UNIVERSITY OF SOUTHAMPTON

FACULTY OF NATURAL & ENVIRONMENTAL SCIENCES

School of Ocean & Earth Sciences

Volume 1

Impacts of oceanic re-emergence on North Atlantic winter climate

by

Jian Buchan

Thesis for the degree of Doctor of Philosophy

November 2017

UNIVERSITY OF SOUTHAMPTON

ABSTRACT

FACULTY OF NATURAL & ENVIRONMENTAL SCIENCES

School of Ocean & Earth Sciences

Thesis for the degree of Doctor of Philosophy

IMPACTS OF OCEANIC RE-EMERGENCE ON NORTH ATLANTIC WINTER CLIMATE

by Jian Robert Campbell Buchan

The aim of this thesis is to provide a more comprehensive understanding of the role played by the North Atlantic Ocean in influencing North Atlantic and European atmospheric circulation and surface temperatures using climate models and observations.

In this thesis the pattern of occurrences of re-emergence of sea surface temperature anomalies and positive and negative North Atlantic Oscillation (NAO) events over the last 140 years (1871-2011) from historical observations are examined to understand the historical relationship between the ocean and atmosphere. The findings are compared with CMIP5 historical ensemble model output (1850-2005). The aim is to understand how these models which have been used to simulate changes in the Earth's climate through the twentieth and early twenty-first centuries perform in terms of their ability to simulate the observed links between re-emergence and the state of the NAO. Finally, in an ocean-atmosphere model simulation, the role played by North Atlantic sea surface temperatures (SSTs) on shorter (monthly) timescales is investigated in two recent European cold weather events that both coincided with similarly low NAO values: the winter of 2009/2010 and the early winter of 2010/2011.

The evidence from the simulation study of the recent cold winters indicates that the NAO was influenced by the pattern of ocean surface temperatures occurring in October to December 2010 and re-emergence of SST anomalies in the North Atlantic contributed towards the development of an SST anomaly pattern, which favoured the persistence of a negative NAO resulting in the cold weather anomaly of December 2010 in Northern Europe. Observations show a link between NAO strength and re-emergence after negative NAO winters. The occurrence of a re-emergence event increases the chance of predicting the atmospheric state in the second winter. The analysis of the CMIP5 model output suggests that the majority of the models do not correctly represent re-emergence processes in the North Atlantic and are limited in their ability to reproduce the variability in oceanic and atmospheric conditions seen in observations.

Historical observations show a link between the NAO strength and re-emergence, but potential re-emergence events cannot be predicted from the atmospheric state alone. Whilst this thesis has identified factors which point to when these events are likely to occur there still remains considerable uncertainty in our ability to predict them.

Contents

List of tables

List of figures

DECLARATION OF AUTHORSHIP

I, Jian Robert Campbell Buchan,

declare that this thesis and the work presented in it are my own and has been generated by me as the result of my own original research.

Impacts of oceanic re-emergence on North Atlantic winter climate

I confirm that:

1. This work was done wholly or mainly while in candidature for a research degree at this University;

2. Where any part of this thesis has previously been submitted for a degree or any other qualification at this University or any other institution, this has been clearly stated;

3. Where I have consulted the published work of others, this is always clearly attributed;

4. Where I have quoted from the work of others, the source is always given. With the exception of such quotations, this thesis is entirely my own work;

5. I have acknowledged all main sources of help;

6. Where the thesis is based on work done by myself jointly with others, I have made clear exactly what was done by others and what I have contributed myself;

7. Parts of this work have been published as: Buchan *et al.* (2014).

Signed: .....

Date: .....

Acknowledgements

I would like to express my sincere gratitude to my supervisors, Joël Hirschi, Adam Blaker and Bablu Sinha for their guidance and encouragement throughout the course of my PhD. In particular I thank Joël Hirschi for his significant contribution in gaining publication of my first scientific paper, which is included in this thesis.

Definitions and Abbreviations

AGCM: Atmospheric General Circulation Model

CMIP5: Coupled Model Intercomparison Project

ENSO: El Nino-Southern Oscillation

EOF: Empirical Orthogonal Function

FORTE: Fast Ocean Rapid Troposphere Experiment

GCM: General Circulation Model

HadISST: Hadley Centre sea Ice and Sea Surface Temperature data

IPCC: Intergovernmental Panel on Climate Change

MLD: Mixed Layer Depth

MOC: Meridional Overturning Circulation

NAO: North Atlantic Oscillation

NCEP: National Centres for Environmental Prediction

NOAA: National Oceanic & Atmospheric Administration

NOC: National Oceanography Centre

OGCM: Ocean General Circulation Model

OHC: Ocean Heat Content

OI: Optimal Interpolation

PC: Principal Component

SSS: Sea Surface Salinity

SST: Sea Surface Temperature

SSTA: Sea Surface Temperature Anomaly

Chapter 1: Introduction

1.1 Motivation for the study

This thesis will examine the impact of oceanic temperatures in the North Atlantic on the atmospheric circulation patterns and consequent climate variations over Western Europe. Changes in climatic conditions have socioeconomic consequence in Western Europe with its high population density the predictability of changes in climate on seasonal and decadal timescales is of significance. European winter extremes are important both socioeconomically and scientifically as they provide observational data which can be used to provide an improved understanding of the underlying mechanisms affecting changes in the climate. In this thesis data from both observations and climate models will be compared to provide a basis to evaluate the impact of oceanic temperatures in the North Atlantic on Western European climate.

The most recent assessment by the Intergovernmental Panel on Climate Change (IPCC, 2013) provides a context to global changes in the Earth's climate and confirmed the ongoing warming of the atmosphere and the ocean, commonly referred to as global warming, and associated changes in the global water cycle, reductions in snow and ice cover, rises in global mean sea level and changes in some climate extremes. One consequence of the increase in global surface temperatures is forecast to be more frequent hot and fewer cold temperature extremes over most land areas on daily and seasonal timescales as global mean temperatures increase. As global mean surface temperatures increase, Arctic Sea ice coverage is expected to reduce along with the wide-spread retreat of glaciers. There is increasing evidence that the higher temperatures are resulting in an increase in extreme precipitation events over most of the mid-latitude land masses and over the wet tropical regions while arid regions are expected to become even drier. Extreme weather and climate events are likely to become more intense and more frequent by the end of the 21st century (IPCC,2013). While hot extremes are expected to clearly increase there will still be potential for very cold climatic events. Examples of the former have been the Russian heat wave in 2010 (Russo *et al*., 2015) and the European heat waves in 2003 and 2015 (Schär and Jendritzky, 2004, Duchez *et al*., 2016) and of the latter are the cold European winters of 2009/10 and December 2010 (Cohen *et al*., 2010, Jung *et al*., 2011, Liu *et al*., 2012, Maidens *et al*., 2013, Osborn, 2011, Taws *et al*., 2011) and the cold Eastern US winters of 2013/14 and 2014/15 (Grist *et al*., 2016). The ability to reliably forecast extreme climate events such as these over months or years is a key challenge to climate scientists. The demand for accurate forecasts has resulted in initiatives to improve the modelling of weather patterns and future climate (Hurrell and Deser, 2009; Folland *et al*., 2012). The distinction is drawn between weather and climate. Weather is a measure of the atmospheric conditions over short periods of

time (days, weeks) whereas climate is measured over longer term (months, years) averages of weather over time and space.

There are many mechanisms that influence the potential predictability of climate conditions in the North Atlantic and Europe. These include El Nino-Southern Oscillation (ENSO) related stratospheric dynamics and sudden stratospheric warmings (Ineson and Scaife, 2009; Fereday *et al*., 2012), the extent of Arctic sea-ice (Strey *et al*., 2010), Eurasian snow cover (Cohen *et al*., 2010), soil moisture (Fischer *et al*., 2007), Sea Surface Temperature (SST) and upper ocean heat content (Folland *et al*., 2012). The extent to which each of these factors influences seasonal forecasts is less certain. A leading pattern of weather and climate variability over the Northern Hemisphere is the North Atlantic Oscillation (NAO, Hurrell and Deser, 2009). The NAO refers to the distribution of atmospheric mass between and Arctic and the substropical Atlantic. The NAO has an important influence on the winter climate and the re-emergence of SST anomalies from one winter to the next, and will be descibed in detail later. The relationship between mid-latitude SST anomalies and atmospheric circulation over the North Atlantic in late winter has been used for the seasonal prediction of the NAO over the following winter (Czaja *et al*., 2002, Rodwell and Folland, 2002), through the re-emergence of remnant late winter mixed layer temperature anomalies after summer stratification (Alexander and Deser, 1995, Taws *et al*., 2011). Confidence in these relations can be enhanced if climate models demonstrate the same relationship and if the underlying physical processes that govern them are identified and correctly represented.

The fifth phase of the Coupled Model Intercomparison Project (CMIP5, Taylor *et al*., 2012) constitutes the most recent set of coordinated climate models and provides the opportunity to compare the skill of a large group of Ocean Atmosphere General Circulation Models (OAGCMs). The skill of CMIP5 models to reproduce spatial patterns of climate (circulation, air temperature) variability has been examined (Davini and Cagnazzo, 2013, Perez *et al*., 2014), as has their skill in simulating the spatial structure of SST variability (Wang *et al*., 2015). However, so far there have been no studies using CMIP5 models to investigate the relationship between patterns of SST variability and atmospheric modes of variability over the North Atlantic region.

Common to all models that are part of the CMIP5 ensemble is that the horizontal resolution in both the ocean and atmosphere components is rather coarse (i.e. typically around 1-2° in the ocean and about 1°-3° in the atmosphere). As a consequence these models cannot accurately represent features such as the narrow western boundary currents in the ocean and the associated sharp temperature fronts. Recent work using models with increased resolution in the ocean and the atmosphere can simulate much more realistic circulation patterns in the ocean with more

realistic air-sea exchanges (Hewitt *et al*. 2016). Benefits of higher resolution can be seen in the improved skill in long-range (i.e. seasonal to interannual) predictions of European and North American winters compared to the earlier generation of foreasting systems which used resolutions similar to those in the CMIP5 ensemble (Scaife *et al*., 2014; Dunstone *et al*., 2016). Nevertheless, the CMIP5 ensemble and more generally coarse resolution models represent an immensely valuable resource as they allow to cover a broader range of assumptions for the model physics (e.g. mixing scheme, cloud parameterisations, grid type, etc) made when setting up simulations. Due to their comparatively low computational cost coarse resolution models are also highly configurable and therefore suited for hypothesis testing, in particular when a large ensemble of simulations is required (as will be the case later in this thesis). Even with today's computational resources studies using cutting edge high resolution OAGCM typically consist of one single realisation (e.g. Hewitt et al. 2016) where little can be said about sensitivity to parameter choices.

In this thesis the skill of the CMIP5 OAGCM ensembles to reproduce the historical variability of North Atlantic winter weather events driven by both the atmosphere and the ocean is examined. It will go on to investigate the ocean's role in influencing North Atlantic and European climate on shorter (monthly) timescales with the employment of an OAGCM in which observed SST anomalies are used to force the atmospheric model.

1.2 Aims and Objectives

The primary aim of this thesis is to examine the role played by the North Atlantic Ocean in influencing North Atlantic and European atmospheric circulation both in climate models and by the use of new simulations specifically targeting the cold winters of 2009/2010 and 2010/2011. The research objectives will focus on three scientific questions (SQ). These are:

SQ1: What can historical records tell us about the influence of the ocean on atmospheric conditions?

SQ2: How good are climate models at simulating extreme winter weather events and the underlying mechanisms?

SQ3: What can model simulations tell us about how ocean conditions may affect the atmospheric circulation?

In this thesis the pattern of occurrences of re-emergence and positive/negative NAO events over the last 140 years (1871-2011) from historical observations will be examined to understand the historical relationship between the ocean and atmosphere (SQ1). These will be compared with

CMIP5 historical ensemble model output (1850-2005) to understand how they have simulated changes in the North Atlantic winter climate through the twentieth and twenty-first centuries (SQ2). Specifically the relationship between SST variability and atmospheric modes will be investigated. Finally, in an ocean-atmosphere model simulation, the role played by North Atlantic SSTs on shorter (monthly) timescales is investigated in two recent European cold weather events that both coincided with similarly low NAO values: the winter of 2009/2010 and during the early winter of 2010/2011 (SQ3). Specifically, the sensitivity of the atmospheric circulation over the North Atlantic to observed variations in North Atlantic SSTs during the winter of 2009/2010 and the early winter of 2010 are examined.

The focus of this thesis is on the North Atlantic Ocean. This is for several reasons. Firstly, the coupled ocean-atmosphere interaction that occurs in the North Atlantic plays an important role in moderating the climate of North Western Europe. The ocean exerts an active role in this coupling and a detailed examination of its variability has implications for future European climate predictions. Secondly, the good coverage of surface ocean temperature and atmospheric data enables the temporal variations to be investigated with a high level of confidence.

In order to provide a broader context for the research a description of the general principles of oceanic heat transport, the thermohaline circulation, the re-emergence mechanism and ocean-atmosphere coupling is given in Section 1.3. An outline of the thesis is then presented in Section 1.4.

1.3 General principles of oceanic heat transport and air-sea interactions

The global heat balance can be summarised as a balance between incoming solar radiation and outgoing long wave radiation. The incoming radiation is "sunlight", shortwave radiation, some of which is reflected back into space. The fraction of energy reflected is called the albedo (α), and the albedo is higher over lighter areas like snow and ice and lower over darker areas like the ocean. The rate at which incoming radiation arrives at the Earth is known as the solar constant and has a value of 1365 Wm^{-2}. On average over the Earth's surface and over a day, one quarter of this energy 341 Wm^{-2} reaches the top of the atmosphere (i.e. the radiation intercepted by the Earth's cross sectional area (πR^2) is spread across its entire surface area ($4\pi R^2$) over the course of a day), the average albedo is about 0.3 so on average the incoming solar radiation taken up over the Earth's surface is about 240 Wm^{-2} (Wild *et al.*, 2012). To maintain the Earth's temperature at near constant values, an equal amount of energy must radiate back to space. The

outgoing radiation is "black body" radiation, which is proportional to the 4th power of the temperature at the top of the atmosphere. This is given by the Stefan-Boltzmann equation:

$$j = \sigma T^4, \tag{1.1}$$

where j is the black body radiation, σ the Stefan-Boltzmann constant and T the surface temperature.

The Earth has an albedo of 0.3, meaning that 30% of the solar radiation that reaches the planet is scattered back into space without absorption. The effect of albedo on temperature can be approximated by assuming that the energy absorbed is multiplied by 0.7. However, long-wave radiation from the surface of the earth is partially absorbed and re-radiated back down by greenhouse gases. Since the emissivity with greenhouse effect is reduced more than the aborptivity is reduced, the equilibrium temperature is higher than the simple black-body calculation estimates. As a result the Earth's actual average surface temperature is about 288 K.

The outgoing long wave radiation is relatively uniform at the top of the atmosphere. However, most of the incoming radiation occurs in the tropical and equatorial regions, so there is more incoming radiation than outgoing radiation for latitudes equatorward of 35°, and there is more outgoing radiation than incoming radiation in sub polar and polar regions. Over long periods the surface temperature is observed to be relatively stable at each latitude, hence the ocean and atmosphere must transport heat poleward away from tropical regions toward polar regions. The maximum combined ocean and atmosphere heat transport occurs at a latitude of about 35°. The atmosphere is a greater contributor to the total heat transport than the ocean and there is asymmetry between the northern and southern hemisphere ocean heat transport because of the overturning circulation in the North Atlantic. This topic will be discussed in more detail in the next section.

The meridional ocean heat transport can be defined as:

$$M = \int\int vT\rho c_p dzdx, \tag{1.2}$$

where M is the meridional heat transport, v is the velocity component through a longitude depth section, T is the potential temperature of the section, ρ the average density, c_p the specific heat capacity ($3850 \text{Jkg}^{-1}\text{K}^{-1}$), z the depth of the section and x the length of the section.

Estimates of meridional ocean and atmosphere heat transports (Trenberth and Caron, 2001) based on energy balance computations of the atmosphere are shown in Figure 1.1.

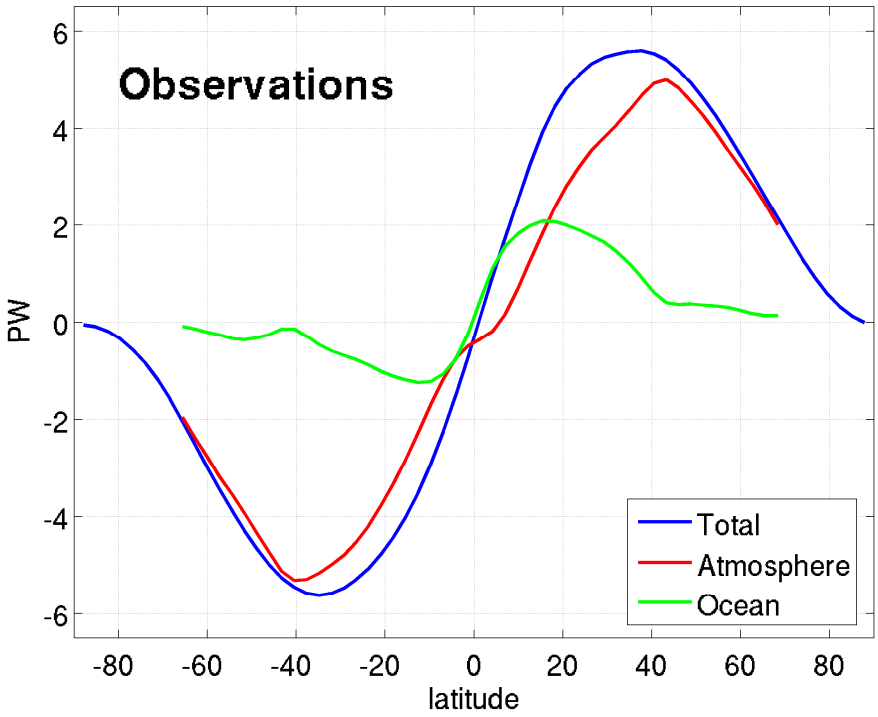

Figure 1.1. Total heat transport (blue) compared with the derived estimate of the adjusted ocean heat transport (green) and implied atmospheric transport (red) from NCEP reanalyses (from Trenberth and Caron, 2001).

The analyses were produced using reanalyses from the National Centres for Environmental Prediction-National Centre for Atmospheric Research (NCEP-NCAR) and the European Centre for Medium Range Weather Forecasts (ECMWF) from 1979 to 1993. The total atmosphere and ocean heat transport is estimated from the difference between estimates of incoming short wave radiation and outgoing long wave radiation at the top-of-the-atmosphere (TOA). The ocean heat transport is estimated independently, and the atmospheric transport is evaluated as the residual between these two quantities. The TOA radiation budget was taken from satellite measurements to provide reliable estimates of the total meridional heat transport. Ocean heat transport was evaluated by comparison of meridional heat transport with alternative estimates from stable coupled climate models that have been run without artificial flux adjustments for several centuries of simulation time and from multiple analyses of direct ocean measurements to determine the extent to which independent means of obtaining these quantities converged. The satellite estimates of the TOA energy budget are adjusted using atmospheric circulation data from NCEP/NCAR reanalysis. As can be seen from Figure 1.1, the ocean meridional heat transport is more asymmetric than the atmosphere with a stronger transport in the Northern Hemisphere. This can be attributed to the contribution of the Atlantic thermohaline circulation which is responsible for a net transport of heat from the Southern to the Northern Hemisphere.

Thermohaline Circulation

Wüst first described the ocean's thermohaline circulation in 1935 (Wüst, 1935). The thermohaline circulation (also referred to as the ocean conveyor belt (Broecker, 1991)) is a part of the large-scale ocean circulation that is driven by global density gradients created by surface heat and freshwater fluxes. Surface currents transport warm water masses northward from the equatorial Atlantic Ocean. As they travel north, these water masses cool, become more dense and eventually sink to depths of ~3000m at high latitudes. This dense deep water then flows southwards and eventually spreads into all the ocean basins. Deep water upwells to the surface in the Pacific and Southern Oceans, where it makes its way back to the Atlantic, either westwards via the Indonesian Throughflow and the Agulhas Current system of South Africa, or eastwards via the Antarctic Circumpolar Current and Drake Passage.The circulation path is shown schematically in Figure 1.2.

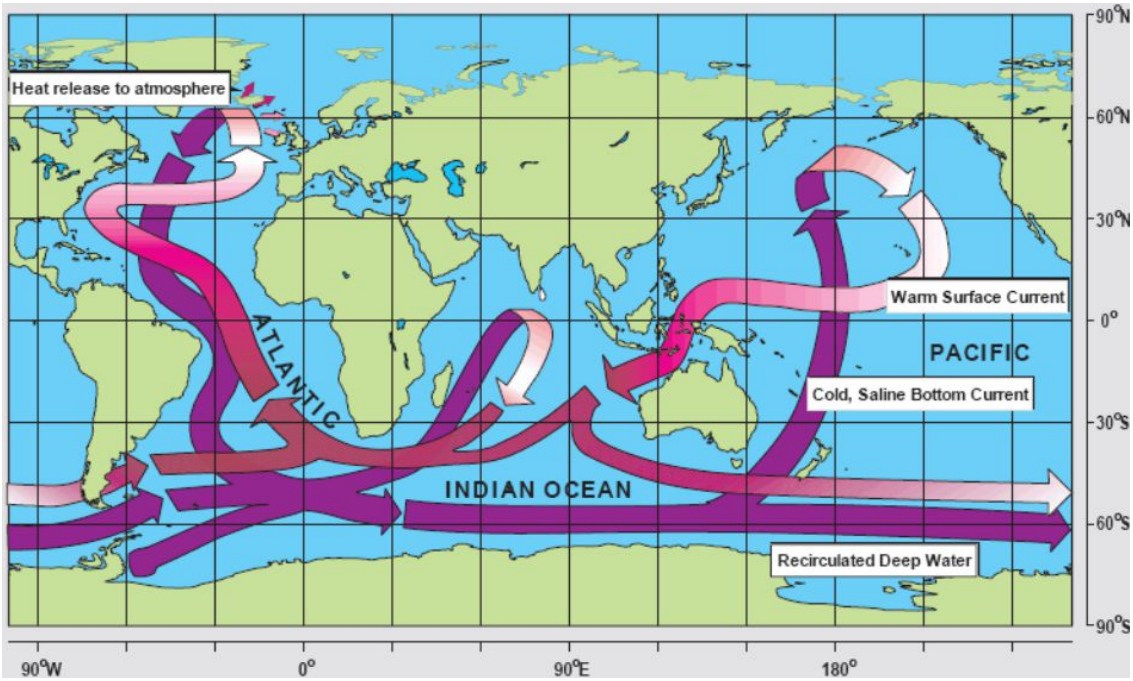

Figure 1.2.Schematic diagram of the global ocean circulation pathways, the conveyor belt (after W. Broecker, modified by E. Maier-Reimer. Source http://www.clivar.org/publications/other_pubs/clivar_transp/d3_transp.htm)

Waters in the vicinity of Iceland are cooled through contact with the cold winter air masses that sweep in from the Canadian Arctic. The cooling increases the density of the surface water to the point where it can sink to the abyss and flow southward, forming the conveyor's lower limb. This flow is depicted as a ribbon of water that flows through the deep Atlantic from Greenland to the tip of Africa. This water mass is known at the North Atlantic Deep Water (NADW). Beneath this water mass in the deep Atlantic is a wedge of Antarctic Bottom Water (AABW),

which under-rides the NADW mass. This intruding water is mixed upward into the southward flowing NADW, increasing the transport by the conveyor's lower limb.

Southward of 30^{o}S the lower limb of the conveyor joins the rapidly moving current that encircles the Antarctic continent, the Antarctic Circumpolar Current. This current blends the NADW exiting the Atlantic with new deep water generated along the perimeter of the Antarctic continent and also with old deep waters recirculated back into the Antarctic from the deep Pacific and Indian Oceans. The lower limb water returns to the surface in the northern Indian and Pacific Oceans. The major route for the return flow to the Atlantic is through the Drake Passage into the South Atlantic. In the North Atlantic the Atlantic Meridional Overturning Circulation (AMOC) is often used synonymously for the Atlantic thermohaline circulation.

It was Henry Stommel (Stommel, 1958) who first showed that the north-south gradient of the Coriolis force was responsible for the observed return flow of the slow wind driven interior gyre circulations being concentrated in fast moving western boundary currents such as the Gulf Stream, in a process known as western intensification. Stommel and Arons (Stommel and Arons, 1959) extended this circulation to the deep ocean, proposing a global circulation in which surface water sinks in the polar regions to feed the deep boundary currents on the western sides of basins.

One of the benefits provided by the conveyor is the heat it releases to the atmosphere over the North Atlantic. This heat transport warms the climate on both sides of the Atlantic and contributes to Europe's mild winters. However, the main reason that Europe is warmer than Newfoundland is due to the prevailing westerly winds (Rahmstorf, 2003). The northward heat transport across 26.5^{o}N in the Atlantic Ocean is obtained using an approximation of equation 1.2 by multiplying the average transport (velocity x area) of 18 Sv (Sverdrups, 1Sv=10^{6}m^{3}s^{-1}) (McCarthy *et al*., 2012) by the vertical temperature difference (7^{o}C), the specific heat capacity and the density of sea water and is estimated at 1.3 PW (Petawatts, 1PW=10^{15}W) (Johns *et al*., 2011). The thermohaline circulation and gyre circulation of the Atlantic maintains high surface water temperatures in the northern Atlantic. Furthermore the geographical pattern of the winter air temperature is affected by the conveyor's heat output and the release of seasonal heat stored in the ocean. This is illustrated in Figure 1.3, which shows the deviations from zonally averaged winter (DJF) surface air temperatures based on 1948-2010 NCEP/NCAR reanalysis.

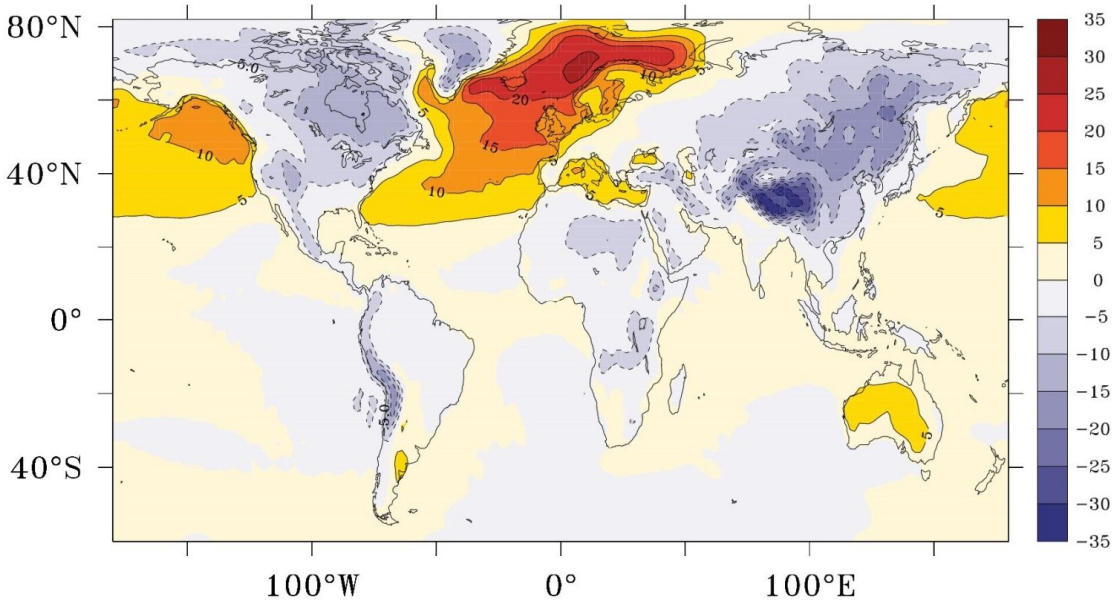

Figure 1.3 Deviations from zonal mean winter (DJF) surface air temperatures from1948-2010 from NCEP/NCAR reanalysis. Units are ^{o}C.

Warm temperature anomalies are found in both the North Atlantic and North Pacific. However those found in the North Atlantic are significantly higher providing an indication of the contribution of the AMOC which is not present in the North Pacific. In the North Atlantic both the seasonal heat storage and AMOC contribute to the temperature anomalies. For the Pacific the warm winter anomaly largely reflects the summer heat storage. In the annual mean there is a much smaller warm anomaly over the North Atlantic than the winter anomaly shown in Figure 1.3 as the contribution from seasonal heat storage cancels out. The differences in the albedo between the ocean and land also contributes to differences. The oceans have a relatively low albedo so will reflect little of the incoming radiation whereas the land has a higher albedo and will reflect more of the incoming heat.

The heat content of a body of water (*OHC*) is defined as:

$$OHC = \int dy \int dz \int \rho c_p T dx \,, \tag{1.3}$$

where T is the potential temperature, ρ the average density (1025kgm^{-3}), c_p the specific heat capacity (3850Jkg^{-1}K^{-1}) and x, y and z the zonal, meridional and depth dimensions. Its evolution is determined by the energy flux through its boundaries.

$$\frac{dOHC}{dt} = Q_{net} + \rho c_p \nabla v T \,, \tag{1.4}$$

where Q_{net} is the net heat content and ∇v the change in horizontal advection.

Variations in ocean heat content can stem from divergence of oceanic heat transport or from exchange with the atmosphere. OHC varies in response to both oceanic and atmospheric exchanges on short and long timescales (Bryden *et al*., 2014, Cunningham *et al*., 2013, Sonnewald *et al*., 2013, Robson *et al*., 2016, Grist *et al*., 2015, Duchez *et al*., 2016). As will be explained in the next section OHC anomalies are not confined to the surface ocean. They have the potential to persist sub-surface for many months and to re-emerge from one winter to the next, in a mechanism which is known as re-emergence.

The re-emergence mechanism

Michael Alexander and Clara Deser first introduced the term re-emergence in the mid-1990s (Alexander and Deser, 1995). They examined surface and sub-surface temperature data from Ocean Weather Ships and using a 1D model of the well-mixed surface layer of the ocean they confirmed a correlative link between the sub-surface temperature anomalies in summer and SSTAs during the previous and subsequent winter seasons.

The sea surface temperature is the surface manifestation of a well mixed layer of water whose depth varies from a maximum in winter (due to mechanical stirring by winter storms and convective overturning as a result of radiative and turbulent heat losses) to a minimum in summer when increasing surface radiation creates buoyant water at the surface, inhibits vertical mixing and stratifies the water column. The mixed layer is bounded below by a strong temperature gradient known as the seasonal thermocline (in this thesis the seasonal thermocline, in context, is referred to simply as the "thermocline"). As the mixed layer deepens in winter it thus entrains water from below the thermocline, and conversely, when the mixed layer is shoaling during the spring and summer it de-entrains water and leaves it below the thermocline.

Re-emergence is the process whereby ocean temperature anomalies established over the deep winter mixed layer are sequestered beneath the seasonal thermocline in summer and reappear at the surface the following winter season. The mechanism is illustrated schematically in Figure 1.4.

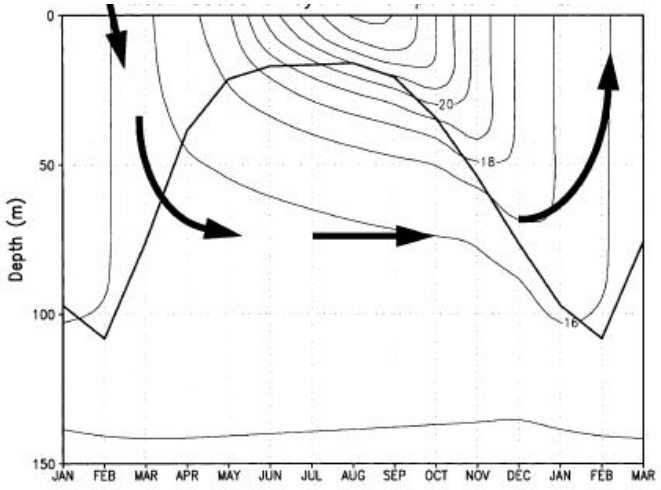

Figure 1.4 Schematic illustration of the re-emergence mechanism showing mean seasonal cycle of upper ocean temperature (^{o}C) and mixed layer depth (m) (black line). The arrows indicate the path of the re-emergence mechanism where anomalies created in winter are stored below the summer seasonal thermocline and are re-entrained into the mixed layer when it deepens in the following autumn. Figure from Alexander *et al*. (2001).

Ocean atmosphere heat exchange generates ocean temperature anomalies that extend from the sea surface down to the base of the deep winter mixed layer (Alexander *et al*., 2001). As the mixed layer shoals throughout spring and summer, due to the increased input of solar radiation and reduced wind stirring, the winter anomalies are trapped below the surface mixed layer and isolated from air-sea interaction by the seasonal thermocline. Strong vertical mixing during the subsequent autumn and winter triggers an increase in the mixed layer depth, and the reentrainment of remnant temperature anomalies back into the mixed layer the following winter. Temperature anomalies situated at deeper depths in the water column reemerge later the following winter, than those situated nearer the surface. The reentrained temperature anomalies can subsequently influence the following winter SSTA pattern. They can cause the winter-to-winter persistence of similar SSTA patterns without persisting at the surface through the intervening summer months and enhance the persistence of wintertime SSTAs from one winter to the next. This has implications for weather forecasting as the resultant SSTAs can actively feed back onto winter atmospheric circulation (Cassou *et al*, 2007, Czaja and Blunt, 2011, Gastineau and Frankignoul, 2015). Indeed this will be one of the main foci in the remaining chapters of this thesis. Re-emergence seems to occur after persistent atmospheric circulation patterns over the North Atlantic in the preceding winter (e.g. in winters where the NAO is negative for prolonged periods) (Blaker *et al*., 2015).

The North Atlantic Oscillation

The atmospheric response to extratropical oceanic variability is a key issue in climate research. The atmospheric circulation of the North Atlantic may be modulated through variability intrinsic to the atmosphere, through external forcing such as the solar cycle and through coupling with the ocean and/or the stratosphere. The leading pattern of weather and climate over the Northern Hemisphere is the North Atlantic Oscillation (NAO) (Hurrell and Deser, 2009). The NAO refers to a redistribution of atmospheric mass between the Icelandic Low and the Azores High, and swings from one phase to another producing large changes in surface air temperature, winds, storminess and precipitation over the Atlantic as well as the adjacent continents. The NAO also affects the ocean through changes in heat content, gyre circulations, mixed layer depth, salinity, high latitude deep water formation and sea ice cover (Hurrell and Deser, 2009). Thus, indices of the NAO have become widely used to document and understand how this mode of variability interacts with the ocean.

The NAO is linked to other modes of variability. On interannual time scales, atmospheric circulation anomalies over the North Pacific, including the Pacific-North American (PNA) patterns are linked to changes in tropical Pacific sea surface temperatures associated with the El Niño/Southern Oscillation (ENSO) phenomenon (Hurrell and Deser, 2009). This association reflects mainly the dynamical teleconnection to higher latitudes forced by deep convection in the tropics. A study by Huang *et al*. (1998) showed significant coherence between the NAO and Niño3 SST in about 70% of the warm ENSO events during the 20th century. The dominant teleconnection pattern associated with changes in the mean atmospheric circulation during the initial winter event was a positive phase of the PNA. More recent studies by Moron and Gouirand (2003) and Brönnimann (2007) provide evidence that the pattern of the North Atlantic sea level pressure anomalies (SLPA) associated with the tropical Pacific SSTA in November-December is different from that found in January-March. In November-December, the warm El Niño events are associated with negative SLPA extending from the Hudson Bay to Scandinavia and positive SLPAs over the Azores high, characteristc of a positive NAO. In contrast cold La Niña events are associated with a postive SLPA over Greenland and a negative SLPA toward western and central Europe, characteristic of a negative NAO. In January, and mainly in February-March, the warm El Niño events are associated with a positive SLPA north of 50^{o}N and a negative SLPA extending to central Europe (typical of NAO negative). The cold La Niña events exhibit almost reversed SLPA patterns.

There is no unique way to define the NAO. Most NAO indices are derived either from simple differences in surface pressure anomalies between various northern and southern locations or from the principal component (PC) time series of the leading empirical orthogonal function

(EOF) of sea level pressure. A disadvantage of station-based indices is that they are fixed in space. In contrast the advantage of EOF analysis is that it takes into account large scale atmospheric patterns and is therefore a better indicator of the state of the NAO than the index based on two stations. However, the shortcoming of EOF analysis is that eigenvectors are mathematical constructs, constrained by their mutual orthogonality. There is no guarantee they represent physical modes of the climate system. The positive phase is characterised by high SLP anomalies over the Azores and low SLP anomalies over Iceland. In contrast a negative phase is characterised by low SLP anomalies over the Azores and high SLP anomalies over Iceland. Figure 1.5 illustrates the SLP anomalies associated with the NAO as well as with two others modes of variability that are prevalent in the North Atlantic. The first is a "Blocking" regime with high pressure centred over Northern Europe and the second the "Atlantic Ridge" with high pressure centred over the North Atlantic.

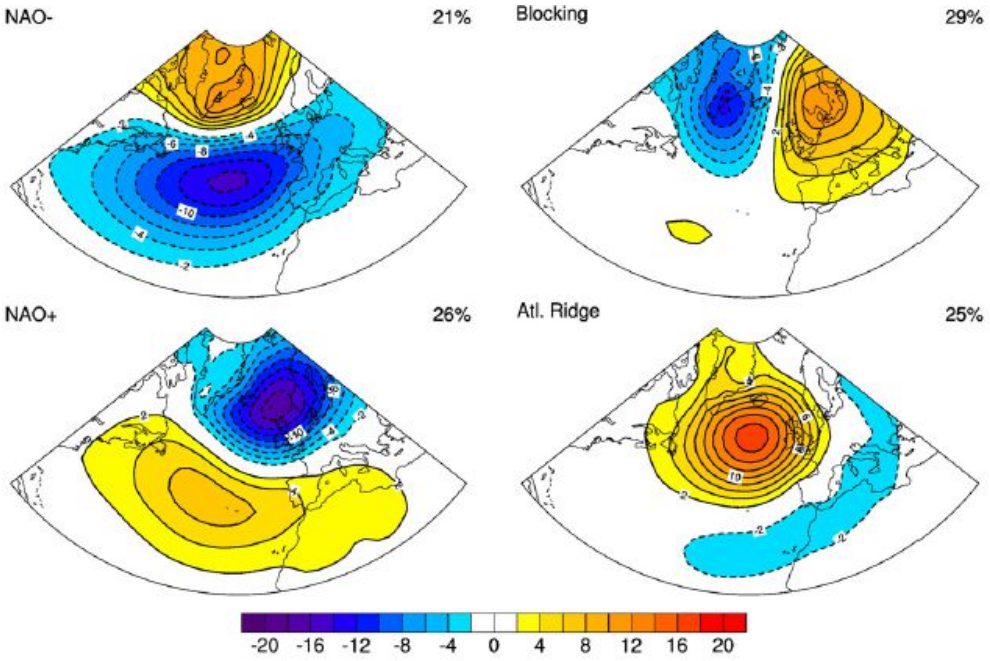

Figure 1.5. Boreal winter (December-March) climate regimes in sea level pressure anomalies (hPa) over the North Atlantic domain (20°-70°N, 90°W-40°E) using daily data over 1950-2006. The percentage at the top right of each panel expresses the frequency of occurrence of a cluster out of all winter days since 1950. Figure from Hurrell and Deser, 2009.

The climate regimes can be further categorised into various circulation types. The relation between pressure pattern circulation type and wind direction, as described by Neal *et al*. (2016), is shown in Figure 1.6 and Table 1.1. They derived weather patterns objectively by clustering daily mean sea level pressure (MLSP) data into a set of 30 then grouped into 8 patterns.

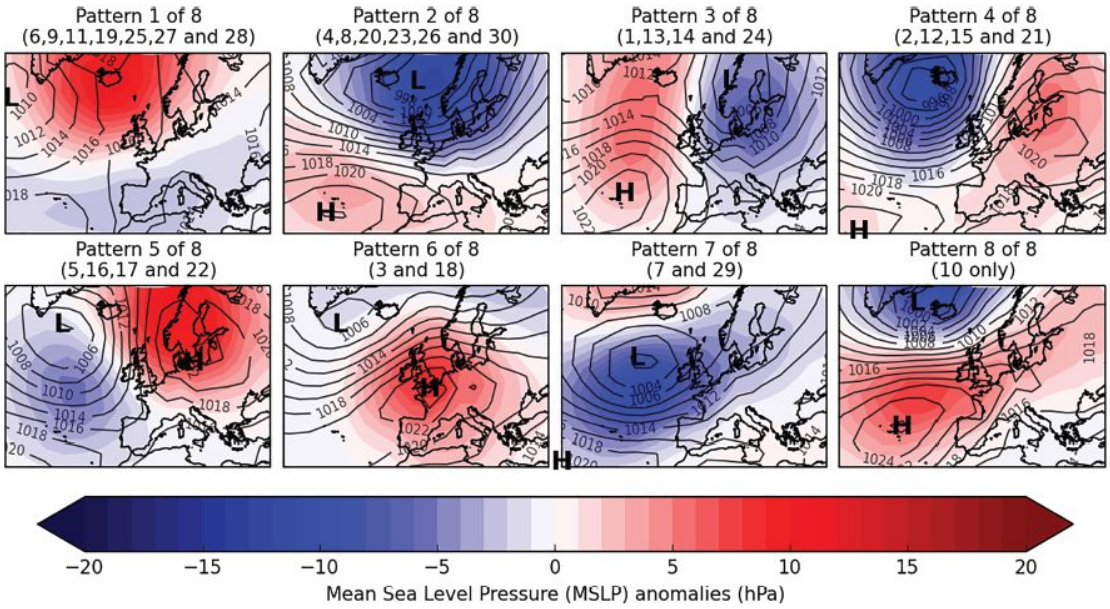

Figure 1.6 Composites from eight weather patterns, the numbers in brackets show the sub-patterns from the set of 30 used to form the composites. Mean sea level pressure (MSLP) anomalies plotted as filled contours (hPa) and MSLP values plotted in foreground from Neal *et al* (2016).

Weather pattern	Description	Percentage Occurance
1. NAO-	Positive MSLP anomalies to the north of UK and negative MSLP anomalies to the south, resulting in a negative NAO pattern.	21%
2. NAO+	Negative MSLP anomalies to the north of the UK and positive MSLP anomalies to the south, resulting in a positive NAO pattern.	18%
3. Northwesterly	Negative MSLP anomalies to the northeast of the UK and positive MSLP anomalies to the southwest of the UK, resulting in a north-westerly flow, varying between cyclonic and anticyclonic.	15%
4. Southwesterly	Negative MSLP anomalies to the northwest of the UK and positive MSLP anomalies to the southeast of the UK, resulting in a south-westerly flow, varying between cyclonic and anticyclonic.	15%
5. Scandinavian high	Negative MSLP anomalies to the west of the UK and positive MSLP anomalies to the east of the UK, resulting in a south to south easterly flow, mostly anticyclonic.	12%
6. High pressure centred over UK	Positive MSLP anomalies over the UK and to the south of the UK, with weak negative MSLP anomalies to the north of the UK, resulting in an anticyclonic westerly or southwesterly flow.	8%
7. Low close to UK	Negative MSLP anomalies are centred just to the west of the UK, resulting in a cyclonic southwesterly flow.	6%
6. Azores high	Positive MSLP centered over the Azores with anticyclonic westerly flow over the UK.	4%

Table 1.1 Description of the eight weather patterns and percentage occurrences from European and North Atlantic Daily to Multi-decadal Climate Variability (EMULATE) MSLP (EMSLP) data (1850-2003) from Neal *et al*. (2016).

The eight patterns help to identify key differences in the circulation flow types of different MSLP patterns. Patterns 1 and 2 represent the negative and positive phases of the NAO. In addition pattern 8 shows a slight variation to the NAO+ pattern. The NAO- and two NAO+ patterns represent 43% of the total variability (Table 1.1). The remaining five patterns represent the other key weather regimes over Europe and are described in Table 1.1. These patterns also provide an understanding of the advection of air masses. Whilst the predominant winds across the North Atlantic are westerlies, those from a northern or northwestern quadrant will draw in cold sub-polar air whilst those from a southern or southwestern quadrant will draw in warm sub-tropical air. This has a direct impact on the resultant surface air temperatures over Northwestern Europe.

The NAO and its different states coincide with different preferred paths for the Northern Hemisphere jet stream. The jet stream is a key determinant of European weather patterns. The Northern Hemisphere jet stream flows over the mid- to northern latitudes of North America, the North Atlantic and Europe at altitudes of 30,000 to 39,000 ft. The jet stream is the product of the solar radiation which drives the Polar, Ferrel and Hadley circulation cells and the action of the Coriolis force on moving air masses. The Coriolis force is caused by the planet's rotation around its axis. The Polar jet stream forms near the the interface of the Polar and Ferrel cells (commonly between 45^{o} and 50^{o}N in winter, but meanders on shorther timescales between 30^{o} and 60^{o}N), while the subtropical jet forms near the boundary of the Ferrel and Hadley circulation cells. The path of the jet stream affects cyclonic storm systems at lower levels in the atmosphere (Woollings *et al.* 2014). Most of the meteorological and climate patterns in the extra tropics are associated with the jet streams, which are stronger over ocean basins. A persistent jet location in winter can lead to extreme weather (Mitchell et al., 2017). The extremely persistent southerly jet throughout winter led to the extremely cold winter of 2009/10 over Europe due to cold air being advected equatorward from high latitudes. In contrast, the extremely persistent northerly jet position of 2011/12 led to a very dry winter, particularly over the south of England, because less moisture was picked up over the Atlantic.

When two air masses of different temperatures or densities meet, the resulting pressure gradient caused by the density difference is highest within the transition zone. The wind does not flow directly from the hot to cold area, but is deflected by the Coriolis effect and flows along the boundary of the two air masses. This is shown schematically in Figure 1.7.

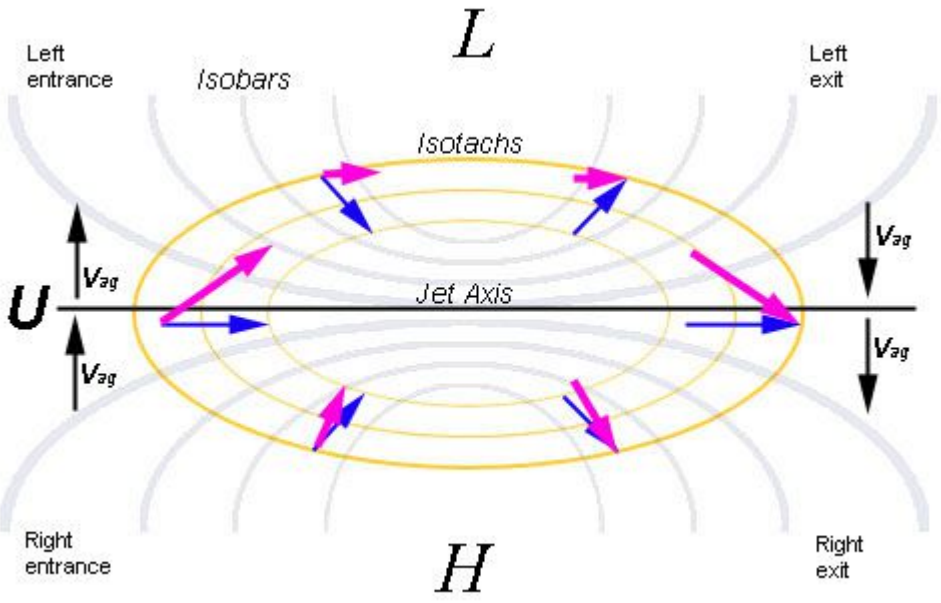

Figure 1.7 A schematic of the height contours between low and high pressure areas and a jet orientated from west to east. The geostropic component of the wind is represented by the blue arrows which are parallel to the isobars, and the isotachs are shown in yellow. Due to an increase in gradient of height contours, air will accelerate in the entrance region, whereas on the exit side, the gradient of the contours slackens, leading to a decelleration of the air flow. Source http://www.eumetrain.org/data/3/3/Content/fi.htm.

Because air flows counterclockwise around low pressure and clockwise around high pressure in the northern hemisphere, westerly flow across the mid-latitudes of the Atlantic occurs throughout the year. The vigor of the flow is related to the north-south pressure gradient, and winds are strongest during the winter when they average near 5 ms^{-1} from the eastern United States across the Atlantic onto northern Europe (Hurrell and Deser, 2009). These mid-latitude westerly winds extend throughout the troposphere and reach their maximum (up to 40 ms^{-1}) at a height of about 12 km in the core of the jet stream.The jet stream roughly coincides with the path of storms, atmospheric disturbances operating on time scales of days, traveling between North America and Europe. Over the subtropical Atlantic the prevailing surface northeasterly trade winds are relatively steady and strongest during boreal summer. The position of the jet stream is influenced by the extent of the warm tropical air mass and cold polar air mass. Generally, positive NAO winters are associated with a northeastward shift in the Atlantic storm activity and enhanced activity from Newfoundland into northern Europe and a modest decrease in activity to the south. Positive NAO winters are also typified by more intense and frequent storms in the vicinity of Iceland and the Norwegian Sea.

The relationship between North Atlantic SSTs and large-scale atmospheric circulations has been widely discussed in the literature (Rodwell *et al*., 1999) and it is well established that over longer time scales (seasons) the SST pattern can be strongly influenced by large-scale atmospheric circulation through both anomalous heat fluxes and wind stresses. Fluctuations in SST and the strength of the NAO are related (Hurrell and Deser, 2009). The leading pattern of SST variability during boreal winter consists of a tri-polar structure marked by a cold anomaly in the subpolar North Atlantic, a warm anomaly in the middle latitudes centred off Cape Hatteras, and a cold subtropical anomaly between the Equator and 30^{o}N. This structure suggests that the SST anomalies are driven by changes in the air-sea heat exchanges and surface wind induced Ekman currents associated with NAO variations (Visbeck *et al*., 2003). The relationship is strongest when the NAO index leads the SST variability by several weeks, which highlights the process by which large scale SST over the extratropical oceans responds to atmospheric forcing on monthly and seasonal time scales (Deser and Timlin, 1997, Czaja and Frankignoul, 2002, Gastineau and Frankignoul, 2015). Over longer periods, persistent SST anomalies also appear to be related to persistent anomalous patterns of SLP, including those associated with the NAO, but the mechanisms whereby the atmosphere forces SST anomalies on decadal and longer time scales are different from those on interannual time scales (Bjerknes, 1964). Studies by Brayshaw *et al*. (2011) have highlighted the importance of SST anomalies in changing the background meridional SST gradients. SST anomalies can weaken or strengthen the background meridional SST gradient in mid latitudes. A weakening of the SST gradient would be expected to reduce the downstream storm track, producing a weaker eddy-driven jet or shifting the jet equatorward, with reduced poleward eddy momentum transport in the upper troposphere and reduced poleward eddy heat transport in the mid-to-lower troposphere. This has the impact of weakening the downstream storm track in mid latitudes and strengthening it at lower latitudes. Thus the SST tripole seen in the North Atlantic can provide the mechanism for changes in the atmosphere with the jet in turn altering the SST patterns.

Ocean atmosphere coupling

Following the Alexander and Deser (1995) paper comparable observational analyses have documented the presence of re-emergence across the North Pacific (Alexander *et al*., 2001; Deser *et al*., 2003) and North Atlantic (Timlin *et al*., 2002, DeCoetlogon and Frankignoul, 2003). In the basin-wide analysis of re-emergence by DeCoetlogon and Frankignoul (2003), re-emergence was apparent throughout most of the North Atlantic, excluding the central portion of the subtropical gyre. These studies confirmed the contribution from the re-emergence process to winter-to-winter persistence of large-scale SSTA patterns in the North Atlantic. Kushnir *et al*. (2002) and Deser *et al*. (2003) shared this conclusion and provided statistical evidence for winter-to-winter recurrence of the leading principal component time series of basin wide North

Atlantic SST. Kushnir *et al*. (2002) also found evidence of an active atmospheric response to the recurring SSTA pattern, which supported similar studies by Czaja and Frankigoul (2002) and Rodwell and Folland (2002).

The suggestion that ocean temperature anomalies could actively influence the atmospheric circulation of the North Atlantic and Europe, and be used in monthly and seasonal climate predictions originates from studies by Bjerknes (1964) and Folland *et al*. (1982). The study by Folland *et al*. (1982) revealed a lagged feedback relationship between Atlantic SSTs in the area south of Newfoundland and atmospheric circulation anomalies over north western Europe. Colder SST anomalies south of Newfoundland were associated with a blocked atmospheric pattern over northwest Europe one month later. Since these studies there have been numerous observation based and statistical analyses supporting the hypothesis that North Atlantic SST anomalies influence atmospheric circulation including Czaja and Blunt, 2011, Gastineau and Frankignoul, 2015 and Gastineau *et al*., 2016. Atmospheric models forced with SST anomalies and coupled ocean-atmosphere model experiments have been used to explore the different physical mechanisms involved.

The role of SSTA re-emergence on the atmospheric circulation of the North Atlantic has been the subject of several climate studies following the initial identification of the process by Alexander and Deser (1995). Czaja and Frankignoul (2002) examined the mean correspondence between SSTAs and 500 hPa geopotential height anomalies at different lags over an entire year, and revealed evidence of a winter atmospheric response to SSTAs from up to 6 months in advance. This enhanced seasonal predictability of the winter atmospheric circulation was consistent with an atmospheric response to reemerging SSTAs from the previous spring. Kushnir *et al*. (2002) reported similar findings. Rodwell and Folland (2002) conducted a study of SSTA re-emergence and North Atlantic climate. In this study they obtained a statistically significant relationship between the forthcoming phase of the winter NAO and SSTs from the previous spring. They devised a method of forecasting winter conditions over Europe based on the covariance between North Atlantic SSTA patterns in May and 500 mbar geopotential heights in the following winter. This statistical regression model formed the basis for operational seasonal forecasting by the UK Met Office (Folland *et al*., 2012). More recently advances in fully coupled dynamics based GCMs have led to increased skill in the seasonal predictability of winter North Atlantic climate. These models employ high ocean resolution, comprehensive representation of the stratosphere and interactive sea ice physics (Scaife *et al*., 2014, Dunstone *et al*., 2016).

Quantitative investigation of the effects of re-emergence on the atmospheric circulation of the North Atlantic with coupled ocean-atmosphere model experiments have been undertaken by

Mosedale *et al*. (2006) and Cassou *et al*. (2007). Cassou *et al*. (2007) directly quantified a significant wintertime atmospheric response to re-emerging remnant ocean temperature anomalies in the North Atlantic. The amplitude of the re-emergence induced response represented 20-25% of the total atmospheric variance and was considered comparable in scale to any other externally forced signal. The nature of the atmospheric response was comparable to the circulation that created the re-emerging temperature anomalies the previous winter that is a winter-to-winter recurrence of the same phase of the NAO. Cassou *et al*. (2007) went on to investigate the physical mechanisms responsible for the atmospheric response to re-emergence. They demonstrated that the reemerging temperature anomalies affected the wintertime atmospheric circulation through transient eddy perturbations along the North Atlantic storm track and changes in the occurrence of key teleconnection patterns.

The results of these studies raise the potential for further investigation of this topic. Firstly, would other coupled models produce similar results in simulating the re-emergence of North Atlantic SSTAs and the atmospheric response? Secondly these results are only theoretical; observational evidence for a significant atmospheric response to actual re-emergence events is limited. Such observations would strengthen the validity and value of model experiments. In this thesis a comprehensive quantitative investigation into the impact of SST anomalies on atmospheric circulation in the North Atlantic is provided together with a detailed assessment of these issues.

The intense re-emergence event of 2009-2010

The winters of 2009/10 and 2010/11 recorded extreme negative phases of the NAO, with December 2010 seeing the lowest NAO index (-4.62) since December 1996 and the 2nd lowest December value since records began in 1825 (Osborn, 2011). This coincided with the re-emergence of SST anomalies in the North Atlantic (Taws *et al*., 2011). This event will be used to study the influence of the oceanic conditions on the atmosphere in Chapter 5.

1.4 Thesis outline

This chapter has provided a review of the literature on the general principles of oceanic heat transport and ocean re-emergence and the key scientific questions that this thesis will address have been introduced. In Chapter 2 the observational data and GCM models that will be used in this thesis are described. In Chapter 3 re-emergence of North Atlantic sea surface temperature anomalies from historical observations from 1871 to 2010 are examined and in Chapter 4 these are compared with re-emergence in a multi model ensemble of historical climate simulations. In Chapter 5 experiments using North Atlantic sea surface temperature anomalies from the winter

of 2009/10 and December 2010 and their impact on north European weather events are described. In Chapter 6 the main findings of this thesis are discussed in relation to the scientific literature presented in this chapter. A more detailed description of each chapter is provided now:

Chapter 2: Data and Methods

In Chapter 2 the observational data (NOAA OI, HadISST and 20th Century Reanalysis) and GCMs (FORTE, CMIP5 contributions) used to investigate the relationship between oceanic heat transport fluctuations on the atmosphere in the North Atlantic are described.

Chapter 3: Re-emergence of North Atlantic temperature anomalies and their impact on North Atlantic winter weather in observations

In Chapter 3, the re-emergence of ocean temperature anomalies in the North Atlantic from one winter to the next is examined to quantify the memory produced in the climate system and the implications for the variability and predictability of the atmospheric circulation over the North Atlantic region. sea level pressure (SLP) and sea surface temperature (SST) fields are taken from observation based datasets (20th Century Reanalysis; HadISST) to study links between re-emergence and atmospheric circulation.

Chapter 4: Re-emergence of North Atlantic temperature anomalies and their impact on North Atlantic winter weather in CMIP5 models

In Chapter 4, the re-emergence of ocean temperature anomalies in Global Circulation Model simulations from the fifth phase of the Coupled Model Intercomparison Project (CMIP5) are compared to those found in observations to study links between re-emergence and atmospheric circulation.

Chapter 5: North Atlantic SST anomalies and the cold North European weather events of winter 2009/10 and December 2010

In Chapter 5, the role played by North Atlantic SSTs on monthly timescales is examined during the winters of 2009/10 and early 2010/11. The study examines the strength of the feedback from Atlantic SSTs onto the atmospheric circulation by investigating two recent European cold events that both coincided with similarly low NAO values: the winter of 2009/2010 and the early winter of 2010/2011. The sensitivity of the atmospheric circulation over the North Atlantic to observed variations in the North Atlantic SST during the winter of 2009/2010 and the early winter of 2010 are quantified using an ocean-atmosphere model. Observed SST anomalies are applied to the model and the atmospheric responses are analysed. Part of this chapter has been published in a peer-reviewed journal (Buchan *et al*., 2014).

Chapter 6: Discussion and Conclusions

In Chapter 6, the main findings of this thesis are discussed in the context of the scientific questions raised in Chapter 1, and the key conclusions from this thesis are summarised.

Chapter 2: Data and Methods

In this thesis, both observational data (NOAA OI, HadISST and 20th Century Reanalysis) and coupled model outputs (FORTE, CMIP5) are utilised to investigate the relationship between sea surface temperature fluctuations and the atmosphere in the North Atlantic. In this chapter a detailed description of the datasets used is provided. The observational data is described in Section 2.1, the CMIP5 model data in Section 2.2 and the model operation of FORTE in Section 2.3.

2.1 Observational Data

The observational data used in this thesis has been used to either provide input for running the FORTE model or in analysis of historical events and comparison with CMIP5 model output (HadISST, 20th Century Reanalysis). Sea Surface Temperatures (SSTs) were selected from the NOAA (National Oceanic and Atmospheric Administration; Reynolds and Smith, 1994, Reynolds *et al*., 2002) Optimum Interpolation (OI) V2 (NOAA OI) monthly time series to produce SST anomalies used in the FORTE simulations (Chapter 5). The SST analysis is produced on a weekly 1^{o} spatial resolution using both in situ and satellite data from November 1981 to the present. The in situ SST is measured from ships and buoys (both moored and drifting). The satellite data is retrieved through Advanced Very High Resolution Radiometer (AVHRR) which allows better resolution of small scale features, such as Gulf Stream eddies. Optimum Interpolation (Gandin, 1963) has been developed as an objective analysis method for irregularly spaced data. The analysis begins with a background or first-guess field, based on the previous week's analysis. Differences between data and the first-guess field, data increments, are computed. At each analysis grid point, the analysis method objectively determines a series of weights for each of the data increments. The weights are based on distances between the grid point. Once the weights are defined, they are multiplied by the data increments and summed to produce an analysis increment at each grid point. The completed analysis is determined by adding the analysis increment to the first guess. The analysis is objective if all the errors are known. Of course they are not perfectly known and are only estimated, hence the term optimum interpolation.

The Met Office Hadley Centre's sea ice and sea surface temperature data set (HadISST; Rayner *et al*., 2003) was used in the analysis of historical events. HadISST provides a unique combination of monthly fields of SST on a 1^{o} latitude-longitude grid from 1871to the present day. The primary purpose of HadISST is to force atmospheric models (AGCMs) in the simulation of recent climate and to evaluate coupled atmosphere-ocean models, thereby

improving our understanding of natural and human-induced climatic variations and allowing evaluation of model performance. The HadISST historical data set is based on gridded, quality-controlled in situ SST observations from ships and buoys and SSTs from the satellite-borne Advanced Very High Resolution Radiometer. Data reconstruction techniques based on empirical orthogonal functions (EOFs) are used to capture the major modes of SST variability and are then projected onto the available gridded SST observations to form quasi-globally complete fields. In HadISST broad scale fields of SST are reconstructed using one of these EOF based techniques, reduced space optimal interpolation (RSOI; Kaplan *et al*., 1997). The RSOI is adapted in a two-stage process: first reconstruction of the global pattern of long-term change and then the residual interannual variability. This results in a better representation of trends than by a single application.

The Twentieth Century Reanalysis data (20CR, Compo *et al*., 2011) has been created by the NOAA ESRL/PSD (National Oceanic and Atmospheric Administration Earth System Research Laboratory/Physical Sciences Division) to provide estimates of global tropospheric variability from 1871 to the present at 6-hourly temporal and 2^{o} spatial resolutions. Atmospheric reanalyses are long historical climate reconstructions that can be considered quasi-observed data as they integrate multiple instrument measurements and have been widely validated against independent observations (Compo *et al*., 2011). The 20CR utilises an Ensemble Kalman Filter data assimilation system (Whitaker and Hamill, 2002), and a new version of the NCEP (National Centre for Environmental Prediction) atmosphere-land model to generate first-guess fields with interpolated monthly sea surface temperature and sea ice concentration fields from the HadISST data as prescribed boundary conditions, and newly compiled land surface pressure and sea level pressure (SLP) reports and observations, to produce a reanalysis data set spanning 1871 to the present. The pressure data come from the International Surface Pressure Databank (ISPD), which incorporates pressure observations extracted from leading international archives of meteorological variables and contributing national and international collections.

For the purpose of this thesis, it was necessary to manipulate the data into a form suitable for subsequent analysis. For SSTs this required generating anomaly data, de-trending time series, and producing spatial pattern correlations. For atmospheric data this required generating spatial maps of SLP from the leading empirical orthogonal function. These processes are described in more detail as they are applied to the selected data.

SST anomaly data is generated from both NOAA OI and HadISST data sets by removing the monthly climatological average from 1871 to 2011 to produce anomaly data. Long time series data (over 100 years) are further refined by removing long-term trends. In order to establish the pattern in the reoccurrence of SST anomaly patterns for the North Atlantic from one winter to

the next, described in the re-emergence section of Chapter 1.3, the SST anomalies in March are then correlated with the equivalent monthly anomalies through to March of the following year to identify re-emergence events. An example of the SST anomaly data from HadISST is shown in Figure 2.1.

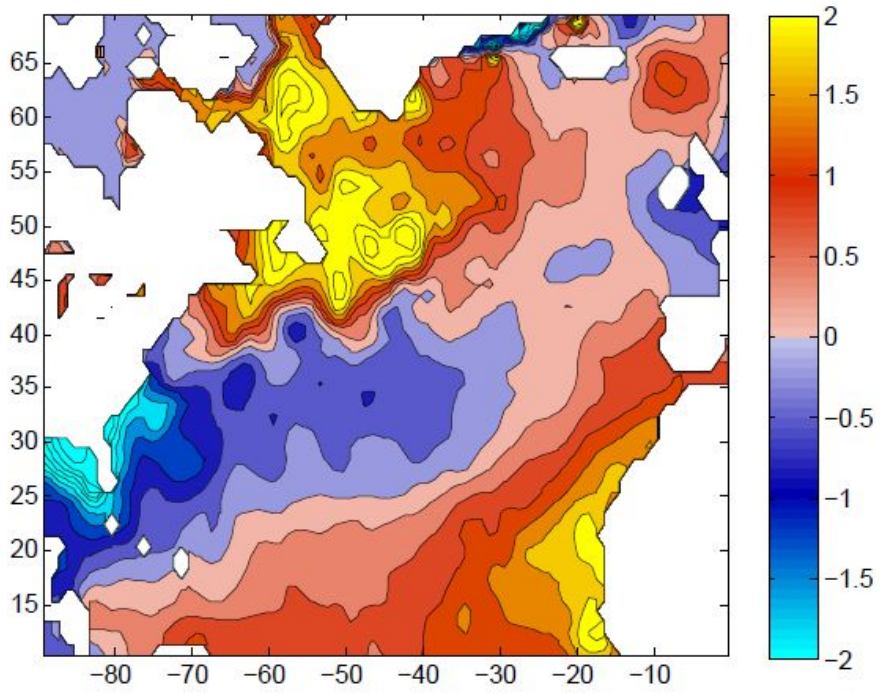

Figure 2.1 An example of winter mean SST anomaly pattern for North Atlantic (10-70°N, 90°W-0) taken from HadISST for December 2009 on 1° grid. Units are °C.

The SST anomalies over long time periods contain a trend in increasing temperatures (Rayner *et al.*, 2003). If left in the data this would introduce a bias into the data with increased occurrence of negative and positive anomalies in the earlier and later years covered by HadISST. In order to better identify the year-to-year variability associated with re-emergence events the anomaly data are detrended by removing a least squares polynomial fit (of degree 15) from the time series. The use of a linear trend is not sufficient because the SSTs are subject to large variability on multiannual to multidecadal timescales. An example of this procedure is shown in Figure 2.2.

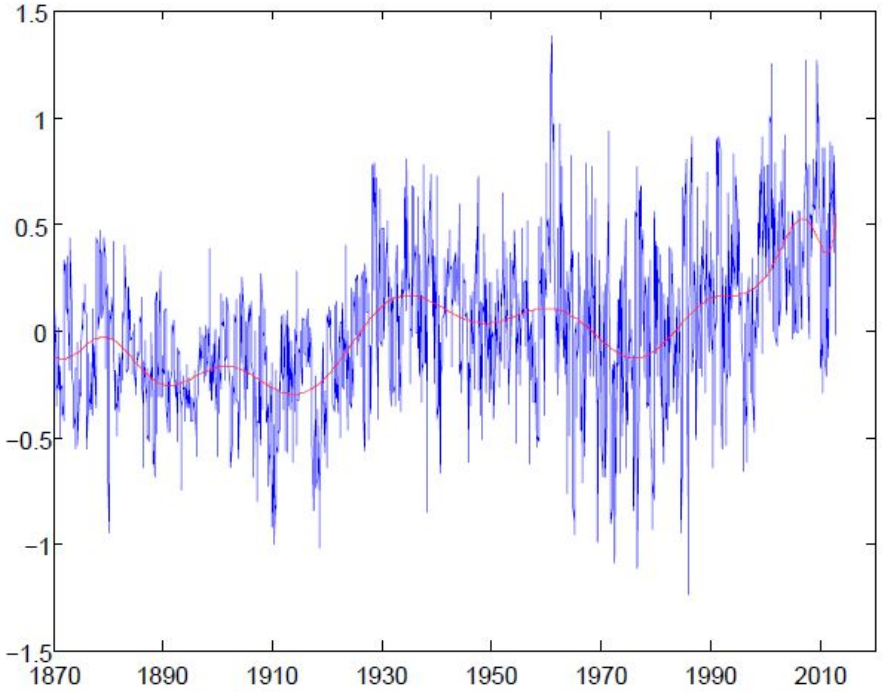

Figure 2.2 Polynomial fit of HadISST SST anomaly data from the North Atlantic (10-65°N, 80-10°W). The blue line shows the mean SST anomaly and red line the least squares polynomial fit, which is removed from the anomaly data. Units are °C.

The SST anomaly patterns for the North Atlantic in March are then correlated with the equivalent monthly anomalies for each month through to March of the following year. The spatial correlation R_t for each month t is calculated according to:

$$R_t = \frac{\sum_{x=1}^{N}\sum_{y=1}^{M}(SST(x,y)_{March} - \overline{SST_{March}})(SST(x,y)_t - \overline{SST_t})}{\sqrt{\sum_{x=1}^{N}\sum_{y=1}^{M}(SST(x,y)_{March} - \overline{SST_{March}})^2 \sum_{x=1}^{N}\sum_{y=1}^{M}(SST(x,y)_t - \overline{SST_t})^2}}, \quad (2.1)$$

where N, M are the number of grid cells with SST values in longitudinal and latitudinal direction and where the overbar denotes the spatial average for the corresponding month:

$$\overline{SST_t} = \frac{1}{NM}\sum_{x=1}^{N}\sum_{y=1}^{M} SST(x,y)_t. \quad (2.2)$$

An example of correlation coefficients from the North Atlantic (10-65°N, 80-10°W) is shown in Figure 2.3.Strong re-emergence patterns are seen for the winters 1940/41, 1969/70 and 2010/11.

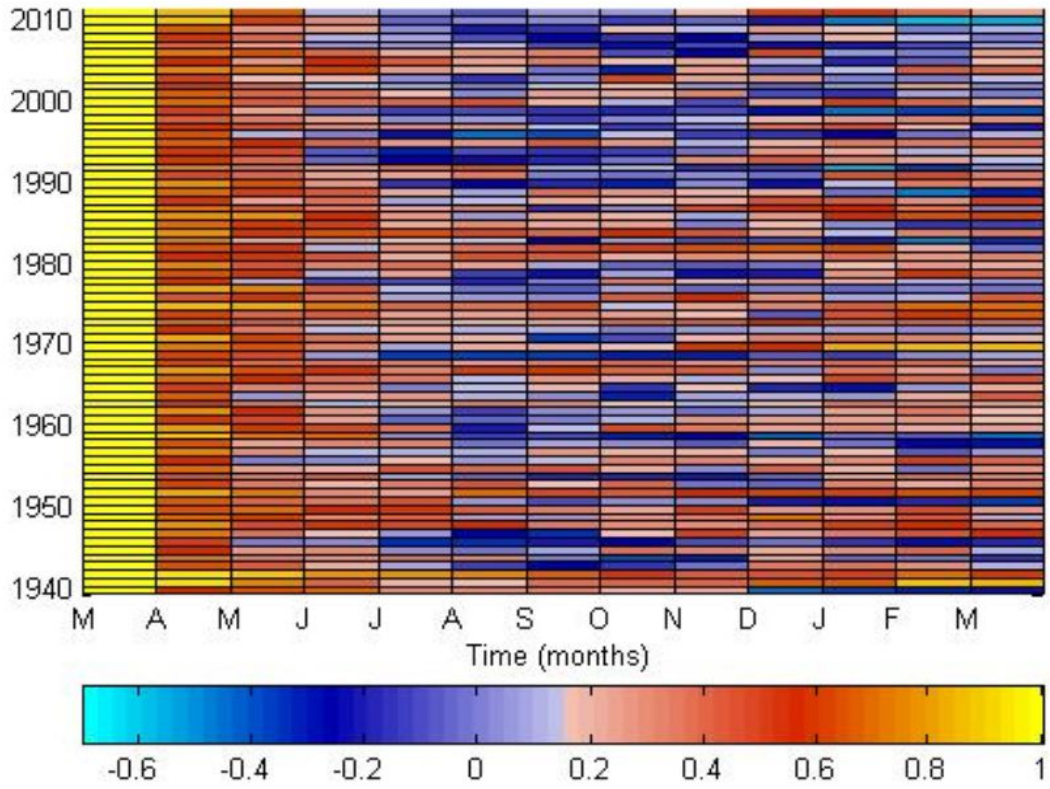

Figure 2.3 Autocorrelation of North Atlantic SST anomalies in March with the equivalent monthly anomalies through March of the following year for 1940 to 2010.

To identify years of interest, in which re-emergence may have occurred, some simple criteria are derived to select years of interest. There are too many years to examine each individually, particularly considering the intention to analyse simulations from the CMIP5 ensemble. To establish the criteria that the physical characteristics of a re-emergence event may be evident SST are considered.

For a re-emergence event to have occurred there must be a significant correlation between SST anomalies from one winter and the next. This was identified by selecting years in which the correlation coefficient between March and the following late autumn to mid-winter (NDJ) reaches or exceeds 0.5 for at least one month i.e.

$$\max(R_{November}, R_{December}, R_{January}) \geq 0.5 .$$

In addition, for re-emergence to have occurred a second criteria must be met to distinguish between years when a high winter to winter correlation reflects persistence rather than re-emergence of the previous winters anomalies. Including a summer minimum criteria provides this, as a given SST anomaly pattern is unlikely to reoccur by chance after disappearing in the summer. The "memory" of the atmosphere typically being short (order of weeks) adding the

criterion of a minimum correlation in summer increases the probability of the method to identify genuine re-emergence events due to the ocean "memory". Years were selected when the ratio between the summer and winter mean correlation coefficients R_{winter} and R_{summer} was less than 0.7:

$$R_{summer} = \left(R_{July} + R_{August} + R_{September}\right)/3,$$
$$R_{winter} = \left(R_{November} + R_{December} + R_{January}\right)/3,$$
$$\frac{R_{summer}}{R_{winter}} \leq 0.7. \qquad (2.3)$$

These criteria were selected to identify years when both a summer minimum and a winter maximum occurred in the spatial SST correlations and to remove years when the high winter correlations reflected persistence of SST anomalies throughout the year rather than re-emergence. The criteria for the ratio between summer and winter correlation coefficients was tested and selected as that which best identified years in which re-emergence had occurred. The method cannot rule out that recurrent SST anomaly patterns from one winter to the next are a mainly passive response of the ocean to similar atmospheric circulation patterns in consecutive winters. In Chapter 3 (section 3.3) a detailed analysis of the selection criteria will show that the method reliably identifies the re-emergence events which have been described in the literature so far and provides some confidence that genuine re-emergence events are identified.

A high correlation R_t between March and the following winter does not necessarily imply large SST anomalies. The anomaly data were therefore tested to see if high correlations coincided with large temperature anomalies. The square root of the sum of the squares of the SST anomalies over the North Atlantic for November, December and January was taken to establish the amplitude of the SST anomalies, defined as:

$$SSTA = \sqrt{SSTA_{nov}^{\ 2} + SSTA_{dec}^{\ 2} + SSTA_{jan}^{\ 2}}, \qquad (2.4)$$

where *SSTA* is the sea surface temperature anomaly

These were then multiplied by the winter correlation coefficient to test for events with a high correlation coefficient and high amplitude. The result of this test is shown in Figure 2.4, where years of strong re-emergence patterns (1969/70, 2010/11) coinciding with a high winter correlation coefficient led to a high product, allowing the re-emergence years to be better identified.

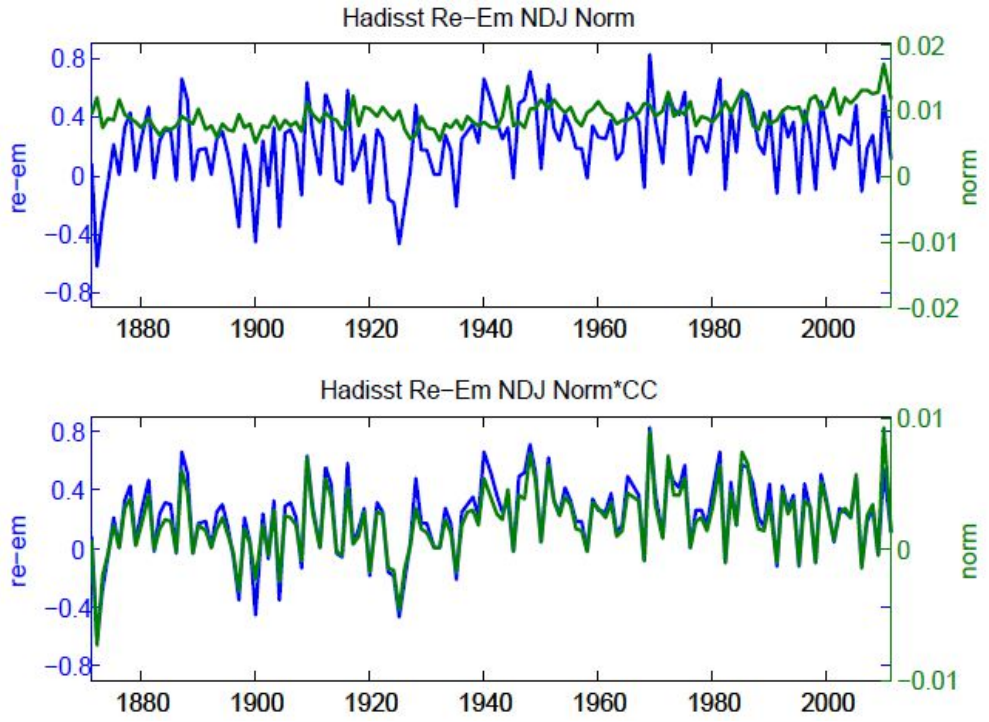

Figure 2.4 Top: Winter mean re-emergence correlation coefficients for North Atlantic (blue) and the square root of the sum of the squares of the SST anomalies (green). Bottom: Winter mean re-emergence correlation coefficients for North Atlantic (blue) and correlation coefficients multiplied by the square root of the sum of the squares of the SST anomalies (green). Units are °C for the sum of the squares.

The spatial structure of the SST variability seen in the HadISST observations was examined by computing the standard deviation of the SST anomalies in the North Atlantic for all months, and is shown in Figure 2.5.

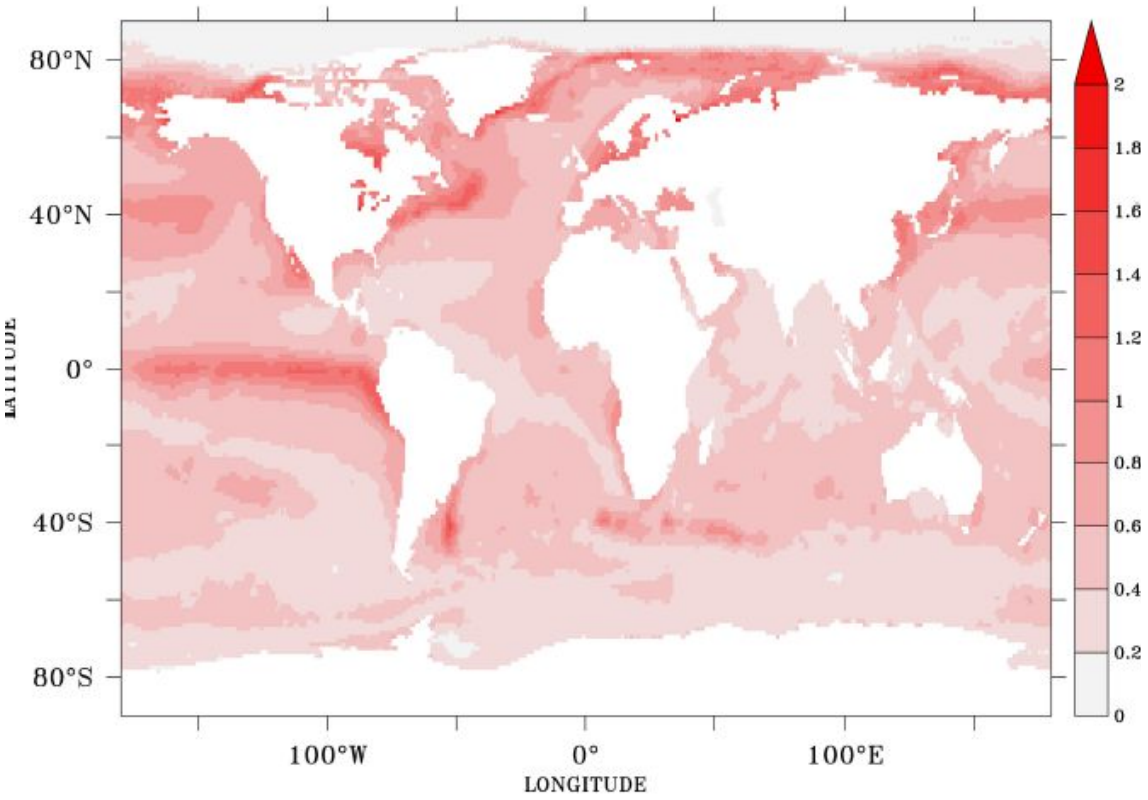

Figure 2.5. Standard deviation of SST anomalies from HadISST for the period 1960-2010.

Regions of higher variability are found in the North Atlantic and North Pacific where large SST fronts are present (note the similarity in pattern to Figure 2.1). Other regions of high variability are seen in the Arctic, along the edge of the sea ice, and along the Equator in the Pacific, indicative of the El Nino Southern Oscillation (ENSO). The highest deviations in the North Atlantic are from the eastern US coast at 40^{o}N along a path across the northeast Atlantic. SST variability is generally lower in the Southern Hemisphere than in the Northern Hemisphere. This is linked to the larger land masses in the Northern Hemisphere which allow the development of sharp land-sea contrasts in atmospheric temperature. This leads to stronger and more frequent outbreaks of continental air masses onto the ocean which enhances SST variability compared to the Southern Hemisphere.

The atmospheric data used in this thesis is taken from sea level pressure (SLP) and surface air temperatures (SAT) from observations (NCEP, 20th Century Reanalysis) and CMIP5 model data. The primary index used to measure atmospheric conditions is the North Atlantic Oscillation which is one of the principal modes of atmospheric variability in the North Atlantic (Hurrell and Deser, 2009). The phases of the NAO are categorized by the variability in sea level pressure over the Northern Hemisphere, from the difference of the Azores high minus the Icelandic low. The NAO can be identified from one-point correlation maps identifying regions

of maximum negative correlation over the North Atlantic (Wallace and Gutzler, 1981; Kushnir and Wallace, 1989). Another technique is EOF (or principal component analysis). In this approach, the NAO is identified from the eigenvectors of the covariance matrix, computed from the time variations of the gridpoint values of sea level pressure. The eigenvectors, each constrained to be spatially orthogonal to the others, are then scaled according to the amount of total data variance they explain. The leading eigenvectors of the covariance matrix calculated from winter mean (DJF) SLP anomalies in the North Atlantic sector (20-70^{o}N, 90^{o}W-40^{o}E) area weighted in the manner of Hurrell and Deser (2009) are shown in Figure 2.6.

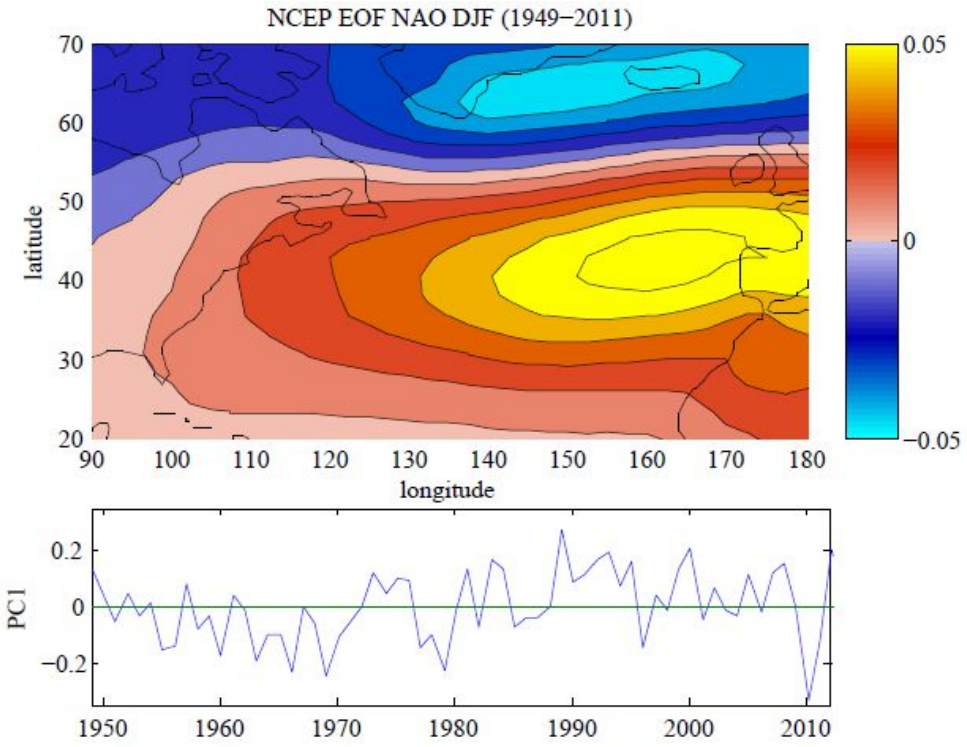

Figure 2.6. (top) Leading empirical orthogonal function (EOF1) of the winter (DJF) mean sea level pressure anomalies in the North Atlantic sector (20-70^{o}N, 90^{o}W-0^{o}E) from 1949-2011 from NCEP. The percentage of total variance explained is 38.5%. (bottom) Time series of EOF1 from 1949 to 2011.

When the NAO index is negative, the SLP anomalies are positive over Iceland and negative over the Azores, resulting in a southward shift in the Jet Stream leading to colder North European winters. The advantage of EOF analysis is that it takes into account large scale atmospheric patterns and is therefore a better indicator of the state of the NAO than the index based on two stations. However, the shortcoming of EOF analysis is that eigenvectors are mathematical constructs, constrained by their mutual orthogonality. There is no guarantee they represent physical modes of the climate system. EOF analysis assumes preferred atmospheric states come in pairs, in which anomalies of opposite polarity have the same spatial structure.

EOFs do not allow for asymmetries between positive and negative phases of the NAO, however, there is evidence that NAO+ and NAO- anomalies are not just the inverse of each other (Hurrell and Deser, 2009).

The results from this method of calculating to NAO were compared with single-point difference of the normalised SLP between Lisbon, Portugal (9°W, 38°N) and Stykkisholmur, Iceland (22°W, 64°N) from Hurrell (https://climateguide.ucar.edu /climate-data/hurrell-nao-index-station-based) are shown in Figure 2.7. Whilst the time series of the two methods show a close correlation and similar distributions, extremes occur more frequently in the single point NAO data. The data does not point to a significant difference in the identification of NAO states between the EOF and single station SLP methods.

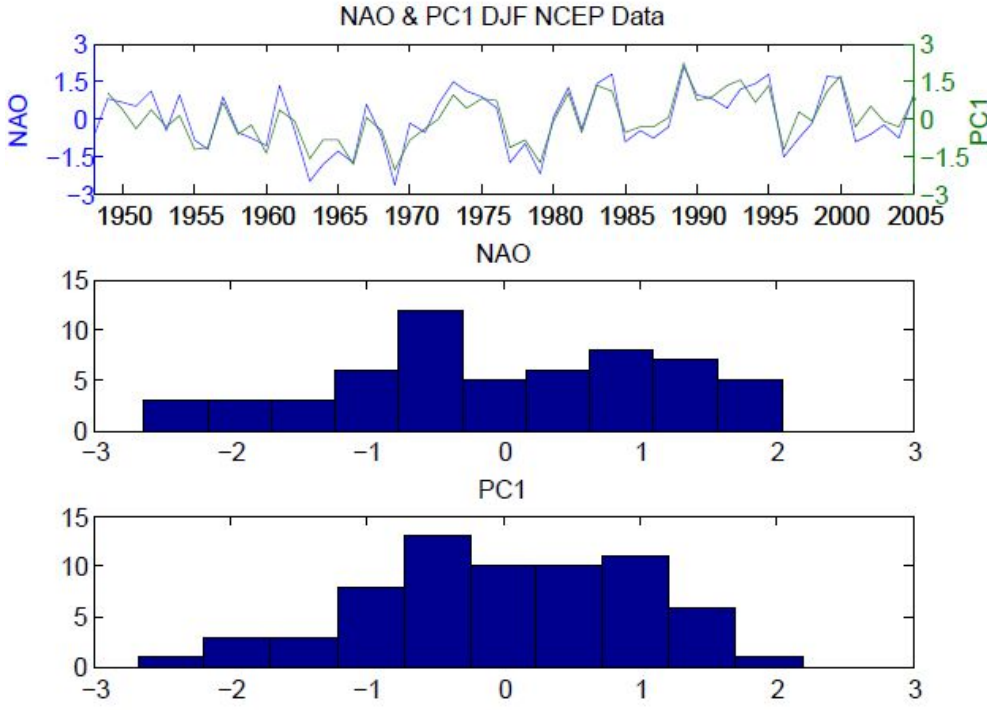

Figure 2.7. (top) Time series of NAO from 1948-2005 of EOF analysis (green) from NCEP data and single-point difference of the normalised SLP between Lisbon, Portugal (9°W, 38°N) and Stykkisholmur, Iceland (22°W, 64°N) (blue) from Hurrell (https://climateguide.ucar.edu /climate-data/hurrell-nao-index-station-based). (middle) Distribution of single-point NAO index. (bottom) Distribution of EOF1 index.

2.2 CMIP5 Model Data

General circulation model output were obtained from the fifth phase of the Coupled Model Intercomparison Project (CMIP5, Taylor *et al.*, 2012). The selected models were taken from the core simulations within the suite of CMIP5 long-term experiments from the "historical" run

which was forced by atmospheric composition changes reflecting both anthropogenic and natural sources from 1850 to 2005. The purpose of the historical ensemble was to evaluate model performance against present climate and observed climate change, provide initial conditions for future scenario experiments and enable assessment of the significance of differences between simulated and observed fields between the different simulations. In this work, 19 different climate models involved in the CMIP5 project have been analysed. A single ensemble member of the historical ensemble (r1i1p1- realisation 1, initialisation 1, perturbation 1) was selected for all models. The names, research centre and country and atmospheric and oceanic resolution are shown in Table 2.1. The CMIP5 data was acquired through the Earth System Grid-Centre for Enabling Technologies (ESG-CET)(http://pcmdi9.llnl.gov/).

Model	Institution	Country	Atmospheric resolution	Oceanic resolution
ACCESS1.0	Commonwealth Scientific and Industrial Research Organisation	Australia	1.25° x 1.9°, L38	1° x 1°, L50
ACCESS1.3	Commonwealth Scientific and Industrial Research Organisation	Australia	1.25° x 1.9°, L38	1° x 1°, L50
BCC-CSM1.1	Beijing Climate Centre	China	1.12° x 1.12°, L26	1° x 0.78°, L40
CanESM2	Canadian Centre for Climate Modelling and Analysis	Canada	2.8° x 2.8°, L35	1.4° x 0.94°, L40
CCSM4	National Centre for Atmospheric Research	USA	0.94° x 1.25°, L26	1.12° x 0.47°, L60
CMCC-CM	Centro Euro-Mediterraneo per I Cambiamenti Climatici	Italy	0.75° x 0.75°, L31	1.97° x 1.2°, L31
CNRM-CM5	Centre National de Recherches Meteorologiques	France	1.4° x 1.4°, L31	0.99° x 0.62°, L42
CSIRO-Mk3.6.0	Commonwealth Scientific and Industrial Research Organisation	Australia	1.9° x 1.9°, L18	1.9° x 0.94°, L31
EC-EARTH	EC-EARTH consortium	Various	1.1° x 1.1°, L62	0.99 x 0.62°, L31
GFDL-ESM2M	NOAA Geophysical Fluid Dynamics Laboratory	USA	2° x 2.5°, L48	1° x 0.9°, L50
GISS-E2-H	NASA Goddard Institute for Space Studies	USA	2° x 2.5°, L40	2.5° x 2°, L26
HadCM3	Met Office Hadley Centre	UK	2.5° x 3.75°, L19	1.25° x 1.25°, L20
HadGEM2-ES	Met Office Hadley Centre	UK	1.25° x 1.9°, L38	1° x 0.83°, L40
INM-CM4	Institute for Numerical Mathematics	Russia	1.5° x 2°, L21	1° x 0.52°, L40
IPSL-CM5A-LR	Institut Pierre et Simon Laplace	France	1.9° x 3.75°, L39	1.97° x 1.2°, L31
MIROC5	Model for Interdisciplinary Research on Climate	Japan	1.4° x 1.4°, L40	1.4° x 0.8°, L50
MPI-ESM-LR	Max-Planck-Institut für Meteorlogie	Germany	1.9° x 1.9°, L47	1.4° x 0.82°, L40
MRI-CGCM3	Meteorological Research Institute	Japan	1.1° x 1.1°, L48	1° x 0.49°, L50
NorESM1-M	Norwegian Climate Centre	Norway	1.9° x 2.5°, L26	1.12° x 0.47°, L53

Table 2.1. List of CMIP5 model names, institutions, countries, atmospheric and oceanic horizontal resolution levels in degrees of longitude and latitude, and vertical resolution (e.g. L50 = 50 verical levels).

The spatial patterns of variability within the atmosphere were again analysed using EOF techniques as described in section 2.1. The variance explained by the first 3 EOFs is listed in Table 2.2. It can be seen that first principle component generally explains more variance than in the observations but less for second and third components.

Model	EOF1	EOF2	EOF3
20CR	38.5	16.9	15.2
Access1	56.1	12.0	8.7
Access3	50.3	10.4	7.5
BCCCSM	59.8	13.1	5.5
Canesm	41.6	12.5	10.0
CCSM4	38.2	12.2	10.2
CNRM	39.9	12.7	10.5
CRISO	50.9	15.2	10.2
ECEARTH	54.8	12.1	5.0
GFDLESM2	35.0	15.0	10.0
GISSE2H	33.9	16.0	11.0
HadCM3	38.8	18.4	11.4
HadGEM2	32.8	22.5	14.8
INMCM4	35.2	20.9	7.9
IPSLCM5A	34.8	20.0	9.1
MIROC5	39.5	20.8	9.7
MPIESM	38.6	16.4	12.0
MRICGCM3	29.1	12.5	10.0
NorESM1	45.5	13.8	8.6

Table 2.2. Percentage of variance from principle component analysis (EOF1, EOF2, EOF3) of the winter (DJF) mean sea level pressure anomalies in the North Atlantic sector (20-70^{o}N, 90^{o}W-0^{o}E) from CMIP5 models.

2.3 The FORTE Model

In order to examine the hypothesis that re-emergence had an impact on the atmospheric circulation in the winter of 2009/10 and December 2010 a GCM needed to be selected which would could perform simulations of the impact of sea surface temperature anomalies on the atmosphere. The Fast Ocean Rapid Troposphere Experiment (FORTE) climate model (Sinha and Smith, 2002, Blaker *et al*., 2006, Wilson *et al*., 2009, Sinha *et al*., 2012) was selected to perform these numerical experiments (Chapter 5). FORTE is a coarse resolution ocean-

atmosphere coupled general circulation model capable of integrations over timescales ranging from days to thousands of years. It is also capable of a high degree of flexibility; the model has been designed with the intention of performing experiments using highly idealized configurations (e.g. Smith *et al*. 2004; 2006). The main components of FORTE are ocean and atmosphere General Circulation Models capable of, and originally designed to allow the easy setup of many different configurations. The ocean model is MOMA (Webb, 1996), an adaptation of the well known Modular Ocean Model version 3 code from GFDL (Geophysical Fluid Dynamics Laboratory, Princetown: Pacanowski and Griffies, 1998) designed for Unix based computers and uses the Unix C compiler pre-processor to provide a wider range of model options. The atmosphere is adapted from IGCM3 (Intermediate General Circulation Model 3) a spectral atmosphere GCM developed at Reading University (Forster *et al*., 2000). They are coupled together using OASIS (Valcke *et al*., 2000), which is designed to link the separate computer processors running the two component models (atmosphere and ocean). The ocean component of FORTE, described in detail below, has a horizontal resolution of 2^o x 2^o and 15 z-coordinate layers in the vertical. The model uses the mesoscale eddy parameterisation of Gent and McWilliams (1990).

MOMA is a derivative of the Bryan-Cox-Semtner type of ocean general circulation models widely used for studying the circulation of the ocean (Webb 1996). The basic model, developed by Bryan (1979), is based on differential equations for the conservation of heat, salt and momentum and represents these by finite-difference equations. The basic procedure described by Bryan (1979) starts from the full set of differential equations describing the evolution of the ocean and uses a series of approximations, valid when studying the large-scale circulation, and derives a set of equations usually termed the "primitive equations". MOMA solves the oceanic primitive equations using finite difference methods on a Arakawa 'B' latitude-longitude grid (Arakawa, 1966). A free-surface scheme based on Killworth *et al.,* 1991 is implemented. The ocean circulation is based on conservation laws expressed as equations. These are mass conservation, momentum conservation (zonal, meridional and vertical)(equations 2.5, 2.6, 2.7), energy conservation (2.8), salt conservation (2.9) and the equation of state that relates temperature, salinity and pressure to density of seawater (2.10) and are expressed as:

$$\rho_0 \frac{\partial u}{\partial t} + \rho_0 (u\nabla)u + \rho_0 w \frac{\partial u}{\partial z} - \rho_0 f \times u = -\nabla\rho + A_m \nabla^2 u + K_m \frac{\partial^2 u}{\partial z^2}, \qquad (2.5)$$

$$\frac{\partial p}{\partial z} = -g\rho, \qquad (2.6)$$

$$\frac{\partial w}{\partial z} + \nabla u = 0, \qquad (2.7)$$

$$\frac{\partial T}{\partial t} + (u\nabla)T + w\frac{\partial T}{\partial z} = A_h \nabla^2 T + K_h \frac{\partial^2 T}{\partial z^2}, \quad (2.8)$$

$$\frac{\partial S}{\partial t} + (u\nabla)S + w\frac{\partial S}{\partial z} = A_h \nabla^2 S + K_h \frac{\partial^2 S}{\partial z^2}, \quad (2.9)$$

$$\rho = \rho(T, S, p), \quad (2.10)$$

where u and w are the horizontal and vertical velocities, T and S the potential temperature and salinity, ρ the in situ density, ρ_0 a Boussinesq reference density is 1035 kg m^{-3}, p the pressure, t time, z the vertical coordinate, the acceleration due to gravity is g = 9.806 ms^{-1}, ∇ the horizontal gradient operator, and A_m, K_m, A_h, and K_h the horizontal and vertical diffusion coefficients for momentum and tracers. Here f is the Coriolis vector, equal to $2\Omega n \sin\vartheta$ where n is the unit vertical vector, Ω the Earth's angular velocity is 7.292 x 10^{-5} s^{-1} and ϑ the latitude.

Bryan (1979) divided the ocean into a set of regular boxes whose sides are defined by lines of constant latitude, longitude and depth. The temperature and salinity fields are specified at the centres of these boxes, giving a three-dimensional array of values. The velocity field is specified in a similar way but the field is offset from the tracer fields according to the Arakawa'B' grid and is shown in Figure 2.8.

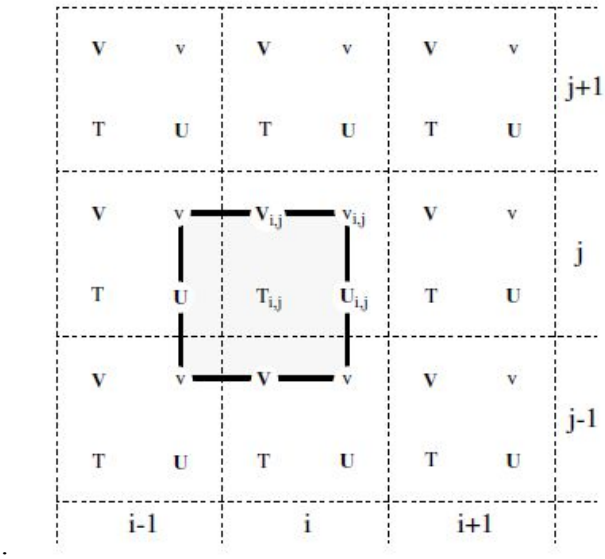

Figure 2.8 The indexing and relative locations of Arakawa 'B' grid. The surface pressure, temperature and tracers are located on the temperature grid (T points), momemtum is located on

the velocity grid (v points) and the zonal and meridional mass fluxes are located at U and V points. The heavy line denotes the boundaries of a temperature grid. Figure from Arakawa, 1966

The finite-difference equations for the temperature and salinity fields are obtained by first integrating equations (2.8) and (2.9) over each of the primary boxes. This gives the "flux" form of the equations in which the advection terms, for example, $(u\nabla)T$, are replaced by the flux of heat and salt due to advection through the side of each of the primary boxes. The diffusion terms are replaced in a similar way by diffusive fluxes through the sides of each box. A similar scheme is used for the momentum equation (2.5) but using boxes centered on the velocity points.

The atmospheric component, IGCM3, is a primitive equation spectral atmosphere model, incorporating realistic coastlines and orography. The primitive equations are solved by expressing the unknown fields (i.e. temperature and velocity etc.) as the weighted sum of a set of spherical harmonic functions. The resolution of the model is then expressed as the number of functions at which the sum is truncated (e.g. T42 means 42 spherical harmonic functions are retained). When the model evaluates variables in real space, the spectral atmosphere model uses a Gaussian grid, which for T42 spectral resolution is approximately 2.8^{o}x2.8^{o}. The prognostic variables are temperature and humidity, vorticity and divergence. The wind field is obtained diagnostically from the latter two. The model is driven by solar radiation incident at the top of the atmosphere and employs a multi-band radiation scheme, including the effects of water vapour, carbon dioxide and ozone. Convection is dealt with via a Betts-Miller (Betts and Miller, 1986) scheme with low, medium and high layer clouds. The atmosphere model in standalone mode incorporates a land surface scheme consisting of a surface and deep soil temperature and moisture content. Each land gridbox is also assigned a vegetation index, which determines the roughness length and albedo. The surface boundary condition over land is thus provided by the land surface scheme and boundary layer sensible and latent heat fluxes and windstresses can be calculated using bulk aerodynamic formulae. Over ocean areas the standalone model incorporates a 25 m deep slab mixed layer model (temperature only, no salinity) with fixed albedo and roughness length. A simple representation of slab-ice is included within the surface boundary scheme. Thus boundary layer fluxes can also be calculated over ocean areas. For the coupled model the mixed layer model over the ocean area is disabled, and the atmosphere is given the SST derived from MOMA at one-day intervals. In order to conserve moisture entering and leaving the ocean it is necessary to account for the excess precipitation over land and deposit the water at the coast as river runoff. At each timestep the latent heat and rainfall are converted into comparable units. Total water in the coupled system is conserved but some will accumulate in reservoirs such as land ice/snow and soil moisture.The precipitation field is passed to the ocean model by moving excess rain (i.e. any more than the fixed amount that can be absorbed by the soil) over land grid points to predetermined coastal points. This is to

simulate river runoff for the coupled model, which otherwise has no way of returning to the sea water that has fallen on land. In order to do this the model grid is divided up into a number of fixed regions, with the rainfall over each region being divided equally between a number of coastal runoff gridboxes for each region.

FORTE model assessment

Starting from rest with the Levitus (temperature, salinity) climatology (Levitus and Boyer, 1998, Levitus *et al*., 1998) the model is spun up for 100 years prior to the main experiments. During this period the ocean reaches a quasi-steady state. The model is then run on for an additional 100 years to generate a control simulation for the subsequent experiments.

A number of broad criteria were used in the assessment of FORTE skill in its control climate. The control simulation was examined to ensure that the output was sufficiently stable to provide a suitable platform for the ensemble experiments. The FORTE control simulation produces a realistic climate as illustrated by the average surface air temperatures for January and July when compared to observational data from NCEP/NCAR reanalysis (Figure 2.9).

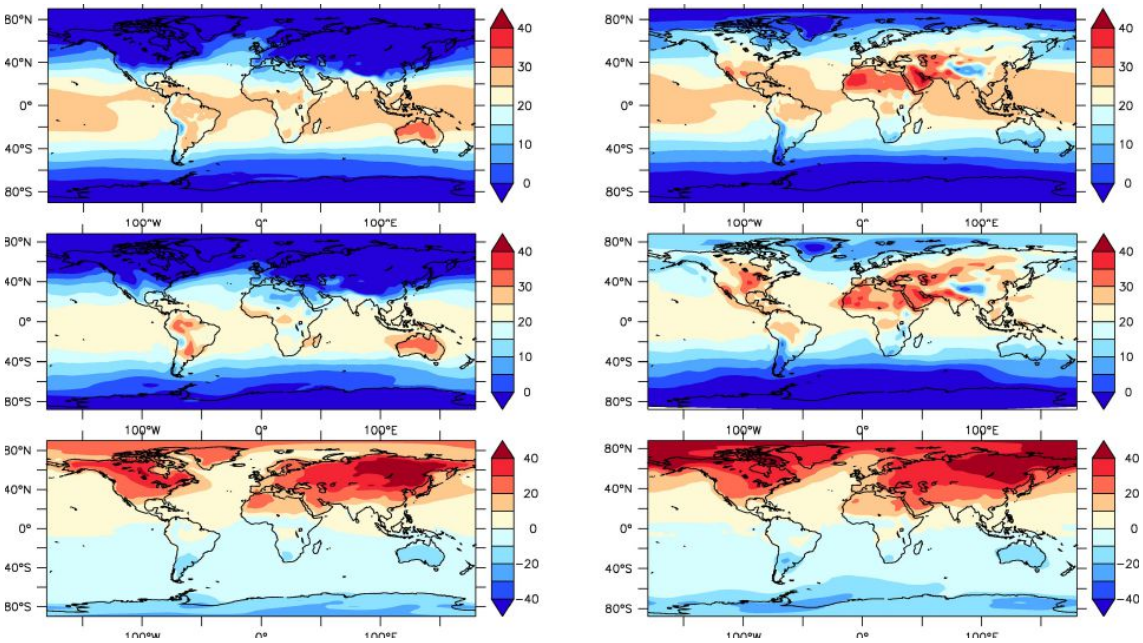

Figure 2.9 Average surface air temperatures from NCEP/NCAR reanalysis from 1948-2011 (top) and FORTE control for last 20 years of 100 year spinup (middle) (^{o}C) for January (left) and July (right) and temperature difference between July and January for NCEP/NCAR (bottom left) and FORTE (bottom right).

The seasonal temperature range shows that FORTE can simulate the amplitude of the seasonal temperature cycle with the largest values found over Eurasia (Siberia) and North America and

much smaller ranges over the oceans. Whilst FORTE produces similar temperatures to those found in observations, simulated continental summer temperatures tend to be higher (over Eurasia, North America, South America and Australia). The Arctic summer temperatures are also higher than those found in observations.

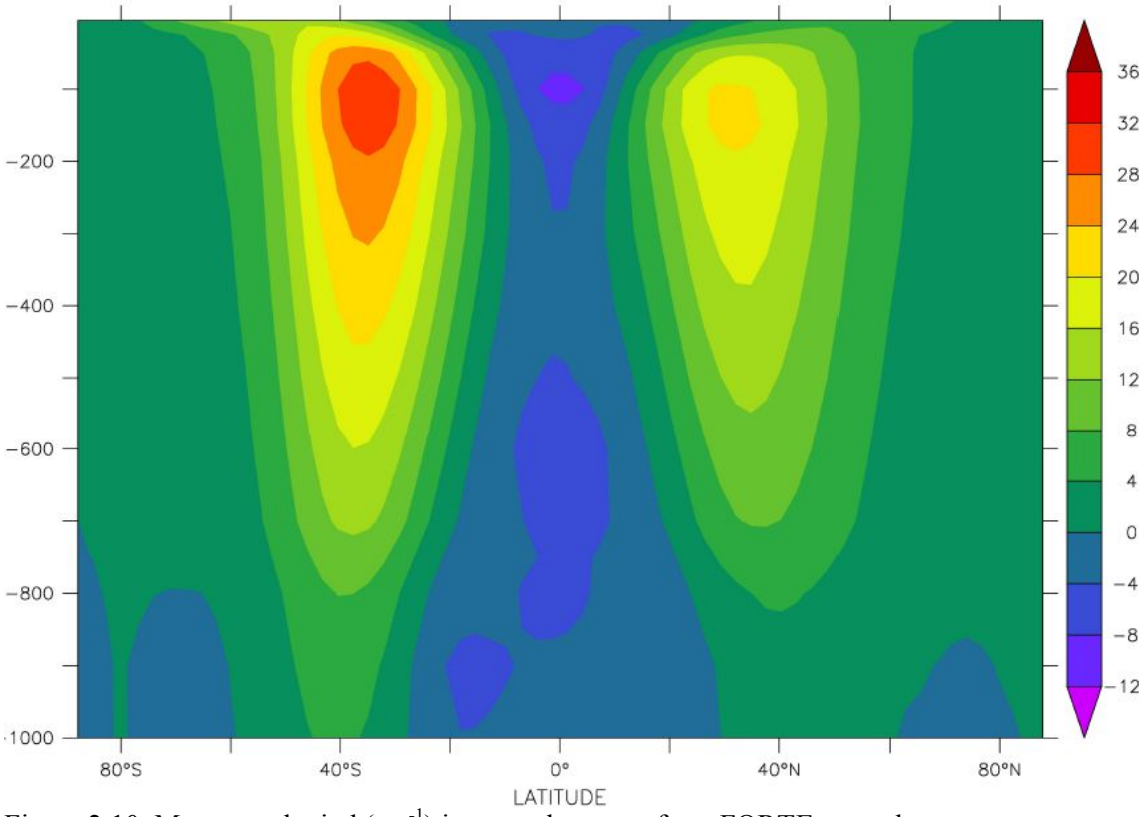

Figure 2.10. Mean zonal wind (ms^{-1}) in second century from FORTE control run.

The zonal mean zonal wind flow is shown in Figure 2.10. The wind flow in the upper atmosphere is predominately westerly with two cells, one in the northern hemisphere and one in the southern, centred around 40^{o} and at 150 mb. This is the level at which the Jet Stream reaches its maximum velocity in both the Northern and Southern Hemispheres. There is a slight asymmetry between the Hemispheres and the wind speeds in the Southern Hemisphere are higher than in the Northern Hemisphere. The amplitude of the velocities simulated in FORTE compares well with the values found in the NCEP/NCAR reanalysis. The mean wind velocities at 250 hPa geopotential height (Figure 2.11) show the track of westerly winds, most pronounced in the southern Hemisphere centred around 40^{o}S and the northen Hemisphere aound 40^{o} N.

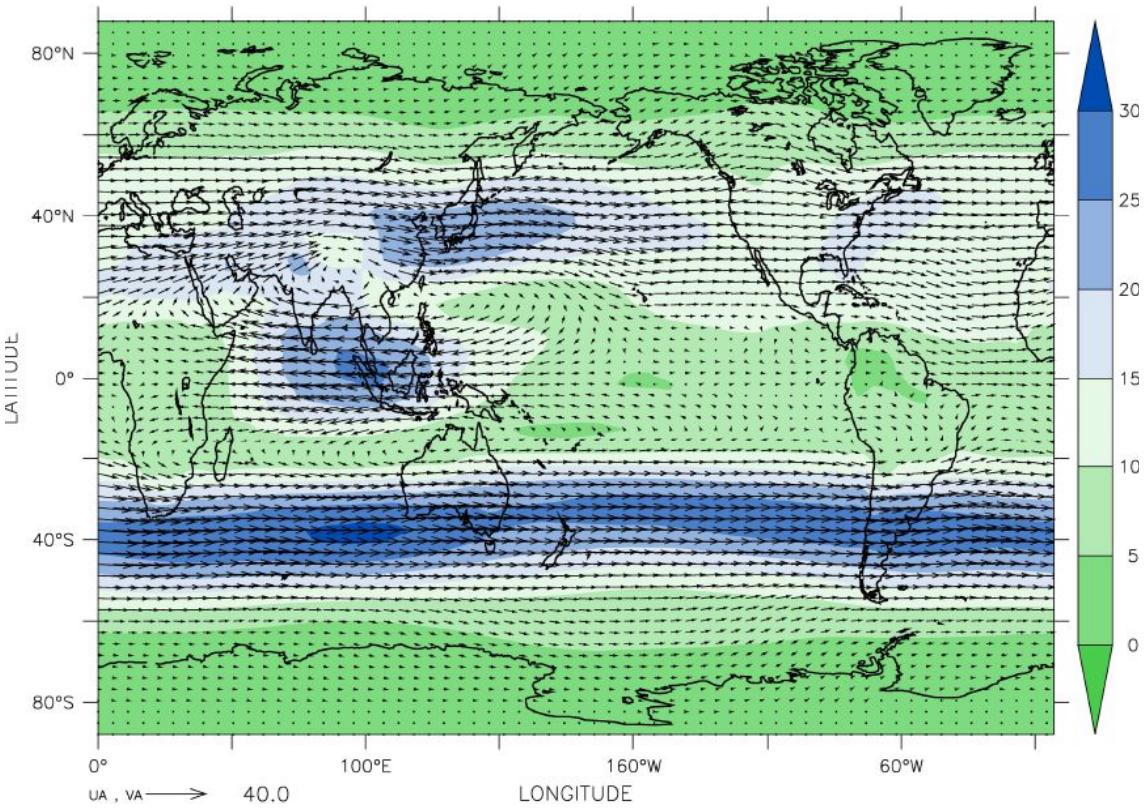

Figure 2.11 Mean atmospheric velocities (ms^{-1}) at 250 hPa geopotential height with mean wind speeds superimposed.

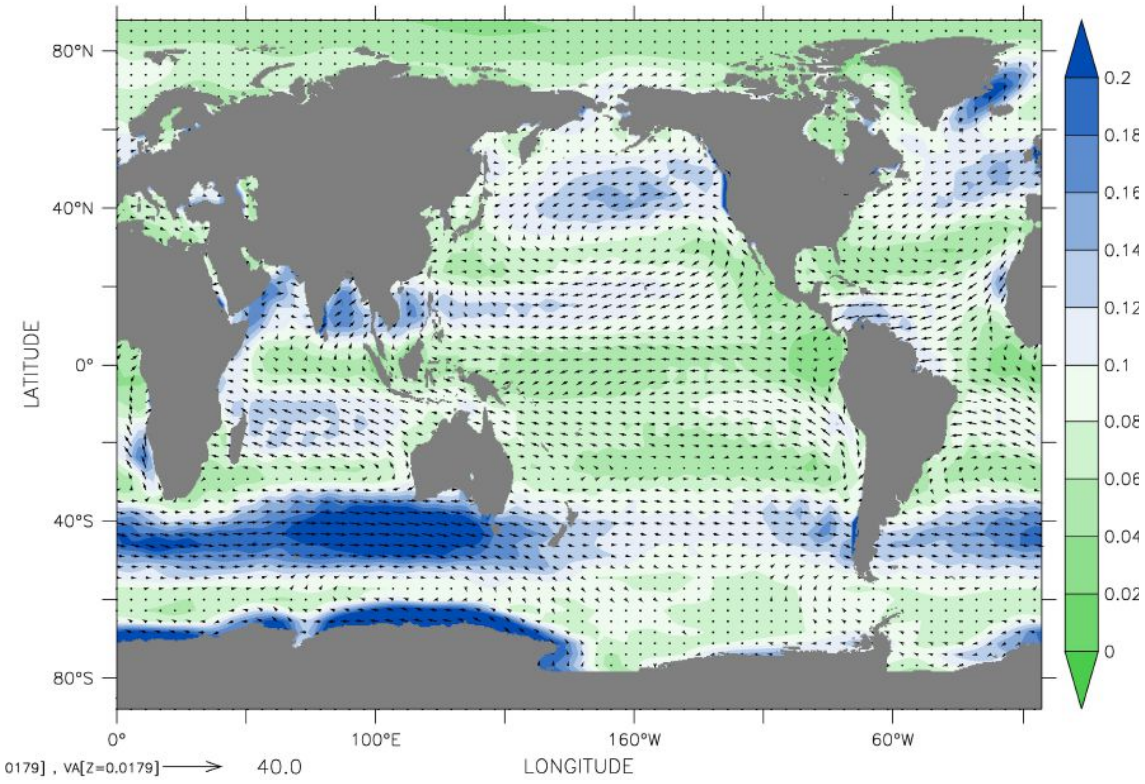

Figure 2.12 Mean surface wind stress (Nm^{-2}) with mean wind speeds (ms^{-1}) superimposed

The mean surface wind stress over the oceans (Figure 2.12) is strongest over the Southern Ocean and in the Northern Hemisphere over the subtropical gyres in the North Pacific and North Atlantic.

The top-of-atmosphere (TOA) radiation in FORTE exhibits an imbalance of ~0.2 W m^{-2} over the second century indicating a net warming of the climate system. As the heat capacities of the atmosphere and land are small, this residual energy must be taken up by the ocean.

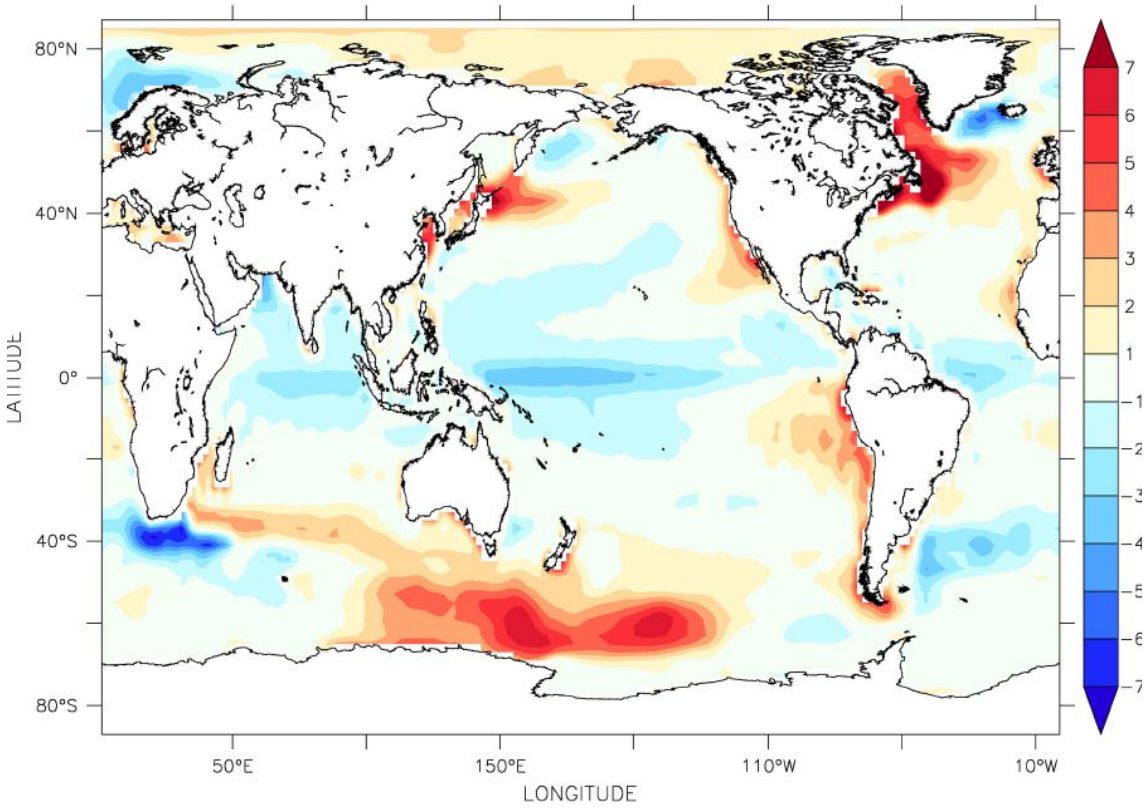

Figure 2.13 Annual mean SST differences (error patterns, in units ^{o}C) , 30 year average after 100 year spinup relative to EN3 v2a from 1960-1989.

The model simulation of SST and SSS is extremely important as it is the primary mechanism for ocean-atmosphere coupling. The SST errors in FORTE relative to EN3 v2a (1960-1989) (Figure 2.13) show warm biases off the Northern Atlantic US coast which reach 4-5^{o}C for most of the Labrador Sea and can exceed 7^{o}C off Newfoundland Additional warm biases are found in the Northern Pacific north of Japan and the Southern Ocean south of Australia and New Zealand and there is a cold bias off the tip of South Africa.

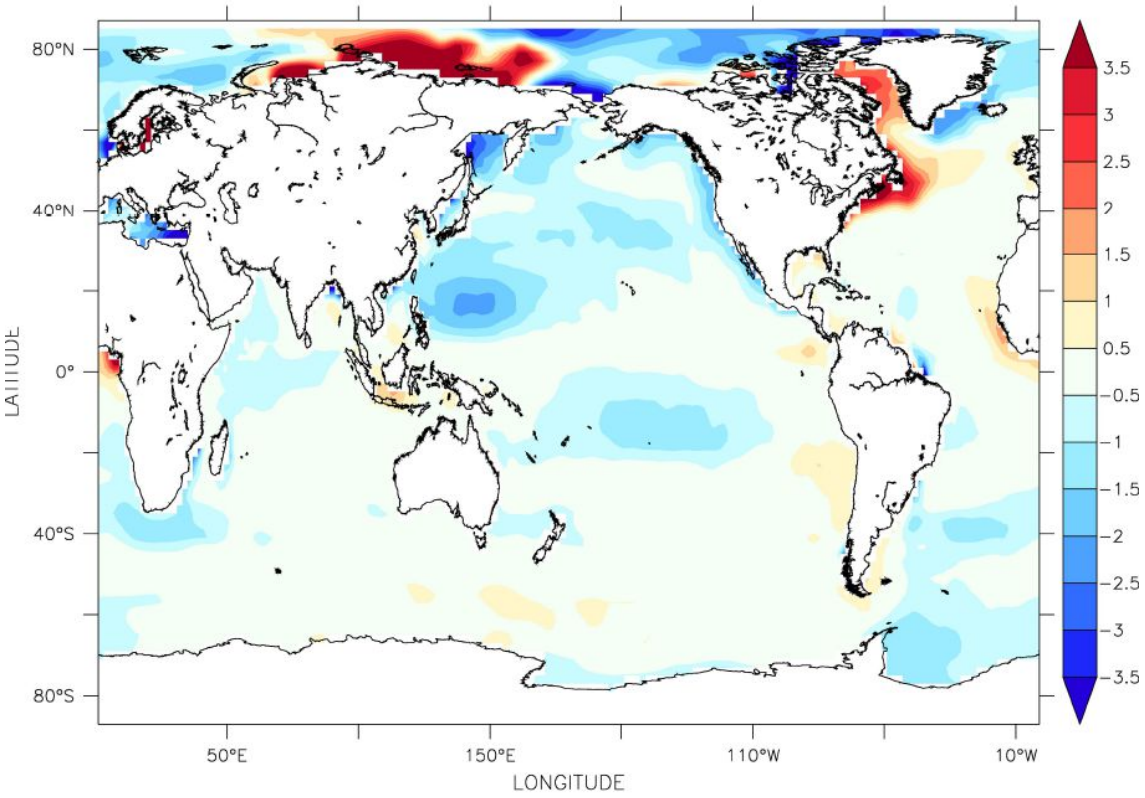

Figure 2.14 Annual mean SSS differences (error patterns) 30 year average after 100 year spinup relative to EN3 v2a from 1960-1989.

The SSS errors in FORTE relative to EN3 v2a (1969-1989) (Figure 2.14) show saline biases in the Northern Atlantic US coast off Newfoundland and in the Labrador Sea, which broadly correspond to the warm biases in this region, and a strong saline bias in the Asian Arctic which may indicate a deficiency in the river runoff to this region. The Northern Pacific and North American Arctic show a fresh bias.

The sea surface height relative to the geoid from FORTE is shown in Figure 2.15. The sea surface height provides information on the position of the main ocean gyres seen in the sub-tropical North Atlantic and North Pacific, and an indication of the strength of ocean currents from the gradient of the contours as seen in the Southern Ocean. Whereas the overall agreement with data from 2004-06 Ocean Atlas is reasonable there are differences most prominently the reduced meridional SSH gradient across the ACC which is consistent with the weaker than observed ACC transport simulated in FORTE Both data show positive anomalies in the North and South Pacific gyres and negative anomalies in the Southern Ocean (Forget, 2010; http://www.ecco-group.org/products: Figure 2.16).

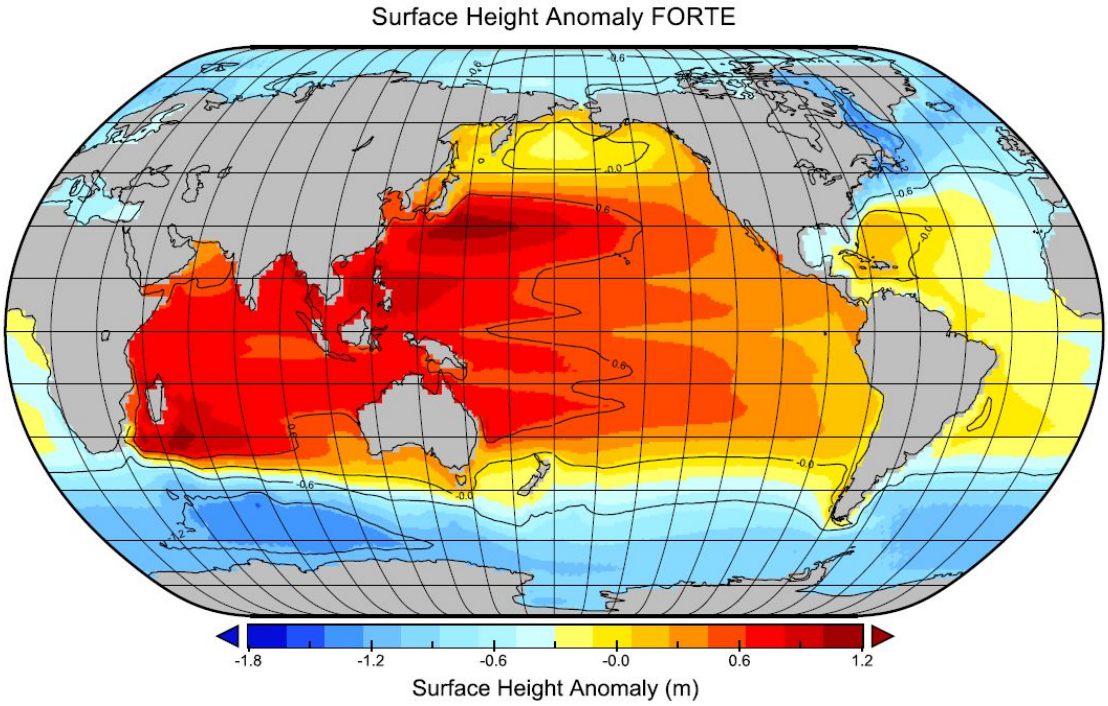

Figure 2.15 Sea surface height above geoid (m) 30 year mean from FORTE.

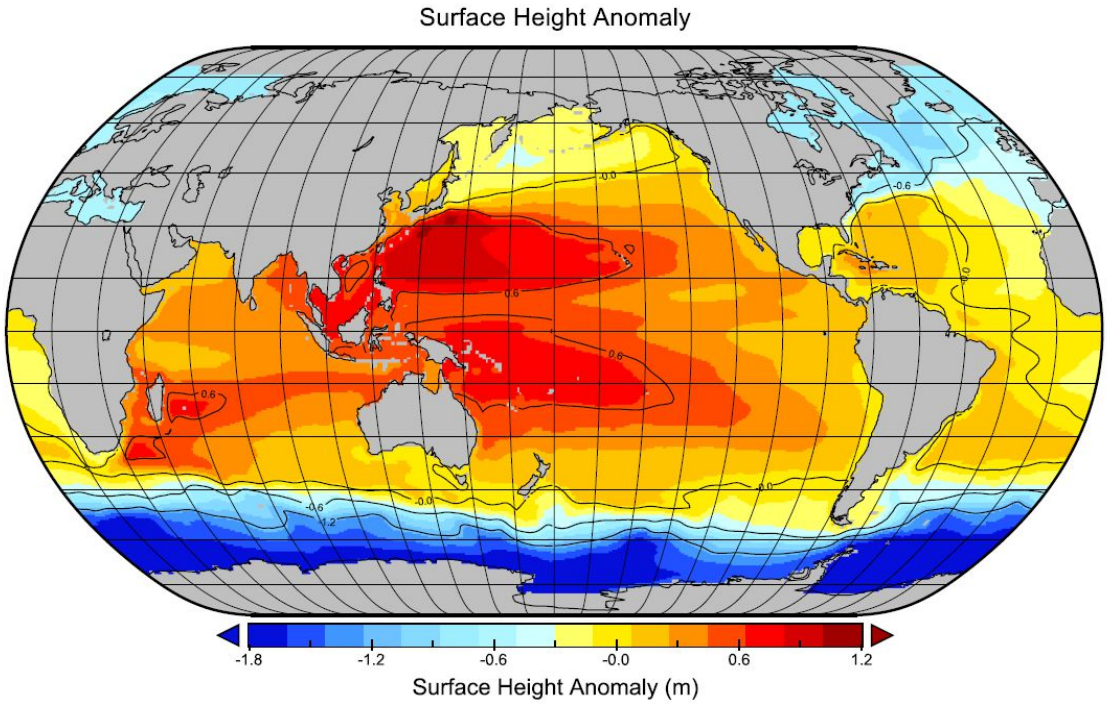

Figure 2.16 Sea surface height above geoid (m) 2004-2006 mean from 2004-06 Ocean Atlas (Forget, 2010; http://www.ecco-group.org/products.htm).

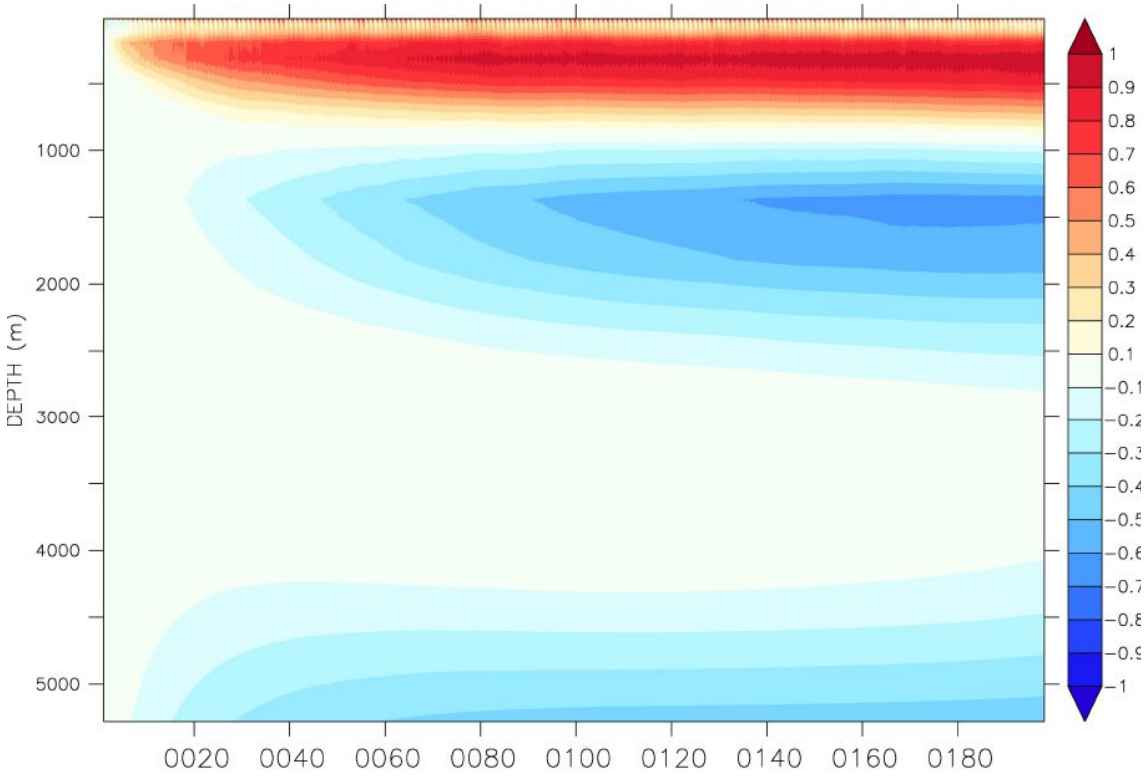

Figure 2.17. Time series of global drift in monthly mean temperature (^{o}C) on level surfaces over 200 years relative to the first year of the simulation.

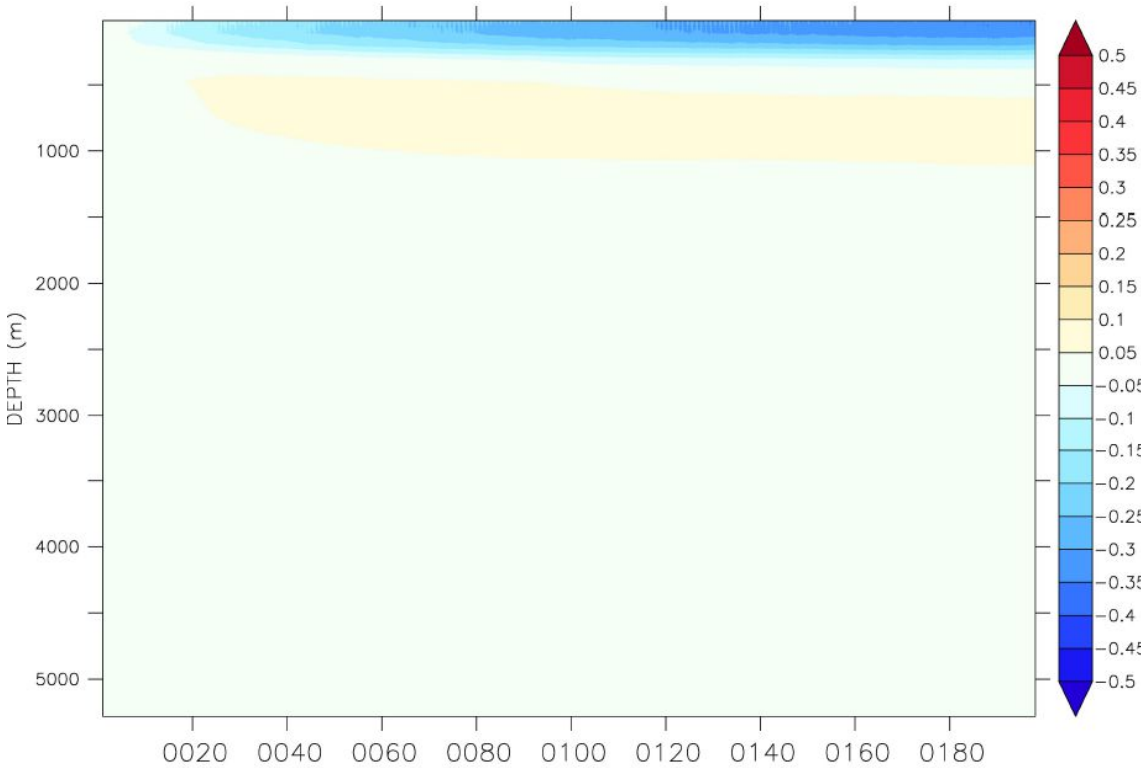

Figure 2.18. Time series of global drift in monthly mean salinity (psu) on level surfaces over 200 years relative to the first year of the simulation.

The global temperature and salinity drifts in the first two centuries of FORTE are shown in Figures 2.17 and 2.18. A warming occurs in the upper 700 m which stablises over the second century. The ocean bottom waters cool slowly over time, but again appear relatively stable during the second century. The corresponding salinity drifts indicate a slow freshening in the upper 250 m of the ocean over time, which is occurring mainly in the North Pacific and Arctic (Figure 2.14).

Key to simulating a realistic North Atlantic climate is a model's ability to simulate a realistic meridional overturning circulation. Figure 2.19 shows the mean Atlantic meridional overturning streamfunction from FORTE taken after the 100 year spinup.

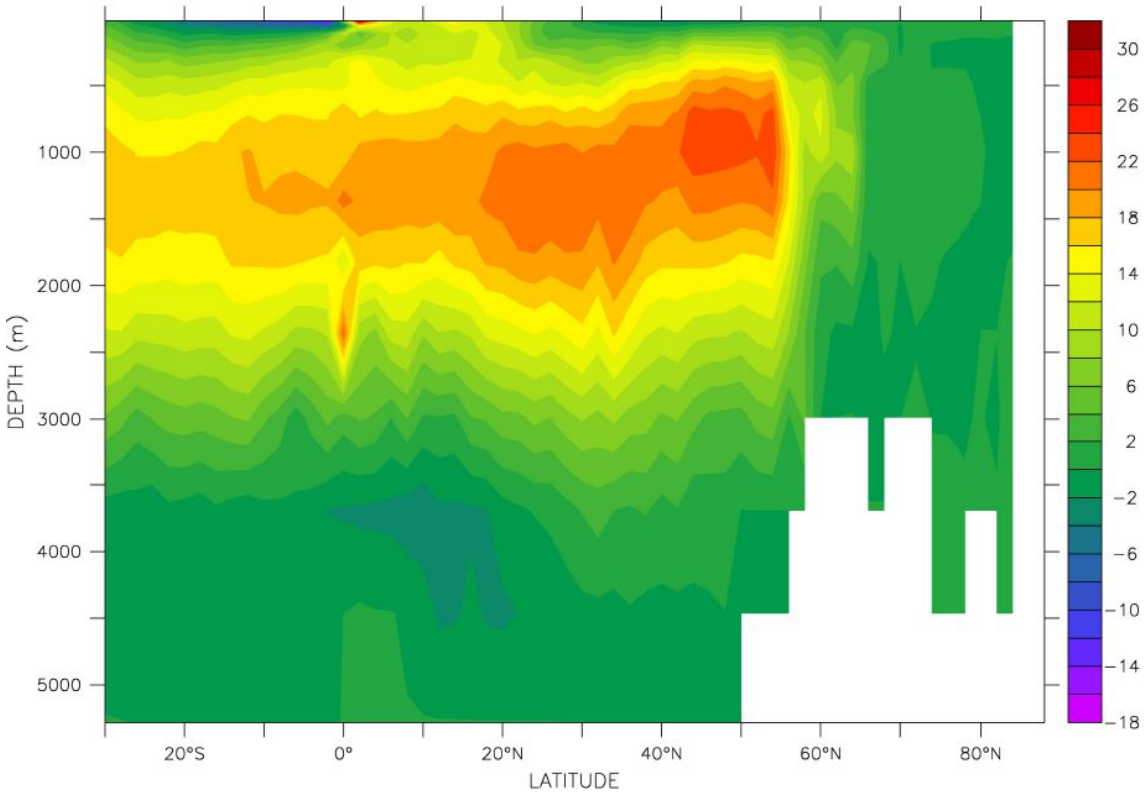

Figure 2.19 The mean Atlantic Meridional Overturning streamfunction (Sv) from FORTE control run after 100 year spinup.

The overturning circulation can be seen with an upper current flowing northward from the Equator to 55^{o}N between the surface and 1000 m with a maximum flow of 22 Sv. Between 1000 m and 4000 m there is a southward flow representing the model analogue of North Atlantic Deep Water (NADW). Beneath this water at 4000 m to 5000 m is the lower limb of the Antarctic Bottom Water (AABW) cell flowing northward with a strength of 2 Sv. An instability

can be seen on the equatorial thermohaline circulation. This effect was identified by Weaver and Sarachil (1990) in the Bryan-Cox GCM and is attributed to the model resolution producing an artifical cell at the equator. The temporal evolution of the Atlantic Meridional Overturning Circulation (AMOC) during the spinup phase and during the main experiment is illustrated with the maximum AMOC at 30^{o}N in Figure 2.20 After the initial spinup period the AMOC stabilises at about 28 Sv for the first 100 years and then shows a slow decline in the second 100 year period from 26 Sv to 17 Sv. This is most likely as a result of a fresh water anomaly originating in the Arctic which extends down into the Nordic Seas. Once it reaches the sills it causes a slowing of the AMOC.

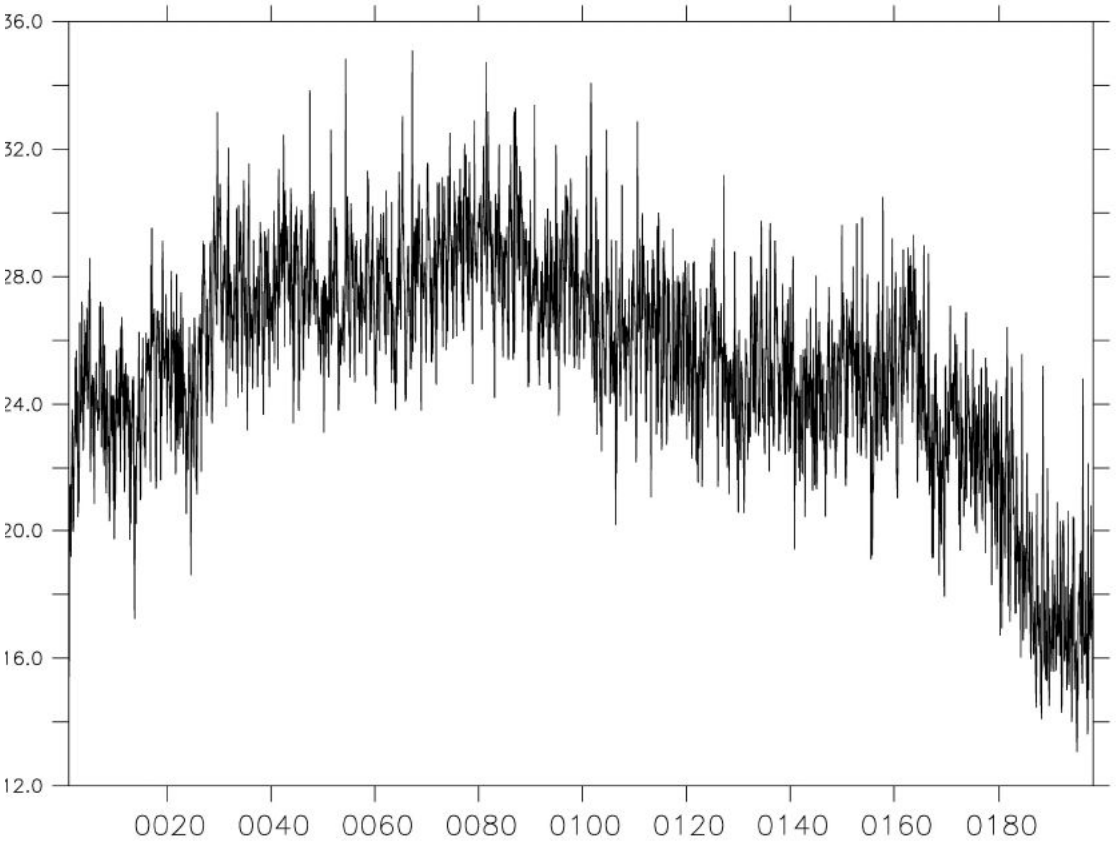

Figure 2.20. The Atlantic Meridional Overturning Circulation (Sv) at 30^{o}N from FORTE control run over 200 years.

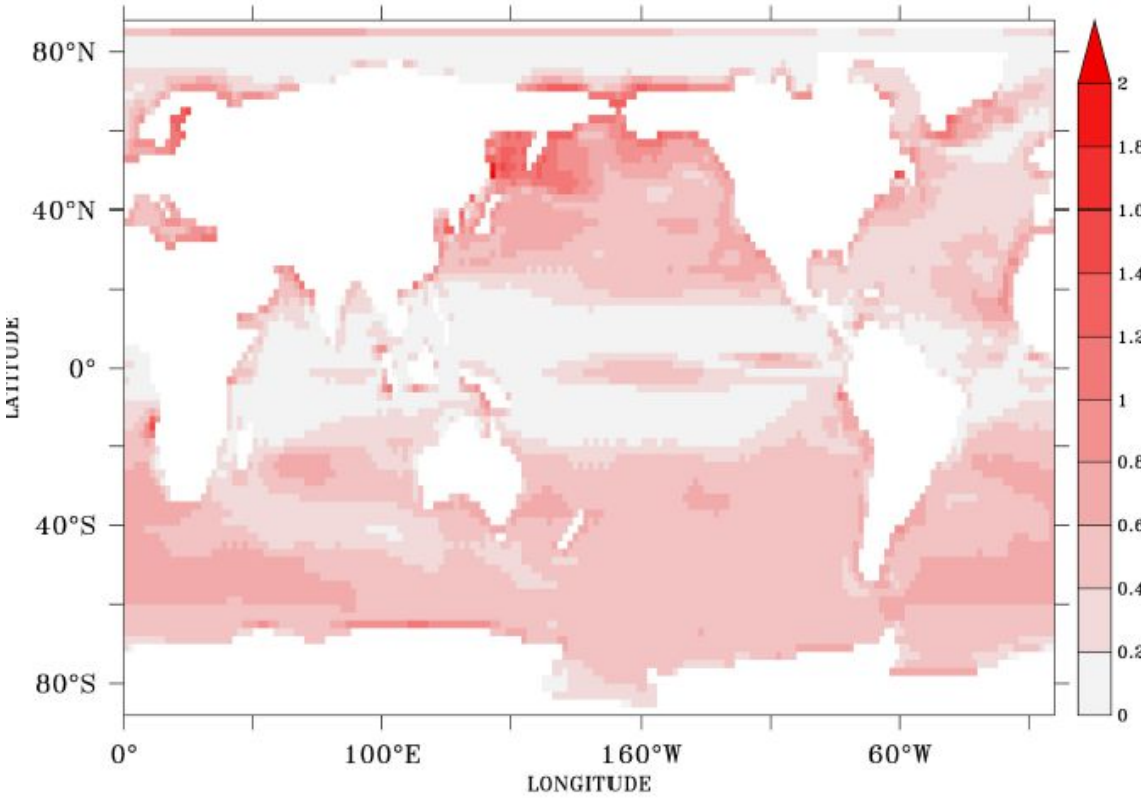

Figure 2.21. Standard deviation in SST anomalies taken from FORTE control simulation over first 100 years.

Finally, the standard deviation of SST anomalies in the FORTE control run were examined and compared with those found in HadISST observations (Figure 2.5 and 2.21). In the North Atlantic the Gulf Stream region shows high standard deviation in both FORTE and HadISST data although FORTE has less variability than HadISST. It is pleasing to see that the variability in this region is not strongly affected by the warm biases around Newfoundland and the Labrador Sea. The most striking difference between FORTE and HadISST is found over the equatorial region where FORTE clearly underestimates the SST variability in the Pacific, Indian and Atlantic Oceans. This is most pronounced over the equatorial Pacific where the tongue of higher variability seen in HadISST is barely visible suggesting that ENSO is weaker in FORTE than observed. In contrast, the SST variability is higher in FORTE in the Northeast Pacific, especially around Kamchatka. The asymmetry in terms of SST variability between the Northern and Southern Hemispheres (i.e. larger SST variability in the Northern Hemisphere than in the Southern Hemisphere), which was described for HadISST earlier is not seen as strongly, and FORTE overestimates SST variability over most parts of the Southern Ocean. It is worth noting though that despite marked differences from observations the FORTE model is not worse at simulating SST variability than many models of the CMIP5 ensemble that was introduced earlier and which will be used in Chapter 4.

Overall the results obtained from the FORTE simulation compare favourably with CMIP5 class models, such as those reported for HadCM3 and HadGEM1 by Johns *et al*. (2006), Davini and Cagnazzo (2014) and Perez *et al*. (2014).

Chapter 3: Re-emergence of North Atlantic temperature anomalies and the impact on North Atlantic winter weather in observations

3.1 Introduction

Re-emergence of ocean temperature anomalies in the North Atlantic from one winter to the next provides memory to the climate system with implications for the variability and predictability of the atmospheric circulation over the North Atlantic region. In this thesis sea level pressure (SLP) and Sea-Surface Temperature (SST) fields are taken from either observation based datasets (20th Century Reanalysis; HadISST) and in Chapter 4 from Global Circulation Model simulations from the fifth phase of the Coupled Model Intercomparison Project (CMIP5) to study links between re-emergence and the atmospheric circulation.

As explained in Chapter 1 re-emergence is the process whereby ocean temperature anomalies established in a deep winter mixed layer are sequestered beneath the seasonal thermocline in summer and reappear at the surface as the mixed layer deepens during the onset of the following winter season. The re-emergence mechanism (Alexander and Deser, 1995) can enhance the persistence of winter Sea Surface Temperature (SST) anomalies from one winter to the next. The impact of re-emergence in the North Atlantic upon the climate system has been investigated by Cassou *et al*. (2007) using the NCAR Community Atmosphere Model. They concluded that the atmospheric response to reemerging SST anomalies resembled the atmospheric circulation that created them the previous winter but with reduced amplitude. Re-emergence was important in the re-establishment of the North Atlantic SST anomaly tripole pattern between the winters of 2009/10 and 2010/11 (Taws *et al*., 2011) and between the winters of 1968/69 and 1969/70 (Blaker *et al*., 2015). The anomaly pattern is characterised by a tripole of warm anomalies in the Labrador Sea region, cold anomalies that extend across the North Atlantic from 25 to 50^{o}N and warm anomalies south of 25^{o}N (Figure 3.1).

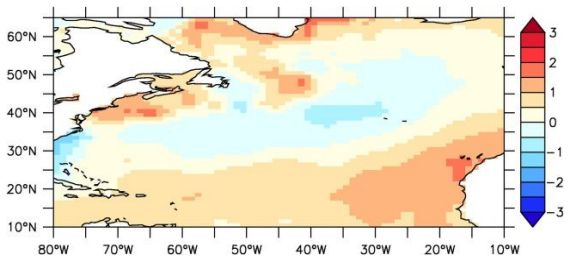

Figure 3.1. An example of the winter mean SST anomaly pattern over the North Atlantic taken from HadISST for December 2009 to March 2010 by removing the 1871-2011 climatological winter mean.

The SST anomaly pattern in the first of a pair of consecutive winters with similar SST anomalies can provide memory to the atmosphere (Buchan *et al*., 2014) and the presence of a persistent winter monthly (DJF) mean negative NAO state during the first winter seems to be key to the occurrence of reemergent SST anomalies in the following winter (Cassou *et al*, 2007; Blaker *et al*., 2015). Kushnir *et al*. (2006) noted that the thermal memory of the ocean mixed layer could be responsible for the persistence of the NAO beyond the time scales of atmospheric dissipation. This implies a two-way interaction between the atmosphere and the ocean, which could contribute to interseasonal or interannual predictability and the contribution of re-emergence to the persistence of atmospheric conditions from one winter to the next.

Northern Europe has experienced severe winter weather events over the last century. Most recently in the winters of 2009/10 and 2010/11 extremely cold temperatures were experienced over northern and central Europe (Cohen *et al*., 2010, Li *et al*., 2015). Studies based on observational data have identified that when extremely cold winters occur in consecutive years the atmospheric conditions correspond to a strongly negative phase of the Arctic Oscillation during the first winter of the pair (Blaker *et al*., 2015). During the winter of 2009/10 the North Atlantic Oscillation (NAO) and Arctic Oscillation (AO) indices reached some of the most negative values recorded and there is evidence that re-emergence of North Atlantic SST anomalies (Taws *et al*., 2011) contributed to the renewal of negative NAO conditions in late 2010 (Buchan *et al*., 2014). These events have also been linked to an observed reduction of the Atlantic meridional overturning circulation by the RAPID 26^{o}N array, which showed a pronounced minimum in northward transport over the winter of 2009/10, followed by a second minimum in the winter of 2010/11 (McCarthy *et al*, 2012; Sonnewald *et al*., 2013, Smeed *et al*., 2013; Bryden *et al*., 2014; Blaker *et al*., 2015).

The North Atlantic Oscillation is one of the principal modes of atmospheric variability in the North Atlantic (Hurrell and Deser, 2009). Introduced in Chapter 1 the NAO describes the distribution of atmospheric mass between the Arctic and the subtropical Atlantic, which produces large changes in surface air temperatures, storm-track position, and precipitation over the North Atlantic and Western Europe. The phases of the NAO are categorized by the variability in sea level pressure (SLP) over the Northern Hemisphere. In this chapter, the NAO index is computed using empirical orthogonal functions (EOF) of SLP over the North Atlantic sector. When the NAO index is negative, the SLP anomalies are high over Iceland and low over the Azores, resulting in a southward shift in the Jet Stream leading to colder North European winters.

The relationship between fluctuations in North Atlantic SSTs and the strength of the NAO has long been recognised (Bjerknes 1964). In a study on the low-frequency variability of the surface

climate over the North Atlantic during winter using 90 years of weather observations, Deser and Blackmon (1993) identified that an important mode of wintertime climate over the North Atlantic was characterised by a dipole pattern of SSTs and surface air temperatures (SAT). Czaja and Frankignoul (2002) investigated the covariability between monthly SSTs and SLP anomalies in the Atlantic as a function of time. They concluded that in Atlantic SST patterns could precede the winter NAO by up to 6 months. The link between the Atlantic Ocean and the atmospheric circulation was further explored in recent studies (e.g. Gastineau and Frankignoul, 2015; Gastineau *et al*, 2016) and it is clear that the issue of if and how the North Atlantic Ocean influences the atmospheric circulation is still ongoing (e.g. Yamamoto and Palter, 2016).

In this chapter the pattern of occurrences of re-emergence and positive and negative NAO events over the last 140 years (1871-2011) from historical observations will be examined and in Chapter 4 compared with CMIP5 historical ensemble model output (1850-2005). In the remainder of this chapter the methodology introduced in Chapter 2 will be applied to HadISST and 20CR with the main aims to (i) identify how frequently re-emergence events are likely to have occurred in the North Atlantic since 1871 and (ii) to establish whether there is a statistically significant link between the occurrence of re-emergence and atmospheric circulation patterns, in particular the NAO. The main goal under (ii) is to understand if the ocean is always preconditioned in a similar way by the atmosphere i.e. does re-emergence in the North Atlantic always follows a winter with negative NAO conditions (as in the event documented in Taws *et al*. 2011) or can both positive and negative NAO winters be conducive to the occurrence of oceanic re-emergence?

3.2 Results from historical records

Lagged pattern correlations referenced to March (March to April of the following year) of SST anomalies for the North Atlantic computed from HadISST data according to equation 2.1 allows identification of years when re-emergence is likely to have occurred (Figure 3.2). Over the period 1870-2011, there have been 11 winters when the maximum re-emergence correlation coefficient exceeds 0.5 and the ratio between the summer mean and winter mean correlation coefficients is less than 0.7. There were 6 events where a winter to winter correlation of more than 0.5 is found (Figure 3.2) which are excluded based on the summer criterion. This suggests that persistence of SSTs anomaly patterns throughout the year is not uncommon. The selection of the winter maximum and summer ratio criteria is discussed in more detail in section 3.3. The method clearly identifies the re-emergence events that have been described in the literature before. The most prominent example is the recent event in the winter of 2009/2010 which was described in Taws *et al*. 2011 but also the event in 1969 (Blaker *et al* 2015; Taws *et al*. 2011)

clearly stands out. With an additional 9 events identified here this initial result suggests that re-emergence is a regular occurrence.

The main aim of this thesis is to explore whether ocean conditions and SST anomalies in particular can influence the atmospheric circulation or whether ocean anomalies are just a passive response to atmospheric forcing with little or no feedback onto the atmosphere. In a first step to understand the ocean-atmosphere links the 11 re-emergence events are examined to establish the NAO state in the preceding winter to illustrate if the ocean tends to be preconditioned in a similar manner in all events. Over the period 1870-2011 there are 65 years with negative winter mean NAO and 76 with a positive winter mean NAO. There is an approximately even distribution with 6 re-emergence events preceded by an NAO- and 5 events preceded by a NAO+ (Figure 3.2). This suggests that there is no bias for re-emergence events to be preceded by a negative NAO, contrary to what might be expected since previous studies have so far only identified re-emergence events associated with negative NAO (Taws *et al*., 2011; Blaker *et al*., 2015).

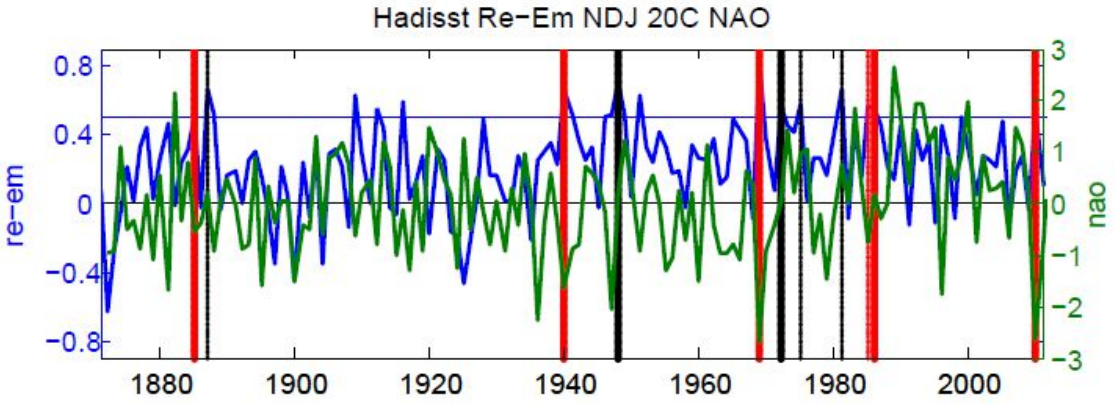

Figure 3.2. Time series of maximum winter (NDJ) re-emergence correlation coefficient from HadISST data (1871-2011, blue), the horizontal blue line indicates the 0.5 coefficient criteria and time series of winter mean (DJFM) NAO based on the leading empirical orthogonal function from 20CR data (1871-2011, green). The years when re-emergence is preceded by a negative NAO are shown in red, the bold lines indicate negative NAO reoccurrence, and years when re-emergence is preceded by a positive NAO are shown in black, the bold lines indicate positive NAO reoccurrence.

The re-emergence events preceded by either negative or positive NAO winters are now discussed separately in more detail. Figures 3.3a and 3.3b show time series of the North Atlantic SST anomaly pattern correlation coefficient during re-emergence events from the preceding to the following month of March.

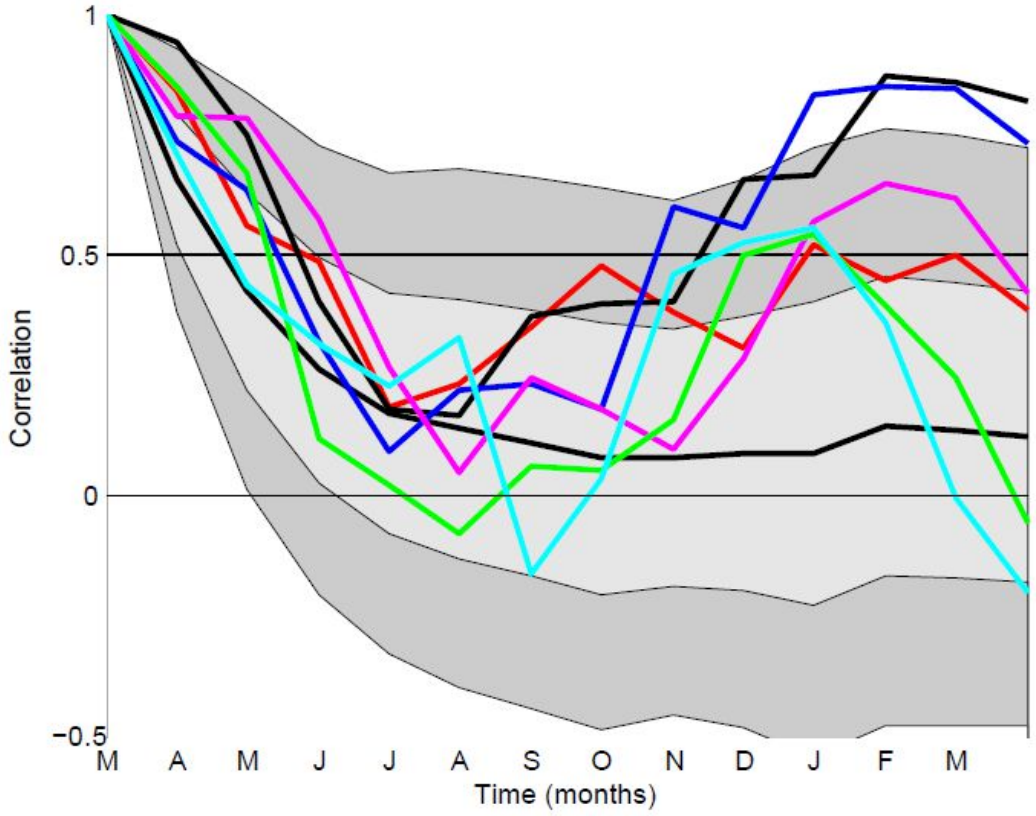

Figure 3.3a. One-year pattern correlations for North Atlantic SST anomalies (10-60°N, 80-10°W) for re-emergence events preceded by negative NAO winters. Values obtained from HadISST from March 1885 - March1886 (magenta), March 1940 - March 1941 (black), March 1969 - March 1970 (blue), March 1985 - March 1986 (red), March 1986 - March 1987 (cyan), March 2010 - March 2011 (green), and 141-year (1871-2011) average (black). The light grey shading denotes the standard deviation range, and the dark grey two standard deviation range.

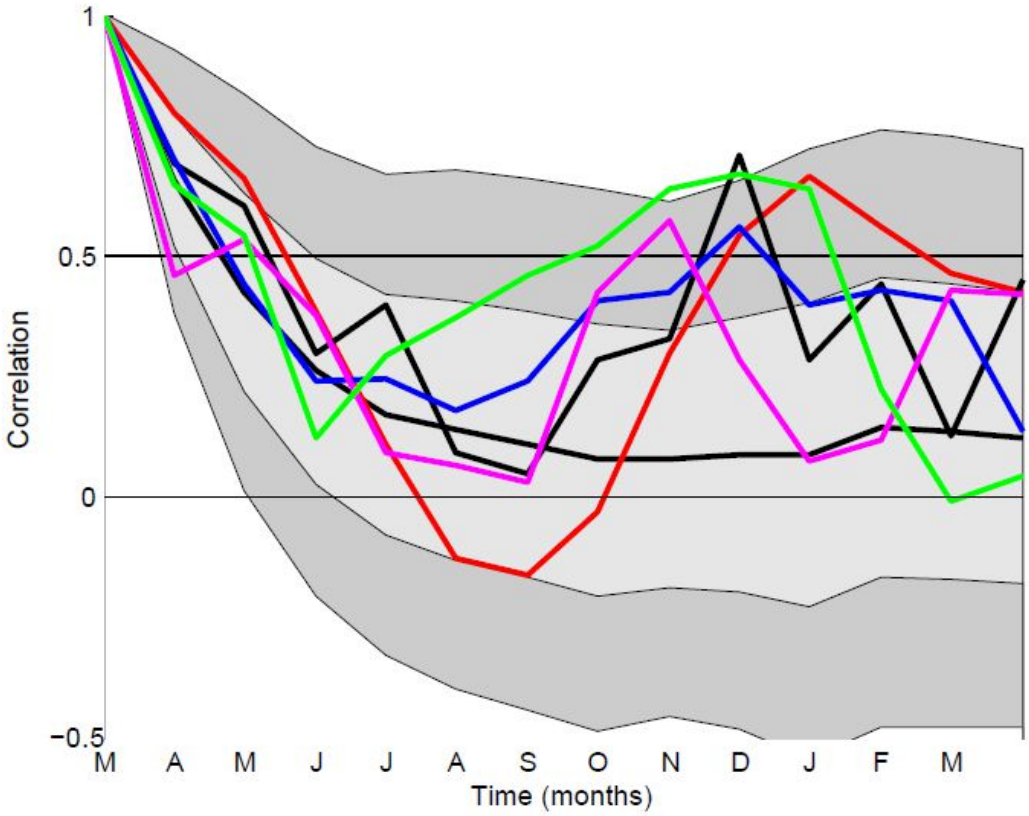

Figure 3.3b. One-year pattern correlations for North Atlantic SST anomalies (10-60°N, 80-10°W) for re-emergence events preceded by positive NAO winters. Values obtained from HadISST data from March 1887 - March 1888 (red), March 1948 - March 1949 (black), March 1972 - March 1973 (blue), March 1975 - March 1976 (magenta), March 1981 - March 1982 (green) and 141-year (1871-2011) average (black). The light grey shading denotes the standard deviation range, and the dark grey two standard deviation range.

The 6 cases preceded by a negative NAO occurred during the winters of 1884/85, 1939/40, 1968/69, 1984/85, 1985/86 and 2009/10. The winters of 1940/41 and 1969/70 have a pronounced re-emergence with the maximum winter correlation exceeding 2 standard deviations from the mean whereas the winters of 1885/86, 1985/86, 1986/87 and 2010/11 are less pronounced with the maximum correlation coefficient between 1 and 2 standard deviations (Figure 3.3a). These results differ slightly from Taws *et al*. (2011) and Blaker *et al*. (2015) who used SST data from EN3_v2a SST. Whereas 1968/1969 and 2009/2010 were also seen in Taws *et al*. (2011) and Blaker *et al*. (2015) they did not identify the winters of 1985/86 and 1986/87, suggesting that there may be some sensitivity in the results to the choice of observational dataset. A negative NAO state reoccurs in the following winter in all these years. The events have not occurred at regular intervals, after 1884 there was a 55 year gap until 1939, a 29 year gap until 1968 and after 1985 a 24 year gap until 2009.

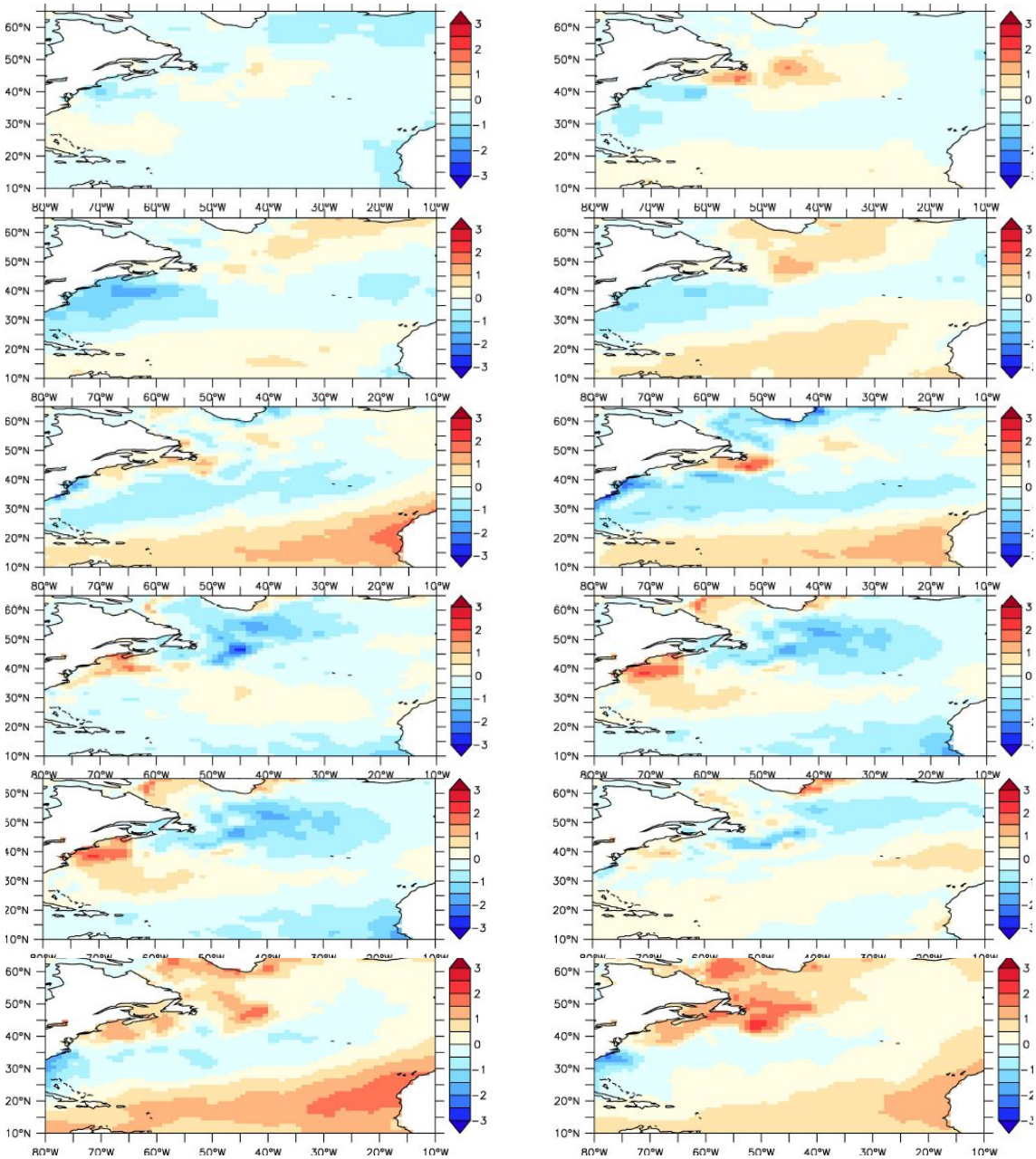

Figure 3.4a. Winter mean North Atlantic SST anomalies from HadISST for years with re-emergence and negative NAO (from top to bottom) 1884/85 & 1885/86, 1939/40 & 1940/41, 1968/69 & 1969/70, 1984/85 & 1985/86, 1985/86 & 1986/87 and 2009/10 & 2010/11.

Pairs of spatial plots of the winter mean SST anomalies for each of the six events show that while the high correlation is indicative of re-emergence the tripole pattern differs from event to event (Figure 3.4a). The winters of 1884/85, 1939/40, 1968/69 and 2009/10 show the formation of a characteristic cold SST band from the US to Northern Europe whereas 1984/85 and 1985/86 show a cold anomaly formation further north in the subpolar North Atlantic with a positive anomaly towards the subtropical North Atlantic. The SST anomaly patterns for the

second winter show variations in the level of correlation but in each case the patterns from the first winter are broadly similar to the patterns seen for the second winter.

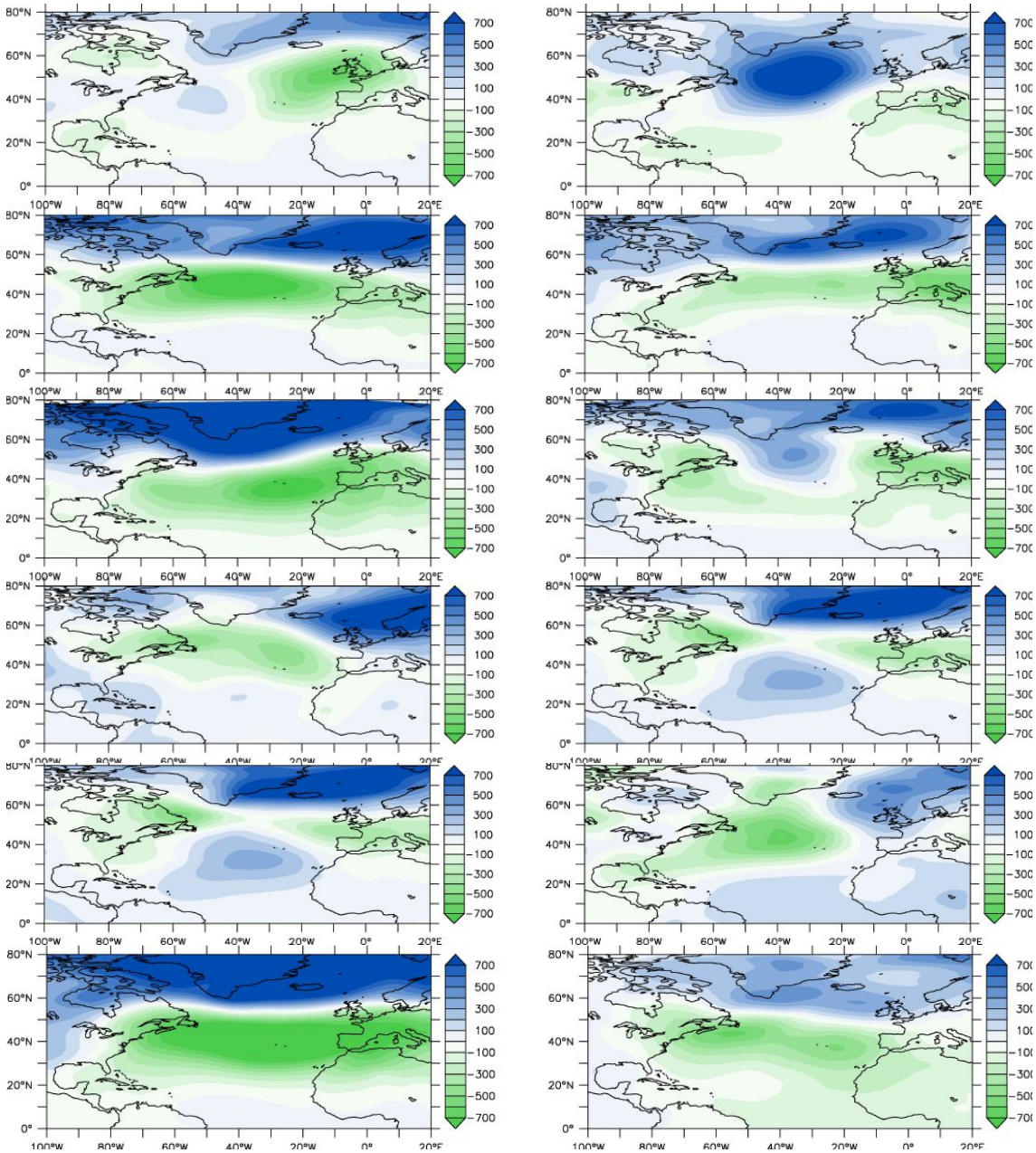

Figure 3.5a. Winter mean SLP anomalies from 20CR for years with re-emergence and negative NAO, (from top to bottom) 1884/85 & 1885/86, 1939/40 & 1940/41, 1968/69 & 1969/70, 1984/85 & 1985/86, 1985/86 & 1986/87 and 2009/10 & 2010/11.

The SLP spatial patterns for these winters show the characteristic features of a negative NAO during the first winter (Figure 3.5a). This feature weakens, but persists during the second winters in 1940/41 and 2010/11. In 1969/70 an anticyclonic circulation anomaly forms over the

North Atlantic. The winters of 1984/85 and 1986/87 show a less pronounced negative NAO pattern and in 1885/86 an anticyclonic anomaly forms over the North Atlantic.

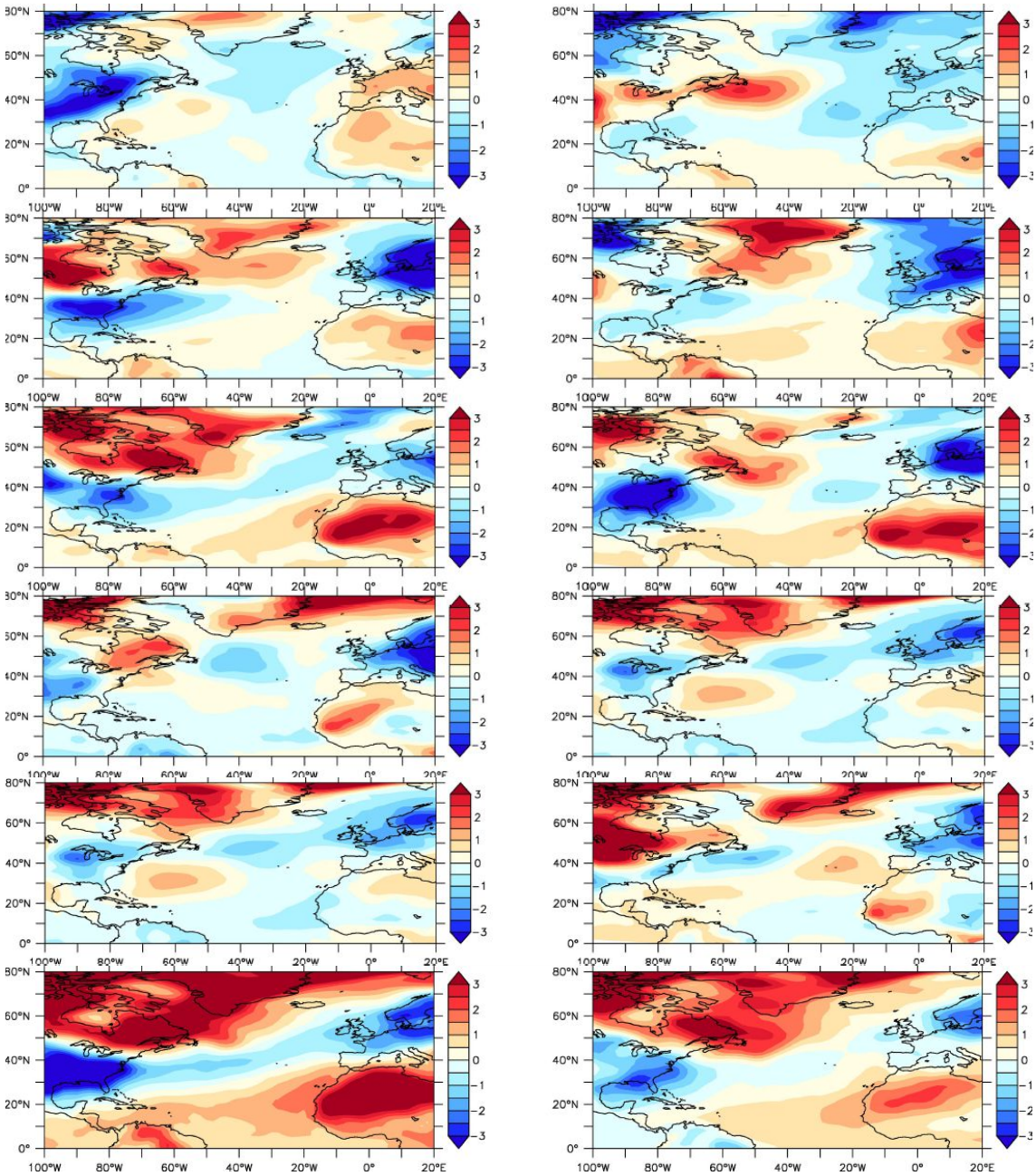

Figure 3.6a. Winter mean SAT anomalies from 20CR for years with re-emergence and negative NAO, (from top to bottom) 1884/85 & 1885/86, 1939/40 & 1940/41, 1968/69 & 1969/70, 1984/85 & 1985/86, 1985/86 & 1986/87 and 2009/10 & 2010/11.

SAT anomalies for 1939/40, 1968/69, 1984/85 and 2009/10 (Figure 3.6a) reveal a widespread cooling anomaly across North West Europe in the first winter, particularly intense in the winter of 1939/40. All these years reveal the characteristic temperature anomalies expected for negative NAO winters with the cold anomalies over Europe coinciding with warm anomalies

over the Labrador region, Canada and the Northern United States. Coversely warm anomalies are present over northern and western regions of Africa and cold anomalies over southern and eastern regions of the U.S. The cold band of temperatures described above for the SST anomalies, which is observed for several events, is clearly reflected in atmospheric temperatures particularly for 1940/41 and 2009/10. For these two events it also becomes clear that there was one coherent band of negative temperature anomalies encompassing much of the US and extending across the Atlantic from southwest to northeast and into Europe. The year to year persistence of this pattern across the entire North Atlantic region is quite remarkable for these events. The winter of 1884/85 is the only case when a warm anomaly occurred over most of Europe with the exception of Scandinavia where a cold SAT anomaly is found. Whereas the temperature anomalies associated with the first winters of the events show a tendency to persist in the following winter this is clearly not the case for 1884/85. For this event the SAT anomaly patterns are almost reversed between the first and the second winter: the warm anomaly over Europe coincided with a cold anomaly over North America in 1884 whereas the opposite is true for the winter of 1885.

Next, the SST and atmospheric patterns coinciding with the 5 re-emergence events that are preceded by positive NAO winters are examined. These occurred in 1887/88, 1948/49, 1972/73, 1975/76, and 1981/82. Whereas the 6 events preceded by a negative NAO are separated by 25 years or more there is a clustering with 3 out of the 5 re-emergence events preceded by positive NAO winters occurring during the comparatively short period from the early 1970s to the mid 1980s (Figure 3.2). For most of the 5 events the NAO index is only slightly positive (in contrast to the strongly NAO negative winters for the events discussed above). A positive NAO state reoccurs in the following winter in four out of five cases: 1948/49, 1972/73, 1975/76 and 1981/82. Events proceeded by positive NAO consistently show re-emergence occurring earlier in the following winter, reaching maximum correlation in November or December (Figure 3.3b). Pattern correlations for re-emergence events preceded by positive NAO conditions fall within 1 standard deviation by late winter, perhaps indicating that atmospheric conditions during the second winter are not strongly influenced by the re-emergence. The associated SST anomaly patterns show different locations of cold and warm anomalies than those found in the NAO negative winters. It is noticeable that the SST anomaly patterns preceding re-emergence are typically not just the inverse of the patterns described earlier for NAO-. The winters of 1971/72 and 1974/75 have extensive cold anomalies over the North Atlantic with the cold anomalies being most pronounced north of about 40°N. All these winters coincided with warm SST anomalies off the US coast which extend across the Atlantic towards Europe in 1974/1975. For the winters of 1886/87, 1947/48 and 1980/81 the SST anomalies are weaker with varying spatial patterns (Figure 3.4b). To some extent the SST anomaly patterns of the first winters

reemerge during the second winter. However, there is less agreement between the SST anomalies in the first and second winters of the re-emergence events when compared with the NAO- cases. This is because in most NAO+ cases the highest winter to winter correlation typically occurs at the beginning of the second winter before tailing off in the later winter months (see Figure 3.3b). It is therefore expected that the agreement between the DJF SST anomalies between the first and second winters is not very good (in contrast to the NAO- cases where correlations during the second winter remain higher throughout the winter months as seen in Figure 3.3a).

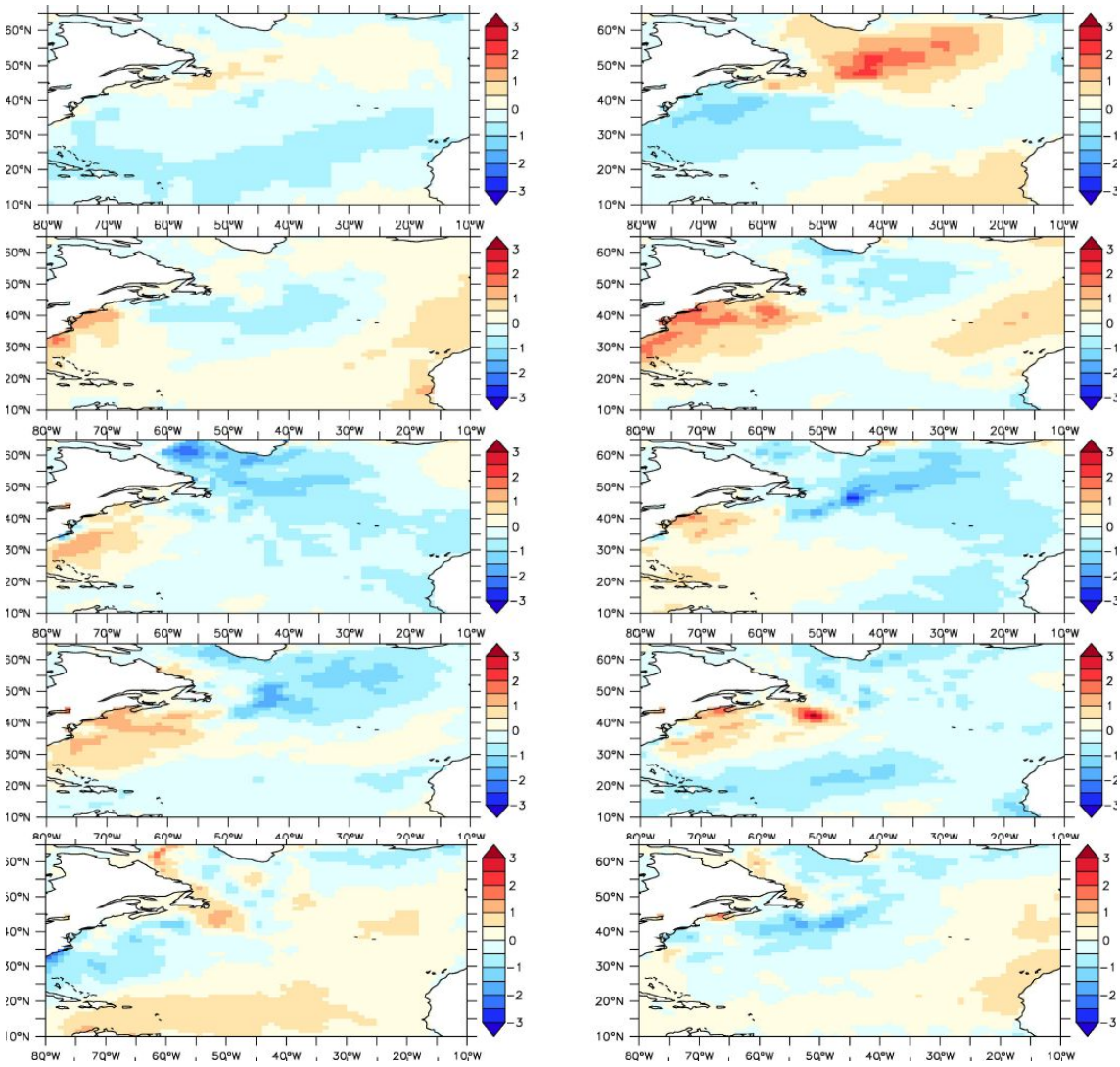

Figure 3.4b. Winter mean North Atlantic SST anomalies from HadISST for years with re-emergence and positive NAO (from top to bottom) 1886/87 & 1887/88, 1947/48 & 1948/49, 1971/72 & 1972/73, 1974/75 & 1975/76 and 1980/81 & 1981/82.

Despite the NAO index being positive for all the first winters there are a range of spatial patterns for the SLP anomalies (Figure 3.5b). None of these actually closely resemble the

"classical" SLP NAO anomaly pattern (see Figure 2.6). Most patterns do show slightly higher than average values for the Azores High and lower than average values for the Icelandic Low.

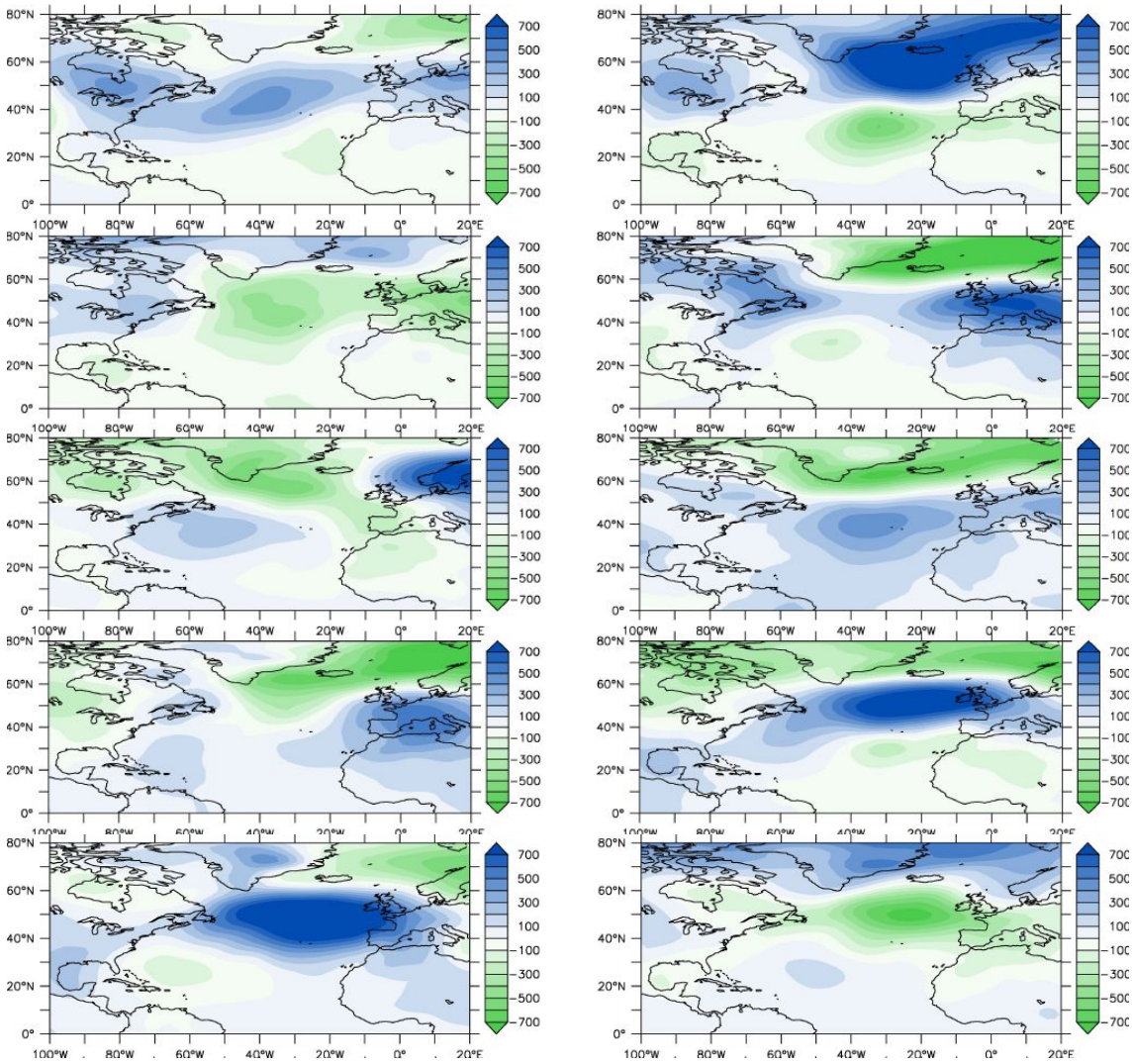

Figure 3.5b. Winter mean SLP anomalies from 20CR for years with re-emergence and positive NAO (from top to bottom) 1886/87 & 1887/88, 1947/48 & 1948/49, 1971/72 & 1972/73, 1974/75 & 1975/76, and 1980/81 & 1981/82.

However, the position of the SLP anomalies either appears to be offset zonally (1971/72) or meridionally (1980/81) or in the case of 1947/48 do not resemble NAO+ anomalies. Given the relatively weak signal found for the NAO+ winters preceding re-emergence this is perhaps not surprising as the DJF mean typically include months with different NAO states which will lead to some non-descript patterns for the seasonal average. Some clear NAO+ patterns are seen in the second winters. This is seen in 1887/88 and 1948/49 where the classical centres of action of the NAO can clearly be identified.

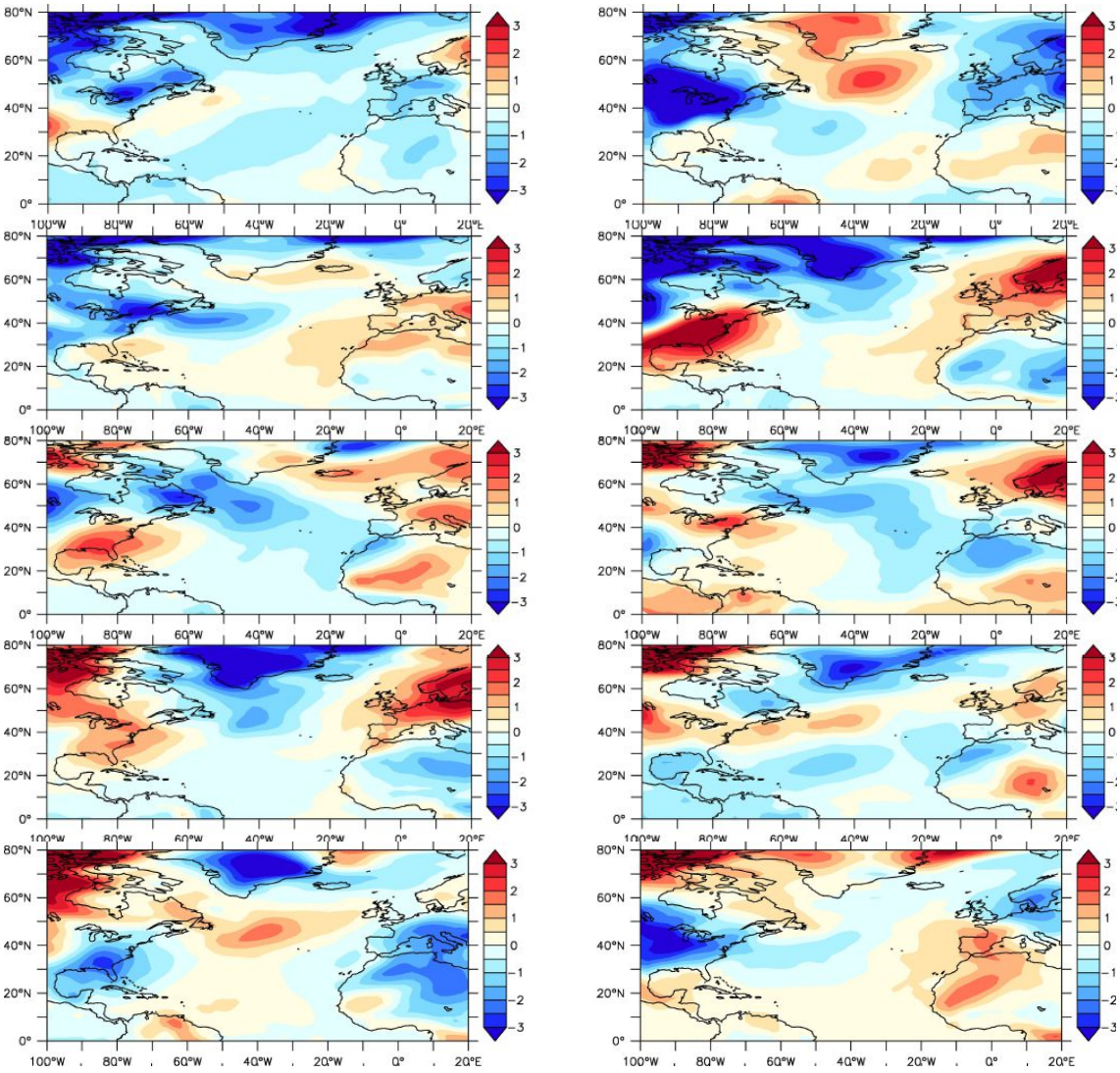

Figure 3.6b. Winter mean SAT anomalies from 20CR for years with re-emergence and positive NAO (from top to bottom) 1886/87 & 1887/88, 1947/48 & 1948/49, 1971/72 & 1972/73, 1974/75 & 1975/76 and 1980/81 & 1981/82.

As expected from the SLP patterns described before different SAT anomaly patterns coincide with the different winters (Figure 3.6b). For three of the winters (1947/48, 1971/72 and 1974/75) warm SAT anomalies are found over Western and North Western Europe which is the expected pattern for NAO+ winters. However, the two remaining winters are characterised by cold anomalies over Western Europe (1886/87 and 1980/81). Interestingly, the SAT anomaly patterns between the first and second winters look similar. The warm (cold) first winters over Europe are all followed by warm (cold) anomalies over most Europe during the second winters.

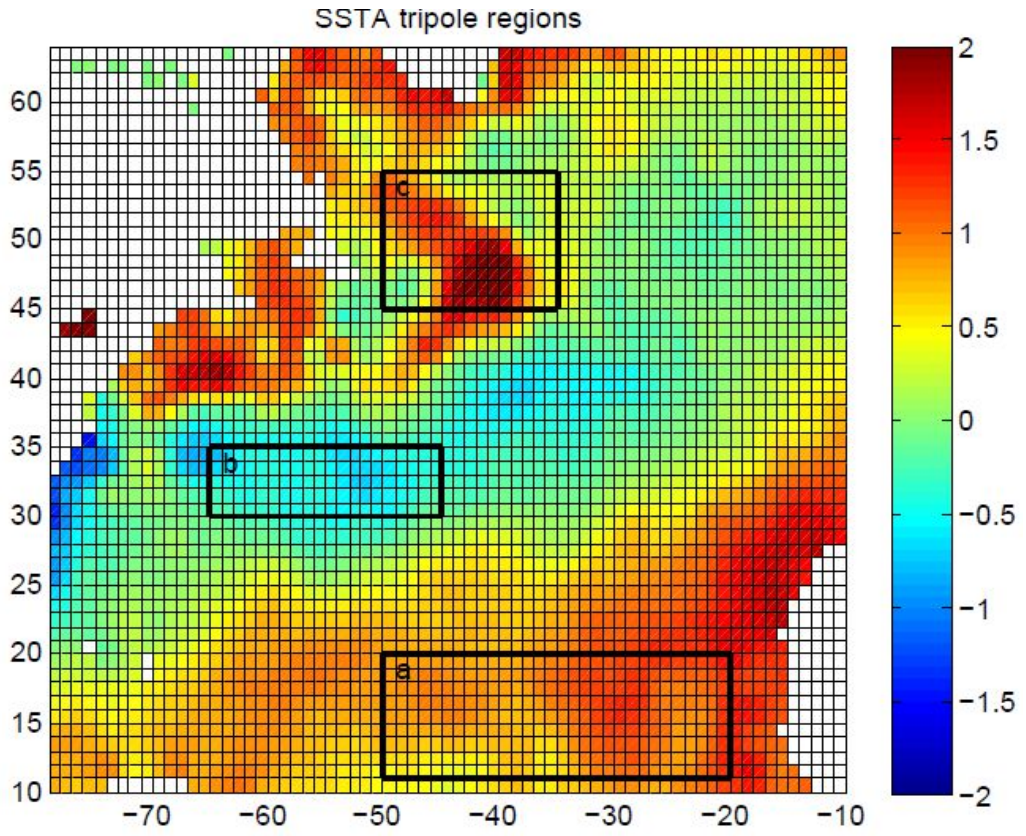

Figure 3.7. SSTA regions selected for tripole index, A (tropics) from 10°N to 20°N, 20°W to 50°W, B (subtropics) 30°N to 35°N, 45°W to 65°W and C (subpolar gyre) 45°N to 55°N, 35°W to 50°W. Example shown January 2010 in deg C.

The selection criteria based on SST correlations cannot rule out false indentification of reemergence events which motivates looking at an additional possible criterion. The relative influence of the SST anomaly patterns in the identified winter events can be further tested by using a simple tripole index. The strength of the tripole patterns were computed from an index.based on the average SSTA temperatures in boxes located over the subpolar gyre, the subtropics and the tropics. The sections were taken from the North Atlantic from 10°N to 20°N and 20°W to 50°W (A, tropics), 30°N to 35°N and 45°W to 65°W (B, subtropics) and 45°N to 55°N and 35°W to 50°W (C, subpolar gyre) shown in Figure 3.7.

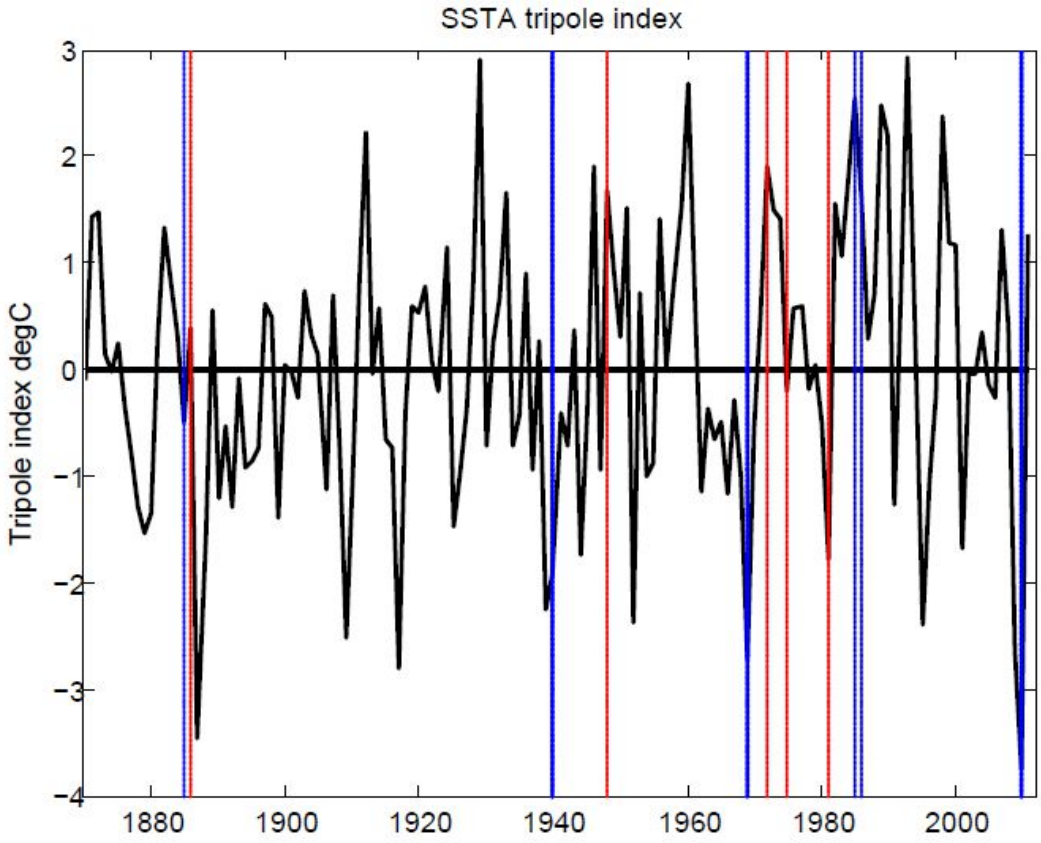

Figure 3.8 SSTA tripole index based on the mean differences in SST anomalies in sections from the North Atlantic from 10°N to 20°N, 20°W to 50°W (A), 30°N to 35°N, 45°W to 65°W (B) and 45°N to 55°N, 35°W to 50°W (C). Index is calculated from (B-A)+(B-C). NAO+ years in red and NAO- years in blue.

The index is calculated using the average temperature anomalies in the boxes A, B, and C. The differences between B and C and B and A are then summed. For NAO+ winters the index is expected to be positive and for NAO- winters negative. The results are shown in Figure 3.8. Taking the NAO- years only 1939/40, 1968/69 and 2009/10 show the expected negative index, 1984/85 and 1985/86 have positive indices. In the NAO+ years the results are less defined with 1947/48 and 1971/72 having positive indices and 1980/81 a negative index. The positioning of the selected regions was varied but found not to change the outcome of the test. Whilst the test is only indicative it does support the earlier comments from Figures 3a and 3b that only 1939/40, 1968/69 and 2009/10 show pronounced and consistent SSTA correlations. As will be shown later these three events all coincided with strongly NAO- conditions and the expected SSTA tripole during the first winter. Despite the NAO index being quite pronounced for some of the NAO+ events (e.g. 1974/1975) the SSTA pattern does generally not resemble a "classical" tripole pattern. However, the absence of a tripolar SSTA pattern does not mean that reemergence did not occur in the NAO+ events identified with the correlation criteria. Recent work strongly suggests that ocean reemergence can indeed also occur after NAO+ winters (Grist

et al. 2016). A further consideration in the use of reanalysis data from the nineteenth century is the scant availability of upper-air and of SST data. The reduced data density could compromise the ability to produce reliable upper-air reanalysis of these earlier periods (Compo *et al*., 2011). The conclusions reached for the earlier years in this study, 1884/85 and 1885/86, should therefore be treated with less confidence than those from the twentieth century. In the remainder of this thesis the events discussed will be those identified using only the summer and winter correlation criteria. Too many events would be discounted when including the tripole criterion described above and as said above there is a priori also no reason for re-emergence to occur only following the development of a clear SST tripole. Furthermore, it will be shown later that for reemergence events preceded by NAO+ the NAO index of the first winters is not very high and hence these winters are not expected to be characterised by a clear SST tripole.

Having identified a set of potential reemergence events and described the patterns of SST, SLP and SAT that coincided with re-emergence preceded by either NAO+ and NAO- winters an important question that remains is whether the link between the NAO state and the occurrence of re-emergence is systematic or if what has been described so far could equally be down to chance. In the following section statistical methods will be used to assess (i) whether the occurrence of positive and negative NAO winters during the first winter suggest that the NAO state can be used to predict the occurrence of re-emergence the following winter and (ii) whether there is a statistically significant influence of re-emergence on the atmospheric circulation (i.e. the state of the NAO) during the second winter. Over the period 1870-2011 there have been 65 years with negative winter mean NAO and 76 with a positive winter mean NAO. Since the 11 re-emergence events are approximately evenly distributed into 6 preceded by an NAO- and 5 preceded by a NAO+ there is no evidence to suggest that ocean re-emergence preferentially follows one atmospheric state over another. Apart from the probability for a positive or negative NAO sign for the winters preceding re-emergence it is instructive to quantify how pronounced the NAO actually was in the two cases. As was shown in Figure 3.2 and later in the description of the SST, SLP and SAT pattern the NAO index is more pronounced when re-emergence is preceded by a negative NAO. However, is the mean NAO value for winters preceding re-emergence significantly different from what one would expect by chance? To assess this a Monte-Carlo statistical method is applied. The mean winter NAO index coinciding with the 11 winters preceding the re-emergence events identified in HadISST is computed and compared to the average NAO with the distribution of the mean NAO index of 10,000 samples for the same number of winters (i.e. 11) taken at random with replacement from the 141 year time series. The results from the 20CR data for the 11 re-emergence events give a mean NAO index of -0.545 in the years preceding re-emergence and when compared to the distribution of the mean NAO index of 10,000 samples gives a probability of 0.04 (i.e. 96% of

the values in the distribution obtained through random sampling are higher than -0.545). This suggests that, despite there being more NAO positive than NAO negative cases; the preceding NAO states are on average significantly negatively shifted. Consistent with the results shown in Figures 3.4a to 3.6a this shows that a clearly defined NAO pattern is only found when re-emergence is preceded by NAO- winters. Table 3.1 lists the average NAO indices for each pair of winters when re-emergence occurred.

	1st winter				2nd winter			
	Dec	**Jan**	**Feb**	**DJF Mean**	**Dec**	**Jan**	**Feb**	**DJF Mean**
1884/85	2.1	-0.4	-1.8	-0.03	-1.3	0.3	-0.1	-0.37
1886/87	-0.2	1.7	1.1	0.87	-2.7	-1.5	-1.6	-1.93
1939/40	-1.7	-2.6	-2.1	-2.13	-0.1	-2.9	-0.9	-1.30
1947/48	-1.0	0.6	0.5	0.03	-0.5	0.9	1.9	0.77
1968/69	-1.4	-3.3	-3.2	-2.63	1.3	-2.9	1.1	-0.17
1971/72	0.8	0.4	0.6	0.60	1.7	0.5	2.3	1.50
1974/75	1.8	1.3	-0.6	0.83	-0.6	0.7	1.2	0.43
1980/81	1.5	1	1.2	1.23	-1.6	-1.3	1.7	-0.40
1984/85	1.5	-2.7	-1.5	-0.90	-1.2	2.4	-2.7	-0.50
1985/86	-1.2	2.4	-2.7	-0.50	1.9	-3.5	-0.7	-0.77
2009/10	-4.6	-1.9	-3.6	-3.37	-5.6	-1.3	1.9	-1.67

Table 3.1 December, January, February and winter mean NAO index for first and second winters when re-emergence events occurred.

The average winter NAO index for the 6 NAO- winters is -1.59 compared to an average of only 0.71 for the 5 positive NAO winters preceding re-emergence. Despite the positive NAO cases being less pronounced Figure 3.6b suggests similar temperature anomalies over Europe for the first and second winters of the 5 pairs of consecutive winters. For the three events when most of Europe was anomalously warm during the first winter (1947/48, 1971/72, 1974/75), warm anomalies occurred again in the following winters (1948/49, 1972/1973, 1975/76). The same is true for the events where most of Europe experienced colder than average conditions in the first winters (1886/87, 1980/81) and where cold anomalies occurred again in the second winter (1887/88, 1981/82).

The similarity of the anomalies found between consecutive winters raises the question whether the atmosphere responds consistently to re-emergence events (Buchan *et al*., 2014; Blaker *et al*., 2015) and in particular if it does so regardless of whether the NAO in the preceding winter is negative or positive. The results described so far suggest that this might be the case. However, is

the link between the identified re-emergence events and the NAO stronger than can be expected by chance? To investigate whether ocean re-emergence results in a statistically significant atmospheric response in the subsequent winter the Monte-Carlo method is used again, comparing the NAO average of the 12 winters making up the 6 pairs of winters where re-emergence coincides with a negative NAO in the preceding winter with the distribution of the mean NAO index from randomly selected 6 pairs of consecutive winters where the first winter is picked (with replacement) from the pool of 65 NAO negative winters. A mean NAO index of -1.194 is found with a probability of 0.01 when compared to the distribution obtained by randomly selecting 6 pairs of winters (with the first winter picked from the pool of NAO negative winters). This process is then repeated for the 5 pairs of winters where re-emergence coincides with a positive NAO in the preceding winter. The mean NAO index is compared with the distribution derived from 10,000 draws of randomly selected 5 pairs of consecutive winters where the first winter is picked (with replacement) from the pool of 76 NAO positive winters. The mean NAO index for the 5 observed pairs is 0.393 with a probability of 0.39 when compared to the randomly selected group (Figure 3.9).

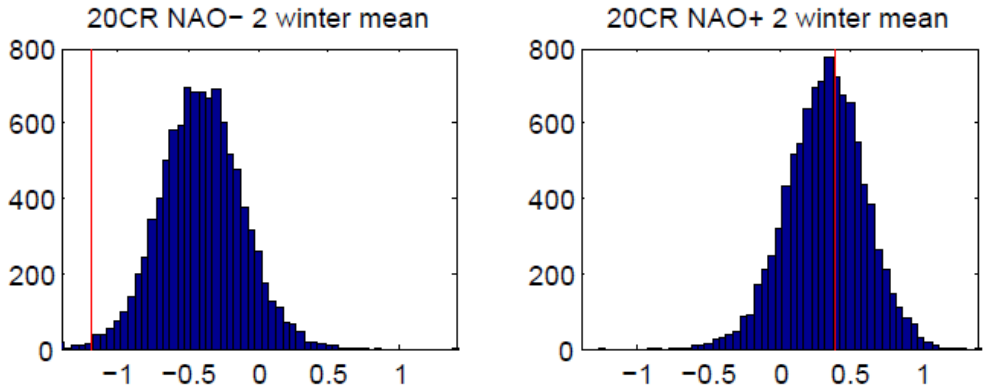

Figure 3.9. The mean winter NAO index averaged for the winter preceding re-emergence and the re-emergence years from 20CR data (red line) for NAO negative lead (left) and NAO positive lead (right) winters compared with the distribution of 10,000 random winter NAO index samples for NAO negative lead and NAO positive lead winters.

These tests reveal an asymmetry to the re-emergence events preceded by NAO+ and NAO- winters. Only strongly NAO negative winters appear conducive to re-emergence. However, our results show that of the 5 events where re-emergence is preceded by a positive NAO winter none were preceded by a strongly NAO positive winter. Instead, they were all preceded by a weakly NAO positive winter (Figure 3.2, Table 3.1). For the 6 events where the winter preceding re-emergence is NAO- the following winter is also NAO negative supporting the findings of earlier studies into the 2009/10 event and 1968/69 events (Taws *et al*. 2013, Buchan *et al*., 2014, Blaker *et al*., 2015). The mean value of the NAO index is -1.594 for the first winter

and -0.794 for the second winter. The probability of getting an average NAO value of -0.794 for 6 winters randomly selected out of 141 years is 0.09. This compares with the findings for the cases when re-emergence events are preceded by a positive winter NAO that have a mean value of the NAO index of 0.713 for the first winter and 0.073 for the second winter. The probability of getting an average NAO value of 0.073 for 5 winters randomly selected is 0.38. The statistical significance of the atmospheric response is significantly lower for re-emergence events preceded by negative NAO winters.

3.3 Robustness of re-emergence selection criteria

The identification of re-emergence events has been based on two criteria, the winter maximum and ratio of summer to winter correlations. The choice of threshold values for both criteria (0.5 and 0.7, respectively) is subjective and in this section a closer examination is made into the impact of these thresholds on the number of identified potential re-emergence events. As well as being used for actual data the same method will be employed on the CMIP5 data (Chapter 4) so the criteria need to be appropriate for these data as well. As has been described earlier (Chapter 2) the criteria selected need to identify when there is a significant correlation between SST anomalies from one winter to the next and that the winter to winter correlation reflects re-emergence rather than persistence in SSTA patterns. Thus both a winter maximum and summer minimum are required to identify years where re-emergence is likely to have occurred.

The suitability of the choice of thresholds for the winter and summer criteria for re-emergence systematically were systematically tested. This was done by varying the values for the two criteria over a wide range. The number of events obtained were then compared against the number of events expected to be found by chance. To achieve this the Monte Carlo method was used. The actual number of events obtained by a given choice of thresholds was compared against the nunber of events found in synthetic 141-year long time series of SSTA data which were generated by randomly selecting months (with replacement) from the actual SST anomalies. For example, January was randomly selected from the 141 available Januaries, February from the 141 available Februaries, and so on until a 141 year long time series was created. Pattern correlations were then computed using the synthetic data in the same manner as presented for the actual SST anomaly time series. A comparison between the correlations found for the actual data and an example of randomly generated data is shown in Figure 3.10.

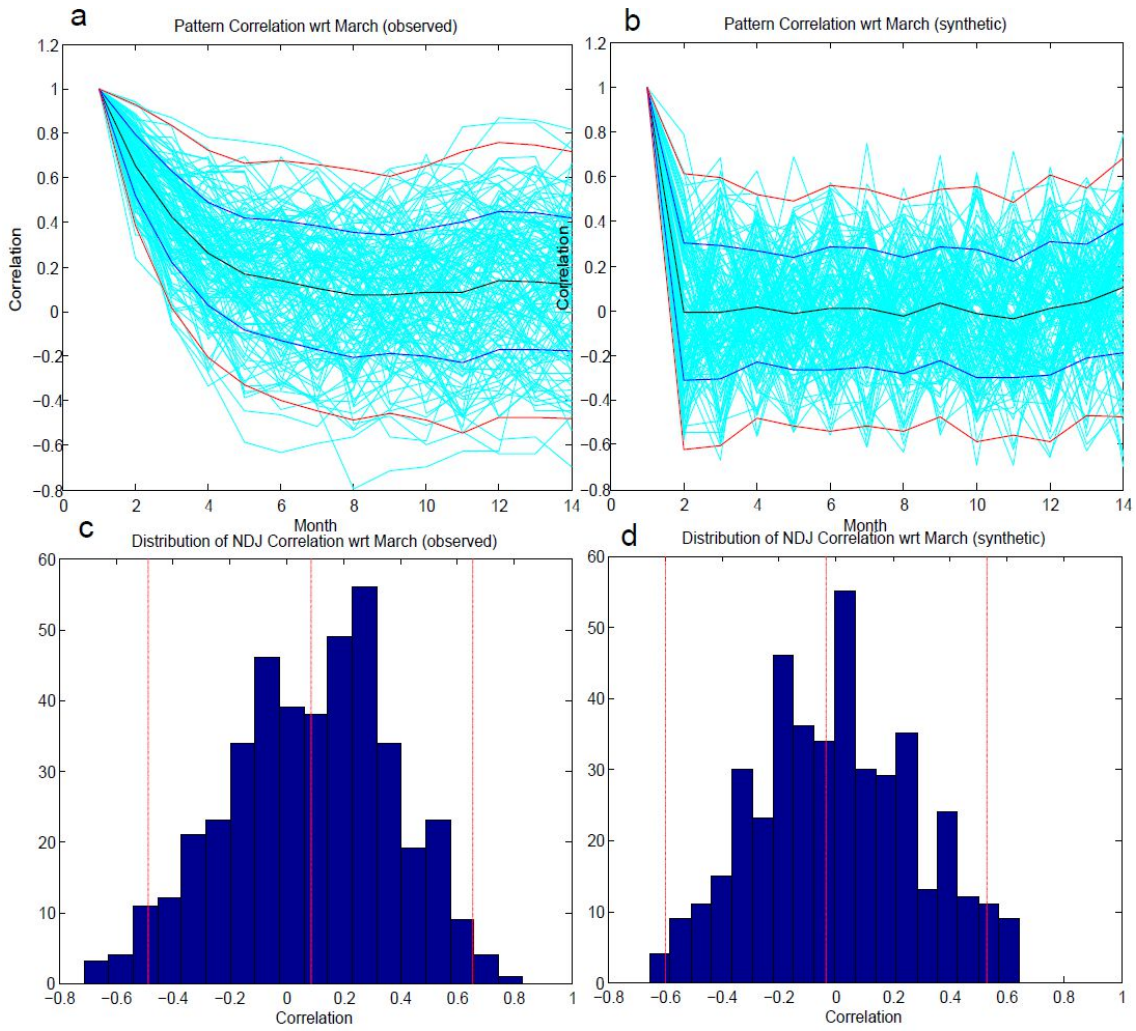

Figure 3.10 a) One year pattern correlations for North Atlantic SST anomalies for 141 years observed data (1870-2011), mean (black) and mean plus +/- 1 and 2 standard deviations (blue/red). b) as a using 141 years from randomly selected months. c) Distribution of correlation coefficents for NDJ months for 141 years observed data, red lines at mean and mean plus +/- 2 standard deviations. d) as c using 141 years from randomly selected months.

The mean correlations from the observed data (Figure 3.10a, c) give a mean NDJ correlation of 0.1 and standard deviation of 0.3. This compares with a sample from the randomly selected months (Figure 3.10b, d) with a mean NDJ correlation of 0.0 and a standard deviation of 0.3. The autocorrelation seen for the actual data is lost in the randomly selected months, illustrated by the sudden reduction in average correlation from 1 to about zero when moving from March to April (Figure 3.10b) compared to the gradual reduction in correlation seen in the observed data (Figure 3.10a). For the winter months the increase in the average correlation seen in the observed timeseries is absent in the correlations based on the randomly selected months. Nevertheless, it is possible to find events that fulfill both criteria in the random data.

The number of re-emergence events were counted for specific winter maximum and summer to winter minimum ratio criteria. The count was repeated for all values of the winter maximum in the range 0 to 1 and for values of the summer ratio in the range 0 to 1, both in increments of 0.05. This process was repeated 1,000 times to produce a distribution of the number of re-emergence events for any given winter maximum and summer ratio. To better understand the impact of having no autocorrelation the analysis described above is carried out using either NDJ winter months (as done in the remainder of the thesis) or using December only for the winter criterion.

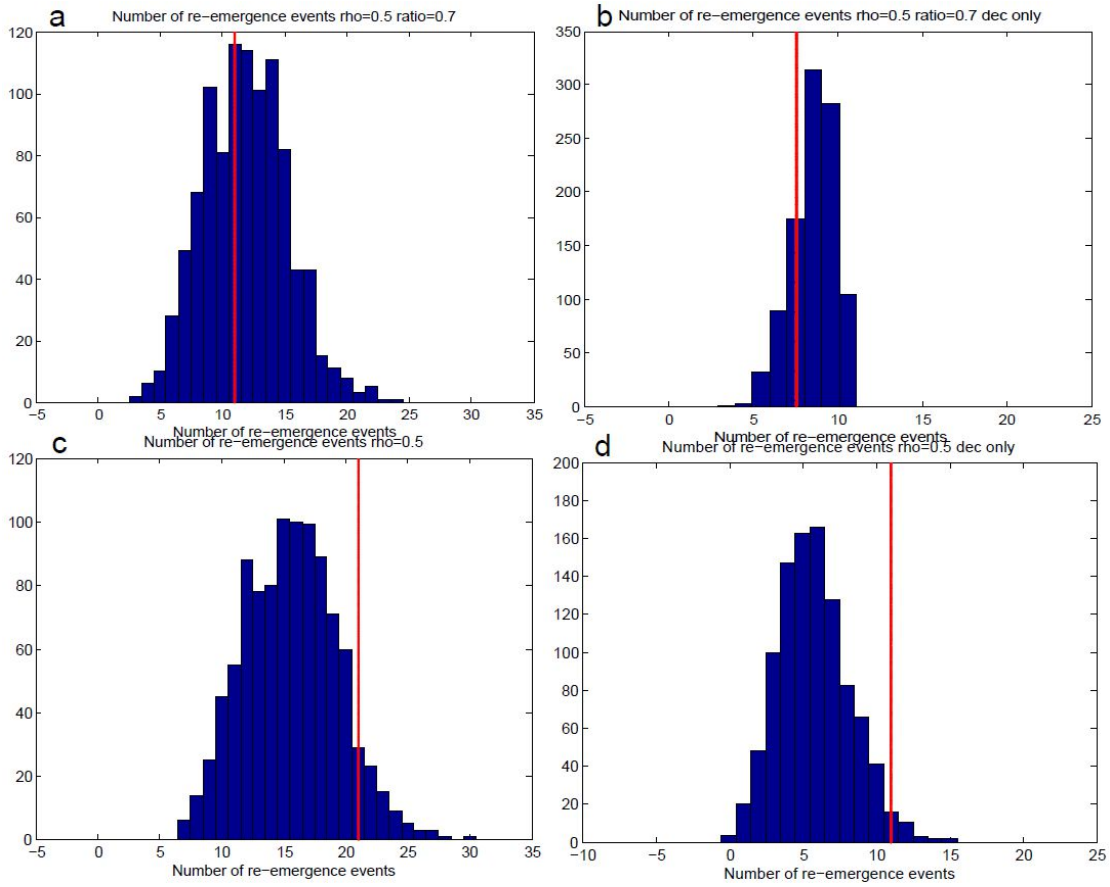

Figure 3.11a). Distribution of the number of re-emergence events identified in 1,000 randomly generated 141-years timeseries for SST anomalies. The threshold for the winter maximum is 0.5 and the summer to winter mean ratio < 0.7. b) as panel a) but using only December for the winter criterion (i.e. December correlatino < 0.5). c) as panel a) but counting events found when using only the winter criterion (max{NDJ} > 0.5). d) as panel b) but using only December i.e. December correlation > 0.5. The vertical red lines show the number of events found using the actual SSTA data.

Figures 3.11a and 3.11b show the distribution of the number of events derived from the synthetic data compared to the actual number of events for a winter maximum of 0.5 and

summer and winter mean ratio less than 0.7 (see Chapter 2). For a maximum winter correlation > 0.5 the observed case lies in the centre of the distribution of the random samples The method was also applied using just December to assess by how much picking from 3 months (NDJ) at random increases the probability of fullfilling the winter criterion. Comparison of the results in Figures 3.11a and 3.11b show a tighter clustering of the number of events when the single month is selected. Randomly selecting from NDJ results in a wider spread of values with a mean that is close to the number of events found using the actual SSTA data. .

Figure 3.11c shows the number of reemergence events using a threshold of 0.5 for the winter criterion without using the summer criterion. In this case the number of events both actual and random are larger than the numbers shown in Figure 3.11a. The actual number of values is now clearly higher than the mean of the random distribution. This illustrates that the summer ratio criterion filters out more actual than random events. For the actual events Figure 3.11c shows that 21 events pass the winter criterion. Applying the summer criterion removes 10 of these events leaving the 11 actual events seen in Figure 3.11a. For the random events the distribution in Figure 3.11c is centered around 16 events and the summer criterion only shifts the number of random events to a distribution centered around 12 (Figure 3.11a). Figure 3.11d shows the number of random and actual events found using only December for the winter criterion. Compared to Figure 3.11c the actual number of events are found further to the right of the distribution. In both these cases the actual number of events exceeds the random number mean in contrast to the results including the summer criterion (Figure 3.11a and 3.11b) showing that the summer criterion is more likley to cull events when using the actual data than when using the random data.

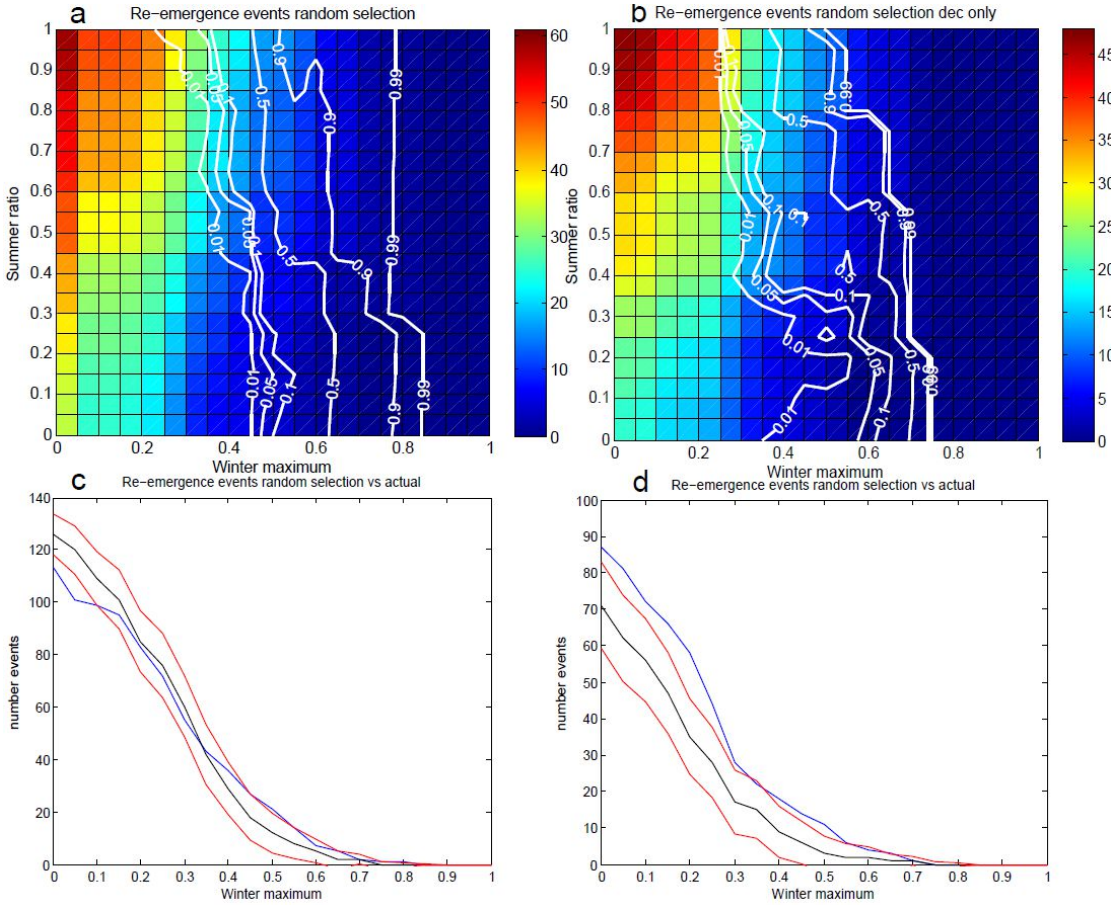

Figure 3.12a). The number of re-emergence events as a function of the winter maximum and summer ratio criteria for NDJ months. b) as panel a) for December. The significance level compared to mean distribution of random samples for p values of 0.01, 0.05, 0.1,0.5, 0.9 and 0.99 (contours). c) The number of re-emergence events as a function of the winter maximum for NDJ months, actual (blue), random sample (black), random sample +/- 2 standard deviations (red). d) as panel c) but using December only.

In a next step the re-emergence selection criteria are systematically tested by varying the threshold levels of the winter maximum, from 0 to 1, and the ratio between the summer and winter mean correlation coefficients from 0 to 1 for both the actual data and from synthetically derived data as described above. The numbers of actual events were plotted as a 2-D plot against the winter and summer criteria (Figure 3.12a and 3.12b) and the significance levels (p) computed from the ratio A/B where A is the number of random realisations where the number of events is lower or equal to the observed number of events and B (=1000) is total number of realisations.

The number of identified re-emergence events reduces as the winter maximum is increased and the summer ratio is reduced. The number of actual events varies from zero when requiring a very high correlation for the winter criterion to 60 when requiring the winter correlation to be

>0. One noteworthy, and at first sight perhaps unexpected feature which was already hinted at in Figure 3.11 is that the random number of events often exceeds the number of actual events. This is the case when the thresholds for the criterion are lower than 0.5 to 0.6. For very low values of the winter criterion the number of random events is significantly (low values of p) higher than the number of actual events. Determining the number of events by selecting only December months (Figure 3.12b) shows slightly reduced significances compared to Figure 3.12a but the number of random events still often exceeds the number of actual events. This reduction in signficance is consistent with the description of Figure 3.11. Using just December (or generally just a single month) means that the results will not depend on whether the data is autocorrelated or not. There is autocorrelation in the actual data (reflected in the average correlations of about 0.1 in Figure 3.10a) which means that NDJ are not independent when applying the winter criterion. For the randomly generated data there is no autocorrelation (Figure 3.10b) and NDJ are largely independent when applying the winter criterion. Picking just one month (December in this case) therefore increases the probability of finding a higher number of actual events than random events. This is illustrated further in Figure 3.12c,d where only the winter criterion is applied. Figure 3.12c shows the number of reemergence events using the winter criterion without using the summer criterion. A higher number of actual events are seen than in Figure 3.12a and a higher probability that the actual number of events is higher than the random number of events except for the lowest values of the winter criterion. When using December only, the number of events is lower than in Figure3.12c but now the number of actual events is always higher than the number of random events.

In conclusion, the stricter the winter criterion the lower the number events for both the actual and the random data. Whereas the number of actual events exceeds that of random events for high values for the winter criterion the opposite is true for low thresholds for the winter criterion where the random number of events significantly exceeds the number of actual events. Figure 3.12 also suggests a much smaller sensitivity to changes in the value of the summer ratio criterion. However, on closer inspection it becomes clear that summer ratio is playing a major role when looking at the ratio between actual and random events. Just using the winter criterion to determine the number of events shows that the number of actual events is more likely to exceed the number of random events for values greater than 0.5 (Figure 3.12c). Applying the summer ratio increases the chance of the number of random events exceeding the number of actual events. This can be explained when looking at Figures 3.10a and 3.10b. The average correlation is always clearly positive (around 0.1) throughout the year for the actual data. In contrast, this correlation is around zero for the random data. Thus when looking at the summer ratio criterion one is likely to find a low average summer correlation making it likely that the summer ratio criterion will be fulfilled by many random events. This will be particularly

pronounced for low values of the winter criterion. For many of the actual events where the maximum winter correlation is for example 0.1 the summer ratio criterion will often not be fulfilled (e.g. summer ratio = 0.7) since the average summer correlation is close to 0.1. This will increase the difference between the actual and random numbers of events and lead to the high significances shown in Figure 3.12a. Even if the significances reduce somewhat, this remains true when using only December for the winter threshold criterion (Figure 3.12b). For high thresholds for the winter criterion most events (both actual and random) that pass the winter criterion will also pass the criterion for the summer ratio. In summary the summer ratio is a large contributor to the very high significance levels found for winter criterion thresholds. The fact that there is still slightly higher number of random events for very low thresholds when using only the winter criterion (Figure 3.12c) can be explained by higher temporal autocorrelation in the actual than in the random data. The actual SST anomaly patterns typically do not fundamentally change from one month to the next. This, in contrast, can often happen in the randomly reorganised SST data. Whilst on average the correlation is close to zero over the 141 years the actual correlation values swing back and forth from one month to the next when using the randomly generated time series (Figure 3.10b) hence slightly increasing the chance that either November, December or January fulfil the winter criterion. Even though such swings are not impossible in the actual data they are less common than in the randomly generated data.

What does this mean for the choice of the criteria of winter maximum > 0.5 and summer to winter ratio < 0.7? Are these criteria too tolerant and let through too many non-genuine reemergence events? It has to be noted here that there is no completely objective way to find the reemergence events from SST data alone. There will always be a risk of being too strict and exclude genuine events or too lenient and consider events that are not linked to re-emergence. The choosen criteria would appear to be on the lenient side with 11 events identified. With thresholds of 0.5 and 0.7 for the winter maximum and summer ratio the number of actual and random events is similar. However, what this shows is that SST anomaly patterns from unrelated years can look similar and not that the 11 events identified are not genuine. Figure 3.12a shows that the choosen citeria threshold of 0.5 and 0.7 are where there is a strong gradient in the significance values. This means that only a small increase in the threshold for the winter criterion shifts the actual number of events to the right of the distributions of random events and more actual events are found than by chance. This would suggest that increasing the value of the winter criterion might be indicated. However, the choosen criteria for the winter maximum and summer to winter ratio clearly identify the years which are known to be, or very likely to be, genuine re-emergence events (i.e. 1968/69, 2009/10) and which show a strong tripole index. Interestingly the winter 2009/2010, when re-emergence has been identified, only just qualifies with the winter maximum criteria. Only a slight increase in the threshold for the

winter criterion (increase from 0.5 to 0.55) leads to the events of 1887 and 2009 being removed from the list. A slight tightening of the summer criterion (0.7 to 0.65) leads to the event of 1887 to be removed from the list. As it is very early in the observational period the SST will not be well constrained in 1887 so this event is less significant. However, 2009 is the probably best documented event when re-emergence occurred (Taws *et al*. 2011) and the thresholds should clearly be chosen such that this event and similar events are identified and flagged as potential re-emergence years. Finally, it is also worth noting that when using only the winter threshold criterion, the number of actual events is typically higher than the number of events found by chance (Figure 3.12c). The significance is highest for a winter threshold around 0.5 (Figure 3.12c) suggesting that it is around this level that one is most likely to find significantly more actual than random events after the first step of the event selection procedure. It is the application of the summer criterion which then culls more actual than random events. In summary varying the thresholds for the summer and winter criteria reveals the sensitivity of the number of identified events to a tightening of the winter and summer criteria. The number of identified events is most sensitive to a tightening of the winter criterion. However, it was also found that a tightening of the winter criterion removes events that are known to be genuine. This suggests that on balance the thresholds used for the winter and summer ratio criteria are appropriate for the analysis done in this thesis.

3.4 Discussion and Conclusions

Analysis of the 20CR historical record shows that 11 events that meet our re-emergence criteria occurred during the period 1870 to 2011. Of these 11 events six were preceded by a negative winter mean NAO and five were preceded by a positive winter mean NAO. The ocean may be preconditioned by the atmosphere during the first winter which may lead to the re-emergence of temperature anomalies in the following winter, but there appears to be no bias in the number of re-emergence events occurring following a negative or positive winter mean NAO. However, a clear asymmetry can be seen in the strength of the NAO signal: Whereas positive NAO winters that precede re-emergence are typically unremarkable (average NAO index of 0.7), a strongly negative index (average of -1.6) is found for preceding negative NAO winters. The asymmetry in the NAO strength for the first winter gives different probabilities for the NAO sign to be repeated in second winter.

An interesting observation is the difference in the timing of re-emergence when preceded by positive or negative NAO states with the highest correlations reached in early winter (positive NAO precedes) or late winter (negative NAO precedes; Figure 3.3). Exploring in detail why this happens is beyond the scope of this thesis but a tentative explanation could be through the impact of the atmosphere on the ocean circulation during the first winter. Negative NAO

winters have been shown to coincide with a weakening of the Atlantic meridional overturning circulation (Blaker *et al*. 2015) and of the related meridional heat transport and ocean heat content (Sonnewald *et al*. 2013; Cunningham *et al*., 2013; Bryden *et al*. 2014). As a consequence, negative ocean temperature anomalies can develop through both anomalous air-sea fluxes linked to the state of the atmosphere as well as through a reduction in the oceanic MHT. Positive NAO winters favour a stronger AMOC (and related MHT) and the build-up of cold, subsurface anomalies in the ocean will mainly be the result of air-sea fluxes. As a consequence larger cold ocean heat content anomalies are expected to develop during negative than during positive NAO winters making it more likely for the cold anomaly to reemerge throughout the winter as the ocean mixed layer depth gradually deepens.

Chapter 4: Re-emergence of North Atlantic temperature anomalies and the impact on North Atlantic winter weather in CMIP5 models

Using observation based datasets Chapter 3 has shown that re-emergence events have occurred repeatedly during the last 140 years. The results also suggest that re-emergence is preconditioned either by strongly NAO- winters or weakly NAO+ winters and that re-emergence can affect the state of the atmosphere. Oceanic re-emergence and its links to the atmosphere therefore are important to North Atlantic winter climate and ideally coupled climate models should be able to simulate a similar relationship between re-emergence and the atmospheric circulation over the North Atlantic region. In this chapter the ability of current state-of-the-art GCMs to reproduce these characteristics of re-emergence will be tested in a subset of the CMIP5 models, which were introduced in Chapter 2.

Global Circulation Models are one of the most important sources of information for understanding changes in the Earth's climate through the twentieth and twenty-first centuries. The skill of different GCMs is determined by the different methods used to solve the equations that describe atmospheric and oceanic dynamics, different parameterisations as well as by the resolution of the model grid. The fifth phase of the Coupled Model Intercomparison Project (CMIP5, Taylor *et al*., 2012) constitutes the most recent set of coordinated climate model experiments and provides the opportunity to compare the skill of a large group of GCMs. The skill in CMIP5 models to reproduce atmospheric circulation patterns, wintertime NAO and the Atlantic Jet Stream have been examined (Davini and Cagnazzo, 2013, Perez *et al*., 2014) as has their skill in simulating the spatial structure of SST variability (Wang *et al*., 2015). However, thus far there have been no studies investigating the relationship between SST variability and atmospheric modes.

4.1 Results from CMIP5 Models

Following the method used in Chapter 3, SST and SLP anomaly fields from the CMIP5 models for the period 1850-2005 are computed by removing the 1850-2005 monthly climatology from the GCM output and the SST anomalies are detrended by removing a polynomial spline fit. The re-emergence correlation coefficients and NAO indices are calculated in the same manner as used for the reanalysis products. The re-emergence correlations varied considerably (Table 4.1, Figure 4.1). The models were assessed against observations using five criteria:

1) The mean winter and summer correlation coefficients for SSTs. The criteria of a mean winter correlation coefficient in the range 0.10 to 0.18 was used (compared to 0.104 in HadISST)

2) The number of re-emergence events, defined as occurances when the winter maxima correlation coefficient is greater than 0.5 and the ratio of the summer mean and winter mean correlation is less than 0.7. The criteria of a number of events in the range 7 to 15 was used (compared to 11 in HadISST)

3) A similar total number and ratio of re-emergence events preceded by NAO- or NAO+ winters (compared to 11 in total, comprising 6 negative and 5 positive in HadISST).

4) Asymmetry of the NAO state in winters preceding re-emergence (NAO negative on average, as found with results from 20CR).

5) Influence of reemergent SST anomaly patterns on the NAO state (i.e. winters when the mean NAO state is repeated in the second winter) compared with results from 20CR.

The atmosphere data for the CMCC-CM and CNRM-CM5 models was limited to the period 1950 to 2005 but their results are also included. A summary of the results is shown in Tables 4.1, which is colour coded to identify the specific criteria.

Model	Mean summer JAS re-em corr coeff	Mean winter NDJ re-em corr coeff	Std Dev winter re-em corr coeff	#events winter max re-em >0.5 & r <0.7	#events negative winter NAO	#events re-em>.5 & NAO-	#events re-em>.5 & NAO- y1 & y2	#events re-em>.5 & NAO+	#events re-em>.5 & NAO+ y1 & y2
HadISST/20C	0.075	0.104	0.304	11	65	6	6	5	3
ACCESS 1.0	0.261	0.290	0.189	15	75	7	4	8	3
ACCESS 1.3	0.217	0.292	0.194	19	73	10	5	9	6
BCC_CSM	0.218	0.242	0.229	23	71	11	5	12	4
CanESM2	0.194	0.149	0.210	7	70	7	4	0	0
CCSM4	0.169	0.131	0.254	10	67	1	0	9	7
CMCC_CM	0.178	0.240	0.197	22	25	5	3	3	0
CNRM_CM5	0.065	0.128	0.221	1	24	0	0	1	1
CSIRO	0.317	0.319	0.247	16	70	9	3	7	5
EC_EARTH	0.101	0.181	0.239	19	72	11	7	8	6
GFDL_ESM2	0.192	0.401	0.206	52	76	28	14	24	8
GISS_E2_H	0.109	0.161	0.240	22	76	10	6	12	7
HadCM3	0.185	0.144	0.172	3	69	1	1	2	1
HadGEM2-ES	0.122	0.106	0.213	3	67	0	0	3	2
INMCM4	0.203	0.135	0.164	1	79	0	0	1	1
IPSL_CM5A	0.143	0.225	0.268	28	75	11	5	17	9
MIROC5	0.256	0.202	0.251	13	77	5	2	8	6
MPI_ESM_LR	0.172	0.163	0.159	2	71	1	1	1	0
MRI_CGCM3	0.085	0.003	0.208	1	77	0	0	1	0
NorESM	0.194	0.145	0.248	11	73	5	0	6	2

Table 4.1. Performance of CMIP5 models compared to observations. Columns from left to right: summer mean (JAS) re-emergence correlation coefficient, winter mean (NDJ) re-emergence correlation coefficient, winter mean re-emergence correlation standard deviation, number of re-emergence events with winter maxima greater than 0.5 and ratio summer mean and winter mean correlation <0.7, number of mean winter (DJFM) negative NAO, number of events where re-emergence preceded by a negative NAO, number of events where re-emergence coincides with negative NAO in year 1 and year 2, number of events where re-emergence preceded by a positive NAO, number of events where re-emergence with positive NAO in year 1 and year 2. The colours highlight which criteria the models fulfil compared to observations (cyan: criterion 1 - mean winter and summer correlations coefficients for SSTs; yellow: criterion 2 – number of re-emergence events; magenta: criterion 3 – similar number of re-emergence events preceded by NAO+ or NAO- winters; see main text.). Models for which more than one colour is used fulfil more than one criterion. Grey shading is used to highlight models that fulfil at least one criterion.

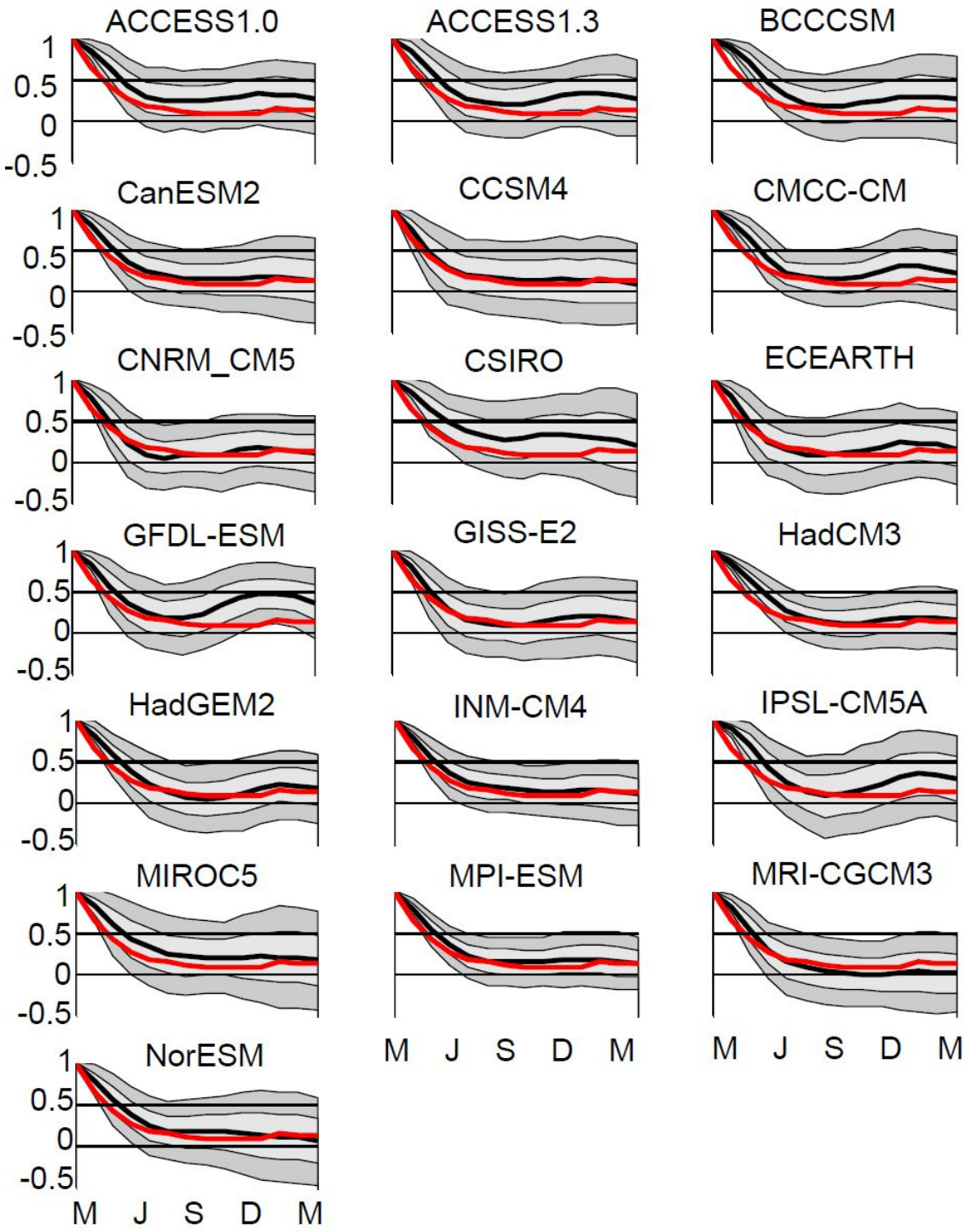

Figure 4.1. One-year pattern correlations for North Atlantic SST anomalies (10-60°N, 80-10°W) taken from CMIP5 models for 155-year (1850-2005) average. The light grey shading denotes the standard deviation range and the dark grey two standard deviation range. The black line is the mean correlation for the CMIP5 model and the red line for HadISST.

Ten models produced mean re-emergence correlations where the winter correlation is close to that found in observations (CanESM2, CCSM4, CNRM-CM5, EC-EARTH, GISS-E2-H, HadCM3, HadGEM2-ES, INMCM4, MPI-ESM-LR, NorESM; highlighted in cyan in Table

4.1). Some models, such as the ACCESS1.0, ACCESS1.3, GFDL-ESM2M and CSIRO models produced winter SST pattern correlations significantly higher than the observed values suggesting that the surface ocean retains a memory from previous winters or that the atmosphere has preferred modes of variability that vary little in their spatial pattern and which therefore often impose similar SST anomaly patterns on the North Atlantic. The MRI-CGCM3 model produced mean winter re-emergence correlations of zero suggesting that the ocean has not retained a memory from previous winters or that the imprint of oceanic memory on SSTs is overwritten by the atmosphere.

The time series of the winter maximum re-emergence correlation coefficients are examined for all CMIP5 models to assess the number of events where the re-emergence criteria are met, when the maximum re-emergence correlation coefficient exceeds 0.5 and the ratio between the summer mean and winter mean correlation coefficients is less than 0.7.

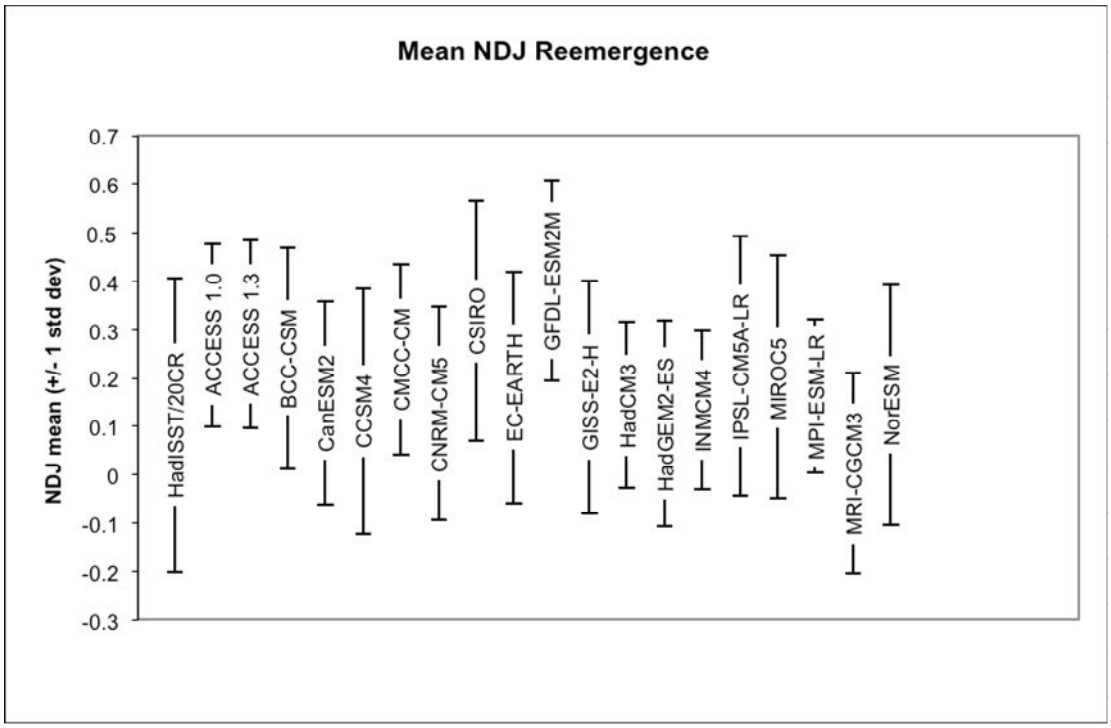

Figure 4.2.(a) Comparison of the mean and standard deviation in the mean winter re-emergence correlation coefficient between HadISST observations and CMIP5 models.

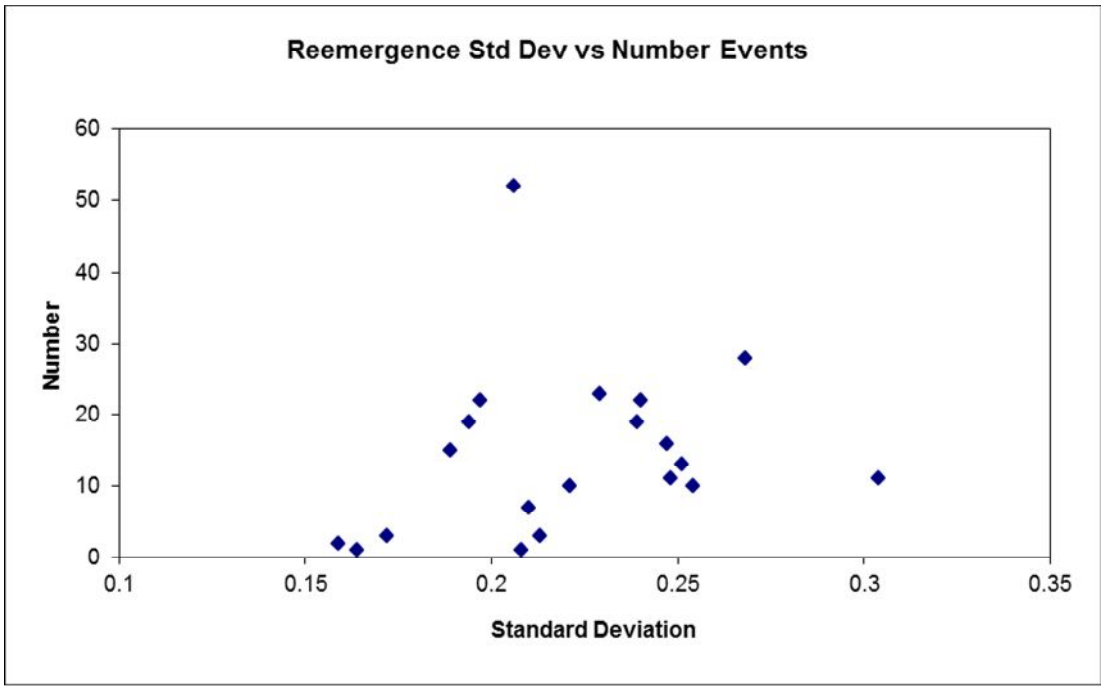

Figure 4.2. (b) Correlation between the number of re-emergence events and the standard deviation between HadISST observations (11 events, standard dev 0.304) and CMIP5 models .

The models produced a wide variation in the number of re-emergence events (Table 4.1, Figure 4.2). Six models simulated a similar number of events to the 11 identified in the HadISST data (ACCESS1.0, CanESM2, CCSM4, CSIRO, MIROC5, NorESM; highlighted in yellow in Table 4.1). The GFDL-ESM2M model produced the highest number of events (52), whilst 6 models produced 3 or fewer events (CNRM-CM5, HadCM3, HadGEM2-ES, INMCM4, MPI-ESM-LR, MRI-CGCM3). The CMIP5 time series are about 15 years (~10%) longer than 20CR. statistically therefore a slightly higher number of re-emergence events in the CMIP5 models are expected. It is worth noting that the interannual variability for the mean winter NDJ correlation coefficient is smaller than observed for all the models analysed here (Figure 4.2a). This is particularly pronounced for ACCESS1.0/1.3 and INMCM4. It is also interesting to note that it is mainly the occurrences of low and negative correlations that the models do not reproduce well. Apart from MRI-CGCM3 no model simulates correlations as negative as those found in HadISST (note that this model fails to reproduce the higher positive correlations). In contrast many models produce situations where the spatial correlations are as high or higher than the upper bound of values found in HadISST. There is only a weak relationship between the number of re-emergence events and the standard deviations in the spatial correlation patterns, with models with larger standard deviations producing more events that are identified as re-emergence (Figure 4.2b). The clear outlier with the highest number of events despite a rather small standard deviation is GFDL-ESM2M.

Next, the time series of the winter mean NAO index is examined, taken from the principal component of the leading EOF, from all the CMIP5 models in the period 1850-2005. The shape of the distribution is comparable to that found in the 20CR data for most models (Table 4.1, Figure 4.3) although for some models the distributions are more asymmetric (e.g. HadGEM2-ES, ACCESS1.3, CCSM4) than in 20CR.

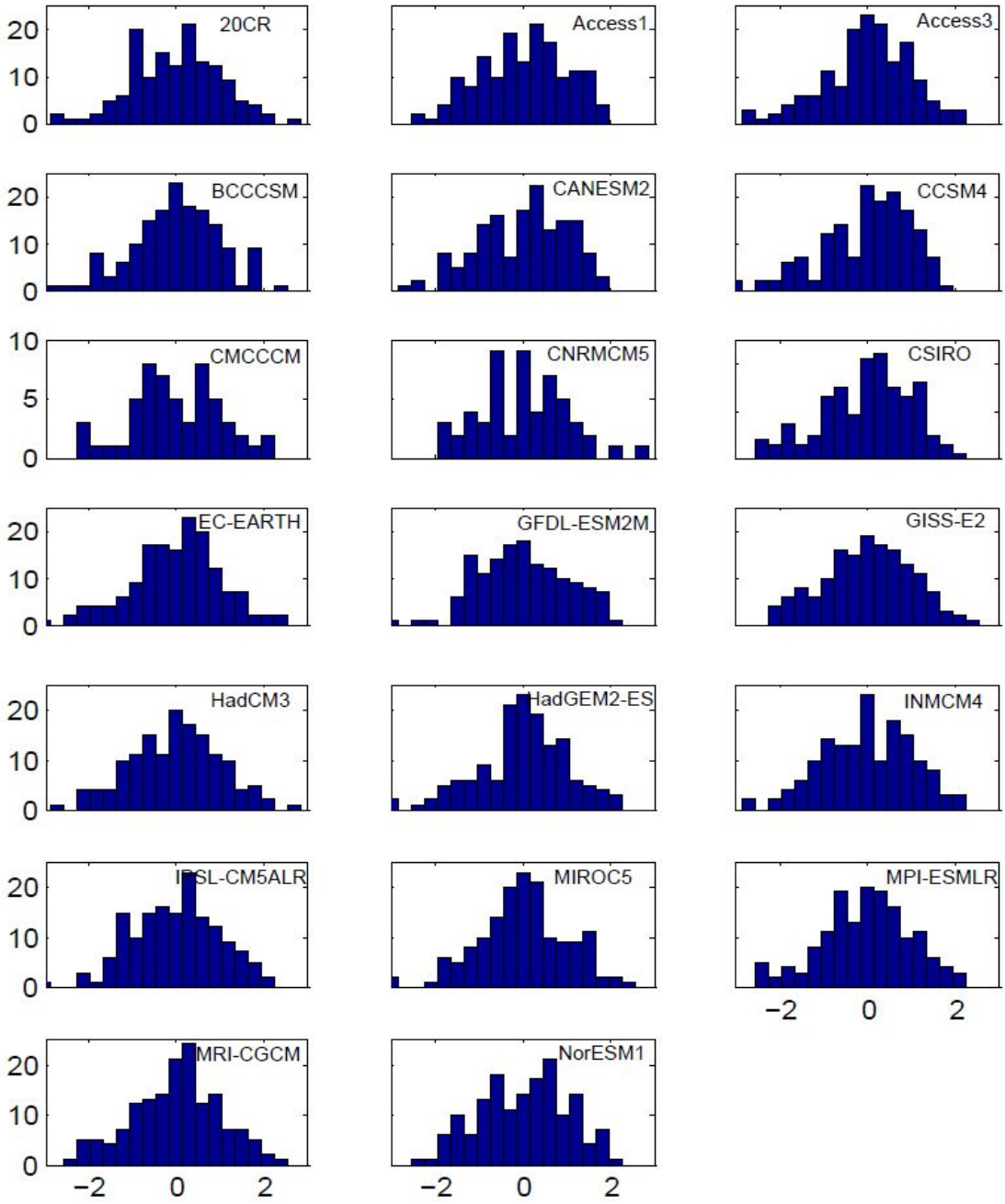

Figure 4.3. Distribution of the mean winter (December-March) NAO index from the leading empirical orthogonal function (EOF1) of North Atlantic sector (20-70°N, 90°W-40°E) SLP from 20CR data (1871 to 2011) and CMIP5 models (1850 to 2005).

An estimate of the agreement of the observed (F_o) and simulated (F_s) NAO distributions can be obtained by applying a Kolmogorov-Smirnov test (Massey, 1952, Wilcox, 2005). In a first step the normalised cumulative sums C_o and C_s from the distributions F_o and F_s are computed:

$$C_o(k) = \frac{1}{n}\sum_{i=1}^{k} F_{oi}\,, \tag{4.1}$$

$$C_s(k) = \frac{1}{m}\sum_{i=1}^{k} F_{si}\,,\ k = (1,.....,L)\,, \tag{4.2}$$

where n, m are the number of winters in 20CR and in the CMIP5 models respectively; L is the number of bins into which the NAO values are grouped. Whether the observed and simulated distributions are significantly different from each other can then be decided from the maximum distance D between C_o and C_s:

$$D = (\,|C_{oki} - C_{ski}|),\ i = (1,.....,L)\,. \tag{4.3}$$

Similarity should be rejected if:

$$D > c\sqrt{n+m/n*m}\,, \tag{4.4}$$

where c = 1.22, 1.36, 1.48, 1.63 for significance levels of 0.1, 0.05, 0.025 and 0.01, respectively

In all the CMIP5 models the maximum distance (D) was less than 0.1 confirming that the simulated and observed NAO distributions shown in Figure 4.3 were similar at a significance level of 0.1.

Mirroring the observational analysis in Chapter 3 the CMIP5 model output was examined for winters where reemergent SST anomalies were preceded by either a negative or a positive NAO state (Table 4.1, Figure 4.4).

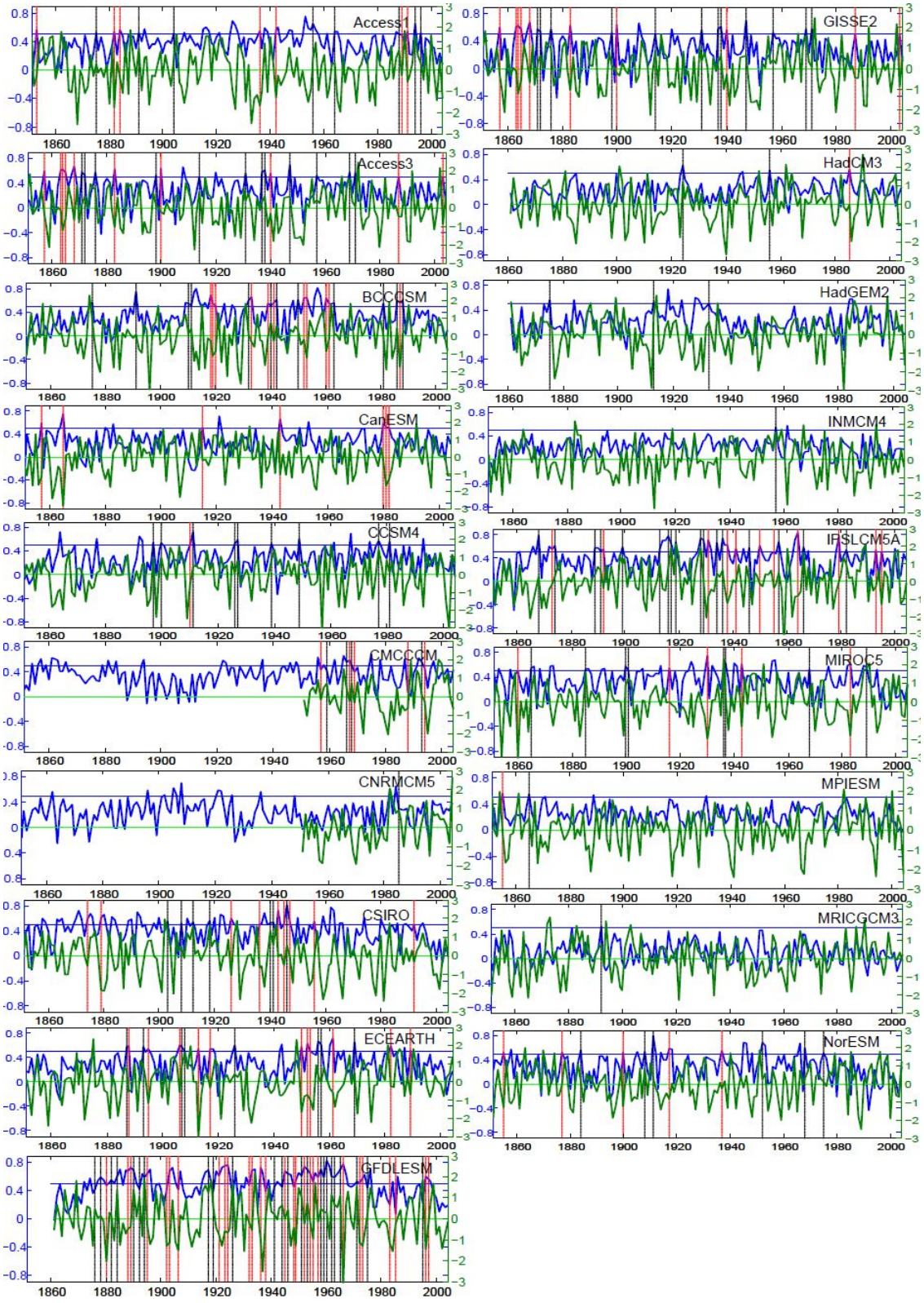

Figure 4.4. Time series of maximum winter (NDJ) re-emergence correlation coefficient (blue) and winter mean NAO from leading empirical orthogonal function (green) from CMIP5 models (1850-2005). The red lines indicate years when re-emergence is preceded by a negative NAO and black lines when preceded by a positive NAO.

These results are compared with results from HadISST and 20CR data. Eleven models have a probability of re-emergence events preceded by a negative or positive NAO winter broadly as suggested in observations (highlighted in magenta in Table 4.1). Of the 8 remaining models seven had a markedly lower incidence of negative NAO states preceding re-emergence with 0 or 1 events (CCSM4, CNRM-CM5, HadCM3, HadGEM2-ES, INMCM4, MPI-ESM-LR, MRI-CGCM3) but with the exception of the CCSM4 model, these models also had a low number of re-emergence events. In the CanESM2 model all seven re-emergence events are preceded by negative NAO winters.

As for the observations the Monte-Carlo tests are applied to assess if a significant link with either NAO+ or NAO- can be found in the CMIP5 models (Figure 4.5, Table 4.2). Only one model (CanESM2) had an extreme negative winter mean NAO index, which reflects that all 7 identified re-emergence events coincide with preceding negative winter mean NAO states. Five models (CCSM4, CNRM-CM5, HadGEM2-ES, INMCM4, MRI-CGCM3) produced strongly positive and statistically significant mean NAO index greater than 0.5 for the preceding winter. Four of these models (CNRM-CM5, HadGEM2-ES, INMCM4, MRI-CGCM3) have a very low incidence of re-emergence events (3 or fewer) and no occurrence of a negative NAO preceding re-emergence. For the re-emergence year (i.e. second winter of an event) fifteen of the CMIP5 models produced a mean NAO index in the range +/-0.5. Two models (HadCM3, MPI-ESM-LR) produced a mean NAO index less than -0.9 and one model (INMCM4) produced a mean NAO index greater than 0.9. However, each of these models had a very low occurrence of re-emergence events and of a negative NAO preceding re-emergence.

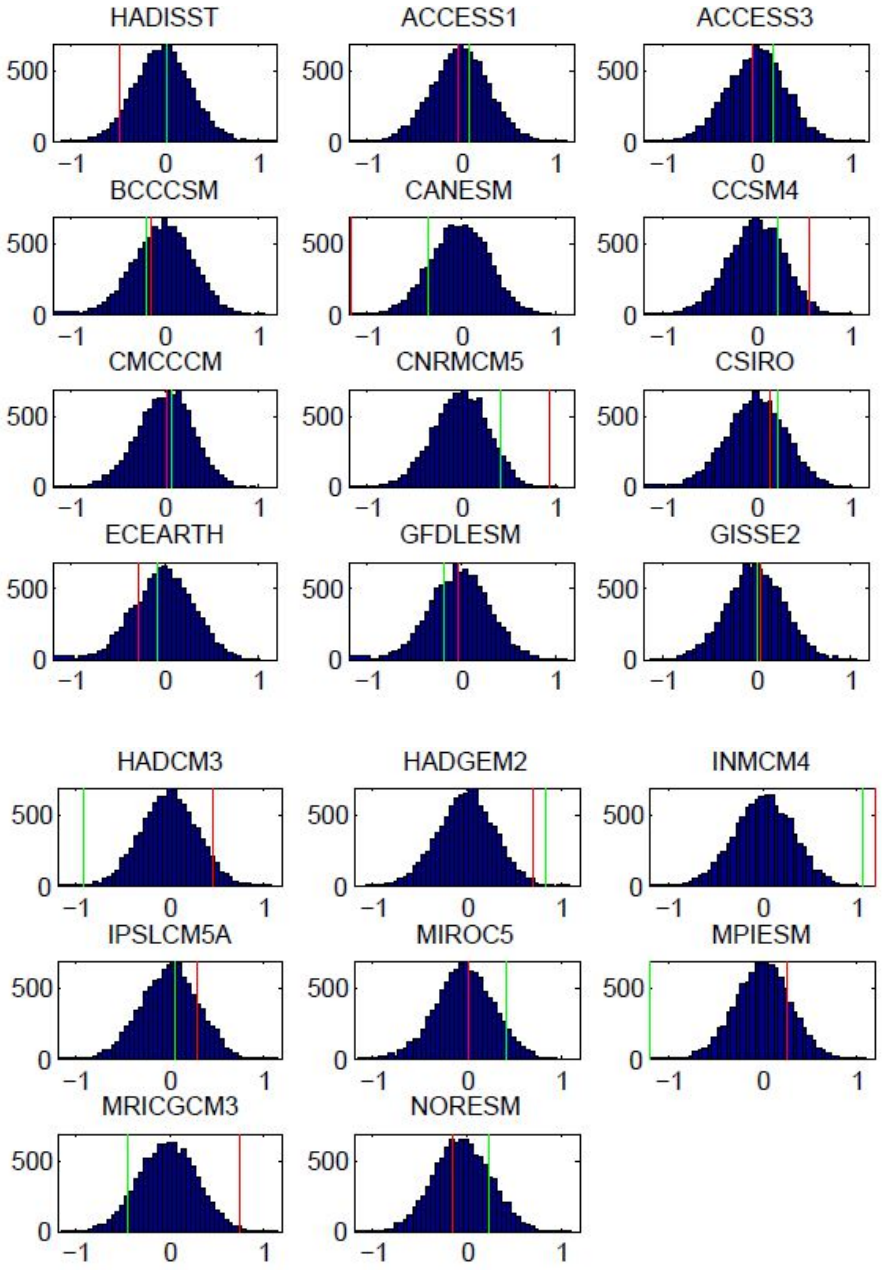

Figure 4.5. The mean winter NAO index from the preceding winter (red) and the re-emergence year (green) for HadISST and CMIP5 models shown with the distribution of 10,000 random winter NAO index samples from the same number of winters from HadISST and CMIP5 models.

Model	Mean NAO 1st winter	Mean NAO 2nd winter	p NAO 1st winter > mean	Mean NAO- 1st winter	Mean NAO- 2nd winter	P NAO- 2nd winter > mean	Mean NAO+ 1st winter	Mean NAO+ 2d winter	p NAO+ 2nd winter <mean
HadISST/20CR	-0.545	-0.400	**0.04**	-1.594	-0.794	**0.09**	0.713	0.073	0.38
ACCESS 1.0	-0.042	0.084	0.45	-0.877	0.115	0.55	0.688	0.050	0.41
ACCESS 1.3	-0.035	0.196	0.43	-0.608	-0.303	0.21	0.605	0.758	**0.01**
BCC_CSM	-0.144	-0.217	0.34	-0.659	0.121	0.57	0.336	-0.528	0.84
CanESM2	-1.180	-0.350	**<0.01**	-1.181	-0.350	0.18			
CCSM4	0.566	0.228	0.98	-0.542	0.425	0.77	0.684	0.204	0.28
CMCC_CM	0.032	0.082	0.51	-0.331	0.400	0.73	0.485	-0.315	0.72
CNRM_CM5	0.956	0.425	0.99				0.956	0.425	0.11
CSIRO	0.154	0.223	0.68	-0.563	0.054	0.48	1.068	0.442	**0.10**
EC_EARTH	-0.268	-0.082	0.18	-0.963	-0.253	0.25	0.631	0.154	0.32
GFDL_ESM2M	-0.042	-0.184	0.45	-0.816	-0.053	0.39	0.859	-0.338	0.73
GISS_E2_H	0.047	-0.006	0.55	-0.586	-0.187	0.29	0.575	0.140	0.32
HadCM3	0.477	-0.938	0.94	-0.009	-1.986	**<0.01**	0.720	-0.403	0.78
HadGEM2-ES	0.716	0.851	0.97				0.716	0.851	**<0.01**
INMCM4	1.543	1.063	1.00				1.543	1.063	**<0.01**
IPSL_CM5A_LR	0.318	0.064	0.84	-0.526	0.133	0.58	0.864	0.013	0.46
MIROC5	0.029	0.432	0.54	-1.707	0.069	0.52	1.116	0.661	**0.03**
MPI_ESM_LR	0.268	-1.260	0.80	-0.078	-1.694	**<0.01**	0.619	-0.836	0.95
MRI_CGCM3	0.749	-0.446	0.99				0.749	-0.446	0.78
NorESM	-0.160	0.254	0.34	-0.757	0.699	0.91	0.337	-0.122	0.54

Table 4.2. The mean NAO from HadISST and CMIP5 models for all winters preceding re-emergence and re-emergence year, the mean NAO for NAO negative leading winters for winters preceding re-emergence and re-emergence year and the mean NAO for NAO positive leading winters for winters preceding re-emergence and re-emergence year. The probability of the mean winter NAO is measured against 10,000 random samples of winter NAOs (p values of 0.1 or lower are highlighted in bold fonts). The colours highlight which criteria the models fulfil compared to observations (cyan: criterion 4 - asymmetry between the strength of the NAO index for positive and negative NAO winters preceding re-emergence; yellow: criterion 5 – cases where re-emergence affects the NAO state i.e. NAO- or NAO+ for the first and second winters of a re-emergence event). Grey shading indicates which models fulfil at least one criterion.

Finally, the asymmetry for the NAO strength is tested for re-emergence events preceded by NAO+ and NAO- winters in the CMIP5 ensemble. The asymmetry was tested in each model by comparing the mean NAO for all winters preceding re-emergence and by looking at the mean NAO values in the first and second year for events where NAO+ or NAO- winters precede re-emergence (Table 4.2). For seven models the mean winter NAO preceding re-emergence is negative (Table 4.2, cyan). Excluding the models with a low number of re-emergence events (CNRM-CM5, HadCM3, HadGEM2-ES, INMCM4, MPI-ESM-LR, MRI-CGCM3) only five models produced (on average) a repeating negative NAO in the second winter (ACCESS1.3, CanESM, EC-EARTH, GFDL-ESM, GISS-E2-H: Table 4.2, yellow). Five models produced a repeating positive NAO in the second winter (ACCESS1.3, CCSM4, CSIRO, EC-EARTH, MIROC5). Only ACCESS1.3 and EC-EARTH produced a balanced distribution of positive and negative NAO states preceding re-emergence comparable to observations, with the first winters being on average NAO negative, and with the second winters being on average NAO negative (positive) for the groups of re-emergence events preceded by negative (positive) NAO winters. The CanESM2 model only had re-emergence events exclusively preceded by negative NAO winters.

4.2 Discussion and Conclusions

The CMIP5 models were analysed to establish if they could simulate a frequency of re-emergence events in the North Atlantic and a link with the NAO that are comparable to the observations.

Ten of the models produced a mean re-emergence correlation coefficient similar to that produced from observations according to criterion 1 (Table 4.1, cyan). However, most of these models, with the exception of CNRM-CM5, EC-EARTH and GISS-E2-H, produced a mean summer correlation coefficient higher than the winter mean suggesting that the winter mean could reflect persistence. The number of winters when the maximum re-emergence correlation coefficient exceeds 0.5 and the ratio between the summer mean and winter mean correlation coefficients is less than 0.7 varied considerably. Six models produced a number of events similar to that found in observations (ACCESS1.0, CanESM2, CCSM4, CSIRO, MIROC5, NorESM; criterion 2, Table 4.1, yellow).

Eleven of the models with 7 or more re-emergence events showed no bias towards either positive or negative NAO winters preceding the occurrence of re-emergence (criterion 3, Table 4.1, magenta). However, most of these models produced a re-emergence frequency that is clearly higher than observed (ACCESS1.3, BCC-CSM, CMCC-CM, EC-EARTH, GFDL-ESM2M, GISS-E2-H, IPSL-CM5A). None of the models can simulate the asymmetry between

the strength of the NAO index for positive and negative NAO winters preceding re-emergence seen in observations (criterion 4, Table 4.2, cyan). Typically, the asymmetry is weaker than observed but it is worth noting that in the CanESM2 model all events are preceded by NAO- winters suggesting unrealistically strong links between NAO and re-emergence.

When only considering models where 7 or more re-emergence events are identified only a few cases were found where re-emergence affects the NAO state i.e. NAO- or NAO+ for both first and second winters of a re-emergence event (criterion 5, Table 4.2, yellow). The most statistically significant impact on the NAO is found in CanESM2 but as stated earlier the link between NAO and re-emergence is too strong in this model. Although not statistically significant ($p=0.25$) the most realistic model for criterion 5 appears to be EC-EARTH. This is the only model for which the NAO average of all preceding winters is clearly negative (implies asymmetry), and where NAO- in the first winter is on average followed by NAO- in the second winter (Table 4.2).

Overall the CMIP5 models assessed fail to reproduce observations and no model can fulfil all the criteria. As shown earlier (Table 4.1) some models do simulate a realistic number of re-emergence events but Table 4.2 suggests that there is no overlap between that group of models and the models that simulate a realistic link between re-emergence and the state of the NAO. EC-EARTH is the model that comes closest to fulfilling all criteria: the number of re-emergence events (19 vs.11 observed events, Table 4.1) is somewhat too high, but could be tolerable given the limited time period and number of observed events (i.e. small sample size), the average winter correlation exceeds the summer correlation (Table 4.1) and the fraction of re-emergence events preceded by either positive or negative NAO winters is realistic (Table 4.1). Finally in EC-EARTH there is also an increased probability for consecutive NAO- winters during re-emergence and for the average NAO preceding re-emergence events to be negative (Table 4.2).

In order to get more insight into the possible reasons why the models are performing poorly in terms of their ability to realistically simulate re-emergence events and their links with the atmospheric circulation it is useful to look at SST variability. The spatial structure of the SST variability simulated in the models was compared to those seen in the observations. The standard deviation found for SST anomalies in the North Atlantic was compared in each model with the standard deviation found in HadISST (Figure 4.6).

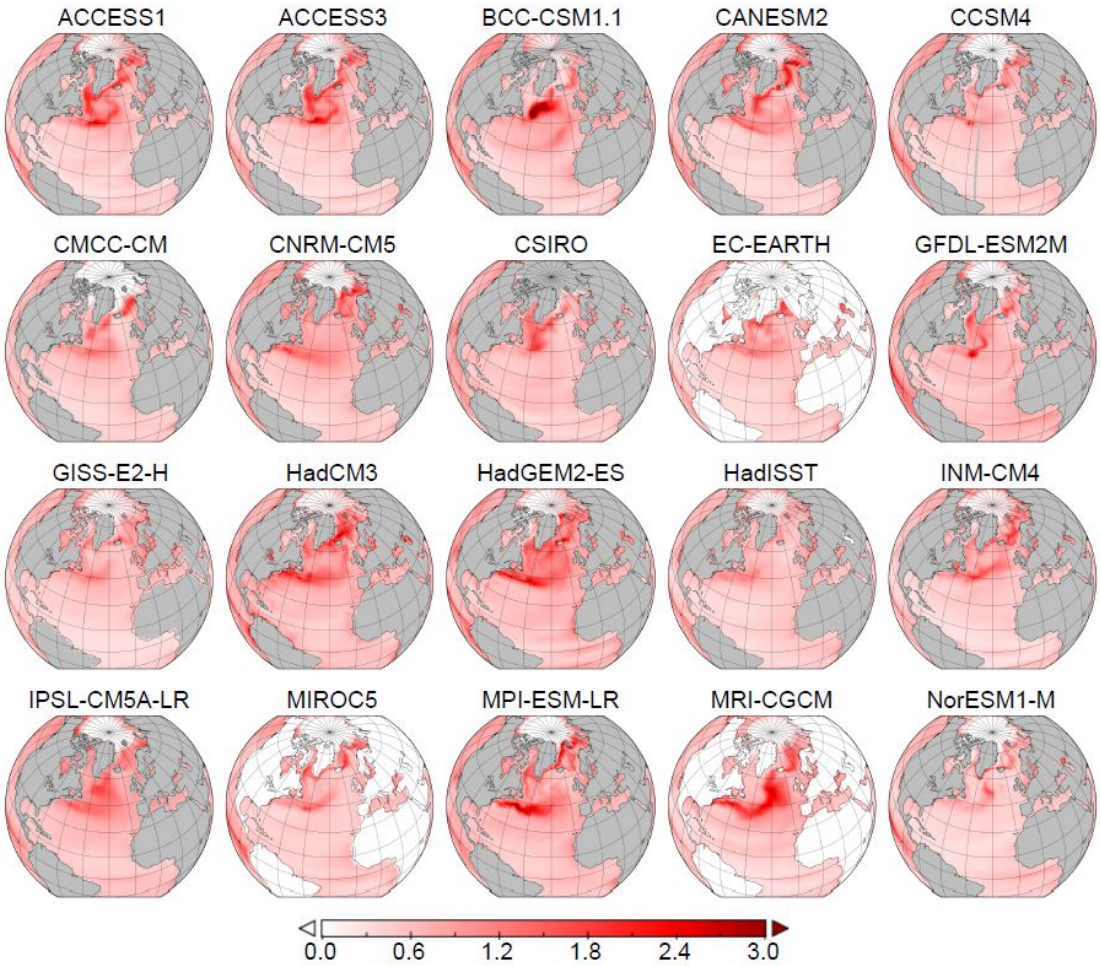

Figure 4.6. Spatial plot of SST anomaly standard deviations from HadISST and CMIP5 models. Units are °C.

The analysis indicates that the majority of the CMIP5 models produce higher SST variability in the North Atlantic compared with observations and simulate too strongly localised patterns of SST variability, in agreement with the previous findings of Wang *et al*. (2015). Fifteen models produced clearly higher standard deviations in SST anomalies in the North Atlantic than those found in observations (ACCESS1.0, ACCESS1.3, BCC-CSM, CanESM2, CCSM4, CMCC-CM, CNRM-CM5, CSIRO, GFDL-ESM2M, HadCM3, HadGEM2-ES, INMCM4, IPSL-CM5A, MPI-ESM-LR, MRI-CGCM3). Four models produced a spatial pattern similar to that found in observations with the region of higher variability extending from the eastern US coast at 40^{o}N along a path across the north-east Atlantic (EC-EARTH, GISS-E2-H, MIROC5, NorESM). Even for these models (most pronounced for EC-EARTH) the variability is typically too high around Greenland and North of Iceland. The number of re-emergence events in the GISS-E2-H model was twice that found in observations. With 19 events the incidence of re-emergence in EC-EARTH was close to the upper limit of 15 events used for criterion 2.

In observations, re-emergence was identified to be equally likely to occur following positive or negative winter NAOs. The results show a link between NAO strength and re-emergence after positive and negative NAO winters. For re-emergence following a positive NAO winter, the NAO of that winter is only weakly pronounced. In contrast, re-emergence only occurs after an NAO negative winter when the NAO index of that winter is strongly negative. However, a weakly positive (or strongly negative) NAO is neither a necessary nor a sufficient condition for re-emergence to occur. Several examples were found of strong negative and weak positive NAO states which did not precede re-emergence. Observing the atmospheric state alone does not therefore mean that re-emergence can be predicted. However, the results suggest that re-emergence events that are preceded by a negative (positive) NAO are statistically more likely to coincide with negative (positive) NAO winters meaning that re-emergence increases the chance of predicting the atmospheric state in the second winter.

For the majority of CMIP5 models used in this study (14) the link between re-emergence and negative NAO events is either too weak or too strong. Overall no model meets all the re-emergence criteria established using observations but the EC-EARTH model most closely reproduces the winter mean correlation coefficient, the links between NAO and re-emergence and also has one of the more realistic SST variability structures in the CMIP5 ensemble analysed.

The CMIP5 models present a highly valued resource to climate science research for the understanding of natural variability and future climate change. However, the findings suggest that the majority of the models do not correctly represent re-emergence processes in the North Atlantic and hence are limited in their ability to reproduce the observed variability in oceanic and atmospheric conditions. These limitations restrict the use of most of these models as tools for predicting the probability of extreme winter weather events such as those recently experienced over the European region in the winters of 2009/2010 and 2010/2011. The results suggest that the models which best simulate SST variability over the North Atlantic provide the most reliable simulations of winter weather events associated with re-emergence. Shortcomings in the ability of the models to simulate the observed spatial structure and frequency of SST variability have been identified as a source of deviation from observations (Wang *et al*., 2015).

Recent results based on the latest version of the UK Met Office seasonal forecasting system GloSea5 (MacLachlan *et al*. 2015) show improvements in the skill in predicting the state of the NAO from one winter to the next. Whilst SSTs are not the only determinant of NAO predictability there is evidence from more recent modelling studies (Scaife *et al*., 2014, Dunstone *et al*. 2016) that using higher resolution ocean models provide a more realistic SST

structure in the North Atlantic, which may provide more realistic links between the SST variability, and the NAO.

Chapter 5: North Atlantic SST anomalies and the cold North European weather events of winter 2009/10 and December 2010

This chapter is based on work published in *Buchan et al.* (2014) – see Appendix 1. Whereas the work presented in Chapters 3 and 4 was concerned with establishing if there is a general link between re-emergence and the NAO this chapter provides a case study for a recent cold event that affected Europe in late 2010 with a particular emphasis on if and how re-emergence affected the atmospheric circulation over the North Atlantic region.

5.1 Introduction

Northern Europe experienced two severe winters in succession in 2009 and 2010. December 2009 to February 2010 was ranked as the coldest winter in Western Europe since 1978/79. This was followed by an extremely cold period during December 2010 with the coldest UK December temperatures in over 100 years (http://www.metoffice/gov.uk/climate/uk/dec2010). As stated previously, the leading mode of interannual to decadal variability of the atmosphere over the North Atlantic in winter is the North Atlantic Oscillation (NAO) (Hurrel and Deser, 2009). A number of different mechanisms which could influence the state of the NAO have been proposed. Changes in the rate and location of tropical heating have been shown to influence the atmospheric circulation over the North Atlantic and, in particular, the NAO. Tropical convection, in turn, is sensitive to the underlying SST distribution, which exhibits much more persistence than SST variability in middle latitudes (Hurrel and Deser, 2009). Recent modelling work has shown that the atmospheric response to the re-emerging North Atlantic SST tripole resembles the phase of the NAO that created the SST tripole the previous winter, thereby modestly enhancing the winter-to-winter persistence of the NAO (Cassou *et al.*, 2007, Gastineau and Frankignoul, 2015).

The phases of the NAO are categorised by the variability in sea level pressure (SLP) over the Northern Hemisphere. The NAO index used for this chapter is defined as the normalised difference between mean SLP measured over Portugal and Iceland. The winters of 2009/10 and 2010/11 recorded extreme negative phases of the NAO, with December 2010 seeing the lowest NAO index (-4.62) since December 1996 and the 2nd lowest December value since records began in 1825 (Osborn, 2011). Several mechanisms have been proposed for the anomalously low winter temperatures. These include the teleconnection pattern of the Northern Hemisphere and the El Nino/Southern Oscillation (ENSO) and anomalous Eurasian snow cover (Cohen *et al.*, 2010), anomalous Arctic ice extent (Strey *et al.*, 2010), sudden stratospheric warmings (Fereday *et al.*, 2012) and solar cycle variability (Gray *et al.* 2016). The North Atlantic

experienced anomalous SSTs during these two winters (Taws *et al*., 2011) and these are known to influence atmospheric circulation over northern Europe (Jung *et al*., 2011).

The relationship between fluctuations in North Atlantic SSTs and the strength of the NAO has long been recognised (Bjerknes, 1964, Deser and Blackmon, 1993, Sutton and Allen, 1997, Czaja and Frankignoul, 2002). The patterns of European climate change in the 1990s and 2000s have been linked to the observed warming of the North Atlantic during this period (Hirschi, 2008, Sutton and Dong, 2012). The influence of North Atlantic SST anomalies on the atmospheric circulation over the North Atlantic during winter has been investigated by performing experiments with atmospheric general circulation models (Grötzner *et al*, 1998, Davies *et al*, 1997, Rodwell *et al*., 1999, Robertson *et al*., 2000, Cassou *et al*., 2007, Brayshaw *et al*., 2011). Rodwell *et al*. (1999) used observed SST patterns as surface boundary conditions for a global atmospheric model. On interannual to decadal timescales the simulated temporal evolution of the NAO index was significantly correlated with the observed NAO values. Strong spatial correlations were observed between SST anomalies and surface evaporation with increased (decreased) evaporation in regions of positive (negative) SST anomalies resulting in increased (decreased) mean sea level pressure downstream. Robertson *et al.* (2000) investigated the influence of Atlantic SST anomalies on the atmospheric circulation over the North Atlantic sector during winter by performing experiments with an atmospheric general circulation model. These consisted of a 30-year run with observed SST anomalies for the period 1961-90 confined geographically to the Atlantic Ocean, and a control run with climatological SSTs prescribed globally. Circulation patterns that resemble the positive phase of the NAO became more pronounced in terms of the leading EOF of winter means. Interannual fluctuations in the simulated NAO were found to be significantly correlated with SST anomalies over the tropical and subtropical South Atlantic. The response to North Atlantic SSTs is known to be highly sensitive to the background state (Kushnir *et al*., 2002). Brayshaw *et al*., (2011) identified the importance of changes in SST gradients for understanding the atmospheric response to SST anomalies. In their most recent study the impact of the SST structure in the North Atlantic on the storm track and large-scale atmospheric flow was examined using a hierarchy of GCM simulations. Two key regions of the North Atlantic were identified: a western region with a strong meridional temperature gradient across the Gulf Stream and an eastern region in midlatitudes associated with the North Atlantic Drift. Individually a strong Gulf Stream meridional SST gradient in the western North Atlantic was found to strengthen the downstream storm track while the North Atlantic Drift pattern reduces it. When the combined SST pattern is used their results suggested that the North Atlantic storm track is enhanced.

In contrast to these previous studies the aim of this study is to examine the role played by North Atlantic SSTs on shorter (monthly) timescales. The strength of the feedback from Atlantic SSTs onto the atmospheric circulation is shown to vary by investigating two recent European cold events that both coincided with similarly low NAO values: the winter of 2009/2010 and the early winter of 2010/2011. The sensitivity of the atmospheric circulation over the North Atlantic to observed variations in the North Atlantic SST during the winter of 2009/2010 and the early winter of 2010 is investigated using an ocean-atmosphere model. Observed SST anomalies are applied to the model and the atmospheric responses are analysed. The method is described in section 5.2. Observed SST anomalies and their impact on the atmospheric circulation are described in sections 5.3 and 5.4 and a discussion of the findings and conclusions are given in sections 5.5 and 5.6.

5.2 Method

Observed sea surface temperatures from the NOAA Optimum Interpolation (OI) SST V2 monthly time series (Reynolds and Smith, 1994, Reynolds *et al*., 2002) are used which is derived by linear interpolation of the weekly OI version 2 fields to daily fields then averaged over a month. The analysis uses in situ and satellite SSTs and is produced on a 1°x1° grid. The SST anomalies are obtained by removing the 1981 to 2010 climatology.

The Fast Ocean Rapid Troposphere Experiment (FORTE) climate model (Sinha and Smith, 2002, Blaker *et al*., 2006, Wilson *et al*., 2009, Sinha *et al*., 2012) is used to perform numerical experiments. The FORTE model and its ability to simulate a realistic climate were discussed in detail in Chapter 2 but worthy of note is the absence of a stratosphere in FORTE, which is likely to reduce possible atmospheric teleconnections between the tropical Pacific and the North Atlantic region (Bell *et al*., 2009).

Starting from rest with the Levitus (temperature, salinity) climatology (Levitus and Boyer, 1998, Levitus *et al*., 1998) the model is spun up for 100 years prior to the main experiments. During this period the ocean reaches a quasi-steady state. The model is then run on for an additional 100 years to generate a control simulation for the subsequent experiments. Henceforth, this experiment will be referred to as "CONTROL". For the whole duration of CONTROL the SSTs and the fluxes exchanged daily between the ocean and atmosphere are saved. Every two years a restart file, corresponding to 1 January, is generated which provides a set of 50 different initial atmospheric conditions from where further experiments can be started. Based on the restart files for the atmosphere two sets of 50 x 24-month long experiments are performed. In these ensemble experiments the SSTs are prescribed with no feedback from the atmosphere onto the ocean. The prescribed SSTs consist of the stored SSTs from CONTROL to

which are added the observed SST anomalies from the NOAA-OISST dataset for the 24 months from January 2009 to December 2010. A simulation is also conducted using the unmodified CONTROL SSTs, confirming that the response of the atmosphere is identical to the original and that there was no "decoupling" effect in the simulations. The two ensemble experiments with prescribed SSTs differ in the area over which the observed SST anomalies are applied. In ensemble SSTA observed monthly mean Atlantic SST anomalies covering the Atlantic region from 30°S to 80°N are used. The second ensemble GSSTA repeats the previous experiment using observed global SST anomalies for the same period. The ensembles SSTA and GSSTA allowed the isolation of the influence of North tropical and South Atlantic SST anomalies to establish the main contributor to the atmospheric response.

5.3 Sea Surface Temperature Anomalies winter 2009 and 2010

The global SST anomalies from December 2009 and December 2010 are firstly examined to identify similarities and differences between the two winters (Figure 5.1).

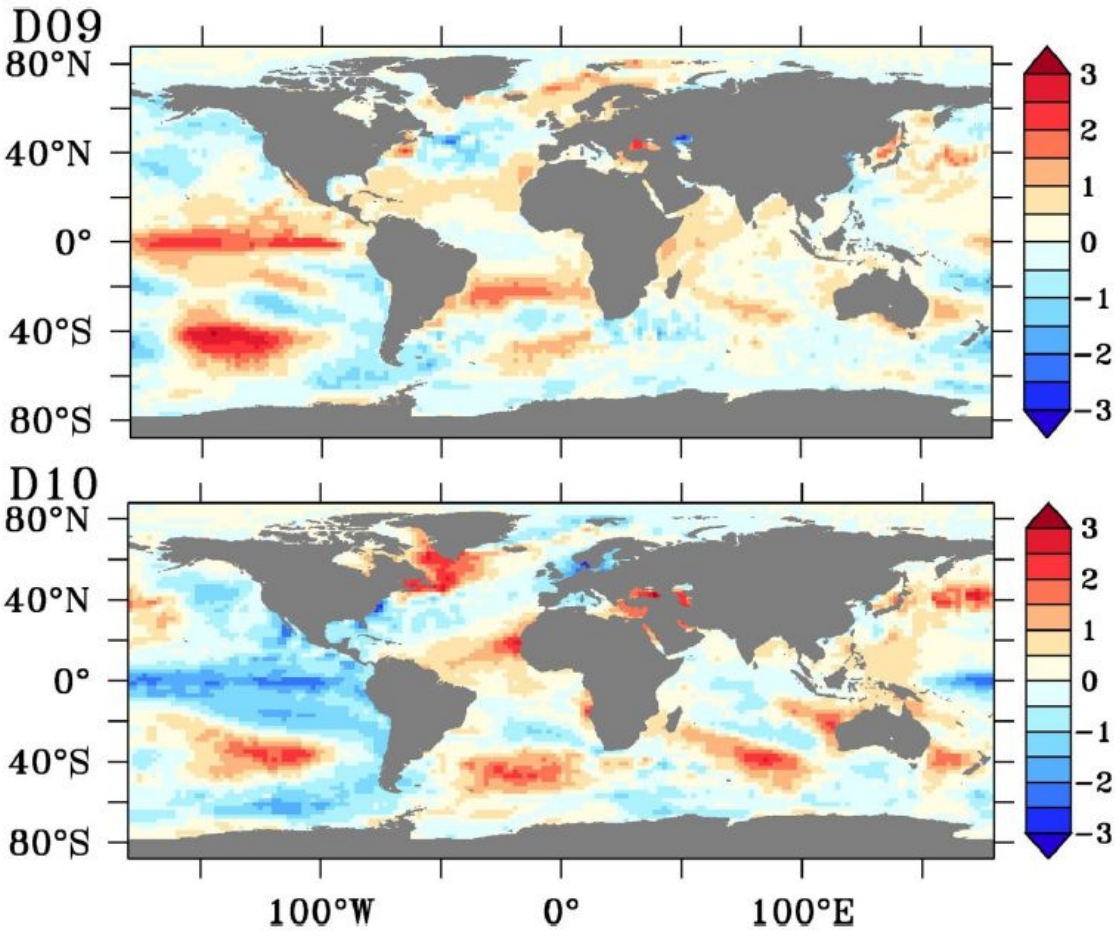

Figure 5.1 Global SST anomalies (°C) from NOAA OI v2 SST data for December 2009 (D09), December 2010 (D10).

Both winters were characterised by a tripole pattern in North Atlantic SST anomalies. Cold anomalies in the mid sub-tropical North Atlantic were flanked by warm anomalies to the south and north. In the Pacific the warm anomalies from an El Niño event (Nino3 index =1.6) in 2009 are replaced by cold anomalies from a La Niña (Nino3 index =-1.5) event in 2010.

A more detailed examination of North Atlantic SST anomalies from December 2009 and December 2010 (Figure 5.2) reveals more pronounced SST anomalies in 2010.

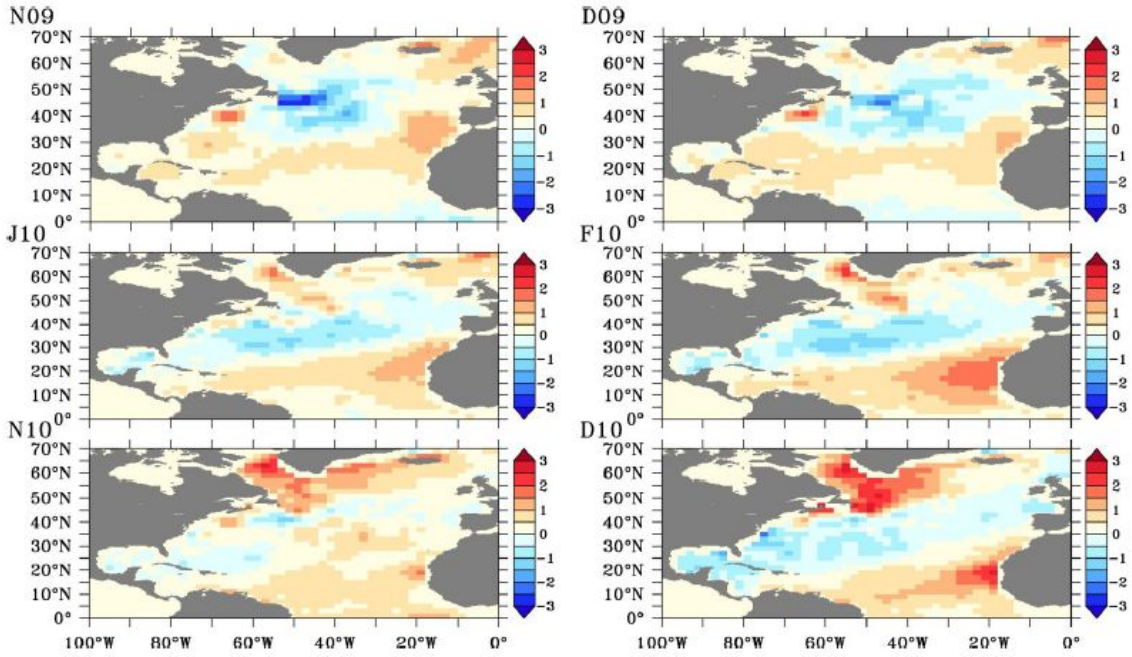

Figure 5.2 North Atlantic SST anomalies (°C) from NOAA OI v2 SST data for November (N09), December 2009 (D09), January (J10), February (F10), November (N10), December 2010 (D10).

Whilst both winters have the characteristic tripole pattern of cold SST anomalies in the central sub-tropical Atlantic between 30°N to 50°N and 70°W to 20°W in 2009, this extends to the west and south in 2010 from 20°N and 80°W. Warm SST anomalies over the Labrador Sea in 2009 intensify and extend south and west in 2010 to 45°N and 30°W. The warm SST anomalies in the south eastern tropical Atlantic extended westward from 20°W to 40°W in 2010.

Part of the cold SST anomaly signal from the winter 2009/10 persisted beneath the seasonal thermocline and the sub-surface anomaly pattern subsequently reemerged during late autumn and early winter 2010 (Taws *et al*., 2011) as clearly seen in panels F10 and D10 of Figure 5.2. Re-emergence is the process whereby ocean temperature anomalies established in a deep winter mixed layer are sequestered beneath the seasonal thermocline in the summer and reappear at the

surface as the mixed layer deepens during the following winter season (Alexander and Deser, 1995).

The developing pattern of North Atlantic SST anomalies in November and December 2010 shows the re-emergence of an enhanced tripole pattern from February 2010 (Taws *et al.*, 2011). The large-scale spatial features reveal cold anomalies of –0.5°C to –1.5°C in the central North Atlantic with warm anomalies to the north and south. The most pronounced changes between December 2010 and December 2009 are seen in the Labrador and Irminger Sea basins with significantly higher temperature anomalies in December 2010 (>1.5°C) whilst negative anomalies in the western subtropical Atlantic (20°N-40°N, 80°W-60°W) are more pronounced (down to -1.5°C). The remote influences of a moderate-to-strong La Nina, developing within the equatorial Pacific in 2010 may have influenced the strength of positive SST anomalies apparent in the tropical Atlantic (Enfield and Mayer, 1997).

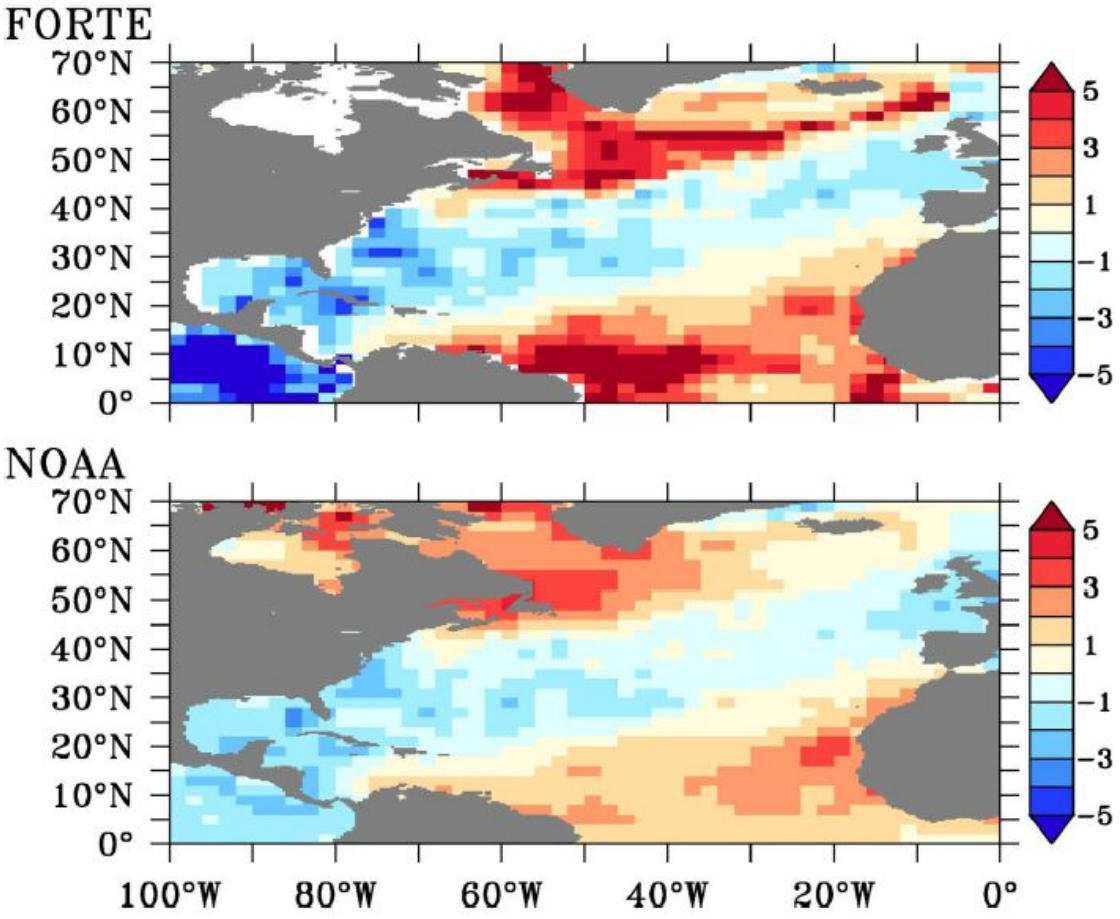

Figure 5.3 The ratio of SST anomalies for December 2010 relative to the standard deviations from the NOAA OI observations (bottom) and FORTE CONTROL ensemble (top).

The SST anomalies in the North Atlantic in December 2010 are significant and were compared to the standard deviations found in both the variability in observed SSTs over a 30-year period (1981-2010) and the free running model. In the Atlantic the SST anomalies were within 3 standard deviations of the variability in observed SSTs over a 30-year period whereas they were within 4 standard deviations of the modelled SSTs over the 100-year CONTROL (Figure 5.3).

5.4 Atmospheric responses to observed SST anomalies

Firstly the atmospheric SLP and surface air temperature (SAT) anomalies occurring during positive and negative NAO phases in CONTROL are described. The impact of SST anomalies on the NAO is then assessed by looking at the differences in SLP and SAT between the SSTA and CONTROL ensembles. The NAO index is calculated from the difference of the normalised SLP between Lisbon, Portugal (9°W, 38°N) and Stykkisholmur, Iceland (22°W, 64°N) (Hurrell and Deser, 2009) for the CONTROL and SSTA ensembles. This is then compared with the distribution and means of the NAO indices for 2009 and 2010 for the CONTROL and SSTA ensembles.

5.4.1 Patterns of Atmospheric Pressure and Surface Atmospheric Temperature

The characteristic SLP and SAT patterns for positive and negative NAO phases in the CONTROL experiment are established by calculating anomalies from the ensemble mean for each month of the 2-year simulations. Initially the patterns of SLP and SAT in the CONTROL ensemble for each 24th month (December of the second simulated year) are examined. The patterns of SLP and SAT anomalies from the CONTROL and SSTA ensembles are grouped into those with NAO indices which were greater than 1 or less than –1. The composite anomalies from the CONTROL and SSTA ensemble based on positive or negative values of the NAO index are computed. The SLP composites are calculated according to:

$$SLPA^{+}_{i,j} = \frac{1}{n}\sum_{l \in l+} SLPA_{i,j} \quad l^{+}, n: \text{ set of time indices and number of NAO+ months,} \qquad (5.1)$$

$$SLPA^{-}_{i,j} = \frac{1}{n}\sum_{l \in l-} SLPA_{i,j} \quad l^{-}, n: \text{: set of time indices and number of NAO- months,} \qquad (5.2)$$

where *i,j* are the zonal and meridional grid cell indices from the FORTE data, and where *l* is index number of the ensemble member.

NAO- responses are characterised by a positive pressure anomaly centred over Iceland and a negative pressure anomaly centred over Portugal. The pressure anomalies are reversed in NAO+

responses (Figure 5.4). The atmospheric circulation patterns from the CONTROL ensemble are reasonably well resolved but model biases are present, which have been previously reported (Wilson *et al*., 2009). Compared with observations the westerly storm track is too broad to the north and extends too far into Europe. However, a comparison of the general structure of the large scale pressure fields from CONTROL and NCEP/NCAR observations showed the locations of the centres of the SLP anomalies from EOF analysis were similar and there was a good correlation between the NAO locations from the CONTROL and observations, as evidenced in Figure 5.4.

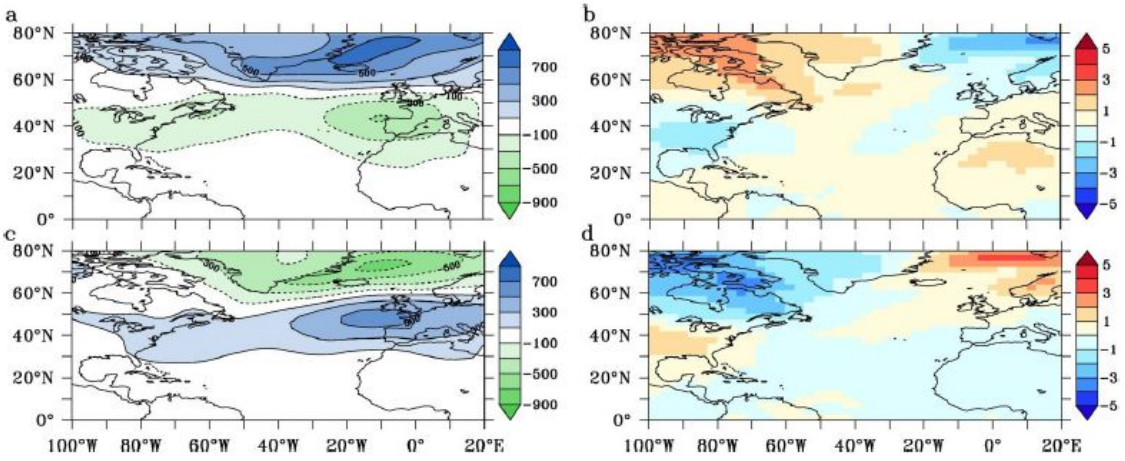

Figure 5.4 Composite SLP anomaly (Pa) (a) and composite SAT anomaly (^{O}C)(b) for December 2010 from CONTROL for NAO negative responses. Composite SLP anomaly (c) and composite SAT anomaly (d) for NAO positive responses.

The NAO surface impacts in the SSTA experiment are stronger than in CONTROL possibly as a result of the size of the SST anomalies lying at the outer bounds of the model variability and because the ensemble sizes are smaller.

In the NAO- state SATs are cooler over the UK and North Western Europe and warmer over South Eastern Europe. In the NAO+ state the polarity is reversed with a warming of SATs over North Western Europe and a cooling over South Eastern Europe. These atmospheric circulation patterns from the CONTROL are used to reference the responses in the SSTA ensemble.

The atmospheric responses from the SSTA ensemble were examined. Initially composites in the 24th month are compared with those from the CONTROL (month 24 in the ensemble is the month that experiences the observed December 2010 SST anomalies) (Figure 5.5).

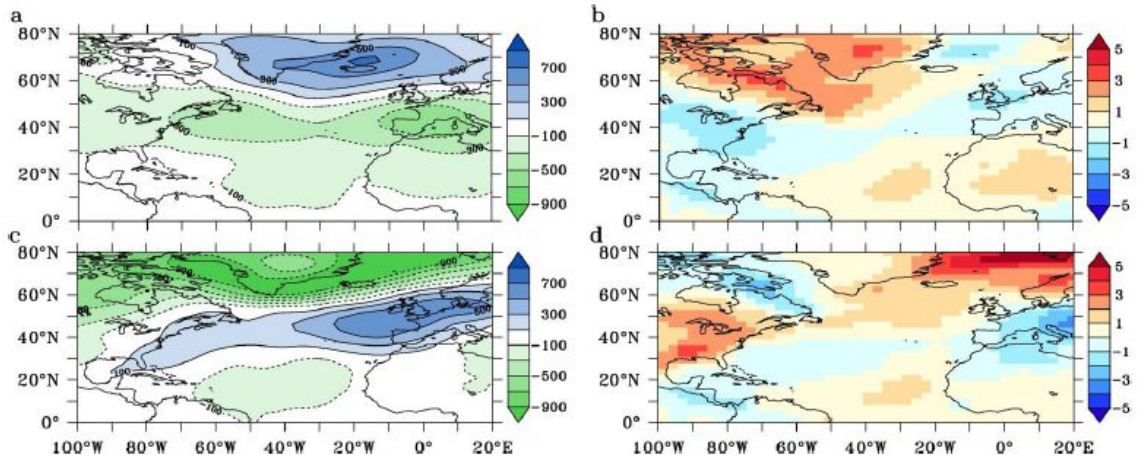

Figure 5.5 Composite SLP anomaly (Pa) (a) and composite SAT anomaly (^{o}C) (b) for December 2010 from SSTA for NAO negative responses. Composite SLP anomaly (c) and composite SAT anomaly (d) for NAO positive responses.

Of the 50 ensemble members of SSTA, 21 exhibit a NAO- state with a positive pressure anomaly over Iceland and a negative pressure anomaly over Lisbon (Figure 5.5a and 5.5b). A NAO+ state is present in 5 cases (Figure 5.5c and 5.5d). The remaining 24 cases produced responses that are NAO neutral, where the index is between –1 and 1. For comparison the distribution in the CONTROL ensemble has 17 negative, 23 positive and 10 neutral cases. The atmospheric circulation patterns for the NAO- members of the SSTA ensemble produced a more widespread cooling of SAT by about 1°C over Western Europe and a more pronounced warming over Greenland. The position of the centres of the temperature anomalies remains similar to that of the CONTROL ensemble. The NAO+ ensemble members show a more pronounced warming of SAT over North Western Europe and cooling over South Eastern Europe.

The NAO+ and NAO- members of the SSTA ensemble also show characteristic differences in atmospheric circulation patterns. NAO+ and NAO- phases are characterised by shifts in the position of the Jet Stream. The position of the Jet Stream from the mean CONTROL atmospheric velocities at 300 hPa geopotential height is centred around 40°N (Figure 5.6a). The influence of the SST anomalies from December 2010 in the NAO- ensemble is to shift the position of the Jet Stream southward with lower velocities over Northern Europe and higher velocities over Southern Europe (Figure 5.6b, c). This shift is consistent with the pressure field for negative phases of the NAO (Rogers, 1996).

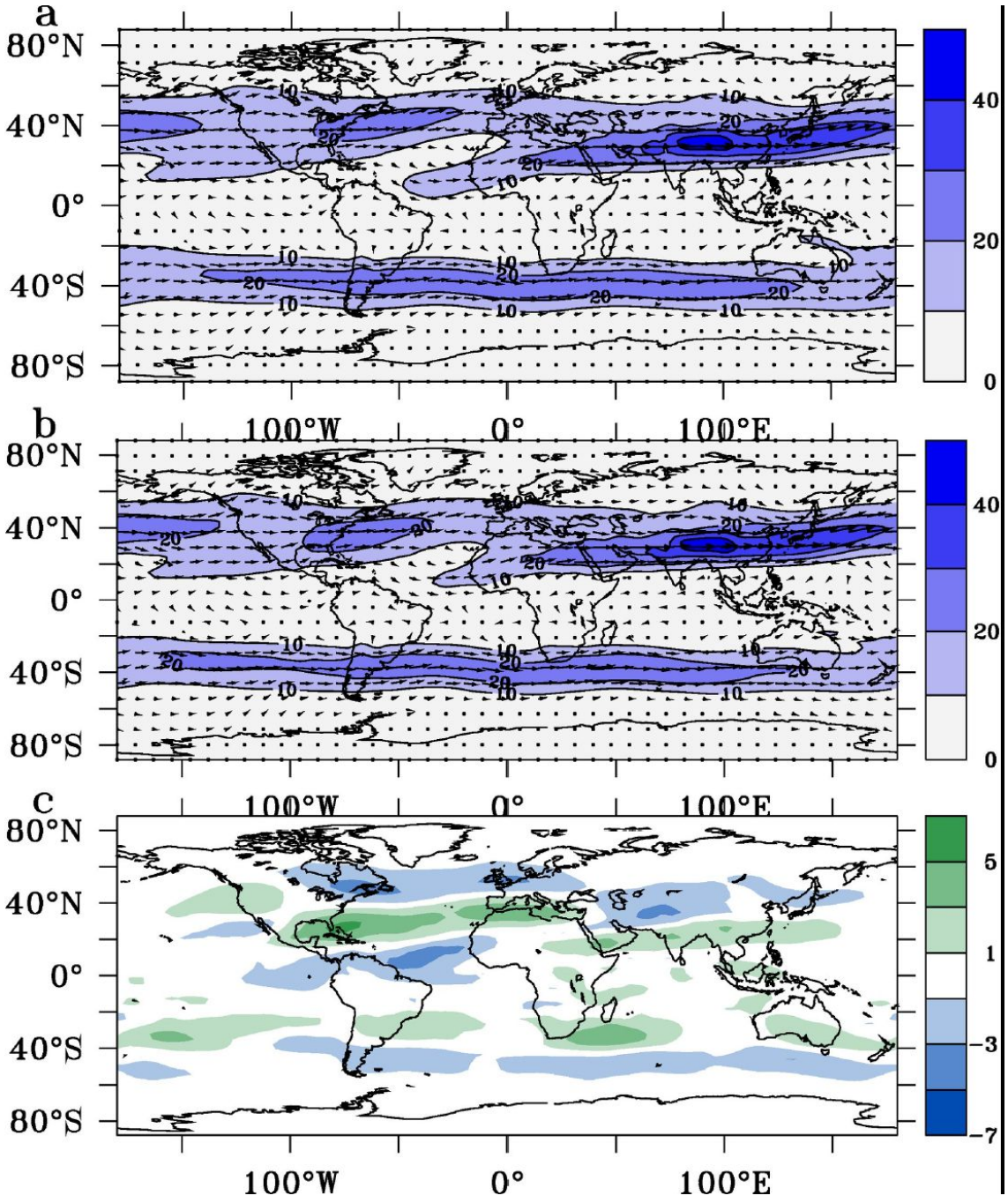

Figure 5.6 (a) Mean CONTROL atmospheric velocities at 300 hPa geopotential height (ms^{-1}) for December 2010 with mean wind speeds superimposed (b) as panel a) for SSTA NAO negative ensemble (c) Difference in atmospheric velocities at 300 hPa between SSTA NAO negative ensemble and CONTROL for December 2010 (ms^{-1}).

The changes in surface heat fluxes between those in the SSTA NAO- ensemble and mean control conditions show the impact of higher SST anomalies in the North Western Atlantic in December 2009 and 2010 (Figure 5.7).

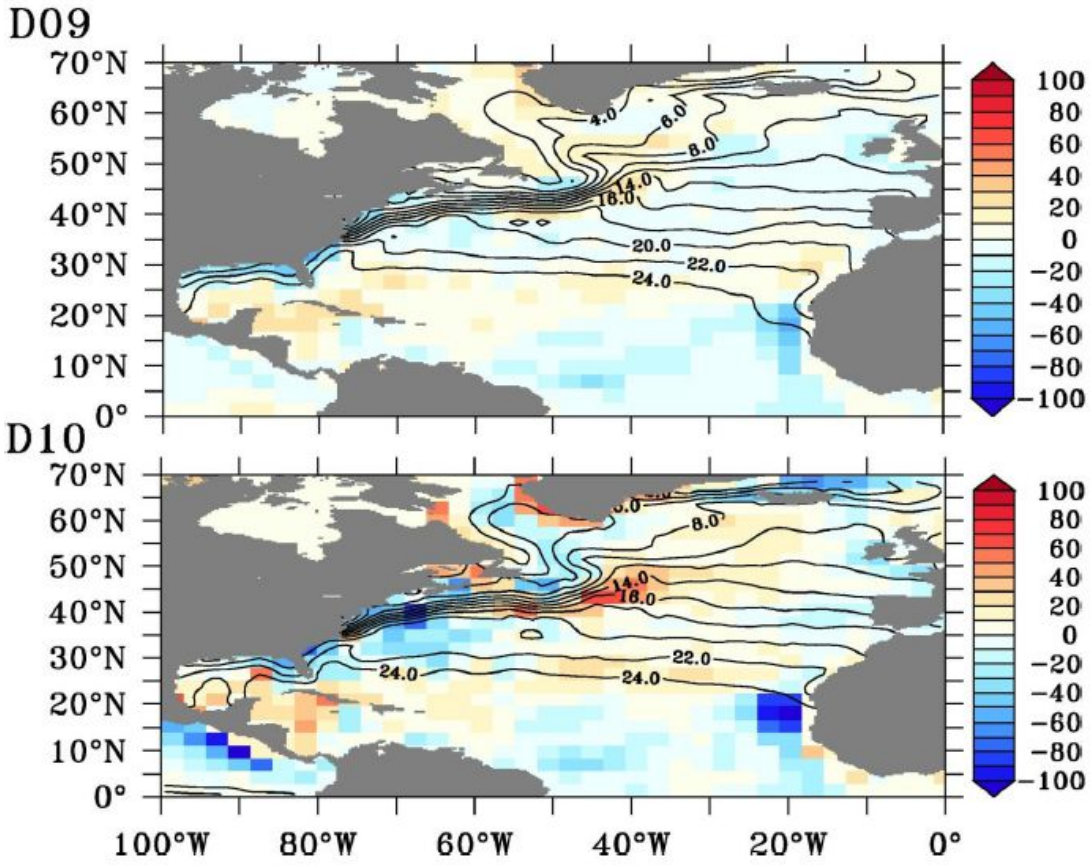

Figure 5.7 Surface upward total heat flux anomalies (wm^{-2}) between SSTA NAO negative ensemble and control mean from December 2009 and December 2010. Contours show SST for December 2009 and December 2010 (^{o}C).

The influence of the SST anomalies in December 2010 compared with December 2009 is particularly significant in the changes in latent heat fluxes to the east of the Labrador/Irminger Sea basins where the positive SST anomalies lead to higher heat loss from the ocean to the atmosphere. The heat flux anomalies in Figure 5.7 lie between the northern two poles in the tripole at 45^{o}N in a region where the SST anomalies collectively most weaken the background meridional SST gradient between northern mid and high latitudes, as can be seen from the SST contours. This is expected to reduce storm activity downstream (consistent with weaker surface baroclinicity) and weaken the surface eddy-driven jet or shift it equator ward (reduced pole ward eddy momentum transport in the upper troposphere and reduced pole ward eddy heat transport in the mid-to-lower troposphere) resulting in the weakening of surface westerlies (Brayshaw *et al*., 2011). This would have the impact of weakening the downstream storm track over the North Atlantic at 45^{o}N and strengthening it at lower latitudes as seen in Figure 5.6.

5.4.2 Frequency in the occurrence of negative NAO indices

The results described in the previous section suggest an increased frequency of NAO- phases for months experiencing the SST anomalies from December 2010 in the ensemble SSTA (21 NAO- responses versus 5 NAO+ responses). However, does this represent a significant shift towards an NAO- state or can a similar response happen by chance? To address this question the extent to which the response of the NAO to SST anomalies is statistically significant and how the level of significance for December 2010 compares to the other 23 months of the 2009 to 2010 period is considered.

The occurrences of atmospheric conditions representative of NAO- phases in the CONTROL and SSTA ensembles are tested by examining the mean NAO indices for a particular month in the 24 month simulation to establish if SST anomalies influence the frequency of atmospheric patterns. The distributions of NAO indices in the 24th month (December 2010) are compared for both the CONTROL and SSTA ensembles. The results indicate a pronounced shift to negative NAO indices in the SSTA ensemble as evidenced by both the ensemble mean and overall distribution (Figure 5.8).

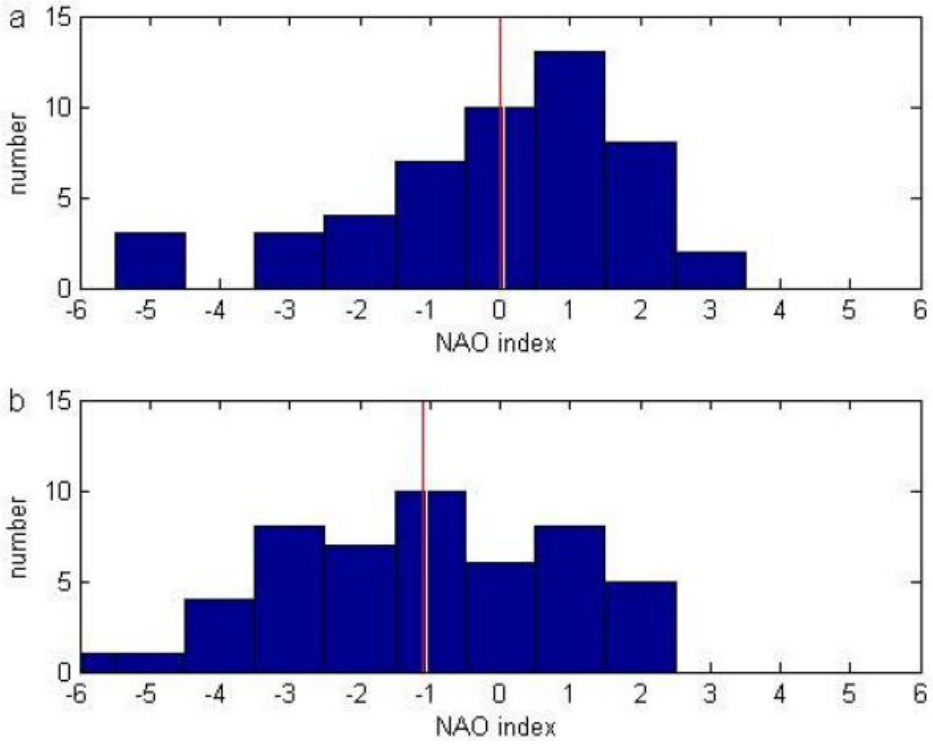

Figure 5.8 Distribution of NAO indices for December 2010 in the CONTROL (a) and SSTA (b) ensembles. Red lines show the ensemble mean.

The CONTROL ensemble has a mean NAO index for month 24 (December 2010) of –0.08 whereas the SSTA ensemble has a mean of –1.1. The SSTA ensemble has 21 outcomes with a mean NAO index less than –1 and only 5 with a mean NAO index greater than +1.

The significance of this result was tested by comparing the mean from the SSTA ensemble against the means of 100,000 random composites of the CONTROL ensemble using 50 samples chosen randomly for December with replacement (Figure 5.9).

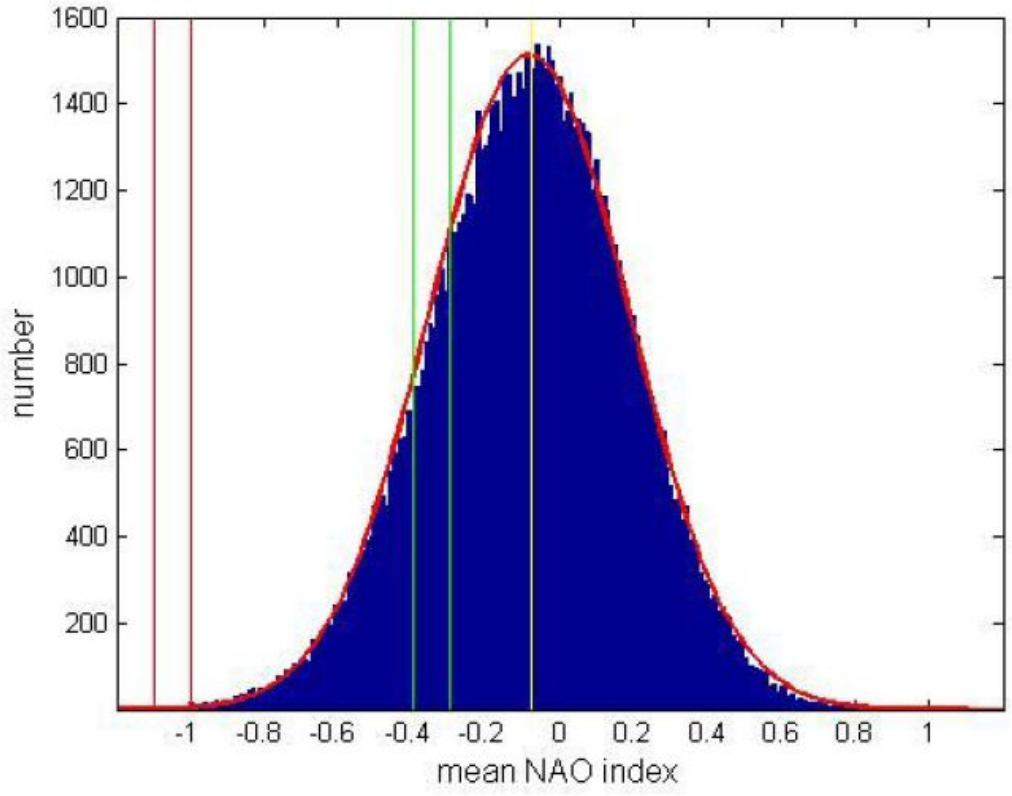

Figure 5.9 Distribution of mean NAO index for December 2010 for 100,000 composites of 50 samples taken randomly from the CONTROL ensemble. CONTROL mean (-0.08) (yellow), SSTA mean November 2010 (-1.0), December 2010 (-1.1) (red), November 2009 (-0.3), December 2009 (-0.4) (green). The distribution calculated from the mean and standard deviation from the CONTROL ensemble for December 2010 is shown in red.

As expected, the means of the NAO taken from the randomly selected composites of the CONTROL ensemble were normally distributed around an NAO index of -0.08. The distribution was further tested using the central limit theorem to create the distribution from the mean and standard deviation from month 24 of the CONTROL ensemble. The result shows good agreement with the distribution from the random composites confirming the two data sets to have the same distribution. Comparing the distribution to the mean NAO index of the SSTA ensemble reveals that the value of –1.1 is significant. A mean NAO index of -1.1 or less would

expect to be found in less than 1 in 1000 randomly chosen 50 member ensembles. The shift towards negative NAO values for December 2010 is statistically significant and very unlikely to have occurred by chance.

A similar level of significance is obtained for the ensemble GSSTA where global SST anomalies are prescribed (mean NAO index of –1.0). However, ENSO teleconnections reliant on the stratosphere are not represented in this model and the contribution of tropical Pacific SST anomalies to a response in the NAO in our experiments cannot be determined.

So far the analysis has concentrated on the NAO response occurring in December 2010. However, pronounced SST anomalies also occurred in other months of the 2009-2010 period (e.g. during the winter of 2009/2010, see Figure 5.2). Is the response found for December 2010 unusual compared to the responses for the other 23 months?

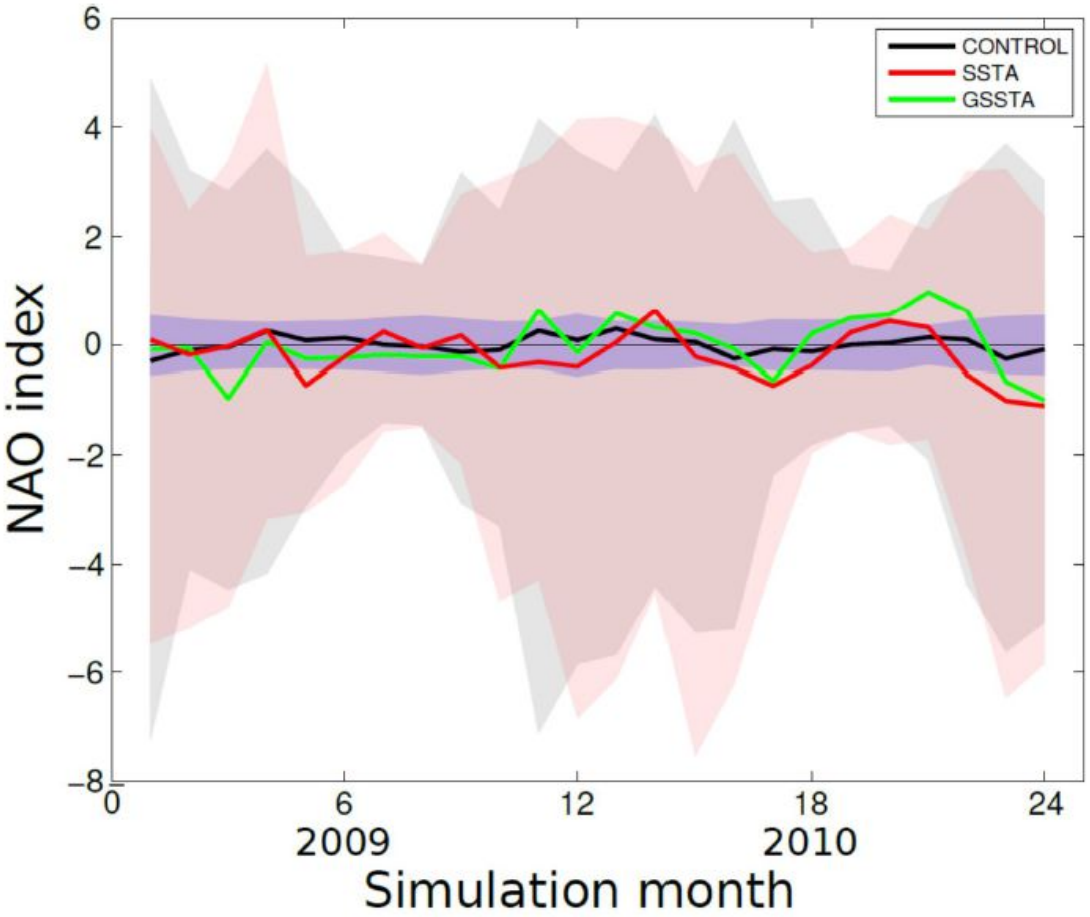

Figure 5.10 Mean monthly NAO indices for CONTROL (black), SSTA (red), GSSTA (green), two standard deviations of monthly mean NAO index sampled randomly from CONTROL (blue). Shaded areas denote the range (maximum and minimum) for each of the 24 months in the CONTROL (black) and SSTA (red) ensembles.

To answer this question the mean monthly NAO indices for every month in the 24-month simulations in the SSTA, GSSTA and CONTROL ensembles are compared (Figure 5.10). The monthly mean of the NAO index in the SSTA and GSSTA ensembles is compared with the corresponding monthly mean found in CONTROL. Even though the NAO extremes for each of the 24 months are similar in the ensembles SSTA and CONTROL the monthly means of the NAO index remain close to 0 in CONTROL. In contrast significant shifts in the NAO index are found for several months in the SSTA and GSSTA ensembles (i.e. shifts in excess of two standard deviations from monthly random composites of the CONTROL ensemble). A weak NAO response is seen in months 11 and 12 (corresponding to November and December 2009) coincident with the first episode of North Atlantic SST anomalies. However, the NAO response is always weaker than for months 23 and 24 (corresponding to November and December 2010) which were both influenced by re-emerging SST anomalies (Taws *et al*., 2011). The negative NAO response for November 2010 is almost as strong as that found for December 2010. This is consistent with the observed values of the NAO index which started its dip toward record low values in November 2010.

Applying observed SST anomalies in experiment SSTA has little impact on the spread of the values of the NAO index (Figure 5.10). As mentioned above the extreme values of the NAO index are similar in CONTROL and SSTA. In addition, for all months the first and third quartiles for the values of the NAO index are comparable in SSTA and CONTROL (and also in GSSTA (not shown)). Both the extreme values of the NAO index and the quartiles show a seasonal cycle with a larger spread of values occurring in winter and spring than in summer and autumn. This reflects the higher atmospheric variability and therefore of the NAO index that characterises the boreal winter season. The similarity in the spread of NAO values in CONTROL and SSTA is a strong indication that the shifts seen for the mean value of the NAO index (Figure 5.10) are not the consequence of increased variability in the NAO index in SSTA compared to CONTROL. In summary, the results suggest that the SST anomalies in November and December 2010 were more conducive to the development of a negative NAO than those in the preceding cold European winter of 2009/2010.

5.5 Dependence of results on ensemble size

The number of ensemble members used in this study is 50 and one question in the design of the experiment using SST anomalies that has not yet been addressed is whether this ensemble size is sufficient to come to robust conclusions. The results discussed above have shown that the average NAO index simulated for December 2010 is -1.1 but the distribution of values (Figure 5.8 bottom, Figure 5.11, top) also show that within the ensemble the NAO index has a wide range of values (-6 to 2.5).

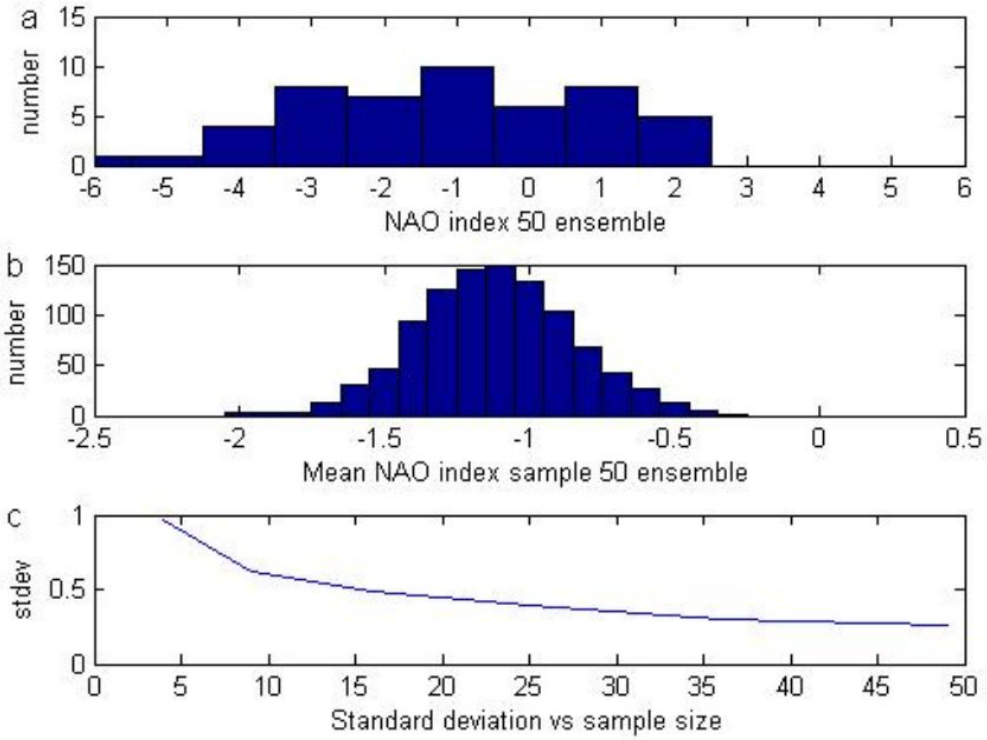

Figure 5.11 Distribution of NAO index from the results of the 50 member ensemble experiment (top). Distribution of mean NAO index from 50 samples selected at random with replacement to generate a population of 1,000 means (middle). Standard deviation of mean NAO index with different ensemble sizes (bottom).

Assessing the significance of the mean of -1.1 can be achieved by randomly sampling the 50 December values in the ensemble with replacement (i.e. by allowing the same value to be selected more than once). Figure 5.11 (middle) shows the distribution of the mean NAO values that are obtained from 1000 random samples of 50 December NAO values. The standard deviation found for the NAO by random selection of 50 Decembers is much smaller (0.28) than the signal of -1.1. This shows that the ensemble size of 50 used here is sufficient and the identified signal of -1.1 for the mean NAO index robust. From 50 the number of randomly selected NAO values is gradually reduced to assess the dependence of the signal to noise ratio on the ensemble size (Figure 5.11, bottom). The results show that the standard deviations gradually increase as the ensemble size is reduced. It is also noticeable that there is initially only a small increase as the ensemble size becomes smaller. Reducing the ensemble size to 25 only increases the standard deviation to 0.37, which would still be small enough for a signal of -1.1 to be statistically significant. It is only when the ensemble size is reduced further that the signal to noise ratio becomes too large to be able to detect a statistically significant signal. It is also evident that an even clearer separation of signal and noise could be achieved by increasing the ensemble size even further. However, for a significant reduction of the standard deviation the

ensemble size would have to be markedly increased. The conclusion reached is that using the ensemble size of 50 is therefore a good compromise between signal to noise ratio and computational cost.

5.6 Discussion and Conclusions

Earlier studies have illustrated that Atlantic SSTs affect the evolution of the NAO on interannual to decadal timescales (e.g. Rodwell *et al*., 1999; Robertson *et al*., 2000). Here in contrast the focus is on shorter (monthly) timescales and the strength of the feedback from Atlantic SSTs onto the atmospheric circulation is shown to vary by investigating two recent European cold events that both coincided with similarly low NAO values: the winter of 2009/2010 and the early winter of 2010/2011. The results suggest that North Atlantic SST anomalies significantly increased the probability of changes in atmospheric circulation affecting Europe in late 2010 but that they had a smaller impact in the preceding winter of 2009/2010. The findings also suggest that the tropical SST anomalies observed in the Pacific are unlikely to have caused the NAO responses observed in the early winter of 2010/2011. Positive SST anomalies in the Labrador/Irminger Sea basins and negative SST anomalies in the subtropical North Atlantic result in changes in the atmospheric pressure structure. The Jet Stream is deflected south giving rise to a band of lower pressure in the Azores around 40^{o}N and high pressure over Iceland resembling a NAO- mode (Rodwell *et al*., 1999).

The absence of a stratosphere in the model limits our ability to model the possible atmospheric teleconnections between the tropical Pacific and the North Atlantic region, although such teleconnections would be expected to operate later in the winter (Bell *et al*, 2009). The SST anomalies experienced in SSTA and GSSTA can be outside the range of the SST variability of CONTROL. This happens as a result of adding the observed SST anomalies to the SSTs of CONTROL which increases the SST variance.

However, this does not affect the main findings. Whilst the applied SST field in ensemble SSTA/GSSTA can be outside the model's natural variability range the use of observed SST anomalies over the 24 month period provides a comparison of the atmospheric responses over that period. The range of variability and distribution of NAO values in SSTA and CONTROL over the 24 months are similar which indicates that the use of observed SST anomalies in the model produce results which are still within the bounds of the natural atmospheric variability of the coupled model (Figure 5.10). The prescribing of observed SST anomalies in un-coupled atmosphere experiments has been used in other studies (e.g. Kushnir *et al*., 2002, Jung *et al*., 2011). Whilst the scale of the SST anomalies could influence the size of the NAO response, the experiments show a larger atmospheric response for November/December 2010 than for any of

the other months of the 2009 to 2010 period. In particular, the study indicates that anomalous SSTs over the North Atlantic region contributed towards forcing the atmosphere towards a negative NAO state in the early winter of 2010/2011.

The results should not be interpreted as the ocean being the sole driver for the extreme cold event in the early winter of 2010/2011. As mentioned earlier, an interesting aspect of the results is the indication that SST anomalies occurring during similarly negative NAO phases (as observed during the cold winter of 2009/2010 and in late 2010) do not necessarily have the same impact on the atmosphere. The strongly NAO- atmospheric circulation pattern that coincided with both periods is itself consistent with the development of an anomalous SST tripole pattern in the North Atlantic (Czaja and Frankignoul, 2002). However, the results suggest that in late 2010 coupled ocean-atmosphere processes over the North Atlantic were particularly important. This is illustrated by the different atmospheric responses found for the winter of 2009/2010 and for late 2010. Both phases coincided with pronounced NAO- phases and an anomalous SST tripole in the North Atlantic. However, in late 2010 the SST anomalies were significantly more pronounced particularly over the Labrador/Irminger Sea basins with anomalous heat flux lying between the northern two poles in the tripole at 45^{o}N weakening the background equator-pole SST gradient. This would be expected to reduce storm activity downstream, weakening the surface eddy-driven jet or shifting it equator-ward and weakening the surface westerlies at this latitude. The stronger NAO responses to November/December 2010 SST anomalies compared to the response found in the winter of 2009/2010 suggest that the conditions in the early winter 2010/2011 were significantly influenced by coupled ocean-atmosphere processes, whereas in 2009/2010 the strong NAO- pattern is more likely to reflect internal variability of the atmosphere with the ocean playing a more passive role.

The work has identified that regional SST anomalies and SST gradients may have been significant in the atmospheric responses. The impact of key regions such as the Labrador Sea and the North Atlantic mid-latitudes to influence atmospheric conditions and identify which areas have the strongest influence on atmospheric conditions was examined. The distribution in NAO results from three 50 member ensemble experiments applying SST anomalies from three different regions, North Atlantic, North Atlantic mid-latitudes and Labrador Sea are shown in Figure 5.12.

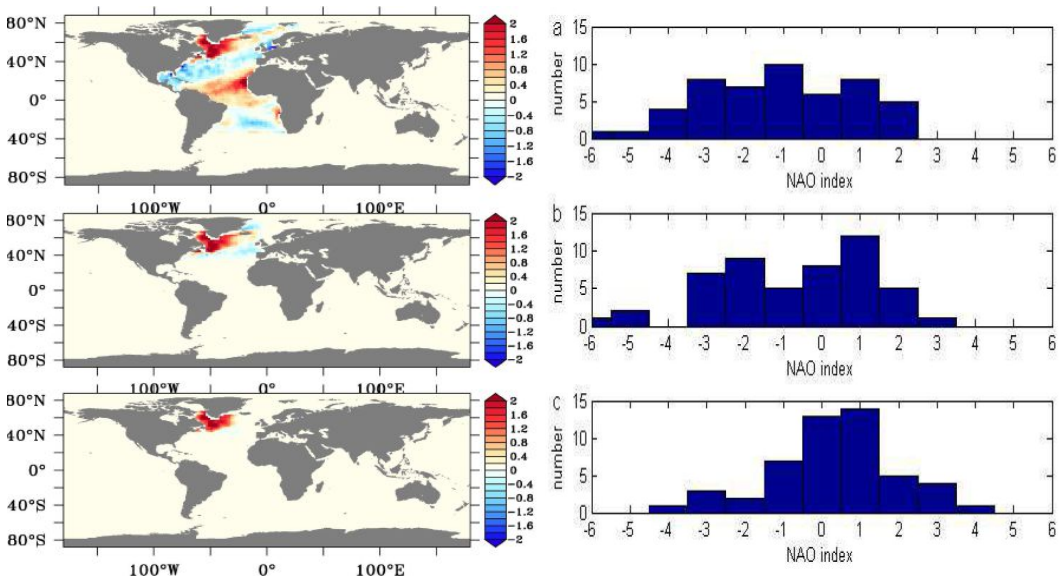

Figure 5.12. The response to three different regions of SST anomalies and the distribution of NAO results from 3 x 50-member ensemble experiments. The SST anomalies are shown on the left for December 2010 for the North Atlantic (top), North Atlantic mid-latitudes (middle) and Labrador Sea (bottom) and the distribution of NAO results from the ensembles on the right when SST anomalies are applied to the whole Atlantic (a), from North Atlantic mid-latitudes northwards (b) and Labrador Sea only (c).

The strongest atmospheric response is found when the whole North Atlantic tripole anomaly is prescribed. However, as shown in Figure 5.12 (middle) removing the southern part of the tripole and prescribing SST anomalies only from the northern mid-latitude onwards only leads to a small weakening of the NAO signal (-0.5) suggesting that the northern part of the tripole is sufficient to recover most of the response. In contrast, no NAO response is found when the SST anomalies are confined to the Labrador Sea. The mean NAO value found in this case is slightly positive (0.4). Given that the Labrador Sea is the region where the largest SST anomalies were observed in December 2010 the absence of an atmospheric response may appear surprising. However, this finding is in line with results from by Brayshaw *et al.*, 2011 who suggest that SST gradients rather than the amplitude of the actual SST values are key to oceanic influence on the atmospheric circulation. By removing the cold SST anomaly that is flanking the warm Labrador Sea anomaly the meridional SST gradient is clearly reduced.

The implication of the results is that the ocean can play an important role in the genesis of certain extreme weather events in the North Atlantic region. The years 2009 and 2010 were particularly interesting from an oceanic point of view. They coincided with observations of a pronounced minimum in the northward transport in the AMOC by the RAPID 26^{o}N array (McCarthy *et al.*, 2012, Rayner *et al.*, 2011) followed by a second minimum in the winter of

2010/2011 (Blaker *et al*., 2015) The AMOC is highly correlated to the oceanic northward transport of heat (Johns *et al*., 2011) and the period of reduced AMOC coincided with a reduction in the North Atlantic Ocean heat content (OHC) in late 2009 (Sonnewald *et al*., 2013). Alongside anomalous Eurasian snow cover (Cohen *et al*, 2010) and anomalous Arctic ice extent (Strey *et al*., 2010, Liu *et al*., 2012), the reduced ocean heat transport may have contributed to the build up of a negative OHC anomaly during the severe winter of 2009/2010 which subsequently re-emerged in the early winter of 2010/2011 (Taws *et al*., 2011).

At this stage the sequence of events described above is speculative. Nevertheless, the evidence presented here indicates that simulations of the NAO are influenced by the pattern of ocean surface temperatures occurring in October to December 2010. The conclusion is that re-emergence of SST anomalies in the North Atlantic contributed towards the development of an SST anomaly pattern, which favoured the persistence of a negative NAO resulting in the cold weather anomaly of December 2010 in Northern Europe.

Chapter 6: Discussion and Conclusions

The primary aim of this thesis was to examine the role played by the North Atlantic Ocean in influencing North Atlantic and European atmospheric circulation using observations (respective reanalyses), output from CMIP5 climate models as well as an in-house GCM (FORTE) which was used to produce simulations. The research objectives focused on the three scientific questions (SQ) introduced in Chapter 1:

SQ1: What can historical records tell us about the influence of the ocean on atmospheric conditions?

SQ2: How good are climate models at simulating extreme North Atlantic winter weather events and the underlying mechanisms?

SQ3: What can model simulations tell us about how ocean conditions may affect atmospheric circulation?

In this chapter the main findings of this thesis are discussed in the context of these scientific questions. In Section 6.1, the main findings from the historical record between the interaction of the ocean and the atmosphere are reviewed. In Section 6.2, the skill of climate models in simulating weather events is considered and in Section 6.3 the role of model simulations in predicting the effect of ocean conditions on atmospheric circulation is discussed. Finally in Section 6.4 the key conclusions from this thesis are summarised.

6.1 What can historical records tell us about the influence of the ocean on atmospheric conditions?

The suggestion that ocean temperature anomalies could actively influence the atmospheric circulation of the North Atlantic and Europe, and be used in monthly and seasonal climate predictions originates from studies by Bjerknes (1964) and Folland *et al*. (1982). Since these studies there have been numerous observation based and statistical analyses supporting the hypothesis that North Atlantic SST anomalies influence atmospheric circulation. The role of SSTA re-emergence on the atmospheric circulation of the North Atlantic has been the subject of several climate studies following the initial identification of the process by Alexander and Deser (1995). Czaja and Frankignoul (2002) examined the mean correspondence between SSTAs and 500 hPa geopotential height anomalies at different lags over an entire year, and revealed evidence of a winter atmospheric response to SSTAs from up to 6 months in advance. This enhanced seasonal predictability of the winter atmospheric circulation was consistent with an

atmospheric response to reemerging SSTAs from the previous spring. In early winter the NAO responds to tripolar SST anomalies amplifying the NAO and acting as a positive feedback (Czaja and Frakignoul, 2002). The conditions for the development of a convective air column from the sea surface to the tropopause frequently occur over all major western boundary currents (Czaja and Blunt, 2011). These frequent occurrences have been shown to be jointly controlled by oceanic advection of warm waters and by atmospheric downward displacement of the tropopause associated with synoptic weather systems. Gastineau and Frankignoul (2015) found that the SST influence is dominated by the Atlantic multidecadal oscillation (AMO). A warm AMO phase leads to an atmospheric warming limited to the lower troposphere in summer, while it leads to a negative phase of the NAO in winter. The winter influence of the AMO is suggested to be primarily forced by the Atlantic SSTs in the northern subtropics. Such influence of the AMO is found in winter instead of early winter because the winter SST anomalies have a larger persistence, because of SST re-emergence.

In Chapter 3, climate observations over the last 140 years were examined to identify patterns in the occurrence of re-emergence and the NAO. The research indicated that there have been 11 re-emergence events occurring during the period 1870 to 2011. Of these 11 events six were preceded by a negative winter mean NAO and five were preceded by a positive winter mean NAO. There appears to be no biases in the number of re-emergence events occurring following a negative or positive winter mean NAO. However, a clear asymmetry was identified in the strength of the NAO signal: Whereas positive NAO winters that precede re-emergence are typically unremarkable a strongly negative index was found for re-emergence events that were preceded by negative NAO winters. The asymmetry in the NAO strength for the first winter resulted in different probabilities for the NAO sign to be repeated in the second winter.

6.2 How good are climate models at simulating extreme North Atlantic winter weather events and the underlying mechanisms?

Quantitative investigation of the effects of re-emergence on the atmospheric circulation of the North Atlantic with coupled ocean-atmosphere model experiments have been undertaken by Mosedale *et al*. (2006) and Cassou *et al*. (2007). Cassou *et al*. (2007) directly quantified a significant wintertime atmospheric response to reemerging remnant ocean temperature anomalies in the North Atlantic. The amplitude of the re-emergence induced response represented 20-25% of the total atmospheric variance and was considered comparable in scale to any other externally forced signal. The nature of the atmospheric response was comparable to the circulation that created the reemerging temperature anomalies the previous winter that is a

winter-to-winter recurrence of the same phase of the NAO. Rodwell and Folland (2012) devised a method of forecasting winter conditions over Europe based on the covariance between North Atlantic SSTA patterns in May and 500 mbar geopotential heights in the following winter. This method formed the basis for operational seasonal forecasting by the UK Met Office. The development of high resolution seasonal forecasting systems (MacLachlan *et al.*, 2014) and improved ocean model resolution (Roberts *et al*., 2016) has lead to significant advances in the forecast skill and reliability in NAO predictions. High levels of prediction skill in the forecasts of the winter NAO have been demonstrated (Scaife *et al*., 2014, Dunstone *et al*., 2016) but some key sources of predictability are still only partially represented and have yet to be resolved.

In Chapter 4, CMIP5 model simulations were examined for the frequency of re-emergence events in the North Atlantic and the link with the NAO that were comparable to those found in observations. The models were assessed against observations using five criteria: the mean winter and summer correlation coefficients for SSTs (1), the number of re-emergence events (2), the number of re-emergence events preceded by NAO- or NAO+ winters (3), asymmetry in winters preceding re-emergence (4) and the influence of reemergent SST anomaly patterns on the NAO state (5).

Most of the analysed models produced a mean summer correlation coefficient (i.e. correlation between March SSTs and the SSTs in the following months of the same year) higher than the winter mean suggesting that the winter mean could reflect persistence. The number of winters when the maximum re-emergence correlation coefficient exceeded 0.5 and the ratio between the summer mean and winter mean correlation coefficients was less than 0.7 varied considerably, with most of the models producing a re-emergence frequency higher than observed. None of the models simulated the asymmetry between the strength of the NAO index for positive and negative NAO winters preceding re-emergence seen in observations, and only a few cases were found where re-emergence affected the NAO state for both first and second winters of a re-emergence event. The most statistically significant impact on the NAO was found in the CanESM2 model but the link between NAO and re-emergence was too strong in this model. Although not statistically significant the most realistic model for criterion 5 appeared to be EC-EARTH. This was the only model for which the NAO average of all preceding winters was clearly negative and where NAO- in the first winter was on average followed by NAO- in the second winter.

Overall the CMIP5 models examined in this thesis failed to reproduce the patterns seen in observations and no model fulfilled all the criteria. Some models simulated a realistic number of re-emergence events but there was no overlap between that group of models and the models that simulated a realistic link between re-emergence and the state of the NAO. The majority of the

CMIP5 models produced higher SST variability in the North Atlantic compared with observations and simulated too strongly localised patterns of SST variability. Only four models produced a spatial pattern similar to that found in observations, and even for these models the variability was typically too high around Greenland and North of Iceland.

6.3 What can model simulations tell us about how ocean conditions may affect atmospheric circulation?

The re-emergence event of 2010/11 (Taws *et al*., 2011) was followed by the return of extremely cold conditions over Northern Europe during December 2010- January 2011, following an extreme cold weather event in the previous winter of December 2009-February 2010 (Osborn, 2011). The severe weather experienced over Northern Europe in December 2010-January 2011 was associated with an extreme negative phase of the NAO (Maidens *et al*., 2013). Many factors could have contributed to the winter atmospheric circulation in that year (Jung *et al*., 2011), such as the teleconnection pattern of the Northern Hemisphere and the El Nino/Southern Oscillation (ENSO, Bell *et al*., 2009), anomalous Eurasian snow cover (Cohen *et al*., 2010), anomalous Arctic ice extent (Strey *et al*., 2010) and sudden stratospheric warmings (Fereday *et al*., 2012). Where pairs of events have occurred in consecutive years the atmospheric conditions during the first winter have been found to correspond to a strongly negative Arctic Oscillation index (Blaker *et al*., 2015). Atmospheric conditions during the second winter were found to be indicative of a more regional negative NAO phase, and this persistence is suggested to be linked to re-emergence of SST anomalies in the North Atlantic for the events of 2009/10 and 1969/70 (Blaker *et al*., 2015). The influence of the ocean through the reoccurrence of SST anomalies was the subject of Chapter 5.

A sudden shift in the monthly NAO index toward more extreme negative values (of –4.62 in December 2010) occurred during the 2010 re-emergence event. The timing of this NAO shift suggests that the occurrence of re-emergence might have provided an impetus for a more extreme atmospheric response than otherwise expected. Specifically the reemerging temperature anomalies may have projected on the overlying atmospheric circulation via transient eddy fluxes and through the emergence of teleconnection patterns that subsequently influenced the return of an extreme negative NAO. The impact of re-emergence on the North Atlantic climate system is widely supported throughout the literature in the statistical analysis of Czaja and Frankignoul (2002), Kushnir *et al.* (2002), Rodwell and Folland (2002), Cassou *et al*., (2007) and Gastineau and Frankignoul (2015). Cassou *et al*., (2007) directly quantified a significant winter atmospheric response to reemerging ocean temperature anomalies in the North Atlantic in coupled ocean-atmosphere experiments.

In Chapter 5, the results from a coupled model forced with the pattern of reemerging SSTAs from the 2010 event (Taws *et al*., 2011) revealed evidence for an ocean-forced NAO shift towards more extreme negative values in December 2010 (Buchan *et al*., 2014). The results suggest that North Atlantic SST anomalies significantly increased the probability of changes in atmospheric circulation affecting Europe in late 2010 but that they had a smaller impact in the preceding winter of 2009/2010. This would indicate that SST anomalies occurring during similarly negative NAO phases do not necessarily have the same impact on the atmosphere. The strongly NAO- atmospheric circulation pattern that coincided with both periods is itself consistent with the development of an anomalous SST tripole pattern in the North Atlantic (Czaja and Frankignoul, 2002, Gastineau and Frankignoul, 2015). However, the results suggest that in late 2010 coupled ocean-atmosphere processes over the North Atlantic were particularly important. This was illustrated by the different atmospheric responses found for the winter of 2009/2010 and for late 2010. The pronounced NAO- phases and an anomalous SST tripole in the North Atlantic coincided with observations of a pronounced minimum in the northward transport in the AMOC by the RAPID 26^{o}N array in the winter 2009/2010 followed by a second minimum in the winter of 2010/2011 (Blaker *et al*., 2015). The stronger NAO responses to November/December 2010 SST anomalies compared to the response found in the winter of 2009/2010 suggest that the conditions in the early winter 2010/2011 were significantly influenced by coupled ocean-atmosphere processes, whereas in 2009/2010 the strong NAO- pattern is more likely to reflect internal variability of the atmosphere with the ocean playing a more passive role.

6.4 Conclusions

This thesis has provided an examination of the role played by the North Atlantic Ocean in influencing North Atlantic and European winter atmospheric circulation from observations (respectively reanalyses), output from CMIP5 climate models and an in house GCM (FORTE) which was used to produce simulations. It has provided quantitative evidence of an ocean forced NAO shift towards more extreme negative values in December 2010. Statistical techniques have been used to examine the pattern of occurrences of re-emergence and positive and negative NAO events over the last 140 years (1871-2011) from observations to understand the historical relationship between the ocean and atmosphere. These were compared with CMIP5 historical ensemble model output (1850-2005) to evaluate the skill of these models in simulating changes in the Earth's climate through the twentieth and twenty-first centuries. The key conclusions from this thesis are summarised as follows:

The evidence from the simulation study presented in Chapter 5 indicates the NAO was influenced by the pattern of ocean surface temperatures occurring in October to December 2010. The conclusion is that re-emergence of SST anomalies in the North Atlantic contributed towards the development of an SST anomaly pattern, which favoured the persistence of a negative NAO resulting in the cold weather anomaly of December 2010 in Northern Europe. The implication of the results from this study is that the ocean can play an important role in the genesis of extreme winter weather events in the North Atlantic region.

The analysis of historical observations revealed that re-emergence is equally likely to occur following positive or negative winter NAOs. The results have shown a link between NAO strength and re-emergence after positive and negative NAO winters. When re-emergence follows a positive NAO winter, the NAO of the following winter is only weakly pronounced. In contrast re-emergence only occurs after an NAO negative winter when the NAO index of that winter is strongly negative. The implication is that observing the atmospheric state alone is insufficient to predict that re-emergence could occur. However the occurrence of a re-emergence event increases the chance of predicting the atmospheric state in the second winter.

The analysis of the CMIP5 model output suggests that the majority of the models do not correctly represent re-emergence processes in the North Atlantic and are limited in their ability to reproduce the variability in oceanic and atmospheric conditions seen in observations. These limitations restrict the use of most of these models as tools for predicting the probability of extreme winter weather events. The results suggest that the models which best simulate SST variability over the North Atlantic provided the most reliable simulations of winter weather events associated with re-emergence. Links between re-emergence and the atmospheric conditions over the North Atlantic have been the subject of considerable scientific investigation. Historical observations reveal that potential re-emergence events cannot be predicted from the atmospheric state alone and that the majority of CMIP5 models do not correctly represent re-emergence processes in the North Atlantic. Prediction of re-emergence events linked with a negative NAO which can be associated with severe climate conditions over North Western Europe is still uncertain. However, there is evidence from more recent modelling studies (Scaife *et al*., 2014, Dunstone *et al*., 2016) that using higher resolution ocean models provides a more realistic SST structure in the North Atlantic and more realistic links between the SST variability, and the NAO and that long-range prediction of European and North American winters is now possible. Whilst this thesis has identified factors which point to the likely timing of these events improving our ability to predict them remains a significant challenge.

Appendix 1

North Atlantic SST Anomalies and the Cold North European Weather Events of Winter 2009/10 and December 2010

JIAN BUCHAN, JOËL J.-M. HIRSCHI, ADAM T. BLAKER, AND BABLU SINHA

National Oceanography Centre, Southampton, United Kingdom

(Manuscript received 28 March 2013, in final form 18 September 2013)

ABSTRACT

Northern Europe experienced consecutive periods of extreme cold weather in the winter of 2009/10 and in late 2010. These periods were characterized by a tripole pattern in North Atlantic sea surface temperature (SST) anomalies and exceptionally negative phases of the North Atlantic Oscillation (NAO). A global ocean–atmosphere general circulation model (OAGCM) is used to investigate the ocean's role in influencing North Atlantic and European climate. Observed SST anomalies are used to force the atmospheric model and the resultant changes in atmospheric conditions over northern Europe are examined. Different atmospheric responses occur in the winter of 2009/10 and the early winter of 2010. These experiments suggest that North Atlantic SST anomalies did not significantly affect the development of the negative NAO phase in the cold winter of 2009/10. However, in November and December 2010 the large-scale North Atlantic SST anomaly pattern leads to a significant shift in the atmospheric circulation over the North Atlantic toward a NAO negative phase. Therefore, these results indicate that SST anomalies in November/December 2010 were particularly conducive to the development of a negative NAO phase, which culminated in the extreme cold weather conditions experienced over northern Europe in December 2010.

1. Introduction

Northern Europe experienced two severe winters in succession in 2009 and 2010. December 2009 to February 2010 was ranked as the coldest winter in western Europe since 1978/79. This was followed by an extremely cold period during December 2010 with the coldest U.K. December temperatures in over 100 years (see http://www.metoffice.gov.uk/climate/uk/2010/december.html). The leading mode of interannual to decadal variability of the atmosphere over the North Atlantic in winter is the North Atlantic Oscillation (NAO; Hurrell and Deser 2009). The NAO defines the distribution of atmospheric mass between the Arctic and the subtropical Atlantic and swings from positive (NAO+) to negative (NAO−) producing large changes in surface air temperatures, storm-track position, and precipitation over the North Atlantic and western Europe. Two other winter climate regimes that display strong anticyclonic ridges over Scandinavia (the "blocking" regime) and off western Europe (the "Atlantic Ridge" regime) are also possible (Hurrell and Deser 2009). A number of different mechanisms that could influence the state of the NAO have been proposed. Changes in the rate and location of tropical heating have been shown to influence the atmospheric circulation over the North Atlantic and, in particular, the NAO. Tropical convection, in turn, is sensitive to the underlying SST distribution, which exhibits much more persistence than SST variability in midlatitudes (Hurrell and Deser 2009). Recent modeling work has shown that the atmospheric response to the reemerging North Atlantic SST tripole resembles the phase of the NAO that created the SST tripole the previous winter, thereby modestly enhancing the winter-to-winter persistence of the NAO (Cassou et al. 2007).

The phases of the NAO are categorized by the variability in sea level pressure (SLP) over the Northern Hemisphere. The NAO index is defined as the normalized difference between mean SLP measured over Portugal and Iceland. The winters of 2009/10 and 2010/11 recorded extreme negative phases of the NAO, with December 2010 seeing the lowest NAO index (−4.62) since December 1996 and the second lowest December value since records began in 1825 (Osborn 2011). Several mechanisms have been proposed for the anomalously

Corresponding author address: Jian Buchan, National Oceanography Centre, European Way, Southampton SO14 3ZH, United Kingdom.
E-mail: jrb1g10@soton.ac.uk

DOI: 10.1175/MWR-D-13-00104.1

Appendix 1

low winter temperatures. These include the teleconnection pattern of the Northern Hemisphere and El Niño–Southern Oscillation (ENSO) and anomalous Eurasian snow cover (Cohen et al. 2010), anomalous Arctic sea ice extent (Strey et al. 2010), and sudden stratospheric warmings (Fereday et al. 2012). The North Atlantic experienced anomalous SSTs during these two winters (Taws et al. 2011) and these are known to influence atmospheric circulation over northern Europe (Cassou et al. 2007).

The relationship between fluctuations in North Atlantic SSTs and the strength of the NAO has long been recognized (Bjerknes 1964; Deser and Blackmon 1993; Sutton and Allen 1997; Czaja and Frankignoul 2002). The patterns of European climate change in the 1990s and 2000s have been linked to the observed warming of the North Atlantic during this period (Hirschi 2008; Sutton and Dong 2012). The influence of North Atlantic SST anomalies on the atmospheric circulation over the North Atlantic during winter has been investigated by performing experiments with atmospheric general circulation models (Grötzner et al. 1998; Davies et al. 1997; Rodwell et al. 1999; Robertson et al. 2000; Cassou et al. 2007; Brayshaw et al. 2011). Rodwell et al. (1999) used observed SST patterns as surface boundary conditions for a global atmospheric model. The simulated temporal evolution of the NAO index was significantly correlated with the observed NAO values especially on interannual-to-decadal time scales. Strong spatial correlations were observed between SST anomalies and surface evaporation with increased (decreased) evaporation in regions of positive (negative) SST anomalies resulting in increased (decreased) mean sea level pressure downstream. Robertson et al. (2000) investigated the influence of Atlantic SST anomalies on the atmospheric circulation over the North Atlantic sector during winter by performing experiments with an atmospheric general circulation model. These consisted of a 30-yr run with observed SST anomalies for the period 1961–90 confined geographically to the Atlantic Ocean, and a control run with climatological SSTs prescribed globally. Circulation patterns that resemble the positive phase of the NAO became more pronounced in terms of the leading EOF of winter means. Interannual fluctuations in the simulated NAO were found to be significantly correlated with SST anomalies over the tropical and subtropical South Atlantic. The response to North Atlantic SSTs is known to be highly sensitive to the background state (Kushnir et al. 2002). Brayshaw et al. (2011) identified the importance of changes in SST gradients for understanding the atmospheric response to SST anomalies. In their most recent study the impact of the SST structure in the North Atlantic on the storm track and large-scale atmospheric flow was examined using a hierarchy of GCM simulations. Two key regions of the North Atlantic were identified: a western region with a strong meridional temperature gradient across the Gulf Stream and an eastern region in midlatitudes associated with the North Atlantic Drift. Individually a strong Gulf Stream meridional SST gradient in the western North Atlantic was found to strengthen the downstream storm track while the North Atlantic Drift pattern reduces it. When the combined SST pattern is used their results suggested that the North Atlantic storm track is enhanced.

In contrast to these previous studies the aim of the present study is to examine the role played by North Atlantic SSTs on shorter (monthly) time scales. We show that the strength of the feedback from Atlantic SSTs onto the atmospheric circulation can vary by investigating two recent European cold events that both coincided with similarly low NAO values: the winter of 2009/10 and the early winter of 2010/11. We investigate the sensitivity of the atmospheric circulation over the North Atlantic to observed variations in the North Atlantic SST during the winter of 2009/10 and the early winter of 2010 using an ocean–atmosphere model. Observed SST anomalies are applied to the model and the atmospheric responses are analyzed. The method is described in section 2. Observed SST anomalies and their impact on the atmospheric circulation are described in sections 3 and 4 and a discussion of our findings and conclusions are given in section 5.

2. Method

We use observed sea surface temperatures from the National Oceanic and Atmospheric Administration (NOAA) optimum interpolation (OI) SST V2 monthly time series (Reynolds and Smith 1994; Reynolds et al. 2002), which is derived by linear interpolation of the weekly OI version 2 fields to daily fields then averaged over a month. The analysis uses in situ and satellite SSTs and is produced on a $1° \times 1°$ grid. The SST anomalies that form the basis of our study are obtained by removing the 1981–2010 climatology.

We employ the Fast Ocean Rapid Troposphere Experiment (FORTE) climate model (Sinha and Smith 2002; Blaker et al. 2006; Wilson et al. 2009; Sinha et al. 2012) to perform our numerical experiments. The ocean component of FORTE contains a simple sea ice model and has a horizontal resolution of $2° \times 2°$ and 15 z-coordinate layers in the vertical. The model uses the mixing parameterization of Gent and McWilliams (1990). The atmospheric component consists of a T42 spectral atmosphere corresponding to a horizontal resolution of

approximately 2.8° × 2.8° and has 15 sigma levels. Both the ocean and the atmospheric components are based on the primitive equations. Coupling between the ocean and atmosphere occurs daily via the Ocean Atmosphere Sea Ice Soil (OASIS; Valcke et al. 2000) coupler. The absence of a stratosphere in FORTE is likely to reduce possible atmospheric teleconnections between the tropical Pacific and the North Atlantic region (Bell et al. 2009).

Starting from rest with the Levitus (temperature, salinity) climatology (Levitus and Boyer 1998; Levitus et al. 1998) the model is spun up for 100 years prior to the main experiments. During this period the ocean reaches a quasi–steady state. The model is then run on for an additional 100 years to generate a control simulation for the subsequent experiments. Henceforth, this experiment will be referred to as "CONTROL." For the whole duration of CONTROL we save the SSTs and the fluxes exchanged daily between the ocean and atmosphere. Every two years a restart file, corresponding to 1 January, is generated that provides us with a set of 50 different initial atmospheric conditions from where we can start further experiments. Based on the restart files for the atmosphere we then perform two sets of 50 24-month-long experiments. In these ensemble experiments the SSTs are prescribed with no feedback from the atmosphere onto the ocean. The prescribed SSTs consist of the stored SSTs from CONTROL to which we add the observed SST anomalies from the NOAA OISST dataset for the 24 months from January 2009 to December 2010. We also conducted a simulation using the unmodified CONTROL SSTs, confirming that the response of the atmosphere is identical to the original and that there was no "decoupling" effect in the simulations. The two ensemble experiments with prescribed SSTs differ in the area over which we apply observed SST anomalies. In ensemble SSTA we use observed monthly mean Atlantic SST anomalies covering the Atlantic region from 30°S to 80°N. The second ensemble GSSTA repeats the previous experiment using observed global SST anomalies for the same period. The ensembles SSTA and GSSTA allow us to isolate the influence of North Atlantic SST anomalies and to establish if they were the main contributor to the atmospheric response.

3. Sea surface temperature anomalies winter 2009 and 2010

The global SST anomalies for December 2009 and December 2010 are first examined to identify similarities and differences between the two winters (Fig. 1). Both winters were characterized by a tripole pattern in North Atlantic SST anomalies. Cold anomalies in the

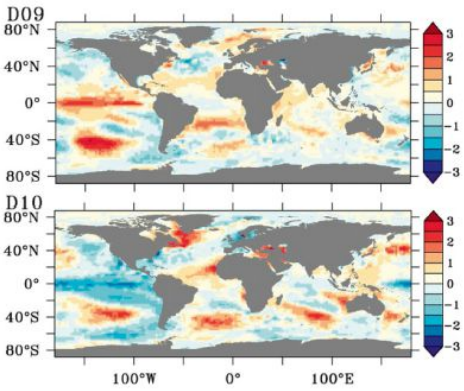

FIG. 1. Global SST anomalies (°C) from NOAA OI v2 SST data for (top) December 2009 (D09) and (bottom) December 2010 (D10).

mid-subtropical North Atlantic were flanked by warm anomalies to the south and north. In the Pacific the warm anomalies from an El Niño event (Niño-3 index = 1.6) in 2009 are replaced by cold anomalies from a La Niña (Niño-3 index = −1.5) event in 2010.

A more detailed examination of North Atlantic SST anomalies for December 2009 and December 2010 (Fig. 2) reveals more pronounced SST anomalies in 2010. While both winters have the characteristic tripole pattern of cold SST anomalies in the central Atlantic between 30° and 50°N and between 70° and 20°W in 2009, this extends to the west and south in 2010 from 20°N, 80°W. Warm SST anomalies over the Labrador Sea in 2009 intensify and extend south and west in 2010 to 45°N, 30°W. The warm SST anomalies in the southeastern tropical Atlantic extended westward from 20° to 40°W in 2010.

Part of the cold SST anomaly signal from the winter 2009/10 persisted beneath the seasonal thermocline and the subsurface anomaly pattern subsequently reemerged during late autumn and early winter 2010 (Taws et al. 2011) as clearly seen in panels F10 and D10 of Fig. 2. Reemergence is the process whereby ocean temperature anomalies established in a deep winter mixed layer are sequestered beneath the seasonal thermocline in the summer and reappear at the surface as the mixed layer deepens during the following winter season (Alexander and Deser 1995).

The developing pattern of North Atlantic SST anomalies in November and December 2010 shows the reemergence of an enhanced tripole pattern from February 2010 (Taws et al. 2011). The large-scale spatial features reveal cold anomalies of −0.5° to −1.5°C in the central North Atlantic with warm anomalies to the north and

Appendix 1

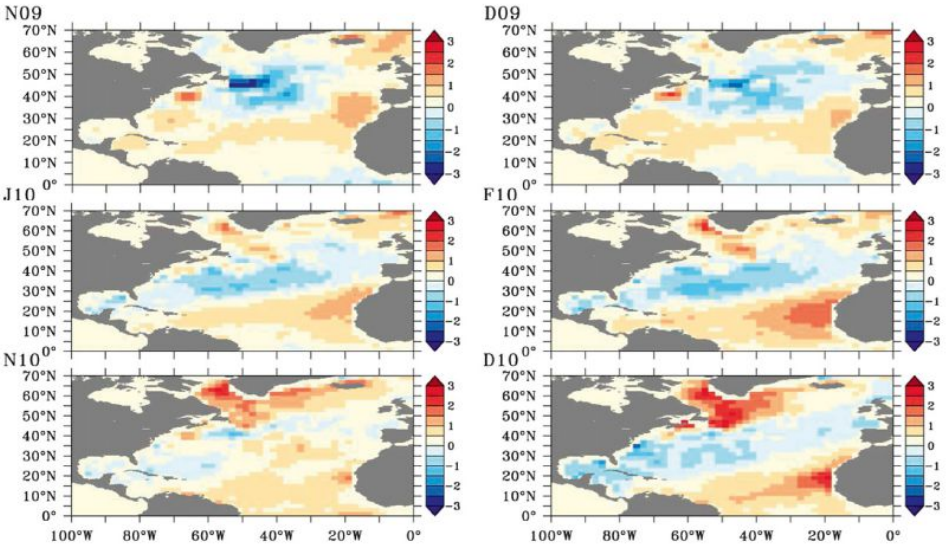

FIG. 2. North Atlantic SST anomalies (°C) from NOAA OI v2 SST data for November 2009 (N09), December 2009 (D09), January 2010 (J10), February 2010 (F10), November 2010 (N10), and December 2010 (D10).

south. The most pronounced changes between December 2010 and December 2009 are seen in the Labrador and Irminger Sea Basins with significantly higher temperature anomalies in December 2010 (>1.5°C) while negative anomalies in the western subtropical Atlantic (20°–40°N, 80°–60°W) are more pronounced (down to −1.5°C). The remote influences of a moderate-to-strong La Niña, developing within the equatorial Pacific in 2010 may have influenced the strength of positive SST anomalies apparent in the tropical Atlantic (Enfield and Mayer 1997).

The SST anomalies in the North Atlantic in December 2010 are significant and were compared to the standard deviations found in both the variability in observed SSTs over a 30-yr period (1981–2010) and the free-running model. In the Atlantic the SST anomalies were within three standard deviations of the variability in observed SSTs over a 30-yr period whereas they were within four standard deviations of the modeled SSTs over the 100-yr CONTROL (Fig. 3).

4. Atmospheric responses to observed SST anomalies

First we describe the atmospheric SLP and surface air temperature (SAT) anomalies occurring during positive and negative NAO phases in CONTROL. The impact of SST anomalies on the NAO is then assessed by looking at the differences in SLP and SAT between the SSTA and CONTROL ensembles. The NAO index is calculated from the difference of the normalized SLP between Lisbon, Portugal (38°N, 9°W), and Stykkisholmur, Iceland (64°N, 22°W; Hurrell and Deser 2009), for the CONTROL and SSTA ensembles. We then compare the

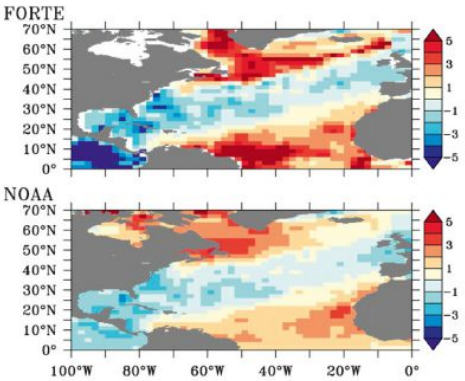

FIG. 3. The ratio of SST anomalies for December 2010 relative to the standard deviations from the (top) FORTE CONTROL ensemble and (bottom) NOAA OI observations.

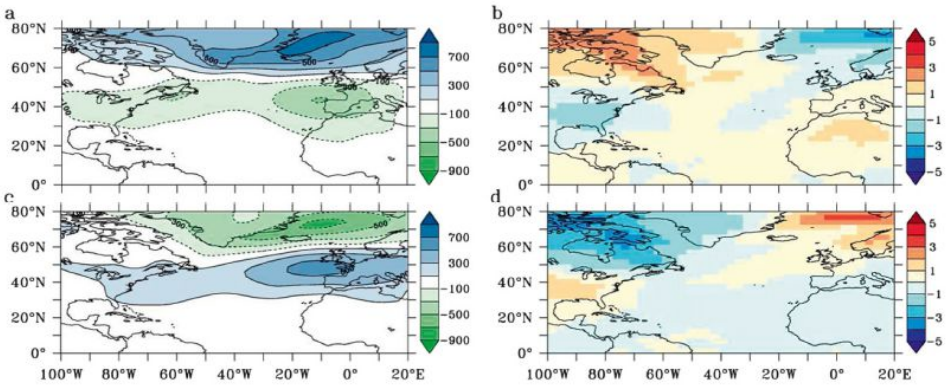

FIG. 4. (a) Composite SLP anomaly (Pa) and (b) composite SAT anomaly (°C) for December 2010 from CONTROL for NAO negative responses. (c) Composite SLP anomaly and (d) composite SAT anomaly for NAO positive responses.

distribution and means of the NAO indices for 2009 and 2010 for the CONTROL and SSTA ensembles.

a. Patterns of atmospheric pressure and surface atmospheric temperature

The characteristic SLP and SAT patterns for positive and negative NAO phases in the CONTROL experiment are established by calculating anomalies from the ensemble mean for each month of the 2-yr simulations. We initially examine the patterns of SLP and SAT in the CONTROL ensemble for each 24th month (December of the second simulated year). The patterns of SLP and SAT anomalies from the CONTROL and SSTA ensembles are grouped into those with NAO indices, which were greater than 1 or less than −1. We compute composite anomalies from the CONTROL and SSTA ensemble based on positive or negative values of the NAO index. The SLP composites are calculated according to

$$\mathrm{SLPA}^{+}_{i,j} = \frac{1}{n}\sum_{l\in l+} \mathrm{SLPA}_{i,j,l^{+}},$$

$n, l+$: set of time indices and number of NAO+ months,

$$\mathrm{SLPA}^{-}_{i,j} = \frac{1}{n}\sum_{l\in l-} \mathrm{SLPA}_{i,j,l^{-}},$$

$n, l-$: set of time indices and number of NAO− months,

where i, j are the zonal and meridional gridcell indices from the FORTE data, and where l is index number of the ensemble member.

NAO− responses are characterized by a positive pressure anomaly centered over Iceland and a negative pressure anomaly centered over Portugal. The pressure anomalies are reversed in NAO+ responses (Fig. 4). The atmospheric circulation patterns from the CONTROL ensemble are reasonably well resolved but model biases are present, which have been previously reported (Wilson et al. 2009). Compared with observations the westerly storm track is too broad to the north and extends too far into Europe. However, a comparison of the general structure of the large scale pressure fields from CONTROL and the National Centers for Environmental Prediction–National Center for Atmospheric Research (NCEP–NCAR) observations showed the locations of the centers of the SLP anomalies from EOF analysis were similar and there was a good correlation between the NAO locations from the CONTROL and observations, as evidenced in Fig. 4. The NAO surface impacts in the SSTA experiment are stronger in CONTROL possibly as a result of the size of the SST anomalies lying at the outer bounds of the model variability and because the ensemble sizes are smaller.

In the NAO− state SATs are cooler over the United Kingdom and northwestern Europe and warmer over southeastern Europe. In the NAO+ state the polarity is reversed with a warming of SATs over northwestern Europe and a cooling over southeastern Europe. These atmospheric circulation patterns from the CONTROL are used to reference the responses in the SSTA ensemble.

We now investigate the atmospheric responses from the SSTA ensemble. Initially composites in the 24th month are compared with those from the CONTROL (month 24 in the ensemble is the month that experiences

Appendix 1

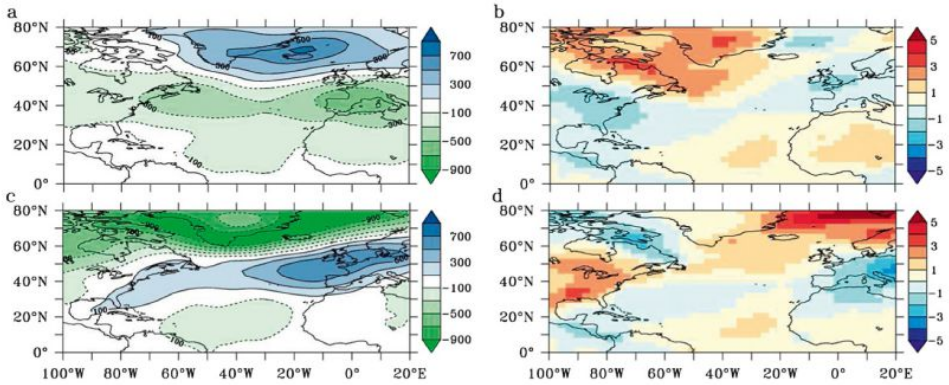

FIG. 5. (a) Composite SLP anomaly (Pa) and (b) composite SAT anomaly (°C) for December 2010 from SSTA for NAO negative responses. (c) Composite SLP anomaly and (d) composite SAT anomaly for NAO positive responses.

the observed December 2010 SST anomalies; Fig. 5). Of the 50 ensemble members of SSTA, 21 exhibit an NAO− state with a positive pressure anomaly over Iceland and a negative pressure anomaly over Lisbon (Figs. 5a,b). An NAO+ state is present in five cases (Figs. 5c,d). The remaining 24 cases produced responses that are NAO neutral where the index is between −1 and 1. For comparison the distribution in the CONTROL ensemble has 17 negative, 23 positive, and 10 neutral cases. The atmospheric circulation patterns for the NAO− members of the SSTA ensemble produced a more widespread cooling of SAT by about 1°C over western Europe and a more pronounced warming over Greenland. The position of the centers of the temperature anomalies remains similar to that of the CONTROL ensemble. The NAO+ ensemble members show a more pronounced warming of SAT over northwestern Europe and cooling over southeastern Europe.

The NAO+ and NAO− members of the SSTA ensemble also show characteristic differences in atmospheric circulation patterns. NAO+ and NAO− phases are characterized by shifts in the position of the jet stream. The position of the jet stream from the mean CONTROL atmospheric velocities at 300-hPa geopotential height is centered around 40°N (Fig. 6a). The influence of the SST anomalies from December 2010 in the NAO− ensemble is to shift the position of the jet stream southward with lower velocities over northern Europe and higher velocities over southern Europe (Fig. 6b). This shift is consistent with the pressure field for negative phases of the NAO (Rogers 1996). The changes in surface heat fluxes between those in the SSTA NAO− ensemble and mean control conditions show the impact of higher SST anomalies in the northwestern Atlantic in December 2009 and 2010 (Fig. 7). The influence of the SST anomalies in December 2010 compared with December 2009 is particularly significant in the changes in latent heat fluxes to the east of the Labrador/Irminger Sea Basins where the positive SST anomalies lead to higher heat loss from the ocean to the atmosphere. The heat flux anomalies in Fig. 7 lie between the northern two poles in the tripole at 45°N in a region where the SST anomalies collectively most weaken the background meridional SST gradient between northern mid- and high latitudes, as can be seen from the SST contours. We expect this to reduce storm activity downstream (consistent with weaker surface baroclinicity) and weaken the surface eddy-driven jet or shift it equatorward (reduced poleward eddy momentum transport in the upper troposphere and reduced poleward eddy heat transport in the mid- to lower troposphere) resulting in the weakening of surface westerlies (Brayshaw et al. 2011). This would have the impact of weakening the downstream storm track over the North Atlantic at 45°N and strengthening it at lower latitudes as seen in Fig. 6.

b. *Frequency in the occurrence of negative NAO indices*

The results described in the previous section suggest an increased frequency of NAO− phases for months experiencing the SST anomalies from December 2010 in the ensemble SSTA (21 NAO− responses vs 5 NAO+ responses). However, does this represent a significant shift toward an NAO− state or can we expect a similar response to happen by chance? To address this question

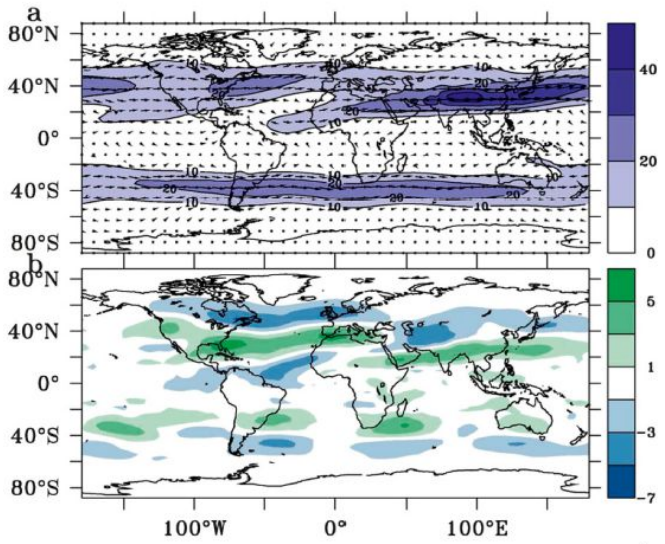

FIG. 6. (a) Mean CONTROL atmospheric velocities at 300-hPa geopotential height ($m\,s^{-1}$) for December 2010 with mean wind speeds superimposed. (b) Difference in atmospheric velocities at 300 hPa between SSTA NAO negative ensemble and CONTROL for December 2010 ($m\,s^{-1}$).

we assess to what extent the response of the NAO to SST anomalies is statistically significant and how the level of significance for December 2010 compares to the other 23 months of the 2009–10 period.

The occurrences of atmospheric conditions representative of NAO− phases in the CONTROL and SSTA ensembles are tested by examining the mean NAO indices for a particular month in the 24-month simulation to establish if SST anomalies influence the frequency of atmospheric patterns. We start by comparing the distributions of NAO indices in the 24th month (December 2010) for both the CONTROL and SSTA ensembles. The results indicate a pronounced shift to negative NAO indices in the SSTA ensemble as evidenced by both the ensemble mean and overall distribution (Fig. 8). The CONTROL ensemble has a mean NAO index for month 24 (December 2010) of −0.08 whereas the SSTA ensemble has a mean of −1.1. The SSTA ensemble has 21 outcomes with a mean NAO index less than −1 and only 5 with a mean NAO index greater than +1.

The significance of this result was tested by comparing the mean from the SSTA ensemble against the means of 100 000 random composites of the CONTROL ensemble using 50 samples chosen randomly for December with replacement (Fig. 9). As expected, the means of the NAO taken from the randomly selected composites of the CONTROL ensemble were normally distributed around an NAO index of −0.08. The distribution was further tested using the central limit theorem to create the distribution from the mean and standard deviation from month 24 of the CONTROL ensemble. The result shows good agreement with the distribution from the random composites confirming the two datasets to have the same distribution. Comparing the distribution to the mean NAO index of the SSTA ensemble reveals that the value of −1.1 is significant. We expect to find a mean NAO index of −1.1 or less in fewer than 1 in 1000 randomly chosen 50-member ensembles. The shift toward negative NAO values for December 2010 is statistically significant and very unlikely to have occurred by chance.

A similar level of significance is obtained for the ensemble global SST anomaly (GSSTA) where we prescribe global SST anomalies (mean NAO index of −1.0). However, ENSO teleconnections reliant on the stratosphere cannot be represented in this model and we are unable to determine if tropical Pacific SST anomalies contributed to a response in the NAO in our experiments.

So far our analysis has concentrated on the NAO response occurring in December 2010. However,

Appendix 1

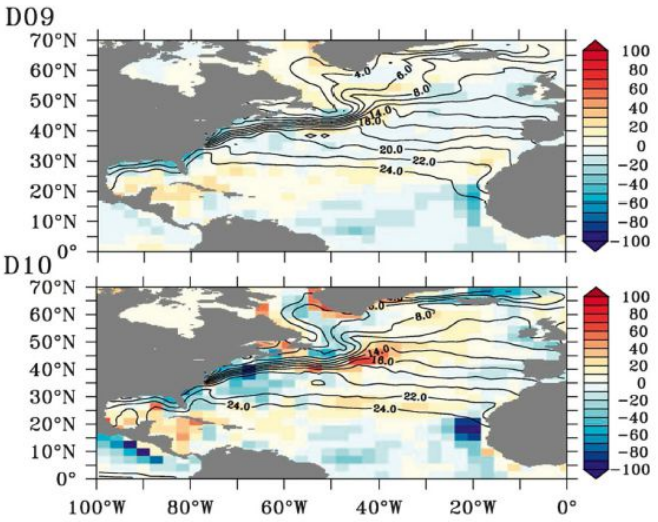

FIG. 7. Surface upward total heat flux anomalies ($W m^{-2}$) between SSTA NAO negative ensemble and control mean for (top) December 2009 and (bottom) December 2010. Contours show SST for December 2009 and December 2010 (°C).

pronounced SST anomalies also occurred in other months of the 2009–10 period (e.g., during the winter of 2009/10, see Fig. 2). Is the response we find for December 2010 unusual compared to the responses for the other 23 months? To answer this question we compare the mean monthly NAO indices for every month in the 24-month simulations in the SSTA, GSSTA, and CONTROL ensembles (Fig. 10). The monthly mean of the NAO index in the SSTA and GSSTA ensembles is compared with the corresponding monthly mean found in CONTROL. Even though the NAO extremes for each of the 24 months are similar in the ensembles SSTA and CONTROL the monthly means of the NAO index remain close to 0 in CONTROL. In contrast we find significant shifts in the NAO index for several months in the SSTA and GSSTA ensembles (i.e., shifts in excess of two standard deviations from monthly random composites of the CONTROL ensemble). A weak NAO response is seen in months 11 and 12 (corresponding to November and December 2009) coincident with the first episode of North Atlantic SST anomalies. However, the NAO response is always weaker than for months 23 and 24 (corresponding to November and December 2010), which were both influenced by reemerging SST anomalies (Taws et al. 2011). The negative NAO response for November 2010 is almost as strong as that found for December 2010. This is consistent with the observed values of the NAO index, which started its dip toward record low values in November 2010.

We note that applying observed SST anomalies in experiment SSTA has little impact on the spread of the values of the NAO index (Fig. 10). As mentioned above the extreme values of the NAO index are similar in CONTROL and SSTA. In addition, we find that for all

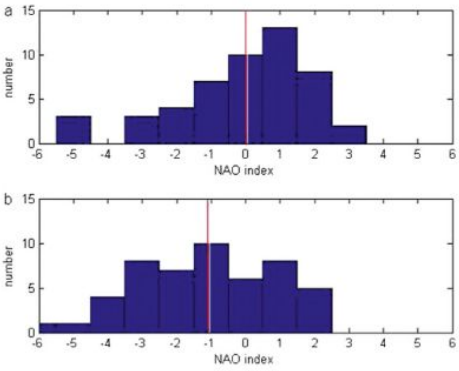

FIG. 8. Distribution of NAO indices for December 2010 in the (a) CONTROL and (b) SSTA ensembles. Red lines show the ensemble mean.

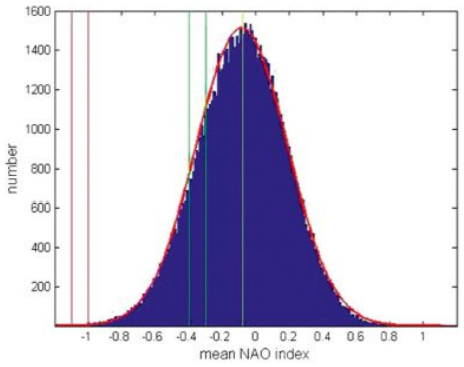

FIG. 9. Distribution of mean NAO index for December 2010 for 100 000 composites of 50 samples taken randomly from the CONTROL ensemble. CONTROL mean (−0.05) (yellow), SSTA mean November 2010 (−1.0) and December 2010 (−1.1) (red), and November 2009 (−0.3) and December 2009 (−0.4) (green). The distribution calculated from the mean and standard deviation from the CONTROL ensemble for December 2010 is shown in red.

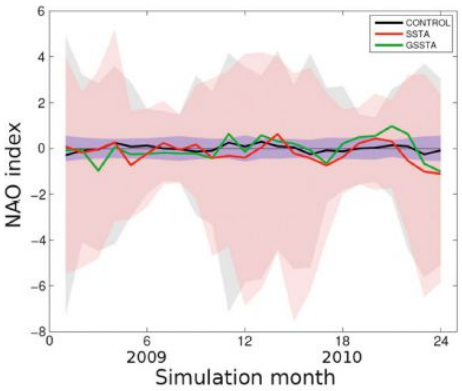

FIG. 10. Mean monthly NAO indices for CONTROL (black), SSTA (red), GSSTA (green), and two standard deviations of monthly mean NAO index sampled randomly from CONTROL (blue). Shaded areas denote the range (maximum and minimum) for each of the 24 months in the CONTROL (black) and SSTA (red) ensembles.

months the first and third quartiles for the values of the NAO index are comparable in SSTA and CONTROL (and also in GSSTA; not shown). Both the extreme values of the NAO index and the quartiles show a seasonal cycle with a larger spread of values occurring in winter and spring than in summer and autumn. This reflects the higher variability of the atmosphere and therefore of the NAO index that characterizes the boreal winter season. The similarity in the spread of NAO values in CONTROL and SSTA is a strong indication that the shifts seen for the mean value of the NAO index (Fig. 10) are not the consequence of increased variability in the NAO index in SSTA compared to CONTROL. In summary, our results suggest that the SST anomalies in November and December 2010 were more conducive to the development of a negative NAO than those in the preceding cold European winter of 2009/10.

5. Discussion and conclusions

Earlier studies have illustrated that Atlantic SSTs affect the evolution of the NAO on interannual to decadal time scales (e.g., Rodwell et al. 1999; Robertson et al. 2000). Here in contrast our focus is on shorter (monthly) time scales and we show that the strength of the feedback from Atlantic SSTs onto the atmospheric circulation can vary by investigating two recent European cold events that both coincided with similarly low NAO values: the winter of 2009/10 and the early winter of 2010/11. Our results suggest that North Atlantic SST anomalies significantly increased the probability of changes in atmospheric circulation affecting Europe in late 2010, but that they had a smaller impact in the preceding winter of 2009/10. Our findings also suggest that the tropical SST anomalies observed in the Pacific are unlikely to have caused the NAO responses observed in the early winter of 2010/11. Positive SST anomalies in the Labrador/Irminger Sea Basins and negative SST anomalies in the subtropical North Atlantic result in changes in the atmospheric pressure structure. The jet stream is deflected southward giving rise to a band of low pressure in the Azores around 40°N and high pressure over Iceland resembling a NAO− mode (Rodwell et al. 1999).

The absence of a stratosphere in our model limits our ability to model the possible atmospheric teleconnections between the tropical Pacific and the North Atlantic region, although such teleconnections would be expected to operate later in the winter (Bell et al. 2009). We also note that the SST anomalies experienced in SSTA and GSSTA can be outside the range of the SST variability of CONTROL. This happens since we add the observed SST anomalies to the SSTs of CONTROL, which increases the SST variance.

However, this does not affect our main findings. While the applied SST field in ensemble SSTA/GSSTA can be outside the model's natural variability range the use of observed SST anomalies over the 24-month period provides a comparison of the atmospheric responses

Appendix 1

over that period. The range of variability and distribution of NAO values in SSTA and CONTROL over the 24 months are similar, which indicates that the use of observed SST anomalies in the model produce results that are still within the bounds of the natural atmospheric variability of the coupled model (Fig. 10). The prescribing of observed SST anomalies in uncoupled atmosphere experiments has been used in other studies (e.g., Kushnir et al. 2002; Jung et al. 2011). While the size of the NAO response could be influenced by the scale of the SST anomalies our experiments show a larger atmospheric response for November/December 2010 than for any of the other months of the 2009–10 period. In particular, our study indicates that anomalous SSTs over the North Atlantic region contributed toward forcing the atmosphere toward a negative NAO state in the early winter of 2010/11.

Our results should not be interpreted as the ocean being the sole driver for the extreme cold event in the early winter of 2010/11. As mentioned earlier an interesting aspect of our results is the indication that SST anomalies occurring during similarly negative NAO phases (as observed during the cold winter of 2009/10 and in late 2010) do not necessarily have the same impact on the atmosphere. The strongly NAO− atmospheric circulation pattern that coincided with both periods is itself consistent with the development of an anomalous SST tripole pattern in the North Atlantic (Czaja and Frankignoul 2002). However, our results suggest that in late 2010 coupled ocean–atmosphere processes over the North Atlantic were particularly important. This is illustrated by the different atmospheric responses we find for the winter of 2009/10 and for late 2010. Both phases coincided with pronounced NAO− phases and an anomalous SST tripole in the North Atlantic. However, in late 2010 the SST anomalies were significantly more pronounced particularly over the Labrador/Irminger Sea Basins with anomalous heat flux lying between the northern two poles in the tripole at 45°N weakening the background equator-to-pole SST gradient. We would expect this to reduce storm activity downstream, weakening the surface eddy-driven jet or shifting it equatorward and weakening the surface westerlies at this latitude. The stronger NAO responses to November/December 2010 SST anomalies compared to the response found in the winter of 2009/10 suggest that the conditions in the early winter 2010/11 were significantly influenced by coupled ocean–atmosphere processes, whereas in 2009/10 the strong NAO− pattern is more likely to reflect internal variability of the atmosphere with the ocean playing a more passive role.

The implication of our results is that the ocean can play an important role in the genesis of certain extreme weather events in the North Atlantic region. The years 2009 and 2010 were particularly interesting from an oceanic point of view. An observing system in the North Atlantic registered a marked decrease of the strength of the Atlantic meridional overturning circulation (AMOC) in 2009 (McCarthy et al. 2012; Rayner et al. 2011). The AMOC is highly correlated to the oceanic northward transport of heat (Johns et al. 2011) and the period of reduced AMOC coincided with a reduction in the North Atlantic ocean heat content (OHC) in late 2009 (Sonnewald et al. 2013). Alongside anomalous Eurasian snow cover (Cohen et al. 2010) and anomalous Arctic sea ice extent (Strey et al. 2010; Liu et al. 2012), the reduced ocean heat transport may have contributed to the buildup of a negative OHC anomaly during the severe winter of 2009/10, which subsequently reemerged in the early winter of 2010/11 (Taws et al. 2011).

At this stage the sequence of events described above is speculative. Nevertheless, the evidence presented here indicates that simulations of the NAO are influenced by the pattern of ocean surface temperatures occurring in October–December 2010. Our conclusion is that reemergence of SST anomalies in the North Atlantic contributed toward the development of an SST anomaly pattern, which favored the persistence of a negative NAO resulting in the cold weather anomaly of December 2010 in northern Europe.

Acknowledgments. The authors thank David Brayshaw and an anonymous reviewer for their thoughtful reviews and comments, which helped to improve this paper. This work was part of the NERC funded project MONACO. Joel Hirschi, Bablu Sinha, and Adam Blaker are supported by National Capability funding provided by the United Kingdom Natural Environment Research Council.

REFERENCES

Alexander, M. A., and C. Deser, 1995: A mechanism for the recurrence of wintertime midlatitude SST anomalies. *J. Phys. Oceanogr.*, **25,** 122–137.

Bell, C. J., L. J. Gray, A. J. Charlton-Perez, and M. M. Joshi, 2009: Stratospheric communication of El Niño teleconnections in European winter. *J. Climate,* **22,** 4083–4096.

Bjerknes, J., 1964: Atlantic air-sea interaction. *Advances in Geophysics,* Vol. 10, Academic Press, 1–82.

Blaker, A. T., B. Sinha, V. O. Ivchenko, N. C. Wells, and V. B. Zalesny, 2006: Identifying the roles of the ocean and atmosphere in creating a rapid equatorial response to a Southern Ocean anomaly. *Geophys. Res. Lett.,* **33,** L06720, doi:10.1029/2005GL025474.

Brayshaw, D. J., B. Hoskins, and M. Blackburn, 2011: The basic ingredients of the North Atlantic storm track. Part II: Sea surface temperatures. *J. Atmos. Sci.,* **68,** 1784–1805.

Cassou, C., C. Deser, and M. A. Alexander, 2007: Investigating the impact of reemerging sea surface temperature anomalies

on the winter atmospheric circulation over the North Atlantic. *J. Climate,* **20,** 3510–3526.

Cohen, J., J. Foster, M. Barlow, K. Saito, and J. Jones, 2010: Winter 2009–2010: A case study of an extreme Arctic Oscillation event. *Geophys. Res. Lett.,* **37,** L17707, doi:10.1029/2010GL044256.

Czaja, A., and C. Frankignoul, 2002: Observed impact of Atlantic SST anomalies on the North Atlantic Oscillation. *J. Climate,* **15,** 605–623.

Davies, J. R., D. P. Rowell, and C. K. Folland, 1997: North Atlantic and European seasonal predictability using an ensemble of multidecadal atmospheric GCM simulations. *Int. J. Climatol.,* **17,** 1263–1284.

Deser, C., and M. L. Blackmon, 1993: Surface climate variations over the North Atlantic during winter: 1900–1989. *J. Climate,* **6,** 1743–1753.

Enfield, D. B., and D. A. Mayer, 1997: Tropical Atlantic sea surface temperature variability and its relation to El Niño–Southern Oscillation. *J. Geophys. Res.,* **102** (C1), 929–945.

Fereday, D. R., A. Maidens, A. Arribas, A. A. Scaife, and J. R. Knight, 2012: Seasonal forecasts of Northern Hemisphere winter 2009/10. *Environ. Res. Lett.,* **7,** 034031, doi:10.1088/1748-9326/7/3/034031.

Gent, P. R., and J. C. McWilliams, 1990: Isopycnal mixing on Ocean Circulation Models. *J. Phys. Oceanogr.,* **20,** 150–160.

Grötzner, A., M. Latif, and T. P. Barnett, 1998: A decadal climate cycle in the North Atlantic Ocean as simulated by the ECHO coupled GCM. *J. Climate,* **11,** 831–847.

Hirschi, J. J.-M., 2008: Unusual North Atlantic temperature dipole during the winter of 2006/2007. *Weather,* **63,** 1, 4–11.

Hurrell, J. W., and C. Deser, 2009: North Atlantic climate variability: The role of the North Atlantic Oscillation. *J. Mar. Syst.,* **78,** 28–41, doi:10.1016/jmarsys.2008.11.026.

Johns, W. E., and Coauthors, 2011: Continuous, array-based estimates of Atlantic Ocean heat transport at 26.5°N. *J. Climate,* **24,** 2429–2450.

Jung, T., F. Vitart, L. Ferranti, and J.-J. Morcrette, 2011: Origin and predictability of the extreme negative NAO winter of 2009/10. *Geophys. Res. Lett.,* **38,** L07701, doi:10.1029/2011GL046786.

Kushnir, Y., W. A. Robinson, I. Blade, N. M. J. Hall, S. Peng, and R. Sutton, 2002: Atmospheric GCM response to extratropical SST anomalies: Synthesis and evaluation. *J. Climate,* **15,** 2233–2256.

Levitus, S., and T. P. Boyer, 1998: *Temperature.* Vol. 4, *World Ocean Atlas 1998,* NOAA Atlas NESDIS 4, 99 pp.

——, R. Burgett, and T. P. Boyer, 1998: *Salinity.* Vol. 3, *World Ocean Atlas 1998,* NOAA Atlas NESDIS 3, 99 pp.

Liu, J., J. A. Curry, H. Wang, M. Song, and R. M. Horton, 2012: Impact of declining Arctic sea ice on winter snowfall. *Proc. Natl. Acad. Sci. USA,* **109** (11), 4074–4079, doi:10.1073/pnas.1114910109.

McCarthy, G., and Coauthors, 2012: Observed interannual variability of the Atlantic meridional overturning circulation at 26.5°N. *Geophys. Res. Lett.,* **39,** L19609, doi:10.1029/2012GL052933.

Osborn, T. J., 2011: Winter 2009/2010 temperatures and a record breaking North Atlantic Oscillation index. *Weather,* **66,** 19–21.

Rayner, D., and Coauthors, 2011: Monitoring the Atlantic meridional overturning circulation. *Deep-Sea Res. II,* **58,** 1744–1753.

Reynolds, R. W., and T. M. Smith, 1994: Improved sea surface temperature analysis using optimum interpolation. *J. Climate,* **7,** 929–948.

——, N. A. Rayner, T. M. Smith, D. C. Stokes, and W. Wang, 2002: An improved in situ and satellite SST analysis for climate. *J. Climate,* **15,** 1609–1625.

Robertson, A. W., C. R. Mechoso, and Y.-J. Kim, 2000: The influence of Atlantic sea surface temperature anomalies on the North Atlantic Oscillation. *J. Climate,* **13,** 122–138.

Rodwell, M. J., D. P. Rowell, and C. K. Folland, 1999: Oceanic forcing of the wintertime North Atlantic Oscillation and European climate. *Nature,* **398,** 320–323.

Rogers, J. C., 1996: Patterns of low-frequency monthly sea level pressure variability (1899-1986) and associated wave cyclone frequencies. *Quart. J. Roy. Meteor. Soc.,* **122,** 1385–1414.

Sinha, B., and R. Smith, 2002: Development of a fast coupled general circulation model (FORTE) for climate studies, implemented using the OASIS coupler. Tech. Rep. 81, National Oceanography Centre, Southampton, United Kingdom, 67 pp.

——, A. T. Blaker, J. J.-M. Hirschi, S. Bonham, M. Brand, S. Josey, R. S. Smith, and J. Marotzke, 2012: Mountain ranges favour vigorous Atlantic meridional overturning. *Geophys. Res. Lett.,* **39,** L02705, doi:10.1029/2011GL050485.

Sonnewald, M., J. J.-M. Hirschi, and R. Marsh, 2013: Oceanic dominance of interannual subtropical North Atlantic heat content variability. *Ocean Sci. Discuss.,* **10,** 27–53, doi:10.5194/osd-10-27-2013.

Strey, S. T., W. L. Chapman, and J. E. Walsh, 2010: The 2007 sea ice minimum: Impacts on the Northern Hemisphere atmosphere in late autumn and early winter. *J. Geophys. Res.,* **115,** D23103, doi:10.1029/2009JD013294.

Sutton, R. T., and M. R. Allen, 1997: Decadal predictability of North Atlantic sea surface temperature and climate. *Nature,* **388,** 562–567.

——, and B. Dong, 2012: Atlantic Ocean influence on a shift in European climate in the 1990s. *Nat. Geosci.,* **5,** 788–792, doi:10.1038/NGEO1595.

Taws, S. L., R. Marsh, N. C. Wells, and J. Hirschi, 2011: Re-emerging ocean temperature anomalies in late-2010 associated with a repeat negative NAO. *Geophys. Res. Lett.,* **38,** L20601, doi:10.1029/2011GL048978.

Valcke, S., L. Terry, and A. Piacentini, 2000: OASIS 2.4 user's guide. CERFACS, 85 pp.

Wilson, C., B. Sinha, and R. Williams, 2009: The influence of ocean dynamics and orography on Northern Hemisphere storm tracks. *J. Climate,* **22,** 3689–3702.

Appendix 1

List of References

Alexander, M. A. and C. Deser, 1995. A mechanism for the recurrence of wintertime mid-latitude SST anomalies, *Journal of Physical Oceanography,* 25, 122-137.

Alexander, M. A., M. S. Timlin and J. D. Schott, 2001, Winter to winter recurrence of sea surface temperature, salinity and mixed layer depth anomalies, *Progress in Oceanography,* 49, 41-61.

Arakawa, A., 1966. Computational design for long term numerical integration of the equations of fluid motion: two-dimensional incompressible flow, *Journal of Computational Physics*, 1, 119-143

Bell, C. J., L. J. Gray, A. J. Charlton-Perez and M. M. Joshi, 2009. Stratospheric communication of El Niño teleconnections in European winter, *Journal of Climate,* 22, 4083-4096.

Betts, A. K. and M. J. Miller, 1986. A new convective adjustment scheme. Part II: Single column tests using GATE wave, BOMEX, ATEX and artic air-mass data sets, *Quarterly Journal of Royal Meteological Society*, 112, 693-7009.

Bjerknes, J., 1964. Atlantic air-sea interaction, *Advances in Geophysics* 10, 1-82.

Blaker, A. T., B. Sinha, V. O. Ivchenko, N. C. Wells and V. B. Zalesny, 2006. Identifying the roles of the ocean and atmosphere in creating a rapid equatorial response to a Southern Ocean anomaly, *Geophysical Research Letters,* 33, LO6720, doi:10.1029/2005GL025474.

Blaker, A. T., J. J-M. Hirschi, G. McCarthy, B. Sinha, S. Taws, R. Marsh, A. Coward and B. de Cuevas, 2015. Historical analogues of the recent extreme minima observed in the Atlantic meridional overturning circulation at 26^{o}N, *Climate Dynamics*, 44, 1, 457-473, doi: 10.1007/s00382-014-2274-6.

Brayshaw, D. J., B. Hoskins and M. Blackburn, 2011. The basic ingredients of the North Atlantic storm track. Part II: Sea Surface Temperatures, *Journal of the Atmospheric Sciences,* 68, 1784-1805, doi:10.1175/2011JAS3674.1.

Broecker, W. S., 1991. The Great Ocean Conveyor, *Oceanography,* 4, 79-89.

Bronnimann, S., 2007, Impact of El Nino-Southern Oscillation on European Climate, *Reviews of Geophysics*, 45,RG3003, doi:10.1029/2006RG000199.

Bryan, K., 1979. Models of the world ocean, *Dynamics of Atmospheres and Oceans,* Elsevier, New York.

List of References

Bryden, H., B. A. King, G. McCarthy and E. L. McDonagh, 2014. Impact of a 30% reduction in Atlantic meridional overturning during 2009-2010, *Ocean Science*, 10, 683-691, doi:10.5194/os-10-683-2014.

Buchan, J., J. J-M. Hirschi, A. T. Blaker and B. Sinha, 2014. North Atlantic SST anomalies and the cold North European weather events of winter 2009/10 and December 2010, *Monthly Weather Review*, 142, 922-932, doi:10.1175/MWR-D-13-00104.

Cassou, C., C. Deser, and M. A. Alexander, 2007. Investigating the impact of reemerging sea surface temperature anomalies on the winter atmospheric circulation over the North Atlantic, *Journal of Climate,* 20 (14), 3510-3526, doi:10.1175/JCLI4202.1.

Cohen, J., J. Foster, M. Barlow, K. Saito, and J. Jones, 2010. Winter 2009–2010: A case study of an extreme Arctic Oscillation event, *Geophysical Research Letters*, *37*, L17707, doi:10.1029/2010GL044256.

Compo, G. P., J. S. Whitaker, P. D. Sardeshmukh, N. Matsui, R. J. Allan, X. Yin, B. E. Gleason *et al*. 2011. The twentieth century reanalysis project, *Quarterly Journal Royal Meteorological Society,* 137, 1-28, doi:10.1002/qj.776.

Cunningham, S. A., C. D. Roberts, E. Frajka-Williams, W. E. Johns, W. Hobbs, M. D. Palmer, D.Rayner, D. A. Smeed and G. McCarthy, 2013. Atlantic Meriodional Overturning Circulation slowdown cooled the subtropic ocean. *Geophysical Research Letters*, 40(23), 6202-6207, doi:10.1002/2013GL058464.

Czaja, A. and N. Blunt, 2011. A new mechanism for ocean-atmosphere coupling in midlatitudes, *Quarterly Journal Royal Meteorological Society,* 137, 1095-1101, doi:10.1002/qj.814.

Czaja, A and C. Frankignoul, 2002. Observed impact of Atlantic SST anomalies on the North Atlantic Oscillation, *Journal of Climate*, 15, 605-623.

Davies, J. R, D. P. Rowell and C. K. Folland, 1997. North Atlantic and European seasonal predictability using an ensemble of multidecadal atmospheric GCM simulations, *International Journal of Climatology,* 17, 1263-1284.

Davini. P and C. Cagnazzo, 2013. On the misinterpretation of the North Atlantic Oscillation in CMIP5 models, *Climate Dynamics*, 43, 1497-1511, doi:10.1007/s00382-013-1970.

DeCoetlogon, G. and C. Frankignoul, 2003. The persistence of winter sea surface temperature in the North Atlantic, *Journal of Climate,* 16, 1364-1377, doi:10.1175/1520-0442-16.9.1364.D.

Deser, C. and M. L. Blackmon, 1993. Surface climate variations over the North Atlantic during winter: 1900-1989, *Journal of Climate*, 6, 1743-1753.

Deser, C. and M. S. Timlin, 1997. Atmosphere-ocean interaction on weekly time scales in the North Atlantic and Pacific, *Journal of Climate,*10, 393-408.

Deser, C., M. A. Alexander and M. S. Timlin, 2003. On the persistence of sea surface temperature anomalies in midlatitudes, *Journal of Climate,* 16, 16, 57-72.

Duchez, A., E. Frajka-Williams, S. A. Josey, D. G. Evans, J. P. Grist, R. Marsh, G. D. McCarthy, B. Sinha, D. J. Berry, J. J-M. Hirschi, 2016. Drivers of exceptionally cold North Atlantic Ocean temperatures and their link to the 2015 European heat wave, *Environmental Research Letters*, 11, 7, doi:10.1088/1748-9326/11/7/074004.

Dunstone, N., D. Smith, A. Scaife, L. Hermanson, R. Eade, N. Robinson, M. Andrews, J. Knight, 2016. Skilful predictions of the winter North Atlantic Oscillation one year ahead, *Nature Geoscience*, 9, 11, doi:10.1038/ngeo2824.

Enfield, D. B and D. A. Mayer, 1997. Tropical Atlantic sea surface temperature variability and its relation to El Nino-Southern Oscillation, *Journal of Geophysical Research*, 102, 929-945.

Fereday, D.R., A. Maidens, A. Arribas, A. A. Scaife, and J. R. Knight, 2012. Seasonal forecasts of Northern Hemisphere winter, *Environmental Research. Letters,* 7, 034031, doi:10.1088/1748-9326/7/3/034031

Feliks, Y., A. W. Robertson and M. Ghil, 2016. Interannual variability in North Atlantic weather: Data analysis and a quasigeostrophic model, *Journal of the Atmospheric Sciences*, 73, 3227-3248, doi:10.1175/JAS-D-15-0297.1.

Fischer, E. M., S. I. Seneviratne, P. L. Vidale, D. Luthi, C. Schär, 2007. Soil moisture-atmosphere interactions during the 2003 European summer heat wave, *Journal of Climate*, 20, 5081-5099, doi:10.1175/JCL14288.1.

Folland, C. K., L. Y. Chan and R. M. Maryon, 1982. Associations between some mid-latitude sea surface temperature anomalies in November and N. Atlantic surface pressure

patterns in early December, *Met Office Memorandum No. 120*. Meteorological Office, Bracknell, U. K.

Folland, C. K., A. A. Scaife, J. Lindesay and D. B. Stephenson, 2012. How potentially predictable is northern Europe winter climate a season ahead? *International Journal of Climatology,* 32(6), 801-808, doi.org/10.1002/joc.2314.

Forget, G., 2010. Mapping Ocean Observations in a Dynamical Framework: A 2004-06 Ocean Atlas, *Journal of Physical Oceanography*, 40(6), 1201-1221, doi:org/10.1175/2009/JPO4043.1

Forster, P. M., M. Blackburn, R. Glover and K. P. Shine, 2000. An examination of climate sensitivity for idealised climate change experiments in an intermediate general circulation model, *Climate Dynamics,* 16, 833-849.

Gandin, L. S., 1963. Objective Analysis of Meteorological Fields, Gidrometeorizad, 238pp.

Gastineau, G. and C. Frankignoul, 2015. Influence of the North Atlantic SST variability on the atmospheric circulation during the twentieth century. *Journal of Climate*, *28*(4), pp.1396-1416.

Gastineau, G., B. L'Hévéder, F. Codron. and C. Frankignoul, 2016. Mechanisms Determining the Winter Atmospheric Response to the Atlantic Overturning Circulation. *Journal of Climate*, *29*(10), pp.3767-3785.

Gent, P. R and J. C. McWilliams, 1990. Isopycnal mixing on Ocean Circulation Models, *Journal of Physical Oceanography*, 20, 150-160.

Gray, L. J., T. J. Woollings, M. Andrews and J. Knight, 2016. Eleven-year solar cycle signal in the NAO and Atlantic/European blocking, *Quarterly Journal of the Royal Meteorological Society,* 142, 698, 1890-1903, doi:10.1002/qj2782.

Grist, J P. S. A. Josey, Z. L. Jacobs, R. Marsh, B. Sinha, and E. V. Sebille, 2016. Extreme air-sea interaction over the North Atlantic subpolar gyre during the winter of 2013-2014 and its sub-polar legacy, *Climate Dynamics*, 46, 4027-4045, doi :10.1007/s00382-015-2819.

Grötzner, A, M. Latif and T. P. Barnett, 1998. A decadal climate cycle in the North Atlantic Ocean as simulated by the ECHO coupled GCM, *Journal of Climate,* 11, 831-847.

Hirschi, J. J.-M., 2008. Unusual North Atlantic temperature dipole during the winter of 2006/2007, *Weather*, 63, 1, 4-11.

Huang, J., K. Higuchi and A. Shabbar, 1998, The relationship between the North Atlantic Oscillation and El Nino-Southern Oscillation, *Geophysical Research Letters*, 25, 14, 2707-2710, doi:10.1029/98GL01936.

Hurrell, J. W and C. Deser, 2009. North Atlantic climate variability: The role of the North Atlantic Oscillation, *Journal of Marine Systems*, 78, 28-41, doi:10.1016/ jmarsys.2008.11.026.

Ineson, S. and A. A. Scaife, 2009. The role of the stratosphere in the European climate response to El Nino, *Nature Geoscience,* 2, 32-36.

IPCC, 2013. Summary for Policymakers. In: Climate Change 2013: The Physical Science Basis. Contribution of Working Group I to the Fifth Assessment Report of the Intergovernmental Panel on Climate Change, Stocker, T. F., D. Qin, G.K. Plattner, M. Tignor, S.K.Allen, J. Boschung, A. Nauels, Y. Xia and P.M. Midgley (eds). Cambridge University Press, Cambridge, U. K.

Johns, T. C., C. F. Durman, H. T. Banks, M. J. Roberts, A. J. McLaren, J. K. Ridley, C. A. Senior, K. D. Williams, A. Jones, G. J. Rickard, S. Cusack, W. J. Ingram, M. Crucifix, D. M. H. Sexton, M. M. Joshi, B. W. Dong, H. Spencer, R. S. R. Hill, J. M. Gregory, A. B. Keen, A. K. Paraens, J. A. Lowe, A. Bodas-Salcedo, S. Stark, Y. Searl, 2006. The new Hadley Centre climate model (HadGEM1): Evaluation of coupled simulation, *Journal of Climate*, 19, 1327-1347.

Johns, W. E, M. O. Baringer, L. M. Beal, S. A. Cunningham, T. Kanzow, H. L. Bryden, J. J.-M. Hirschi, J. Marotzke, C. S. Meinen, B. Shaw and R. Curry, 2011. Continuous, array-based estimates of Atlantic Ocean Heat Transport at 26.5^{o}N, *Journal of Climate*, 24, 2429-2450.

Jung, T, F. Vitart, L. Ferranti, and J.-J. Morcrette, 2011. Origin and predictability of the extreme negative NAO winter of 2009/10, *Geophysical Research Letters*, *38*, L07701, doi:10.1029/2011GL046786.

Kaplan, A., Y. Kushnir, M. Cane and M. Blumenthal, 1997. Reduced space optimal analysis for historical data sets: 136 years of Atlantic sea surface temperatures, *Journal of Geophysical Research,*102, 27,835-27,860.

Killworth, P. D., D. Stainforth, D. J. Webb and S. M. Paterson, 1991. The development of a free-surface Bryan-Cox-Semtner ocean model, *Journal of Physical Oceanography*, 21, 9, 1333-1348.

Kushnir, Y. and J. M. Wallace, 1989. Low frequency variability in the Northern Hemisphere winter, geographical distribution, structure and time dependence, *Journal of Atmospheric Science,*46, 3122-3142.

Kushnir, Y., W. A. Robinson, I. Blade, N. M. J. Hall, S. Peng and R. Sutton, 2002. Atmospheric GCM response to extratropical SST anomalies: Synthesis and evaluation, *Journal of Climate*, 15, 2233-2256.

Levitus, S. and T. P. Boyer, 1998. *World Ocean Atlas 1998*, vol 4, *Temperature, NOAA, Atlas NESDIS 2*, 99pp., NOAA, Silver Spring, Md.

Levitus, S., R. Burgett and T. P. Boyer, 1998. *World Ocean Atlas 1998*, vol 3, *Salinity, NOAA Atlas NESDIS 3*, 99pp., NOAA, Silver Spring, Md.

Li, C., B. Stevens and J. Marotzke 2015. Eurasian winter cooling in the warming hiatus of 1998–2012. *Geophysical Research Letters*, *42*(19), pp.8131-8139.

Liu, J, J. A. Curry, H. Wang, M. Song, and R. M. Horton, 2012. Impact of declining Arctic sea ice on winter snowfall, *Proc. Nat. Acad. Sci.*, 109 (11), 4074-4079, doi:10.1073/pnas.1114910109.

MacLachlan, C., A. Arribas, K. A. Peterson, A. Maidens, D. Fereday, A. A. Scaife, M. Gordon, M. Vellinga, A. Williams, R. E. Comer, J. Camp, P. Xavier and G. Madec, 2015. Global Seasonal forecast system version 5 (GloSea5): a high resolution seasonal forecast system. *Quarterly Journal of the Royal Meteorological Society*, *141*(689), pp.1072-1084.

Maidens, A., A. Arribas, A. A. Scaife, C. Maclachlan, D. Peterson, and J. Knight, 2013. The influence of surface forcings on the prediction of the North Atlantic oscillation regime of winter 2010-2011, *Monthly Weather Review*, 141, 11, 3801-3813, doi:10.1075/MWR-D-13-00033.1

Massey Jr., F. J., 1951. The Kolmogorov-Smimov test for goodness of fit, *Journal of the American Statistical Association*, 46, 253,68-78.

McCarthy, G, E. Frajka-Williams, W. E. Johns, M. O. Baringer, C. S. Meinen, H. L. Bryden, D. Rayner, A. Duchez, C. Roberts and S. A. Cunningham, 2012. Observed interannual variability of the Atlantic meridional overturning circulation at 26.5^{o}N, *Geophysical Research Letters*, 39, L19609, doi:10.1029/2012GL052933.

Mitchell, D., P Davini, B. Harvey, N. Massey, K. Haustein, T. Woolings, R. Jones, F Otto, B. Guillod, S. Sparrow, D. Wallom, M. Allen, 2017, Assessing mid-latitude dynamics in extreme event attribution syatems, *Climate Dynamics*, 48, 12, 3889-3901, doi:10.1007/s00382-016-3308-z.

Moron, V. and L. Gouirand, 2003, Seasonal modulation of the El Nini-Southern Oscillation relationship with sea level pressure anomalies over the North Atlantic in October-March 1973-1996, *International Journal of Climatology*, 23, 143-155, doi:10.1002/joc.868.

Mosedale, T., D. Stephenson, M. Collins and T. Mills, 2006. Granger causality of coupled climate processes: Ocean feedback on the North Atlantic Oscillation, *Journal of Climate,*19, 1182-1194.

Neal, R., D. Fereday, R. Crocker and R. E. Comer, 2016, A flexible approach to defining weather patterns and their application in weather forecasting over Europe, *Meteorological Applications*, 23, 389-400, doi:10.1002/met.1563.

Osborn,T. J., 2011. Winter 2009/2010 temperatures and a record breaking North Atlantic Oscillation index, *Weather,* 66, 19-21.

Pacanowski, R. C. and S. M. Griffies, 1999. The MOMA3 Manual, NOAA/Geophysical Fluid Dynamics Laboratory.

Perez, J., M. Menendez, F.J. Mendez and I. J. Losada, 2014. Evaluating the performance of CMIP3 and CMIP5 global climate models over the north-east Atlantic region, *Climate Dynamics*, 43, 2663-2680, doi:10.1007/s00382-014-2078-8.

Rahmstorf, S., 2003. The current climate, *Nature*, 421, 699.

Rayner, N. A., D. E. Parker, E. B. Horton, C. K. Folland, L. V. Alexander and D. P. Rowell, 2003. Global analysis of sea surface temperature, sea ice, and night marine air temperatures since the late nineteenth century, *Journal of Geophysical Research*, 108, D14,4407, doi:10.1029/2002JD002670.

Rayner, D., J. J.-M.Hirschi, T. Kanzow, W. E. Johns, P. G. Wright, E. Frajka-Williams, H. L. Bryden, C. S. Meinen, M. O. Baringer, J. Marotzke, L. M. Beal and S. A. Cunningham, 2011. Monitoring the Atlantic meridional overturning circulation, *Deep-Sea Research II*, 58, 1744-1753, doi:10.1016/j.dsr2.2010.10056.

Reynolds, R. W. and T. M. Smith, 1994. Improved sea surface temperature analysis using optimum interpolation, *Journal of Climate,* 7, 929-948.

Reynolds, R. W., N. A. Rayner, T. M. Smith, D. C. Stokes and W. Wang, 2002. An improved in situ and satellite SST analysis for climate, *Journal of Climate*, 15, 1609-1625.

Roberts, M. J., H. T. Hewitt, P. Hyder, D. Ferreira, S. A. Josey, M. Mizielinski, A. Shelly, 2016. Impact of ocean resolution on coupled air-sea fluxes and large-scale climate, *Geophysical Research Letters*, 43, 10,430-10,438, doi:10.1002/2016GL070559.

Robertson, A. W., C. R. Mechoso and Y-J. Kim, 2000. The influence of Atlantic Sea Surface Temperature Anomalies on the North Atlantic Oscillation, *Journal of Climate*, 13, 122-138.

Robson, J., P. Ortega and R. Sutton, 2016. A reversal of climatic trends in the North Atlantic since 2005, *Nature Geoscience*, 9, doi:10.1038/NGE02727.

Rodwell, M. J. and C. K. Folland, 2002. Atlantic air-sea interaction and seasonal predictability, *Quarterly Journal of the Royal Meteorological Society,* 128, 1413-1443.

Rodwell, M. J., D. P. Rowell and C. K. Folland, 1999, Oceanic forcing of the wintertime North Atlantic Oscillation and European climate, *Nature*, 398, 320-323.

Rogers, J. C., 1996. Patterns of low-frequency monthly sea level pressure variability (1899-1986) and associated wave cyclone frequencies, *Quarterly Journal Royal Meteorological Society*, 122, 1385-1414.

Russo, S., J. Sillmann and E. M. Fischer, 2015. Top ten European heatwaves since 1950 and their occurrence in the coming decades, *Environmental Research Letters*, 10:124003, doi:10.1088/1748-9326/10/12/124003.

Scaife, A. A., A.Arribas, E. Blockley, A. Brookshaw, R. T. Clark, N. Dunstone, R. Eade, D. Fereday, C. K. Folland, M. Gordon, L. Hermanson, J. R. Knight, D. J. Lea, C.MacLachlan, A. Maidens, M. Martin, K. A. Peterson, D. Smith, M. Vellinga, E. Wallace, J. Waters and A. Williams, 2014. Skillful long-range prediction of European and North American winters, *Geophysical Research Letters*, 41, 2514-2519, doi:10.1002/2014GL059637.

Schär, C. and G. Jendritzky, 2004. Hot news from summer 2003, *Nature*, 432, 559-560, doi:10.1038/432559a.

Sinha, B. and R. Smith, 2002. Development of a fast coupled general circulation model (FORTE) for climate studies, implemented using the OASIS coupler, Technical Report 81, 67 pp., National Oceanography Centre, Southampton, U.K.

Sinha, B., A. T. Blaker, J. J.-M. Hirschi, S. Bonham, M. Brand, S. Josey, R .S. Smith and J. Marotzke, 2012. Mountain ranges favour vigorous Atlantic meridional overturning, *Geophysical Research Letters*, 39, L02705, doi:10.1029/2011GL050485.

Smeed, D. A., G. D. McCarthy, S. A. Cunningham, E. Frajka-Williams, D. Rayner, W. E. Johns, C.S. Meinen, M. O. Baringer, B. I. Moat, A Duchez and H. L. Bryden, 2014. Observed decline of the Atlantic meridional overturning circulation 2004-2012, *Ocean Science*,10, 29-38, doi:10.5194/os-10-29-2014.

Smith, R.S., C. Dubois and J. Marotzke, 2004. Ocean circulation and climate in an idealised Pangean OAGCM. *Geophysical research letters*, *31*(18).

Smith, R.S., C. Dubois and J. Marotzke, 2006. Global climate and ocean circulation on an aquaplanet ocean-atmosphere general circulation model. *Journal of climate*, *19*(18), pp.4719-4737.

Sonnewald, M., J. J-M. Hirschi, R. Marsh, E. L. McDonagh and B. A. King, 2013. Atlantic meridional ocean heat transport at 26^{o}N: impact on subtropical ocean heat content variability. *Ocean Science*, *9*(6), pp.1057-1069.

Stommel, H, 1958. The Gulf Stream: a physical and dynamical description, Berkely: University of California, p234.

Stommel, H. and A. B. Arons, 1959. On the abyssal circulation of the world ocean 1: Stationary planetary flows on a sphere, *Deep Sea Research*, 6, 140-154.

Strey, S.T., W.L. Chapman and J.E. Walsh, 2010. The 2007 sea ice minimum: Impacts on the Northern Hemisphere atmosphere in late autumn and early winter, *Journal of Geophysical Research*, 115, D23103.

Sutton, R. T. and M. R. Allen, 1997. Decadal predictability of North Atlantic sea surface temperature and climate, *Nature,* 388, 562-567.

Sutton, R. T. and B. Dong, 2012. Atlantic Ocean influence on a shift in European climate in the 1990s, *Nature Geoscience,* doi:10.1038/NGEO1595.

Taws, S. L., R. Marsh, N. C. Wells and J. J-M. Hirschi, 2011. Re-emerging ocean temperature anomalies in late 2010 associated with a repeat negative NAO, *Geophysical Research Letters*,38, L20601, doi:10.1020/2011GL048978.

Taylor, K. E., R. J. Stouffer and G. A. Meehl, 2012. An overview of CMIP5 and the experiment design, *Bulletin of the American Meteorological Society*, 93, 485-498, doi:10.1175/BAMS-D-11-00094.1.

Timlin, M. S., M. A. Alexander and C. Deser, 2002. On the re-emergence of North Atlantic SST anomalies, *Journal of Climate,* 15, 9,2707-2712.

Trenberth, K. E. and J. M. Caron, 2001. Estimates of Meridional Atmosphere and Ocean Heat Transports, *Journal of Climate,* 14, 3433-3433.

Valcke, S., L. Terray and A. Piacentini, 2000. OASIS 2.4, Ocean atmosphere sea ice soil: users guide, Technical Report TR/CMGC/00/10, 85pp., CERFACS, Toulouse, France.

Visbeck, M., E. P. Chassignet, R. G. Curry, T. L. Delworth, R. R. Dickson and G. Krahmann, 2003. The ocean's response to North Atlantic Oscillation variability, In: J. W. Hurrell, Y. Kushnir, Y. Otterson, M. Visbeck (Eds.), The North Atlantic Oscillation, Climate Significance and Environmental Impact, AGU Geophysical Monograph, vol. 134, pp. 113-146.

Wallace, J. M. and D. S. Gutzlet, 1981. Teleconnections in the geopotential height field during the Northern Hemisphere winter, *Monthly Weather Review,*109, 784-812.

Wang, G., D. Dommenget and C. Frauen, 2015. An evaluation of the CMIP3 and CMIP5 simulations in their skill in simulating the spatial structure of SST variability, *Climate Dynamics*, 44, 95-114, doi:10.1007/s00382-014-2154.

Weaver, A. J. and E. S. Sarachik, 1990. On the importance of vertical resolution in certain ocean general circulation models, *Journal of Physical Oceanography*, 20, 4, 600-609.

Webb, D. J., 1996. An ocean model code for array processor computers, *Computers and Geosciences*, 22, 5, 569-578.

Whitaker, J. S. and T. M. Hamill, 2002. Ensemble data assimilation without perturbed observations, *Monthly Weather Review,* 130, 1913-1924.

Wilcox, R., 2005, Kolomogorov-Smimov test, *Encyclopedia of biostatistics*.

Wild, M., D.Folini, C. Schär, N. Loeb, E. G. Dutton, G. Konig-Longlo, 2012. The global energy balance from a surface perspective, *Climate Dynamics*, doi:10.1007/s00382-012-1569-8

Wilson, C., B. Sinha and R. Williams, 2009. The influence of ocean dynamics and orography on Northern Hemisphere storm tracks, *Journal of Climate*, 22, 3689-3702, doi:10.1175/2009JCL12651.

Woollings, T, C. Czuchnicki and C. Franke, 2014, Twentieth century North Atlantic jet variability, *Quarterly Journal Royal Meteorological Society*, 140, 680, 783-791.

Wust, G., 1935. Die stratosphere, *Wissenschaftliche Ergebnisse der Deutschen Altantischen Expedition "Meteor",* 6, 109-288.

Yamamoto, A. and J. B. Palter, 2016. The absence of an Atlantic imprint on the multidecadal variability of wintertime European temperature. *Nature communications*, *7*.